

Electrogenerated Films of Carbazole- and Thiophene-Based Microporous Polymer Networks



Dissertation

zur Erlangung des akademischen Grades

Doktor der Naturwissenschaften

(Dr. rer. nat.)

**eingereicht in der Fakultät für Mathematik und Naturwissenschaften
der Bergischen Universität Wuppertal**

von

Alex Uriel Palma Cando

geb. in Quito, Ecuador

Wuppertal 2016

Die Dissertation kann wie folgt zitiert werden:

urn:nbn:de:hbz:468-20170210-142131-6

[<http://nbn-resolving.de/urn/resolver.pl?urn=urn%3Anbn%3Ade%3Ahbz%3A468-20170210-142131-6>]

Para mis queridos padres, Romey y Cecilia.

To my beloved parents.

Meinen geliebten Eltern.

*„All unsere Wissenschaft, gemessen an der Wirklichkeit, ist primitiv und kindlich –
doch ist sie unser kostbarstes Gut.“*

*“All our science, measured against reality, is primitive and childlike –
and yet it is the most precious thing we have.”*

*“Toda nuestra ciencia, comparada con la realidad, es primitiva e infantil –
y sin embargo, es lo más valioso que tenemos.”*

Albert Einstein
(1879 – 1955)

This work was carried out during the period from October 2013 to October 2016 in the Department of Chemistry, Macromolecular Chemistry Group, Bergische Universität Wuppertal, under the supervision of Prof. Dr. Ullrich Scherf.

- 1. Reviewer: Prof. Dr. Ullrich Scherf.**
- 2. Reviewer: Prof. Dr. Bernardo Frontana-Uribe.**
- 3. Reviewer: Prof. Dr. Arne Thomas.**

Dissertation submitted on: 09.11.2016

Oral examination on: 02.02.2017

Abstract

Electrochemical oxidative polymerization of rigid, multifunctional monomers allows for the generation of microporous thin films with high surface areas. In this work, multifunctional carbazole- and thiophene-based rigid monomers were utilized as tridimensional building blocks (tectons) toward the electrogeneration of microporous polymer films. The monomer structure plays an essential role on the properties of the resulting microporous polymer networks. A distinct correlation is observed between the number of electroactive substituents in the monomers and the specific surface area of the corresponding microporous polymer films. Potential applications were explored for the chemical and electrochemical detection of nitroaromatic compounds using optimized microporous polymer films.

Zusammenfassung

Die oxidative, elektrochemische Polymerisation starrer, multifunktionaler Monomere ermöglicht die Erzeugung dünner mikroporöser Filme mit hoher Oberfläche. In dieser Arbeit wurden multifunktionelle, dreidimensionale Carbazol- und Thiophen-basierte rigide Monomere (Tektone) dazu verwendet, elektrochemisch dünne mikroporöse Filme zu generieren. Die Struktur der Monomere spielt für die Eigenschaften der dabei entstehenden mikroporösen Polymernetzwerke eine entscheidende Rolle. Es wird ein Zusammenhang zwischen der Anzahl der elektroaktiven Gruppen des Monomeres und der spezifischen Oberfläche des entsprechenden Polymerfilmes beobachtet. Einige dieser mikroporösen Polymernetzwerke wurden für Anwendungen als Sensormaterial sowohl für die chemische, als auch die elektrochemische Detektion von Nitroaromaten untersucht.

Table of Contents

Chapter 1. Introduction.....	1
1.1. Electrogeneration of Microporous Polymer Networks.....	1
1.2. Films of Carbazole-Based Microporous Polymer Networks.....	2
1.3. Films of Thiophene-Based Microporous Polymer Networks.....	9
1.4. Motivation and Objectives.....	13
1.5. References.....	14
Chapter 2. Electrogenenerated Microporous Polymer Networks from Di-, Tri- and Tetracarbazole-Based Monomer.....	19
2.1. Introduction.....	19
2.2. Results and Discussion.....	20
2.2.1. Synthesis of the Series of Monomers.....	20
2.2.2. Electrochemical Characterization of the Monomers and Polymers at Pt Disc Electrodes.....	21
2.2.3. Porosity Characterization of Bulk Polymers and MPN Films.....	24
2.2.4. Electrochemical Reduction of 1,3,5-Trinitrobenzene at MPN-Modified Glassy Carbon Electrodes.....	26
2.2.5. Mechanism of Electron Transfer for Electrochemical Reduction of Nitroaromatic Analytes at PTPTCz-Modified GC Electrodes.....	29
2.2.6. Gas-Phase Nitroaromatic Analytes Detection by PSpCz Thin Films.....	32
2.3. Conclusions.....	34
2.4. Experimental Section.....	34
2.4.1. Monomers and Bulk Polymers.....	34
2.4.1.1. Synthesis of 4,7-di[4-(carbazol-9-yl)phenyl]benzo[c][1,2,5]thiadiazole (CBPBT).....	35
2.4.1.2. Synthesis of 2,2',7,7'-tetra(carbazol-9-yl)-9,9'-spirobifluorene (SpCz).....	35
2.4.1.3. Synthesis of tetra[4-(carbazol-9-yl)phenyl]methane (TPTCz).....	36
2.4.1.4. Synthesis of bulk polymers.....	36
2.4.2. Electrochemical Studies.....	37
2.4.2.1. Electrochemical polymerization on Pt electrodes.....	37
2.4.2.2. Electrochemical polymerization on glassy carbon (GC) electrodes and electrochemical sensing of TNB, NB and TNP.....	37
2.4.2.3. Electrochemical polymerization on ITO electrodes.....	38

2.4. References.....	38
Chapter 3. Electrogenerated MPNs from Tetra- and Octacarbazole-Based	
Monomers	41
3.1. Introduction.....	41
3.2. Results and Discussion.....	42
3.2.1. Synthesis of the Series of Monomers.....	42
3.2.2. Characterization of Chemically Synthesized Bulk Polymers.....	43
3.2.3. Electrochemical Characterization of the Monomers and Polymers at Pt Disc Electrodes.....	46
3.2.4. Electrochemical Quartz-Crystal Microbalance Studies of the Monomers and Polymers.....	50
3.2.5. Porosity, Optical and Morphological Characterization of Electrogenerated MPN Films.....	52
3.2.6. Electrochemical Reduction of Nitroaromatic Analytes at MPN-Modified Glassy Carbon Electrodes.....	53
3.3. Conclusions.....	57
3.4. Experimental Section.....	57
3.4.1. Monomers and Bulk Polymers.....	57
3.4.1.1. Synthesis of tetraphenylmethane (1).....	58
3.4.1.2. Synthesis of tetra(4-bromophenyl)methane (2)	58
3.4.1.3. Synthesis of tetra[4-(carbazol-9-yl)phenyl]methane (TPTCz).....	59
3.4.1.4. Synthesis of 9-(4-bromophenyl)-carbazole (3).....	59
3.4.1.5. Synthesis of tetra[4-(carbazol-9-yl)phenyl]silane (TPTCzSi).....	60
3.4.1.6. Synthesis of tetra(4-nitrophenyl)methane (4).....	60
3.4.1.7. Synthesis of tetra(4-aminophenyl)methane (5).....	61
3.4.1.8. Synthesis of tetra(3,5-dibromophenyl)methane (6).....	61
3.4.1.9. Synthesis of tetra[3,5-di(carbazol-9-yl)phenyl]methane (TPOcCz).....	61
3.4.1.10. Synthesis of 9,9'-(5-bromo-1,3-phenylene)bis(carbazole) (7).....	62
3.4.1.11. Synthesis of tetra[3,5-di(carbazol-9-yl)phenyl]silane (TPOcCzSi).....	62
3.4.1.12. Synthesis of bulk polymers by oxidative coupling with FeCl ₃	63
3.4.2. Electrochemical Studies.....	63
3.4.2.1. Electrochemical polymerization and characterization on Pt disc and Pt/quartz crystal electrodes.....	64

3.4.2.2. Electrochemical polymerization on ITO electrodes for porosity measurements and morphological characterization.....	64
3.4.2.3. Electrochemical polymerization on glassy carbon (GC) electrodes and electrochemical sensing of TNB.....	64
3.5. References.....	65
Chapter 4. Electrogenerated MPNs from Tetrathiophene-based Monomers.....	67
4.1. Introduction.....	67
4.2. Results and Discussions.....	69
4.2.1. Synthesis of the Series of Monomers.....	69
4.2.2. Characterization of Chemically Synthesized Bulk Polymers.....	69
4.2.3. Electrochemical Characterization of the Monomers and Polymers at Pt Disc Electrodes.....	73
4.2.4. Porosity, Optical and Morphological Characterization of Electrogenerated MPN Films.....	77
4.2.5. Electrochemical Reduction of 1,3,5-Trinitrobenzene at PTPTh-Modified Glassy Carbon Electrodes.....	82
4.3. Conclusions.....	84
4.4. Experimental Section.....	85
4.4.1. Monomers and Bulk Polymers.....	85
4.4.1.1. Synthesis of 2,2',7,7'-tetra(thien-2-yl)-9,9'-spirobifluorene (SpTh).....	85
4.4.1.2. Synthesis of 2,2',7,7'-tetra(thioen-3-yl)-9,9'-spirobifluorene (Sp3Th).....	86
4.4.1.3. Synthesis of tetra[4-(thien-2-yl)phenyl]methane (TPTTh).....	86
4.4.1.4. Synthesis of tetra[4-(thien-3-yl)phenyl]methane (TPT3Th).....	87
4.4.1.5. Synthesis of bulk polymers by oxidative coupling with FeCl ₃	87
4.4.2. Electrochemical Studies.....	88
4.4.2.1. Electrochemical polymerization and characterization on Pt electrodes.....	88
4.4.2.2. Electrochemical polymerization on ITO electrodes for porosity measurements, as well as for optical, and morphological characterization....	88
4.4.2.3. Electrochemical polymerization of TPTTh on glassy carbon (GC) electrodes and electrochemical sensing of TNB.....	89
4.5. References.....	89
Chapter 5. Electrogenerated MPNs from Tetraphenylethene-Cored Multifunctional Monomers.....	93

5.1. Introduction.....	93
5.2. Results and Discussions.....	94
5.2.1. Synthesis of the Series of Monomers.....	94
5.2.2. Characterization of Chemically Synthesized Bulk Polymers.....	95
5.2.3. Electrochemical Characterization of the Monomers and Polymers at Pt Disc Electrodes.....	98
5.2.4. Porosity Characterization of Electrogenenerated MPN Films.....	103
5.2.5. Optical Characterization of the AIE-active Monomers in Solution and Solid State.....	103
5.2.6. Optical and Morphological Characterization of Electrogenenerated AIE-active MPN Films.....	107
5.3. Conclusions.....	109
5.4. Experimental Section.....	109
5.4.1. Monomers and bulk polymers.....	109
5.4.1.1. Synthesis of bis[4-(carbazol-9-yl)phenyl]methanone (1).....	110
5.4.1.2. Synthesis of 1,1,2,2-tetra[4-(carbazol-9-yl)phenyl]ethene (TPETCz).....	110
5.4.1.3. Synthesis of 1,1,2,2-tetra(4-bromophenyl)ethene (2).....	111
5.4.1.4. Synthesis of 1,1,2,2-tetra[4-(4,4,5,5-tetramethyl-1,3,2-dioxaborolan-2- yl)phenyl]ethene (3).....	111
5.4.1.5. Synthesis of 1,1,2,2-tetra[4-(thiophen-2-yl)phenyl]ethene (TPETTh).....	111
5.4.1.6. Synthesis of 9-(4-bromophenyl)-carbazole (4).....	112
5.4.1.7. Synthesis of 1,1,2,2-tetra[4'-(carbazol-9-yl)-(1,1'-biphenyl)-4-yl]ethene (TPETPTCz).....	112
5.4.1.8. Synthesis of 2-(4-bromophenyl)thiophene (5).....	113
5.4.1.9. Synthesis of 1,1,2,2-tetra[4'-(thiophen-2-yl)-(1,1'-biphenyl)-4-yl]ethene (TPETPTTh).....	113
5.4.1.10. Synthesis of 9,9'-(5-bromo-1,3-phenylene)bis(carbazole) (6).....	114
5.4.1.11. Synthesis of 1,1,2,2-tetra[3',5'-di(carbazol-9-yl)-(1,1'-biphenyl)-4- yl]ethene (TPETPOcCz).....	114
5.4.1.12. Synthesis of 2,2'-(5-bromo-1,3-phenylene)dithiophene (7).....	115
5.4.1.13. Synthesis of 1,1,2,2-tetra[3',5'-di(thiophen-2-yl)-(1,1'-biphenyl)-4- yl]ethene (TPETPOcTh).....	115
5.4.1.14. Synthesis of bulk polymers by oxidative coupling with FeCl ₃	116

5.4.2. Electrochemical Studies.....	116
5.4.2.1. Electrochemical polymerization and characterization on Pt disc electrodes	117
5.4.2.2. Electrochemical polymerization on ITO electrodes for porosity	
measurements and optical characterization.....	117
5.5. References.....	118
Chapter 6. Summary and Outlook.....	121
6.1. Summary of Chapters 2 – 5.....	121
6.2. Outlook.....	122
6.3. References.....	123
List of Abbreviations.....	125
List of Publications.....	129
Acknowledgements.....	131

Chapter 1

Introduction¹

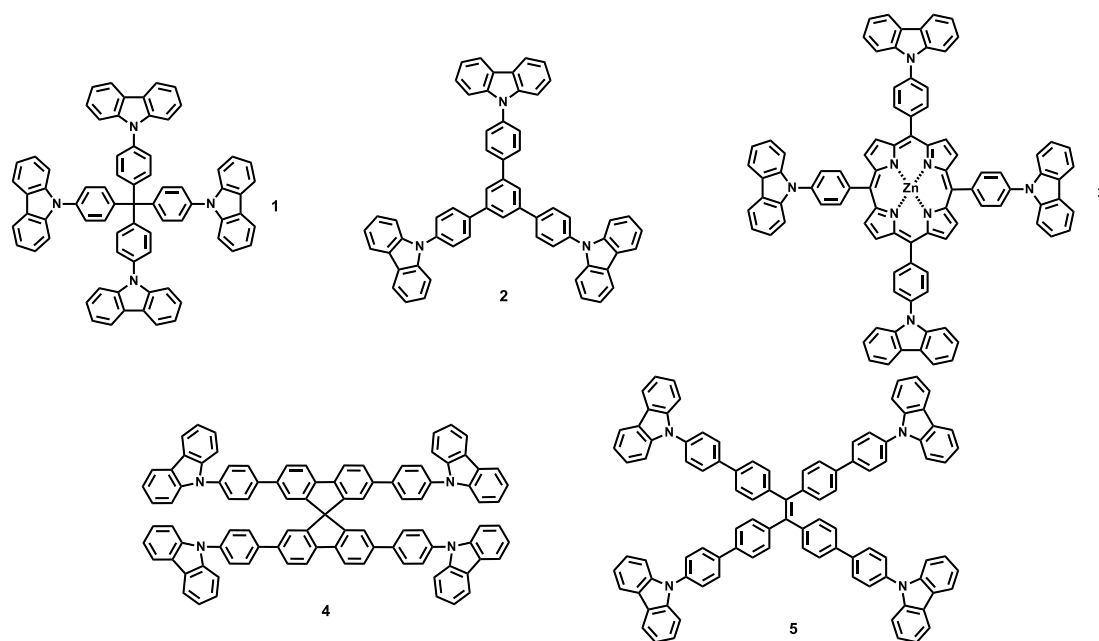
1.1. Electrogeneration of Microporous Polymer Networks

Over the past decade a new class of porous materials, named microporous polymer networks (MPNs), was developed. The mainly non-crystalline materials are covalently bond and highly crosslinked organic structures that often show high porosity and intrinsic surface area. Chemical synthesis of MPNs was mainly accomplished by solution polymerization methods as, among others, Suzuki-type,^{2,3} Sonogashira-type,⁴⁻⁷ or Yamamoto-type C-C couplings,⁸⁻¹¹ direct arylation,¹² polyolefinations,¹³ polyhydroxymethylations,¹⁴ cyclotrimerizations,¹⁵⁻¹⁷ and oxidative couplings.¹⁸⁻²⁰ The final products showed application potential in gas storage and separation,²¹⁻²⁵ heterogeneous catalysis,²⁶⁻²⁸ and photoluminescence-based sensing.²⁹ However, MPNs produced by these methods are insoluble and practically intractable powders (or in some cases, monoliths) which cannot be processed into high quality thin films. The availability of thin films, however, is a desired characteristic for several applications e.g. in organic electronics. Some approaches have been proposed for producing thin MPN films, for example, layer-by-layer (LbL) growth,³⁰ surface-initiated synthesis,³¹ and electrochemical oxidative polymerization.³²⁻³⁶ The electrochemical preparation of conducting polymers (CPs) has been studied for the last three decades including mechanism studies,³⁷⁻³⁹ doping, dedoping and overoxidation processes,^{40,41} as well as the resulting physical properties of the films as electronic and ionic conductivity.^{42,43} Regarding synthesis, the influence of various experimental parameters, e.g. polymerization technique, applied potential or current profile, temperature, solvents, additives and supporting electrolytes; on the properties the electrogenerated CPs have also been investigated.⁴⁴ The electropolymerization method allows for simultaneous polymer formation and deposition in short times, under mild and metal- or catalyst-free conditions. Concerning the mechanism of anodic electropolymerization, a cascade of radical coupling reactions which leads to dimers, tetramers, octamers, up to polymers is well accepted. In more detail, radical cations are first formed by oxidation of the monomer at the electrode followed by dimerization and proton elimination from the charged species. Therefore, suitable monomers with low oxidation potential are required, based on e.g. pyrrole,⁴⁵⁻⁴⁷ aniline,⁴⁸ carbazole⁴⁹⁻⁵¹ or thiophene⁵²⁻⁵⁴ as building blocks. An extensive amount of literature is available regarding synthesis and characterization of mainly linear (1D) CPs made from bifunctional monomers with potential applications in, among others,

optoelectronic^{55,56} or electrochromic devices,⁵⁷ sensors,⁵⁸ and electrocatalysis.^{59,60} Very similar synthetic principles are now applied for the electrochemical, oxidative polymerization of multifunctional carbazole- and thiophene-based monomers leading to the formation of thin films of microporous polymer networks.

1.2. Films of Carbazole-Based Microporous Polymer Networks

Electrochemical polymerization of suitable monomers is usually carried out in a three-electrode cell connected to a potentiostat/galvanostat (electrochemical workstation) that allows control over the potential and current applied to the system. This type of cells involves a counter electrode, a reference electrode, and a working electrode (WE) where oxidation of the monomer and film deposition takes place. Noble metals like gold and platinum as well as other conductor or semiconductor materials e.g. glassy carbon and indium tin oxide (ITO) are utilized as WE. Moreover, the cell should contain at least one supporting electrolyte (e.g. tetrabutylammonium salts) in a proper solvent or solvent mixture (acetonitrile, dichloromethane, chloroform) and, of course, the monomer of low oxidation potential (e.g. carbazole- or thiophene-based building blocks). Electrochemical oxidative polymerization of carbazole was initially describe by Ambrose and Nelson in 1968.⁶¹ By applying oxidative potential, cation radicals are generated that undergo coupling to 3,3'-carbazole. The dimers can experience further reactions, e.g. 6,6'-couplings, into extended oligomers.⁶² Scheme 1 shows the chemical structures of carbazole-based, multifunctional monomers that are discussed in this section.



Scheme 1. Chemical structures of discussed multifunctional carbazole-based monomers.

Introduction

Microporous polymer networks (P1) were prepared by Y. Ma and co-workers in the potentiodynamic electropolymerization of monomer 1 in acetonitrile/dichloromethane (2:3) solution.⁶³ Figure 1a shows cyclic voltammograms of the electropolymerization of 1. The progressively increasing current after each additional cycle reflects the growth of the film on the electrode. Under the applied conditions, a well-defined microporous polymer film was achieved that contained only dimeric carbazole bridges (see Figure 1c). A proof of the microporosity of the material was provided by HR-TEM of P1 film, with pore diameters lower than 1 nm (see Figure 1b). P1 films showed smooth morphology with a root-mean-square roughness (RMS) of 1.6 nm. The surface roughness is a critical issue for applying these materials in organic electronics (e.g. in organic light emitting diodes (OLEDs), organic solar cells (OSCs), organic field effect transistors (OFETs), or supercapacitors). P1-based mi-

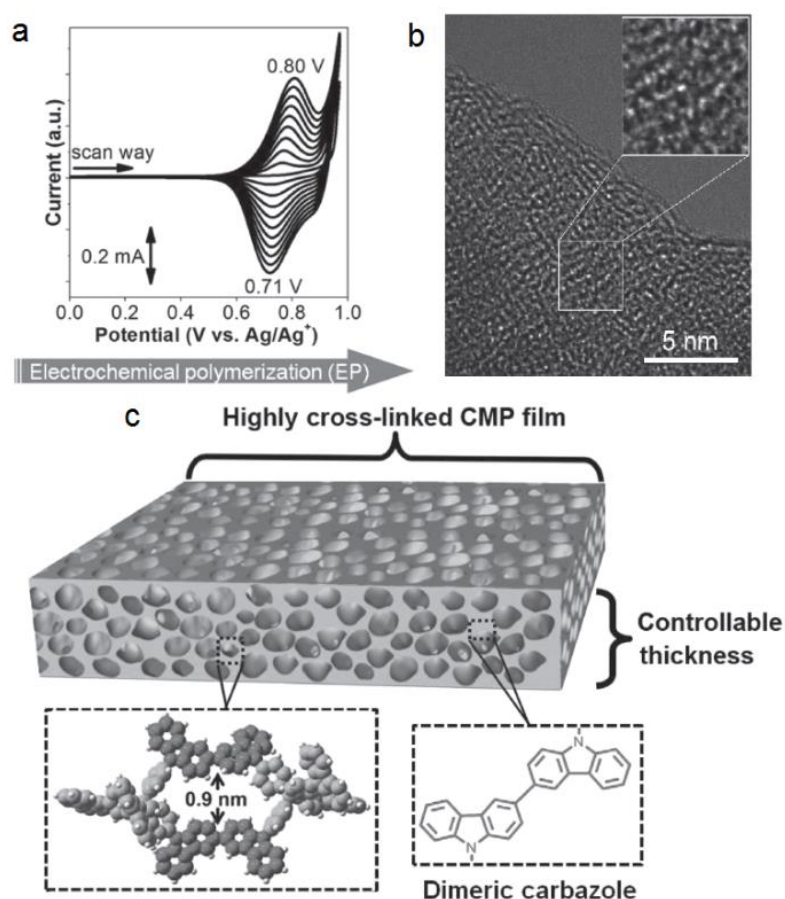


Figure 1. Cyclic voltammograms of electropolymerization of monomer 1 at ITO electrodes by switching the potential between 0 and 0.93 V (0.1 M TBAPF₆ in acetonitrile/dichloromethane (2:3), scan rate of 0.05 Vs⁻¹) (a), HR-TEM image of an electrogenerated P1 film (b), and schematic structure of the microporous P1 film (c). Adapted with permission.⁶³ 2013, WILEY-VCH Verlag.

porous films of different doping level were used as anode interlayer of OLEDs and OSCs in the configuration ITO/PEDOT:PSS (30 nm)/P1 (10 nm)/P-PPV (75 nm)/CsF (1.3 nm)/Al (100 nm), and ITO/PEDOT:PSS (30 nm)/P1 (10 nm)/PCDTBT:PC71BM (90 nm)/LiF (0.5 nm)/Al (100 nm), respectively (see Figure 2). The OLEDs containing the doped P1 interlayers showed a maximum luminous efficiency of 20.7 cd A^{-1} , 37 % higher if compared to OLEDs without anode interlayer. Moreover, optimized OSCs resulted in power-conversion efficiency (PCE) of 7.56 % (V_{OC} of 0.93 V, J_{SC} of 12.44 mAcm^{-2} and FF of 65.7 %) with a strong PCE increase if compared to cells without anode interlayer (PCE of 5.68 %, V_{OC} of 0.91 V, J_{SC} of 10.61 mAcm^{-2} , FF of 58.8 %). These results were explained by an improved electric contact between active layer and microporous polymer film due to their intrinsic high porosity by minimizing the contact resistance, and enhancing the hole-collection capability.

Further optimization of active and cathode interlayers in OSCs with microporous P1 films as hole extracting interlayer led to PCE values of 8.42 %.⁶⁴ Figure 3a shows the architecture utilized in these OSCs: ITO/PEDOT:PSS (30 nm)/P1 (10 nm)/PTB7:PC71BM (100 nm)/LiF or PFN (0.5 nm)/Al (100 nm). The J-V curves display almost similar V_{OC} values (about 0.75 V) and FF (> 60 %) for the OSCs with or without, doped or undoped microporous P1 films (see Figure 3b). However, a distinctly increased J_{SC} value (16.76 mA cm^{-2}) was obtained for OSCs with moderately doped P1 films as anode interlayer. The effect was related to an increased anode work function and electrical conductivity if compared to undoped P1-based interlayers or devices without anode interlayers.

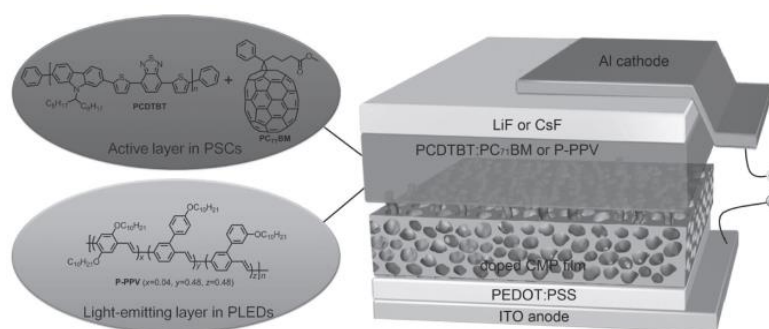


Figure 2. Device structures of OSCs and OLEDs with microporous P1 films as anode interlayers. Adapted with permission.⁶³ 2013, WILEY-VCH Verlag.

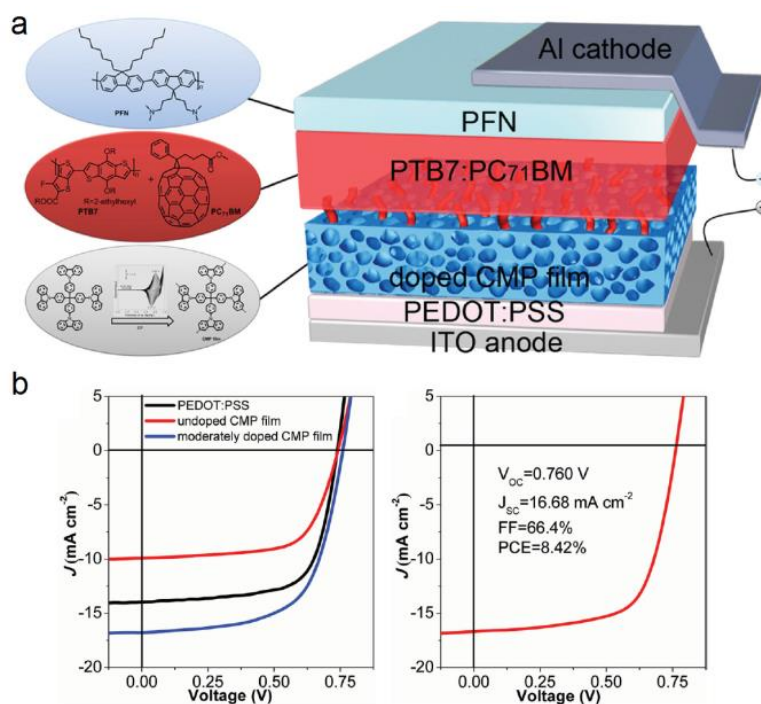


Figure 3. Device structure (a), and current density vs. voltage (J - V) curves under 1000 W m^{-2} AM 1.5G illumination for OSCs with and without microporous P1 films as anode interlayers (b). Adapted with permission.⁶⁴ 2014, WILEY-VCH Verlag.

Jiang and co-workers for the first time reported krypton gas sorption measurements of free-standing MPN films made from monomer 2 (P2).⁶⁵ Nitrogen gas sorption measurements followed by data analysis using the Brunauer-Emmett-Teller (BET) equation is a standard technique for estimating the specific surface area of porous materials.⁶⁶ In the case of electropolymerized MPN films, only small amounts of material (in the milligram range) can be collected. This fact requires the use of gas with low saturation pressure (e.g. Kr, only 2.5 torr compared to 760 torr for N_2 gas). For the measurement, thick films (about $1 \mu\text{m}$) were peeled off from ITO electrodes after potentiostatic polymerization in diluted acetonitrile/water (3:2) solution. A specific BET surface area (S_{BET}) of $1450 \text{ m}^2\text{g}^{-1}$ was calculated for the deposits as a direct proof of the high microporosity of the films. Additionally, thin films of P2 were used in photoluminescence-based chemo- and biosensing experiments with various analytes. Figure 4a and 4b depicts the photoluminescence quenching and enhancement effect when P2 films are exposed to vapors of electron-poor and electron-rich analytes, respectively. The degree of photoluminescence quenching was related to the amount of photoinduced electron transfer from MPN film to the electron-poor analyte. Higher detection sensitivity was observed for analytes with lower LUMO energy levels. Moreover, PL quenching based on the

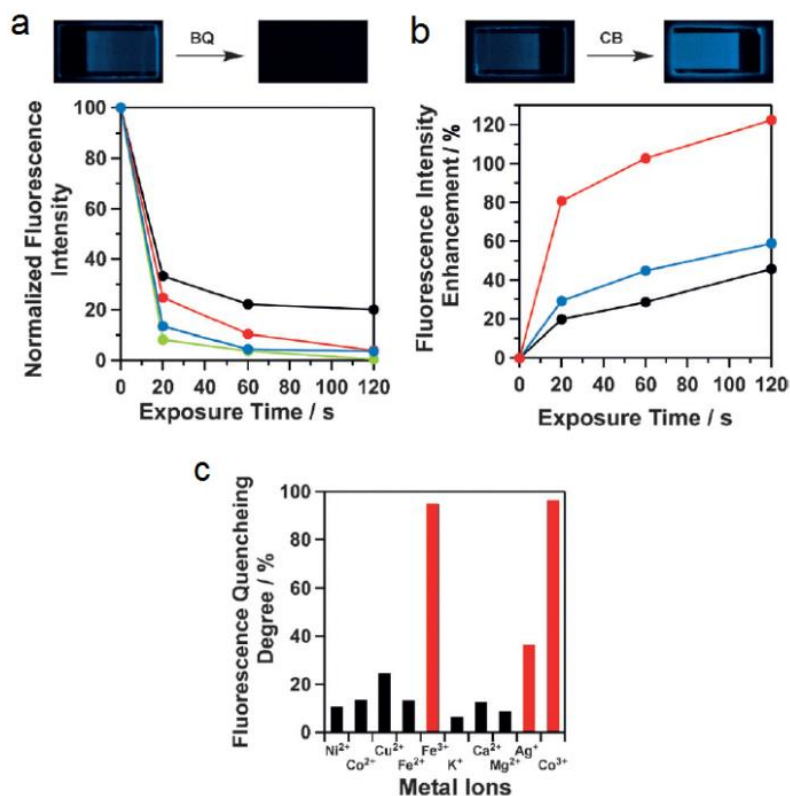


Figure 4. Photoluminescence quenching of P2 films upon exposure to benzonitrile (black line), 1,2-dinitrobenzene (red line), hexafluorobenzene (blue line) and 1,4-benzoquinone (green line, inset: PL quenching images) (a), photoluminescence enhancement of P2 films upon exposure to toluene (black line), benzene (blue line) and chlorobenzene (red line, inset: PL enhancement images) (b), and degree of photoluminescence quenching of P2 films upon treatment with 10^{-4} M aqueous solutions of various metal ions for 1 min (c). Adapted with permission.⁶⁵ 2014, WILEY-VCH Verlag.

oxidation of P2 films were used for sensing of species with a standard reduction potential higher than the oxidation potential of the films such as Fe^{3+} , Ag^+ , Co^{3+} , HClO and dopamine (see Figure 4c). For example, a remarkable PL quenching of 50 % was measured after contacting a P2 film with a 10^{-8} M Fe^{3+} solution for 20 s. The initial photoluminescence of the films were easily recovered by treatment with a NaBH_4 solution.

The use of microporous polymer films in electrochemical supercapacitors has been also explored by Ma and co-workers.⁶⁷ MPN films were produced by potentiodynamic electrochemical oxidative polymerization of a tetracarbazole monomer with a zinc-porphyrin core unit (3) in dichloromethane solution. Cyclic voltammograms of deposits of P3 in monomer-free solution exhibited a reversible redox behavior for a 38 nm-thick film (see Figure 5a). The peak current showed a linear relation with the scan rate, thus indicating the o-

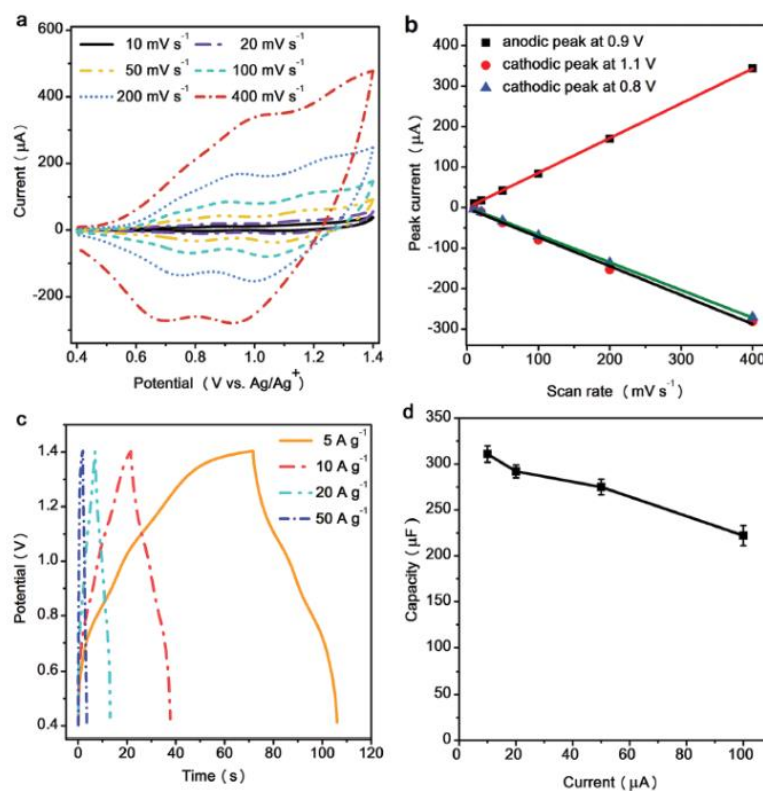


Figure 5. Cyclic voltammograms of P3-films in monomer-free solution at different scan rates (a), relationship between peak currents and scan rates (b), galvanostatic charge/discharge plots at different current densities (c), and capacitance values for different current densities (d). Reproduced with permission.⁶⁷ 2015, WILEY-VCH Verlag.

occurrence of surface-limited redox reactions (see Figure 5b). A maximum capacitance of 142 F g⁻¹ was obtained in galvanostatic charge-discharge tests by applying a current density of 5 A g⁻¹ (see Figure 5c and 5d). These findings were explained by the highly crosslinked and rigid nature of the MPN films thus suppressing volume changes during charging and discharging, and a smooth charge carrier and ion transport between porous film and electrolyte due to an increased number of accessible, electronically active surface sites.

Microporous polymer films (P4) based on monomer 4 have been used as light-harvesting antennae for exciton pumping by Jiang and co-workers.⁶⁸ The thin films of P4 were synthesized on ITO by potentiodynamic electrochemical polymerization in dichloromethane solution. Dedoped films of P4 excited at 350 nm emit brilliant blue light with the photoluminescence (PL) band peaking at 434 nm and a PL quantum yield of 19 % (see Figure 6a). Green coumarin 6 (C6) and Nile red (NR) dyes (see Figure 6b and 6d for PL excitation and emission spectra) were soaked into the micropores of P4 films by immersion with dye solutions. Intrinsic microporosity and high surface area of the films lead to a maximum dye/

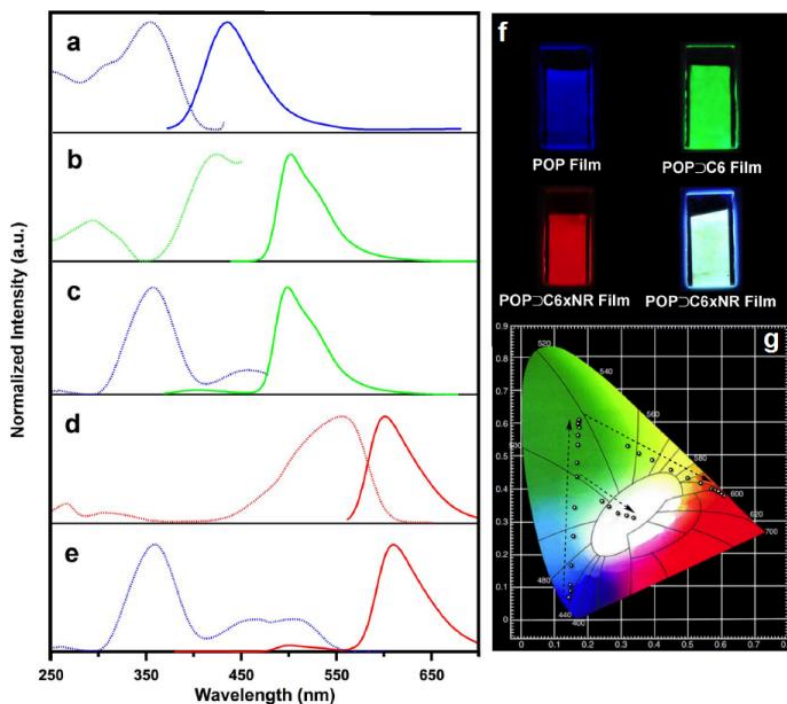


Figure 6. Normalized PL excitation (dotted curves) and emission (solid curves) spectra of P4 films (a), coumarin 6 in DCM (b), P4/C6 films (3.19 mol% C6) (c), Nile red in DCM (d), and P4/C6-NR films (3.19 mol% C6 and 5.41 mol% NR) (e). Photos of dye-infiltrated MPN films showing blue, green, red, and white photoluminescence under UV excitation (g), and Luminescence engineering of thirty dye-infiltrated P4 films with the corresponding Commission Internationale de L'eclairage (CIE) coordinates (h). Adapted with permission.⁶⁸ 2015, Nature Publishing Group.

MPN interfacial area and enable efficient photon harvesting and excitation energy channeling from the P4 films to the dye molecules. Due to the good overlap of emission band of P4 with the respective absorption bands of C6 and NR, an efficient singlet excitation energy transfer is allowed from P4 to C6 (see Figure 6c), and from P4/C6 to NR (see Figure 6e). Hereby, different emission colours were adjusted by tuning the relative concentrations of C6 and NR within the microporous films. Following this line, thirty different emission colours including blue, green, red and white have been realized (see Figure 6f and 6g).

Microporous thin films of P5, made from monomer 5 by Jiang and co-workers, were applied for detection of explosives by PL quenching.⁶⁹ For this, thin microporous polymer films were synthesized containing aggregation-induced emission (AIE)-active tetraphenylethylene building blocks by potentiodynamic electrochemical polymerization in acetonitrile/dichloromethane (1:4). The P5 films emit green light with the PL band peaking at 524 nm (upon excitation at 331 nm). The PL quantum yield for the monomer 5 in solution or

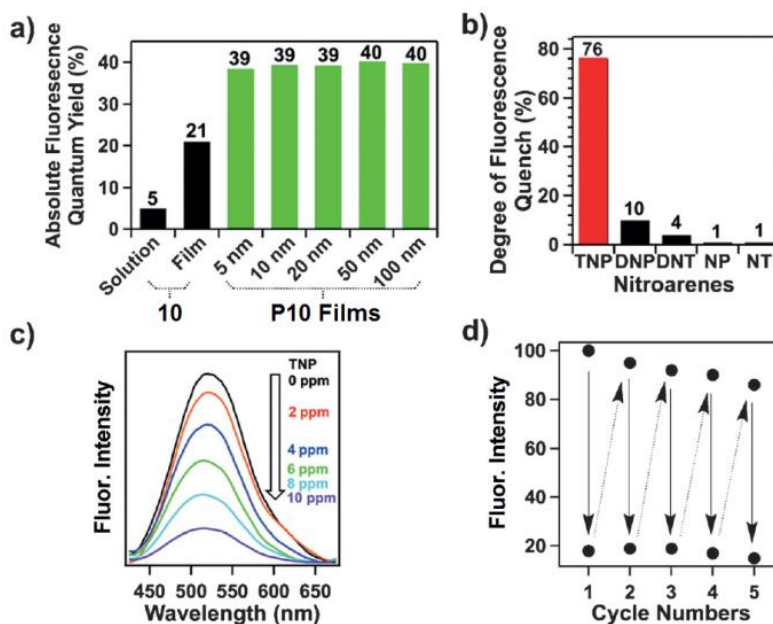


Figure 7. Fluorescence quantum yields of monomer 5 in THF solution or as spin-coated film, and of electrogenerated microporous P5 films of different thicknesses (a), degree of PL quenching of P5 films upon after interaction with various electron-poor nitroarenes in acetonitrile (b), spectral PL changes of a P5 film (thickness of 5 nm) upon immersion in TNP solutions in acetonitrile (1 min) (c), and reversibility of the TNP sensing approach (P5 films, thickness 10 nm) (d). Adapted with permission.⁶⁹ 2015, WILEY-VCH Verlag.

as spin-coated film were estimated to 5 % and 21 %, respectively, thus reflecting the occurrence of the AIE effect.⁷⁰ An almost double quantum yield of ca. 40 % was found for cross-linked films of P5 independent of their thickness of 5 nm – 100 nm (see Figure 7a). Films of P5 were contacted with solutions of different nitroaromatic compounds resulting in a significant PL quenching response for 2,4,6-trinitrophenol (TNP). The high response to TNP was related to the fit of the LUMO energy levels between TNP and P5 with photoinduced electron transfer as driving force for the observed PL quenching (see Figure 7b). The optimum sensitivity towards TNP was observed for very thin P5 films with thickness of 5 nm (see Figure 7c; for the reversibility of the effect see Figure 7d) with 82 % PL quenching for contacting the P10 film for 1 min with a 50 ppm TNP solution.

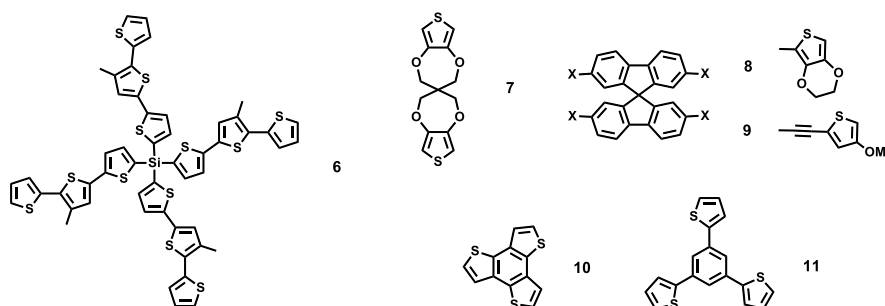
1.3. Films of Thiophene-Based Microporous Polymer Networks

The electrochemical oxidative polymerization of electron-rich heteroaromatic compounds (e.g. pyrroles, thiophenes) follows a mechanism similar to that described for carbazole-based monomers.⁴⁴ After oxidation of the monomer at the anode, the formed cation radicals dimerize at the most reactive positions, and, by consecutive proton elimination, the

aromaticity is restored. The potential required for the oxidation of the monomer is always higher than that needed for oxidation of the oligomeric intermediates (e.g. dimers, tetramers, etc) thus resulting in a simultaneous condensation towards polymeric species. Deposition of the polymer at the working electrode is mainly driven by a reduced solubility of the condensation products.

Recently, Ludwigs and co-workers reviewed synthesis and applications of materials containing the twisted α,β -terthiophene motif including the electrogeneration of microporous polymer films.⁷¹ As another example, Thomas and co-workers produced dithienothiophene-based microporous polymer networks with S_{BET} values of up to $790 \text{ m}^2\text{g}^{-1}$.⁷² Related electrogenerated MPN films on ITO showed interesting electrochromic properties. In an approach reported by Roncali and co-workers,^{73,74} and Thomas and co-workers,⁷ the electrochemical polymerization of multifunctional dithiafulvene-based monomers or the chemical polymerization of tetrathiafulvalene with 1,3,5-triethynylbenzene, respectively, produced microporous polymer networks showing S_{BET} values of up to $434 \text{ m}^2\text{g}^{-1}$ for the chemically synthesized material.

Scheme 2 depicts the chemical structures of the monomers discussed in this section. In 1995 Roncali and co-workers published a preliminary note dealing with the electrochemical, oxidative cross-linking of tetra(terthiophenyl)silane tectons (6).³² Electrodeposition of the corresponding radical cation was carried out by applying the lowest possible oxidation potential of 0.80 V in saturated dichloromethane solution. The absorption spectrum of the resulting electrode deposit shows a long wavelength absorption band centered at 380 nm only slightly red shifted if compared to that of 6 in DCM (373 nm). After successive cycling up to higher potential of 1.4 V, a red shifted absorption peak centered at 460 nm was observed, related to the formation of covalently bond, hexathiophene-bridged polymer networks (see Figure 8).



Scheme 2. Chemical structures of discussed multifunctional thiophene-based monomers.

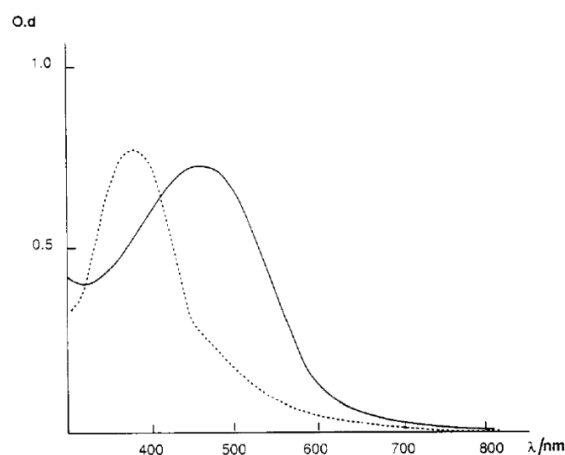


Figure 8. Absorption spectra of electrodeposit of monomeric 6 on ITO (dotted line) and of the relating MPN film (P6) after several cycles in a potential range of 0 V – 1.4 V (solid line). Reproduced with permission.³² 1995, Elsevier B.V.

Reynolds and co-workers reported the electrochemical polymerization of the spiro-type monomer 7.⁷⁵ Synthesis of P7 films was performed by potentiodynamic electropolymerization in acetonitrile/toluene (4:1). The resulting films were insoluble in common organic solvents thus indicating the formation of highly cross-linked materials. Depending on the potential applied the electrochromic P7 films adopt different colours, from red in the neutral to blue in the oxidized state (see Figure 9).

Another comparative study on the electropolymerization of multifunctional thiophene-based monomers with quaterthiophene or spirobifluorene cores (8 and 9) was published by Roncali

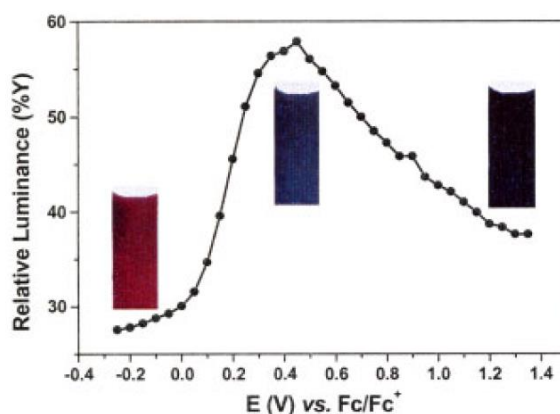


Figure 9. Relative luminance versus applied potential for P7 films. Photographs show the red neutral state, a blue-gray intermediate state, and a dark-blue oxidized state (for a P7 film deposited up to an accumulated charge density of 50 mC cm⁻² on an ITO electrode). Adapted with permission.⁷⁵ 2002, WILEY-VCH Verlag.

and co-workers.⁷⁶ Excitation and fluorescence emission spectra of monomer 9 and a related quaterthiophene-cored monomer are depicted in Figure 10a. A much higher Stokes shift was observed for the quaterthiophene-based monomer if compared to the orthogonally arranged spirobifluorene-based monomer thus reflecting the more rigid structure with only minor geometrical changes between ground and singlet excited state for monomer 9. The different rigidity of both monomers also influence the morphology of the corresponding, electrogenerated polymer networks (see Figure 10b). Scanning electron microscopy images of P8 or P9 films on ITO display a quite compact and homogeneous structure, while electrogenerated films based on the quaterthiophene monomer show a cauliflower-type, rough and inhomogeneous morphology. AFM images show similar results with a low RMS roughness of ca. 1 nm – 4 nm for P8 and P9 films.

Microporous polymer films electrosynthesized from monomers 10 and 11 have been utilized as component of the active layer stacks of bulk-heterojunction-type organic solar cells by Jiang and co-workers.⁷⁷ Thin films of P10 (BTT-CMP) and P11 (TTB-CMP) on ITO were obtained by potentiodynamic electrochemical polymerization from solutions of the corresponding monomers in propylene carbonate (see Figure 11a). The resulting microporous films show S_{BET} values of $> 1000 \text{ m}^2\text{g}^{-1}$ and electrochemical bandgaps of ca. 2 eV (see Figure 11b). The active layer of photovoltaic devices were fabricated by infiltrating P10 and P11 films with PC₆₀BM, simply by soaking a solution of the fullerene derivative into the mi-

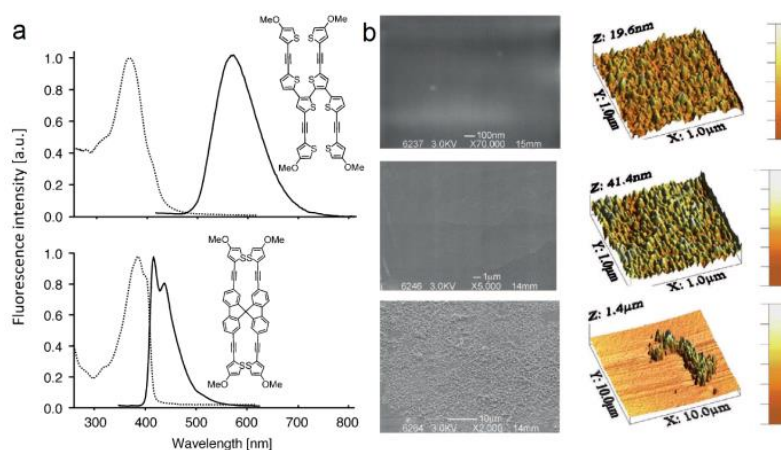


Figure 10. Normalized PL excitation (dotted line) and emission (solid line) spectra of the rigid monomer 9 (bottom) and a semirigid quaterthiophene-cored monomer in DCM (a), and SEM and AFM images of electrogenerated films on ITO (generated under potentiostatic conditions: top: P8, middle: P9, bottom: polymer film made from the quaterthiophene-cored monomer (b). Adapted with permission.⁷⁶ 2014, WILEY-VCH Verlag.

Introduction

ropores of the films thus producing a homogeneously distributed bulk p-n heterojunction morphology. The resulting configuration of the OSCs devices was ITO/PEDOT:PSS/P10 or P11:PC₆₀BM/LiF/Al (see Figure 11c). Optimized P10- and P11-OSCs displayed remarkably high power-conversion efficiencies of 5.02 % (V_{OC} of 0.73 V, J_{SC} of 10.05 mAcm⁻², FF of 68.2 %) and 2.55 % (V_{OC} of 0.86 V, J_{SC} of 4.91 mAcm⁻², FF of 60.5 %), respectively (see Figure 11d). The higher J_{SC} for the P10-based OSC was assigned to a higher hole mobility of P10 film. On the other hand, the higher V_{OC} for the P11-based OSC was attributed to the lower lying HOMO energy level of P11.

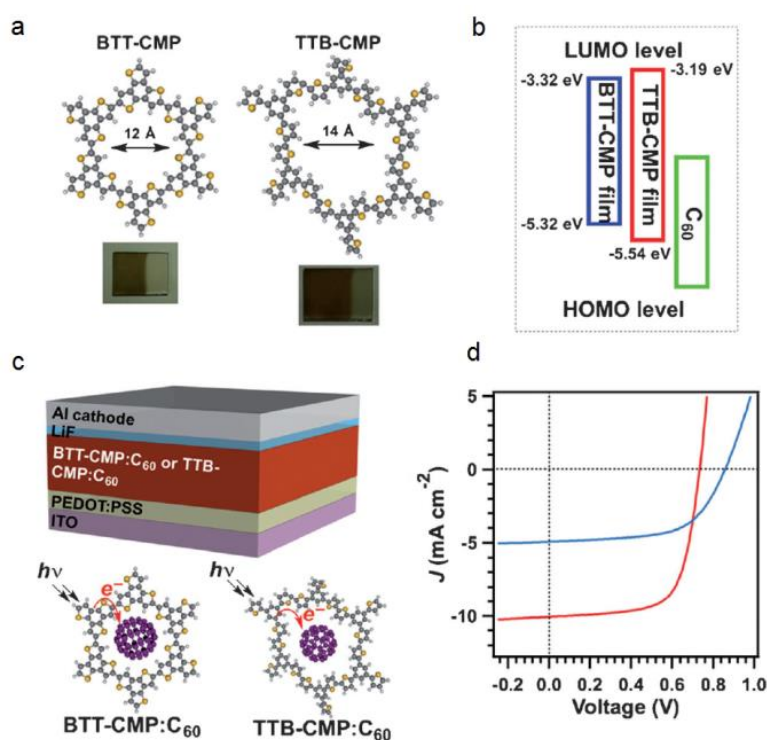


Figure 11. Idealized chemical structures of the pores in P10 and P11 (inset: photographs of the films) (a), HOMO-LUMO energy levels of P10 and P11 films, and of PC₆₀BM (b), OSC device configuration with P10:PC₆₀BM or P11:PC₆₀BM as active layers (c), and J-V curves for OSCs with P10:PC₆₀BM (red curve) or P11:PC₆₀BM (blue line) as active layers (d). Adapted with permission.⁷⁷ 2015, WILEY-VCH Verlag.

1.4. Motivation and Objectives

Electrochemical oxidative polymerization has become a powerful technique to generate thin films of microporous polymer networks (MPNs) with potential applications in the organic electronics field. However, issues as the influence of the chemical structure of the monomers (e.g. type of core, number and size of the linkers) on the properties of the corresponding MPN

films still need to be addressed. The major objectives of this thesis as included in the following chapters are:

- Electrogenation of MPN films from di-, tri- and tetracarbazole-based monomers and their use for electrochemical and chemical detection of nitroaromatic analytes.
- Synthesis of MPN films based on tetra- and octacarbazolyl-substituted tetraphenylmethane or –silane tectons and their application for the high sensitivity electrochemical detection of nitroaromatic compounds.
- Electrodeposition of MPN films from tetrafunctional 2-thienyl- or 3-thienyl-substituted monomers.
- Design of AIE-active, tetraphenylethene-cored, tetra- and octacarbazole- or thiophene-substituted monomers for the electrogeneration of fluorescent MPN films.

1.5. References

- (1) Palma-Cando, A.; Scherf, U. *Macromol. Chem. Phys.* 2016, 217, 827.
- (2) Weber, J.; Thomas, A. *J. Am. Chem. Soc.* 2008, 130, 6334.
- (3) Jiang, M.-Y.; Wang, Q.; Chen, Q.; Hu, X.-M.; Ren, X.-L.; Li, Z.-H.; Han, B.-H. *Polymer* 2013, 54, 2952.
- (4) Jiang, J.-X.; Su, F.; Trewin, A.; Wood, C. D.; Campbell, N. L.; Niu, H.; Dickinson, C.; Ganin, A. Y.; Rosseinsky, M. J.; Khimyak, Y. Z.; Cooper, A. I. *Angew. Chem.* 2007, 119, 8728.
- (5) Jiang, J.-X.; Su, F.; Trewin, A.; Wood, C. D.; Niu, H.; Jones, J. T. A.; Khimyak, Y. Z.; Cooper, A. I. *J. Am. Chem. Soc.* 2008, 130, 7710.
- (6) Zhang, K.; Kopetzki, D.; Seeberger, P. H.; Antonietti, M.; Vilela, F. *Angew. Chem. Int. Ed.* 2013, 52, 1432.
- (7) Bildirir, H.; Paraknowitsch, J. P.; Thomas, A. *Chem. Eur. J.* 2014, 20, 9543.
- (8) Yuan, D.; Lu, W.; Zhao, D.; Zhou, H.-C. *Adv. Mater.* 2011, 23, 3723.
- (9) Schmidt, J.; Werner, M.; Thomas, A. *Macromolecules* 2009, 42, 4426.
- (10) Ben, T.; Ren, H.; Ma, S.; Cao, D.; Lan, J.; Jing, X.; Wang, W.; Xu, J.; Deng, F.; Simmons, J. M.; Qiu, S.; Zhu, G. *Angew. Chem.* 2009, 121, 9621.
- (11) Fischer, S.; Schimanowitz, A.; Dawson, R.; Senkovska, I.; Kaskel, S.; Thomas, A. *J. Mater. Chem. A* 2014, 2, 11825.

- (12) Liu, D.-P.; Chen, Q.; Zhao, Y.-C.; Zhang, L.-M.; Qi, A.-D.; Han, B.-H. *ACS Macro Lett.* 2013, 2, 522.
- (13) Preis, E.; Dong, W.; Brunklaus, G.; Scherf, U. *J. Mater. Chem. C* 2015, 3, 1582.
- (14) Preis, E.; Widling, C.; Scherf, U.; Patil, S.; Brunklaus, G.; Schmidt, J.; Thomas, A. *Polym. Chem.* 2011, 2, 2186.
- (15) Katekomol, P.; Roeser, J.; Bojdys, M.; Weber, J.; Thomas, A. *Chem. Mater.* 2013, 25, 1542.
- (16) Yuan, S.; Dorney, B.; White, D.; Kirklin, S.; Zapol, P.; Yu, L.; Liu, D.-J. *Chem. Commun.* 2010, 46, 4547.
- (17) Preis, E.; Schindler, N.; Adrian, S.; Scherf, U. *ACS Macro Lett.* 2015, 4, 1268.
- (18) Schmidt, J.; Weber, J.; Epping, J. D.; Antonietti, M.; Thomas, A. *Adv. Mater.* 2009, 21, 702.
- (19) Kundu, D. S.; Schmidt, J.; Bleschke, C.; Thomas, A.; Blechert, S. *Angew. Chem. Int. Ed.* 2012, 51, 5456.
- (20) Qiao, S.; Du, Z.; Yang, R. *J. Mater. Chem. A* 2014, 2, 1877.
- (21) Chen, Q.; Liu, D.-P.; Luo, M.; Feng, L.-J.; Zhao, Y.-C.; Han, B.-H. *Small* 2014, 10, 308.
- (22) Chen, Q.; Liu, D.-P.; Zhu, J.-H.; Han, B.-H. *Macromolecules* 2014, 47, 5926.
- (23) Chen, Q.; Luo, M.; Hammershøj, P.; Zhou, D.; Han, Y.; Laursen, B. W.; Yan, C.-G.; Han, B.-H. *J. Am. Chem. Soc.* 2012, 134, 6084.
- (24) Sekizkardes, A. K.; Altarawneh, S.; Kahveci, Z.; İslamoğlu, T.; El-Kaderi, H. M. *Macromolecules* 2014, 47, 8328.
- (25) Sekizkardes, A. K.; Culp, J. T.; Islamoglu, T.; Marti, A.; Hopkinson, D.; Myers, C.; El-Kaderi, H. M.; Nulwala, H. B. *Chem. Commun.* 2015, 51, 13393.
- (26) Zhang, Y.; A, S.; Zou, Y.; Luo, X.; Li, Z.; Xia, H.; Liu, X.; Mu, Y. *J. Mater. Chem. A* 2014, 2, 13422.
- (27) Rose, M. *ChemCatChem* 2014, 6, 1166.
- (28) Bleschke, C.; Schmidt, J.; Kundu, D. S.; Blechert, S.; Thomas, A. *Adv. Synth. Catal.* 2011, 353, 3101.
- (29) Liu, X.; Xu, Y.; Jiang, D. *J. Am. Chem. Soc.* 2012, 134, 8738.
- (30) Kim, M.; Byeon, M.; Bae, J.-S.; Moon, S.-Y.; Yu, G.; Shin, K.; Basarir, F.; Yoon, T.-H.; Park, J.-W. *Macromolecules* 2011, 44, 7092.
- (31) Senkovskyy, V.; Senkovska, I.; Kiriy, A. *ACS Macro Lett.* 2012, 1, 494.

Chapter 1

- (32) Roncali, J.; Thobie-Gautier, C.; Brisset, H.; Favart, J.-F.; Guy, A. *J. Electroanal. Chem.* 1995, 381, 257.
- (33) Tanaka, S.; Kumei, M. *J. Chem. Soc., Chem. Commun.* 1995, 815.
- (34) Zotti, G.; Salmaso, R.; Gallazzi, M. C.; Marin, R. A. *Chem. Mater.* 1997, 9, 791.
- (35) Karpe, S.; Cravino, A.; Frère, P.; Allain, M.; Mabon, G.; Roncali, J. *Adv. Funct. Mater.* 2007, 17, 1163.
- (36) Piron, F.; Leriche, P.; Grosu, I.; Roncali, J. *J. Mater. Chem.* 2010, 20, 10260.
- (37) Diaz, A. F.; Castillo, J. I.; Logan, J. A.; Lee, W.-Y. *J. Electroanal. Chem. Interfacial Electrochem.* 1981, 129, 115.
- (38) Andrieux, C. P.; Audebert, P.; Hapiot, P.; Saveant, J. M. *J. Phys. Chem.* 1991, 95, 10158.
- (39) Heinze, J.; John, H.; Dietrich, M.; Tschuncky, P. *Synth. Met.* 2001, 119, 49.
- (40) Brédas, J. L.; Street, G. B. *Acc. Chem. Res.* 1985, 18, 309.
- (41) Otero, T. F.; Grande, H.-J.; Rodríguez, J. *J. Phys. Chem. B* 1997, 101, 3688.
- (42) Rubinson, J. F.; Kayinamura, Y. P. *Chem. Soc. Rev.* 2009, 38, 3339.
- (43) Suárez, I. J.; Otero, T. F.; Márquez, M. *J. Phys. Chem. B* 2005, 109, 1723.
- (44) Heinze, J.; Frontana-Uribe, B. A.; Ludwigs, S. *Chem. Rev.* 2010, 110, 4724.
- (45) Amemiya, T.; Hashimoto, K.; Fujishima, A.; Itoh, K. *J. Electrochem. Soc.* 1991, 138, 2845.
- (46) Evans, P.; Ratcliffe, N. M.; Smith, J. R.; Campbell, S. A. *J. Mater. Chem.* 1996, 6, 295.
- (47) Almeida, A. K. A.; Dias, J. M. M.; Silva, A. J. C.; Santos, D. P.; Navarro, M.; Tonholo, J.; Goulart, M. O. F.; Ribeiro, A. S. *Electrochim. Acta* 2014, 122, 50.
- (48) Watanabe, A.; Mori, K.; Iwabuchi, A.; Iwasaki, Y.; Nakamura, Y.; Ito, O. *Macromolecules* 1989, 22, 3521.
- (49) Fulghum, T.; Karim, S. M. A.; Baba, A.; Taranekar, P.; Nakai, T.; Masuda, T.; Advincula, R. C. *Macromolecules* 2006, 39, 1467.
- (50) Skompska, M.; Chmielewski, M. J.; Tarajko, A. *Electrochem. Commun.* 2007, 9, 540.
- (51) Tarajko, A.; Cybulski, H.; Chmielewski, M. J.; Bukowska, J.; Skompska, M. *Electrochim. Acta* 2009, 54, 4743.
- (52) Wei, Y.; Chan, C. C.; Tian, J.; Jang, G. W.; Hsueh, K. F. *Chem. Mater.* 1991, 3, 888.
- (53) Lee, H. J.; Lee, J.; Park, S.-M. *J. Phys. Chem. B* 2010, 114, 2660.
- (54) Palma-Cando, A. U.; Frontana-Uribe, B. A.; Maldonado, J. L.; Hernández, M. R. *Procedia Chem.* 2014, 12, 92.

Introduction

- (55) Cravino, A.; Zerza, G.; Neugebauer, H.; Maggini, M.; Bucella, S.; Menna, E.; Svensson, M.; Andersson, M. R.; Brabec, C. J.; Sariciftci, N. S. *J. Phys. Chem. B* 2002, *106*, 70.
- (56) Gurunathan, K.; Murugan, A. V.; Marimuthu, R.; Mulik, U. P.; Amalnerkar, D. P. *Mater. Chem. Phys.* 1999, *61*, 173.
- (57) Argun, A. A.; Aubert, P.-H.; Thompson, B. C.; Schwendeman, I.; Gaupp, C. L.; Hwang, J.; Pinto, N. J.; Tanner, D. B.; MacDiarmid, A. G.; Reynolds, J. R. *Chem. Mater.* 2004, *16*, 4401.
- (58) McQuade, D. T.; Pullen, A. E.; Swager, T. M. *Chem. Rev.* 2000, *100*, 2537.
- (59) Deronzier, A.; Moutet, J.-C. *Coord. Chem. Rev.* 1996, *147*, 339.
- (60) Malinauskas, A. *Synth. Met.* 1999, *107*, 75.
- (61) Ambrose, J. F.; Nelson, R. F. *J. Electrochem. Soc.* 1968, *115*, 1159.
- (62) Koyuncu, S.; Gultekin, B.; Zafer, C.; Bilgili, H.; Can, M.; Demic, S.; Kaya, İ.; Icli, S. *Electrochim. Acta* 2009, *54*, 5694.
- (63) Gu, C.; Chen, Y.; Zhang, Z.; Xue, S.; Sun, S.; Zhang, K.; Zhong, C.; Zhang, H.; Pan, Y.; Lv, Y.; Yang, Y.; Li, F.; Zhang, S.; Huang, F.; Ma, Y. *Adv. Mater.* 2013, *25*, 3443.
- (64) Gu, C.; Chen, Y.; Zhang, Z.; Xue, S.; Sun, S.; Zhong, C.; Zhang, H.; Lv, Y.; Li, F.; Huang, F.; Ma, Y. *Adv. Energy Mater.* 2014, *4*, 1301771.
- (65) Gu, C.; Huang, N.; Gao, J.; Xu, F.; Xu, Y.; Jiang, D. *Angew. Chem. Int. Ed.* 2014, *53*, 4850.
- (66) Sing, K. S. W. *Pure Appl. Chem.* 1985, *57*, 603.
- (67) Zhang, H.; Zhang, Y.; Gu, C.; Ma, Y. *Adv. Energy Mater.* 2015, *5*, 1402175.
- (68) Gu, C.; Huang, N.; Xu, F.; Gao, J.; Jiang, D. *Sci. Rep.* 2015, *5*, 8867.
- (69) Gu, C.; Huang, N.; Wu, Y.; Xu, H.; Jiang, D. *Angew. Chem. Int. Ed.* 2015, *54*, 11540.
- (70) Dong, W.; Fei, T.; Palma-Cando, A.; Scherf, U. *Polym. Chem.* 2014, *5*, 4048.
- (71) Scheuble, M.; Goll, M.; Ludwigs, S. *Macromol. Rapid Commun.* 2015, *36*, 115.
- (72) Bildirir, H.; Osken, I.; Ozturk, T.; Thomas, A. *Chem. Eur. J.* 2015, *21*, 9306
- (73) Cocherel, N.; Leriche, P.; Ripaud, E.; Gallego-Planas, N.; Frere, P.; Roncali, J. *New J. Chem.* 2009, *33*, 801.
- (74) Ripaud, E.; Leriche, P.; Cocherel, N.; Cauchy, T.; Frere, P.; Roncali, J. *Org. Biomol. Chem.* 2011, *9*, 1034.
- (75) Reeves, B. D.; Thompson, B. C.; Abboud, K. A.; Smart, B. E.; Reynolds, J. R. *Adv. Mater.* 2002, *14*, 717.
- (76) Yassin, A.; Mallet, R.; Leriche, P.; Roncali, J. *ChemElectroChem* 2014, *1*, 1219.

(77) Gu, C.; Huang, N.; Chen, Y.; Qin, L.; Xu, H.; Zhang, S.; Li, F.; Ma, Y.; Jiang, D. *Angew. Chem.* 2015, *127*, 13798.

Chapter 2

Electrogenerated Microporous Polymer Networks from Di-, Tri- and Tetracarbazole-Based Monomers^{1,2}

Thin films of microporous polymer networks (MPN) were generated by electrochemical polymerization of a series of multifunctional carbazole-based monomers. The microporous films show high Brunauer-Emmett-Teller (BET) surface areas up to 1300 m²g⁻¹ as directly measured by krypton sorption experiments. A correlation between the number of polymerizable carbazole units of the monomer and the resulting surface area is observed. Electrochemical sensing experiments with 1,3,5-trinitrobenzene as prototypical nitroaromatic analyte demonstrate an up to 180 times increased current response of MPN-modified glassy carbon electrodes in relation to the nonmodified electrode. The phenomenon probably involves intermolecular interactions between the electron-poor nitroaromatic analytes and the electron-rich, high surface area microporous deposits, with the electrochemical reduction at the MPN-modified electrodes being an adsorption-controlled process for low scan rates. Finally, thin films of poly-2,2',7,7'-tetra(carbazol-9-yl)-9,9'-spirobifluorene were used for the gas-phase detection of 2,4,6-trinitrotoluene (TNT) with high sensitivity (up to 5 ppb).

2.1. Introduction

Microporous polymer networks (MPN) have been often related to potential applications for gas capture^{3,4} and separation,^{5,6} catalysis,⁷⁻⁹ organic electronic devices,^{10,11} and solid state sensors.¹² For the latter two applications, the availability of high quality films is required.¹³ The chemical methods, which are commonly used for MPN generation, usually produce powdery and practically intractable samples.^{14,15} The possibility of an electrochemical generation of carbazole-based MPN films has been recently demonstrated.^{16,17} The resulting electrochemically generated MPN films have been used as electrode interlayers of organic electronics devices such as organic light emitting diodes and organic solar cells or as electrode material of supercapacitors.¹⁸ A direct proof for the microporosity and high surface area of such films has been first presented in a recent publication by Jiang and co-workers¹⁹ in krypton gas sorption measurements followed by data analysis based on the Brunauer-Emmett-Teller (BET) equation. On the other hand, films of carbazole-based polymers have been used as sensors for nitroaromatic compounds (NACs) via fluorescence quenching²⁰ or electrochemical reduction.²¹ The latter principle is based on the quantification of the cathodic

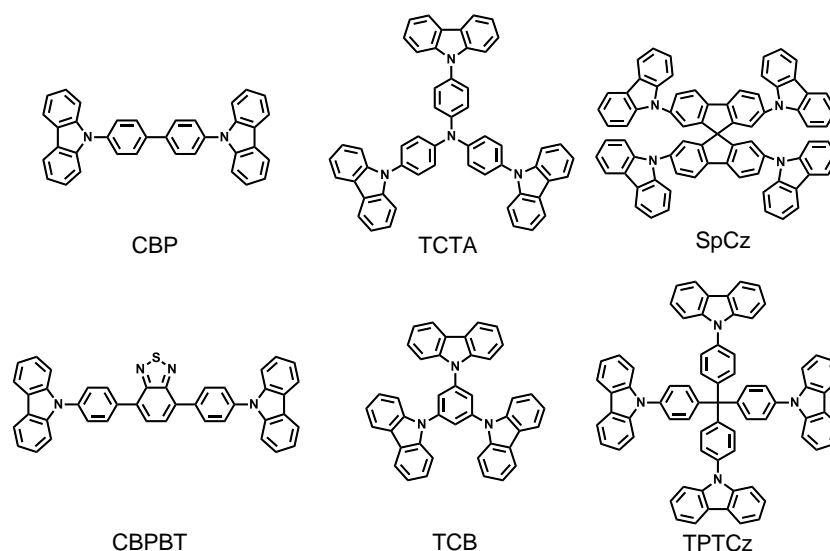
current which is produced during reduction of the nitroaromatic analytes. Zhang and co-workers used films of electropolymerized, carbazole-based monomers for the electrochemical detection of NACs. However, their monomers contain flexible alkylene linkers and should not form microporous networks. Therefore, the novelty of this approach is to combine permanent microporosity of electrochemically deposited films with the electrochemical detection of nitroaromatic analytes.

In this chapter, MPN films were electrochemically generated starting from a series of multifunctional carbazole-based monomers. Direct porosity measurements of the resulting films were calculated by the krypton sorption method. The extracted BET surface area data are compared to the S_{BET} values of corresponding, chemically synthesized bulk MPNs which were obtained as powders. Increased functionality of the multifunctional carbazole-based monomers causes increased BET surface areas, most probably due to an increased rigidity of the networks. Moreover, glassy carbon (GC) electrodes modified with MPN films have been used for the electrochemical sensing of the prototypical nitroaromatic analyte 1,3,5-trinitrobenzene (TNB). Here, a correlation between surface area of the MPN films and the cathodic current response to TNB is observed. The results demonstrate that modification of GC electrodes with microporous polymer coatings can boost the sensitivity to NAC by more than 2 orders of magnitude most probably driven by intermolecular electronic interactions between the electron-poor nitroaromatic analytes and the electron-rich MPN surface. The process is characterized as an adsorption-controlled phenomenon involving an adsorbate layer of the NAC for low scan rates. With increasing scan rate the process becomes diffusion-controlled, since the transport of the analyte molecules is now the limiting process. Finally, the gas-phase detection of nitroaromatic analytes was also explored by using thin MPN films on ITO. The devices show high sensitivity up to ppb concentrations for 2,4,6-trinitrotolunene (TNT) as analyte.

2.2. Results and Discussions

2.2.1. Synthesis of the Series of Monomers

The six carbazole-based monomers were purchased from commercial suppliers or synthesized by us (see Experimental Section for details). Monomers with two, three, and four carbazole substituents have been used: 4,4'-di(carbazol-9-yl)-1,1'-biphenyl (CBP), 4,7-di[4-(carbazol-9-yl)phenyl]benzo[c]-[1,2,5]thiadiazole (CBPBT), tri[4-(carbazol-9-yl)phenyl]amine (TCTA),



Scheme 1. Chemical structures of the investigated carbazole-based monomers.

1,3,5-tri(carbazol-9-yl)benzene (TCB), 2,2',7,7'-tetra(carbazol-9-yl)-9,9'-spirobifluorene (SpCz) and tetra[4-(carbazol-9-yl)phenyl]methane (TPTCz) (Scheme 1).

2.2.2. Electrochemical Characterization of the Monomers and Polymers at Pt Disc Electrodes

Electropolymerization of thiophene^{22,23}, pyrrole²⁴ and carbazole^{25,26} based monomers has been extensively studied due to the interesting properties of the resulting conducting polymer (CP) films, e.g. their electrochromic behavior.²⁷⁻²⁹ Electrochemical oxidative coupling of carbazole was first described by Ambrose and Nelson.³⁰ Applying oxidative potentials, cation radicals are initially generated. Their dimerization and deprotonation lead to the formation of 3,3'-carbazole dimers. The initially formed dimers can undergo further oxidative coupling reactions. Until now the majority of research into CPs has been focused on the synthesis of linear polymers. However, three-dimensional networks have been also proposed as attractive targets for applications in organic electronics devices and sensors.³¹ For obtaining carbazole-based networks with permanent microporosity, the use of monomers (tectons) with multiple carbazole functions that are arranged around a rigid core unit should be favored.

After initial characterization of the electrochemical behavior of the monomers by cyclic voltammetry, polymer formation was carried out by potentiodynamic electrochemical polymerization of 0.5 mM solution of the monomers in acetonitrile/dichloromethane (1:4) by using tetrabutylammonium perchlorate (0.1 M TBAP) as supporting electrolyte. A three-

electrode cell was used with a platinum disc electrode (1 mm diameter) as working electrode (WE), a platinum wire as counter electrode (CE) and $\text{Ag}^\circ/\text{AgNO}_3$ (0.1 M AgNO_3 , 0.60 V vs NHE) as reference electrode (RE). Finally, the deposited polymer films have been again characterized by cyclic voltammetry. Figure 1 depicts the first oxidation scan for all six monomers. CBPBT, CBP and SpCz show a first monomer oxidation peak around 0.97 V. The peak current ratio of ca. 2.1 between the tetra-substituted SpCz and the di-substituted CBP reflects the doubled amount of oxidizable carbazole moieties of SpCz with respect to CBP. A similar ratio is observed for the TPTCz/CBP couple. The low peak current for CBPBT is most probably caused by the low solubility of this monomer; a concentration of 0.5 mM could not be reached in the solvent mixture. For the triphenylamine-cored monomer TCTA, two oxidation peaks at lower potential (0.62 V and 0.77 V) are observed during the first cyclovoltammetric scan. This is probably due to the formation of cation radicals and dication of the 1,4-*N*-substituted phenylene units.³² The observed shoulder at 1.05 V should correspond to the “regular” carbazole dimerization that is observed for the other five monomers within the potential range of 0.93 V – 1.05 V. Therefore, during subsequent cycling, more complicated voltammograms are observed for TCTA monomer if compared to the well-defined voltammograms that are recorded for the other monomers (see Figure 2). For the other five monomers, starting from the second cycle, a couple of reversible oxidation/reduction peaks is formed in the potential range of 0.5 V – 1.0 V reflecting two electron transfer steps during charging/discharging. Repeated sweeps lead to a progressively increasing peak current, thus reflecting the gradual growth of the MPN films on the electrode

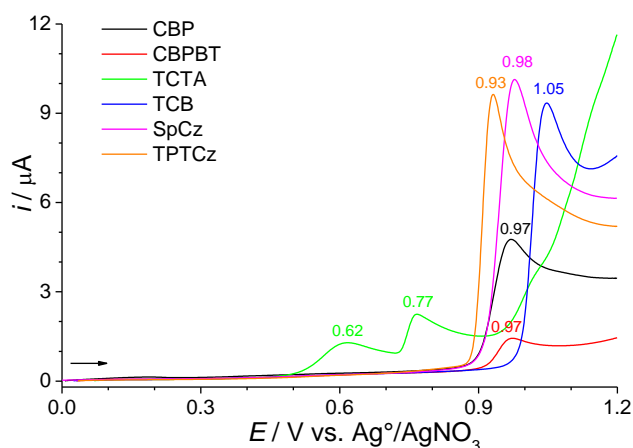


Figure 1. First anodic scan voltammograms for 0.5 mM solutions of the monomers and 0.1 M tetrabutylammonium perchlorate in acetonitrile/dichloromethane (1:4) at a Pt disc electrode. The voltammograms were recorded from 0 V to 1.2 V with a scan rate of 0.10 Vs^{-1} .

Electrogenerated MPNs from Di-, Tri- and Tetracarbazole-Based Monomers

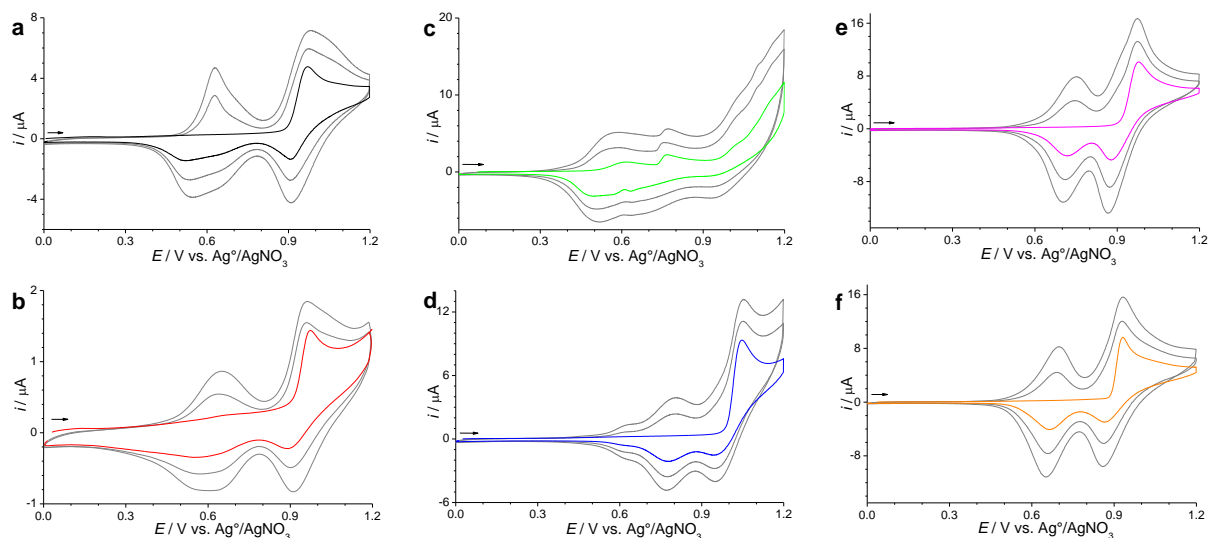


Figure 2. Three successive cyclic voltammograms at Pt disc electrodes for 0.5 mM solutions of the monomers: CBP (a), CBPBT (b), TCTA (c), TCB (d), SpCz (e), and TPTCz (f) and 0.1 M TBAP in acetonitrile/dichloromethane (1:4). Cyclic voltammograms were recorded from 0 V to 1.2 V with a scan rate of 0.10 Vs^{-1} .

(see Figure 3a for TPTCz). The thickness of the MPN films can be precisely controlled by the cycle number. Cyclic voltammograms for PTPTCz deposit on Pt, in monomer-free solution at different scan rates between 0.005 and 0.20 Vs^{-1} are depicted in Figure 3b. The observed linear relationship between peak current and scan rate is characteristic for the formation of an electroactive polymer deposit on the electrode.²²

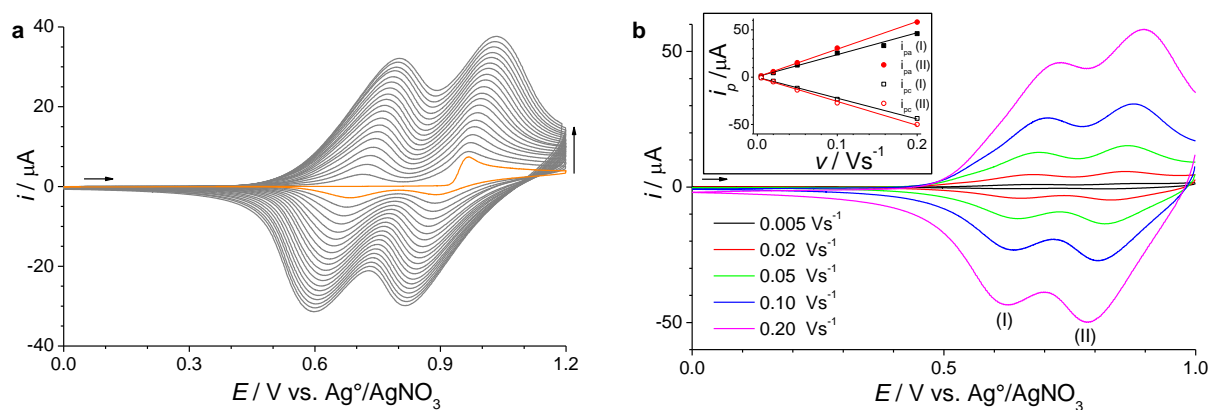


Figure 3. Twenty consecutive cyclic voltammograms at Pt disc electrodes for 0.5 mM TPTCz in acetonitrile/dichloromethane (1:4) mixtures and 0.1 M TBAP as supporting electrolyte potential range: 0 V – 1.2 V, scan rate: 0.10 Vs^{-1} (a). Cyclic voltammograms for an as-prepared PTPTCz film on Pt, in monomer-free acetonitrile solution containing 0.1 M TBAP at scan rates of 0.005 Vs^{-1} – 0.20 Vs^{-1} (b). The inset shows the linear dependence of peak current and scan rate.

2.2.3. Porosity Characterization of Bulk Polymers and MPN Films

Nitrogen gas sorption measurements followed by data analysis using the BET equation belong to the standard techniques for estimating the specific surface area of microporous materials.^{33,34} However, this method is not applicable for the precise characterization of materials with very low surface areas or for very small amounts of microporous materials. A way to overcome this problem is to use krypton gas which has a low saturation pressure of 2.5 torr at 77 K.¹⁹

For Kr sorption measurements, prolonged potentiostatic electrochemical polymerization of the monomers on ITO allows for the generation of free-standing (TCB, SpCz and TPTCz) or easily removable (CBP, CBPBT and TCTA) films due to a reduced adhesion between the ITO electrode and thicker deposits. The MPN films were discharged (dedoped) by applying a potential of 0 V, rinsed with acetonitrile and dichloromethane, removed from the electrode and dried. The film generation was repeated until collection of ca. 2 mg of material. For comparison, all monomers were also chemically coupled into bulk MPN powders by oxidative polymerization with iron(III) chloride. The resulting insoluble powders were purified by washing with aqueous concentrated hydrochloric acid, methanol, THF, ethanol and supercritical CO₂, and dried. In the gas sorption measurements, the isotherms show a fast N₂ uptake at low relative pressure (0 – 0.1), a behavior that is characteristic of permanently microporous materials. The isotherms also display a combination of type I and II behavior (Figure 4).³³ All S_{BET} values are listed in Table 1. The surface area values of films and bulk samples using Kr or N₂ gas, respectively, show similar trends within the P/P₀ range of 0 – 0.6 (Figure 5). Similar S_{BET} values are observed especially for the two tetra-substituted monomers. Very interestingly, a direct relationship between the number of carbazole units of the monomer and the BET surface area of the films is observed. This can be explained by an increased rigidity of the MPNs with increasing cross-linking density, thus leading to an increased permanent microporosity. An unexpectedly low S_{BET} value is observed only for PTCTA. The electrochemical polymerization of monomer TCTA seems problematic due to the presence of the easily oxidizable 1,4-*N*-substituted phenylene units (see Figure 1) thus causing side reactions and a drastically reduced microporosity of PTCTA. The products made from the bi- and trifunctional monomers CBP, CBPBT and TCB all show S_{BET} values of thin films that are ca. 50% of the values of the corresponding chemically (FeCl₃) synthesized bulk

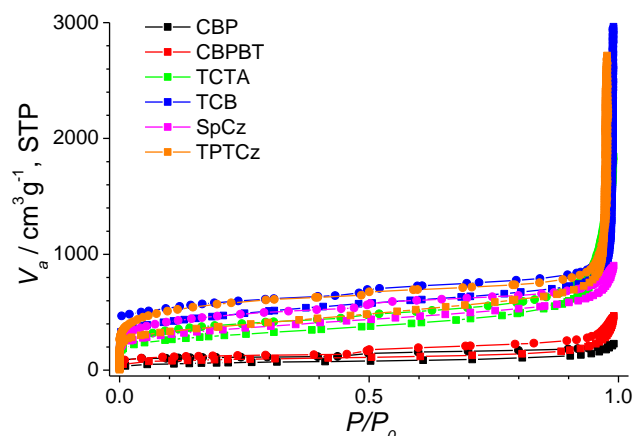


Figure 4. Nitrogen gas sorption isotherms of the chemically synthesized (oxidative coupling with FeCl_3) bulk polymers.

polymers, most probably caused by a reduced cross-linking density during electropolymerization with a preference for the formation of carbazole dimers. Please note that the formation of insoluble MPN films already for the bifunctional monomers CBP and CBPBT shows that dimerization is not the only electrochemical process, a certain amount of further couplings of the initially formed dimers occurs. Chemical polymerization with FeCl_3 may lead to higher crosslinking densities. For the tetrafunctional monomers SpCz and TPTCz the crosslinking density that is obtained by electropolymerization seems high enough to create highly microporous films with BET surface areas in the range of those of the bulk materials, simply as a result of the high functionality of the monomers.

Table 1. Calculated BET surface areas of electropolymerized films and chemically synthesized bulk MPNs, using Kr or N_2 gas, respectively. All S_{BET} film measurements were carried out at least twice.

Polymer	Number of carbazole units in the monomer	S_{BET} Film [m^2g^{-1}]	S_{BET} Bulk [m^2g^{-1}]
PCBP	2	104	225
PCBPBT	2	159	324
PTCTA	3	236	1065
PTCB	3	748	1647
P _{Sp} Cz	4	1297	1249
PTPTCz	4	1106	1322

2.2.4. Electrochemical Reduction of 1,3,5-Trinitrobenzene at MPN-Modified Glassy Carbon Electrodes

Different meso- and macroporous materials have been used in modified electrodes for the electrochemical detection of nitroaromatic compounds³⁵⁻³⁷ driven by the high surface areas of the porous materials as well as molecular interactions between the modified electrodes and the nitroaromatic analytes. To the best of our knowledge, until now MPN films have not been tested in the electrochemical detection of nitroaromatic analytes. Electrochemical studies on the reduction of nitroaromatic compounds in aqueous medium at $\text{pH} < 9.6$ documented the successive formation of nitroso and hydroxylamine functions.³⁸ Four electrons are transferred in the reduction of a nitro to a hydroxylamine group visible as a single reduction wave.

In these experiments, potentiostatic electrochemical polymerization of the carbazole-based monomers on glassy carbon (GC) electrodes was carried out as first step. The MPN films were produced by applying a potential of 1.1 V until an oxidative charge density of 25.5 mC cm^{-2} was accumulated followed by electrochemically discharging (dedoping) at 0 V for 60 s. So, MPN films with a comparable amount of electroactive groups are deposited on the GC electrodes for all monomers. Figure 6 shows tapping mode AFM images of films deposited on ITO using same conditions as for deposits in GC electrodes. MPN films show a similar granular morphology (a so-called cauliflower morphology) with comparable average surface roughness (118 nm to 193 nm) and thickness (748 nm to 870 nm, obtained with a profilometer), except for the thinner PTCB film (111 nm) which shows delamination from the ITO electrodes already for the thin film (see Table 2). Thin films show a rather smooth sur-

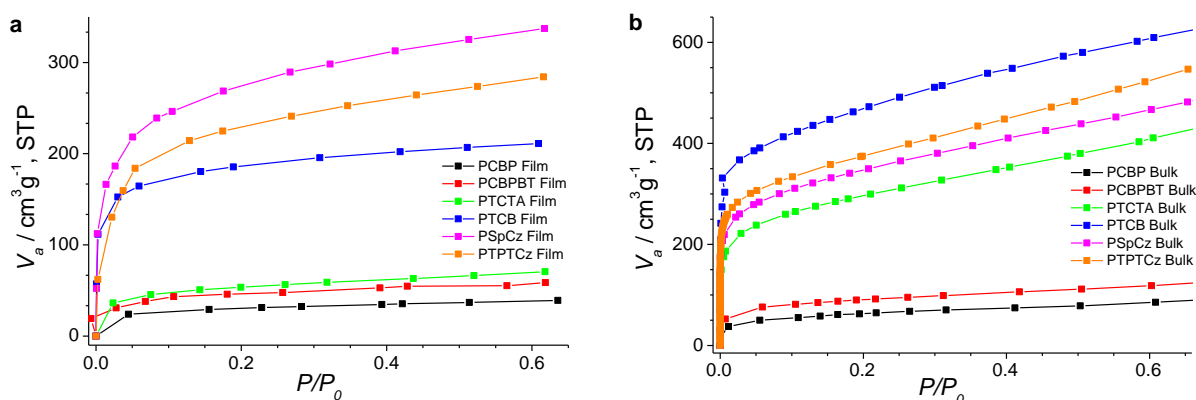


Figure 5. Adsorption isotherms of electropolymerized MPN films (a) and the corresponding bulk polymers made by oxidative coupling with FeCl_3 (b), using Kr or N_2 gas, respectively.

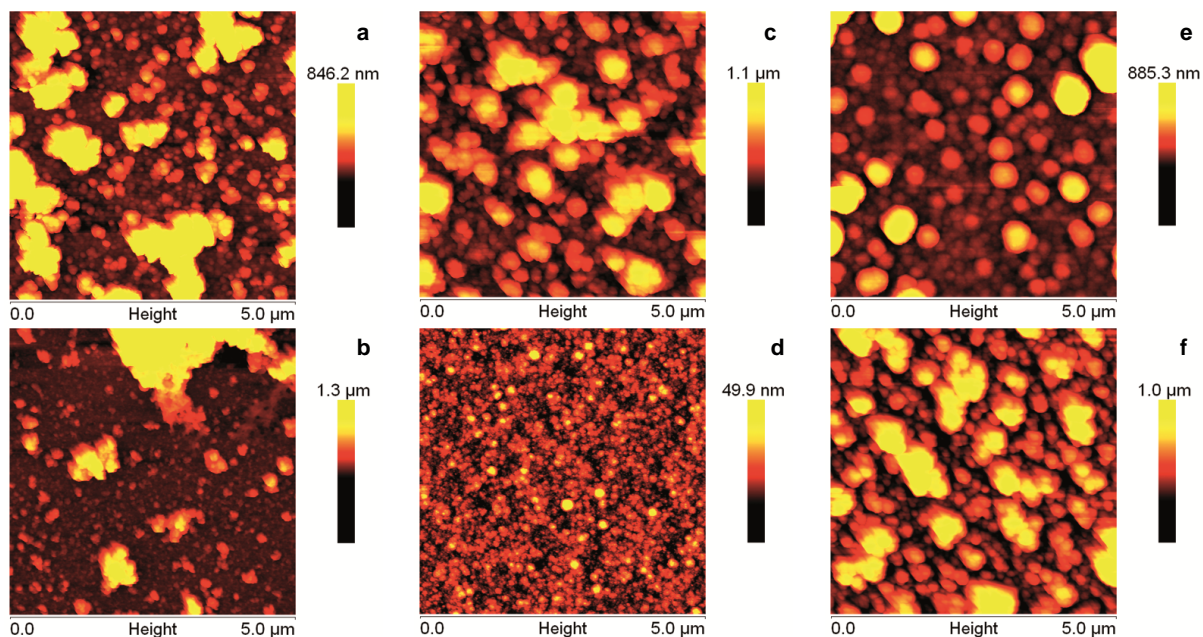


Figure 6. Tapping mode AFM images of MPN films on ITO of PCBP (a), PCBPBT (b), PTCTA (c), PTCB (d), PSpCz (e) and PTPTCz (f).

face (see the average roughness of only 5 nm for the 111 nm PTCB film). MPN-modified GC were introduced as working electrodes into a three-electrode cell with $\text{Ag}^\circ/\text{AgCl}(\text{sat.})$ (NaCl 3 M, 0.21 V vs NHE) as aqueous reference electrode, then used for sensing 1,3,5-trinitrobenzene (TNB) as a prototypical nitroaromatic analyte in aqueous solution containing 0.2 M KCl and 0.1 M PBS (pH 7.4).

Linear scan voltammograms (LSVs) of a $0.5 \mu\text{M}$ aqueous TNB solutions at MPN-modified and non-modified GC electrodes are shown in Figures 7, after background correction by subtraction of the reference voltammogram that was recorded in absence of TNB. Three cathodic peaks for the reduction of the three nitro-substituents of TNB are observed in the

Table 2. Average surface roughness (R_q) and thicknesses of MPN films deposited on ITO.

Polymer	R_q (nm)	Thickness (nm)
PCBP	164	806
PCBPBT	166	859
PTCTA	193	748
PTCB ^a	5	111
PSpCz	118	870
PTPTCz	184	823

^a Delamination already for thin films

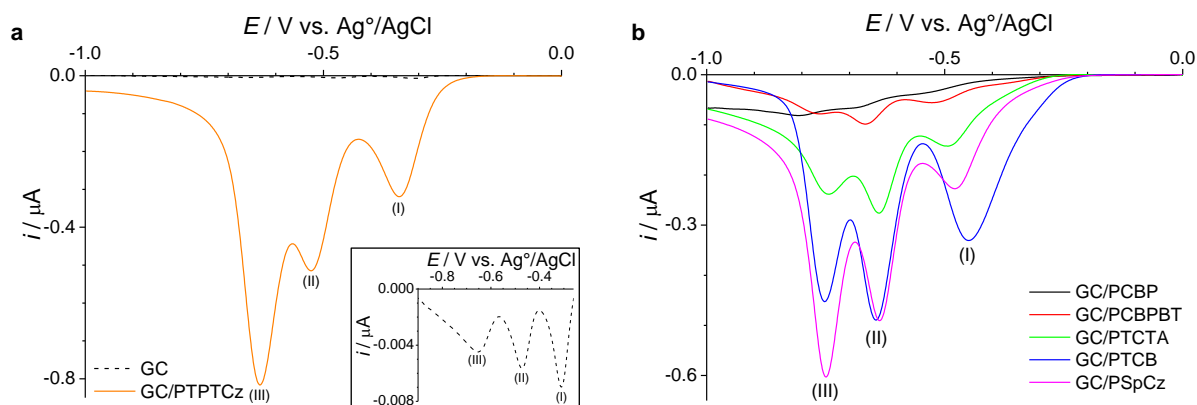


Figure 7. Linear scan voltammograms (after background correction) of 0.5 μM TNB in aqueous 0.2 M KCl and 0.1 M PBS (pH 7.4) solutions at nonmodified (inset) and PTPTCz-modified GC electrodes (a), and at PCBP-, PCBPBT-, PTCTA-, PTCB-, and SpCz-modified GC electrodes (b). The scan rate was 0.01 Vs^{-1} .

voltammograms in the potential range from -0.31 V to -0.81 V. For the nonmodified GC electrode, the peaks are observed at -0.31 (I), -0.47 (II) and -0.65 V (III) (see inset of Figure 7a, similar to reported values³⁹). The modified GC electrodes show slight shifts of the cathodic potentials dependent on the structure of the monomers used for MPN generation. Interestingly, a dramatic enhancement of the current response is observed for the MPN-modified GC electrodes; 17 to 182 times higher as the response for the nonmodified electrode (see Table 3). The electrochemical response nicely correlates with the BET surface area of the MPNs (shown for the intensity of the third cathodic peak in Figure 8a). The observed effect may be driven by intermolecular interactions between the high surface of the electron-rich

Table 3. Current response (after background correction) for the three cathodic reduction peaks of the three aromatic nitro groups in the electrochemical detection of 0.5 μM TNB in aqueous 0.2 M KCl and 0.1 M PBS solutions at nonmodified and MPN-modified GC electrodes. The current ratios of the third peak between MPN-modified and nonmodified GC electrodes are also listed.

Electrode	i_p (I) (μA)	i_p (II) (μA)	i_p (III) (μA)	$i_p/i_{p\text{GC}}(\text{III})$
GC	0.007	0.006	0.004	1
GC/PCBP	0.040	0.071	0.081	18
GC/PCBPBT	0.056	0.098	0.078	17
GC/PTCTA	0.142	0.276	0.238	53
GC/PTCB	0.331	0.489	0.453	101
GC/PTPTCz	0.319	0.515	0.816	182
GC/PSpCz	0.227	0.491	0.603	135

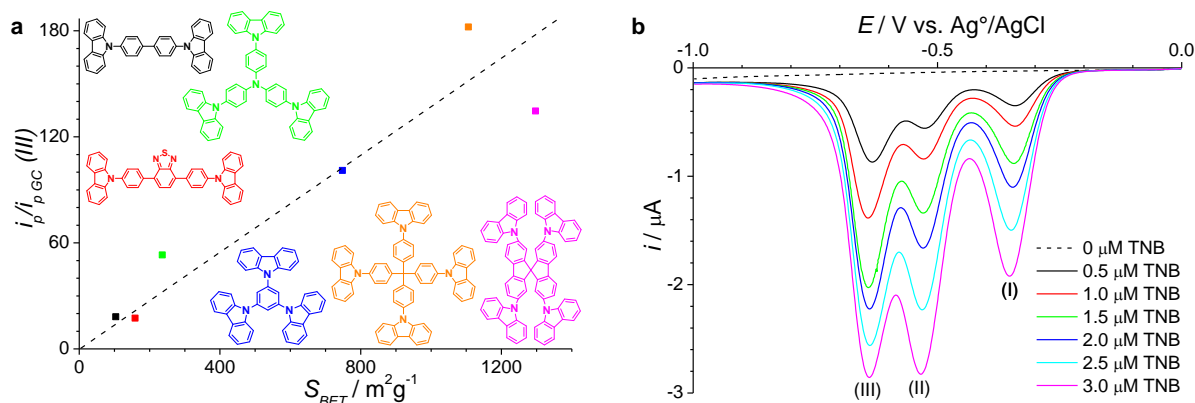


Figure 8. Correlation between the current ratios of the third reduction peaks of 0.5 μM TNB at MPN-modified and nonmodified GC electrodes, and the surface area of the MPN deposits (a). Linear scan voltammograms for the electrochemical reduction of 0 μM to 3.0 μM TNB in aqueous 0.2 M KCl and 0.1 M PBS solutions at PTPTCz-modified GC electrodes (b). The scan rate was 0.01 Vs^{-1} .

carbazole-based microporous polymer networks and the electron-poor nitroaromatic analytes resulting in a thin adsorbate layer. For mesoporous porphyrin-based materials the occurrence of π - π interactions with NACs has been postulated.^{40,41} These results are also consistent with such an assumption due to the correlation between surface area of the MPN films and the electrochemical response. The best results are obtained for coatings based on the tetracarbazolyl-substituted monomers that show the highest specific surface areas. PTPTCz-modified GC electrodes show a current ratio of 182 between modified and nonmodified GC electrodes, thus significantly boosting the sensitivity of the electrodes for electrochemical TNB sensing (see Figure 8b).

2.2.5. Mechanism of Electron Transfer for Electrochemical Reduction of Nitroaromatic Analytes at PTPTCz-Modified GC Electrodes

To extract more information about the mechanism of the process, the electrochemical reduction of nitroaromatic analytes at PTPTCz-modified GC electrodes was investigated by linear scan voltammetry at different scan rates. First, Figure 9a shows linear scan voltammograms for 3 μM nitrobenzene (NB) as analyte and scan rates from 0.005 Vs^{-1} to 0.30 Vs^{-1} . For low scan rates ($< 0.075 Vs^{-1}$) a negatively shifted asymmetrical wave is observed, characteristic for the irreversible reduction of adsorbed molecules.⁴² This behavior is less pronounced for higher scan rates ($> 0.075 Vs^{-1}$). Moreover, there is a linear dependence between cathodic peak current and scan rate for low scan rates, as expected for

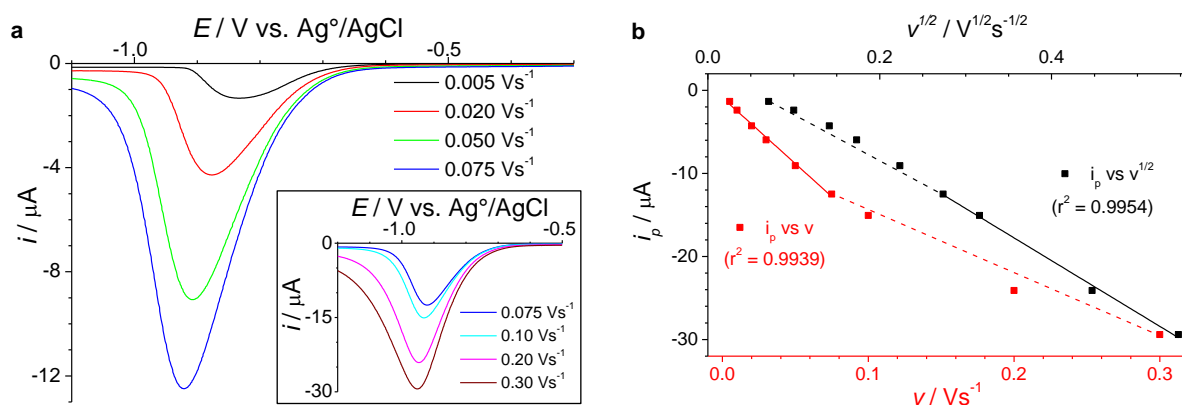


Figure 9. Linear scan voltammograms (a) and cathodic peak current vs scan rate (red line) or square root of scan rate (black line) plots (b) for 3.0 μM NB in aqueous 0.2 M KCl and 0.1 M PBS (pH 7.4) solution at PTPTCz-modified GC electrodes at scan rates of 0.005 Vs^{-1} – 0.075 Vs^{-1} (inset: 0.075 Vs^{-1} – 0.30 Vs^{-1}).

the formation of an adsorbed analyte layer, but a square root dependence for higher scan rates (see Figure 9b). These findings can be interpreted as follows: At low scan rates, the nitrobenzene molecules form a thin adsorbate layer at the MPN surface, an adsorption-controlled process is observed. With increasing scan rate the electron-transfer process becomes diffusion-controlled, since the transport of the nitrobenzene molecules is now the limiting process, the current is now proportional to the square root of the scan rate. Notably, similar results are also obtained for 1,3,5-trinitrobenzene (TNB, Figure 10) and 2,4,6-trinitrophenol (TNP, Figure 11) independent of their very different solubility in water. Linear scan voltammograms for 100 μM TNP showed a better resolution of the three peaks that were expected in the reduction of its three nitroaromatic groups. For comparison, similar experiments for nonmodified GC electrodes show the expected linear relationship between peak current and the square root of the scan rate for NB, TNB and TNP in the scan rate range from 0.01 Vs^{-1} to 0.4 Vs^{-1} (see Figure 12). The obtained linearity indicates a diffusion-

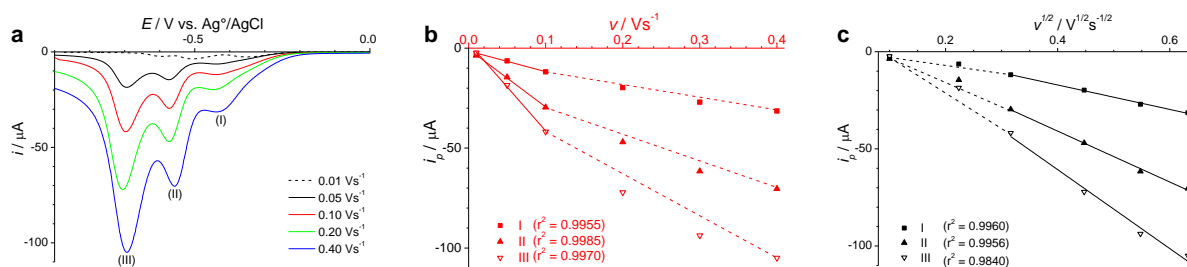


Figure 10. Linear scan voltammograms (a) and cathodic peak current vs scan rate (b) or square root of scan rate (c) plots for 3.0 μM TNB in aqueous 0.2 M KCl and 0.1 M PBS (pH 7.4) solution at PTPTCz-modified GC electrodes with scan rates of 0.01 Vs^{-1} – 0.40 Vs^{-1} .

Electrogenerated MPNs from Di-, Tri- and Tetracarbazole-Based Monomers

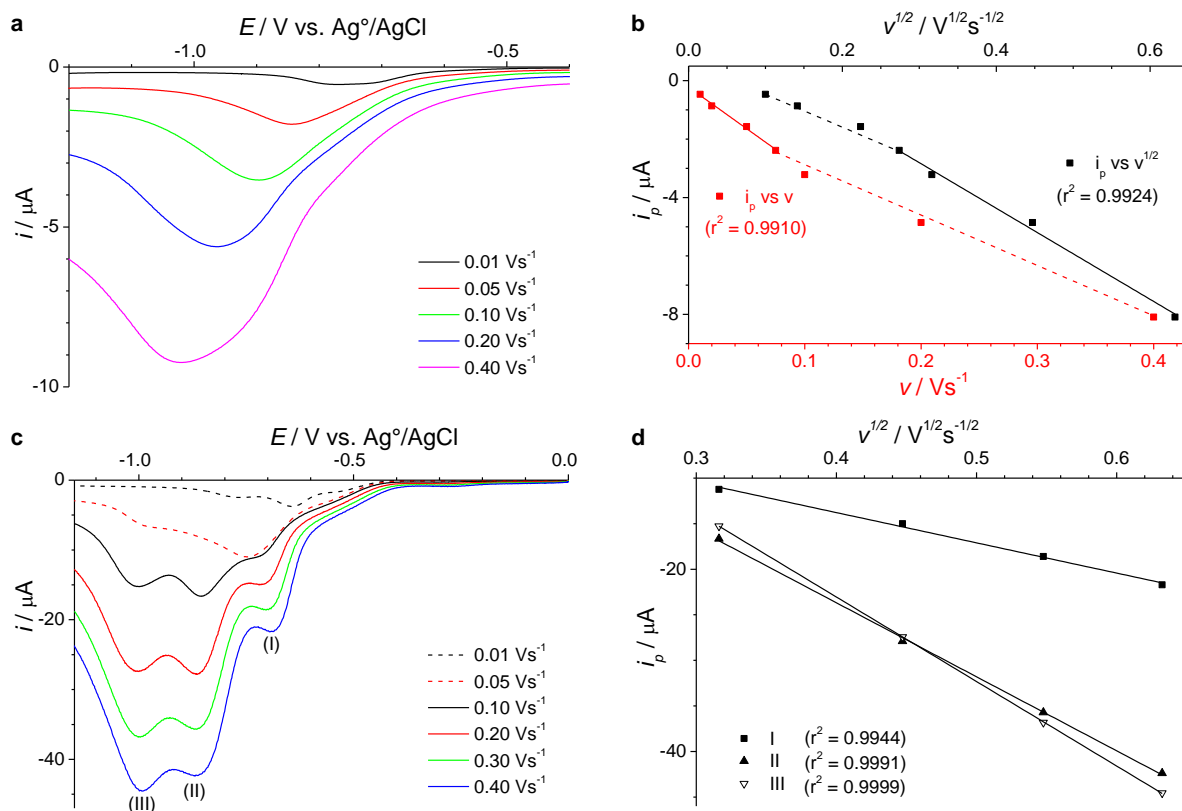


Figure 11. Linear scan voltammograms and cathodic peak current vs scan rate (red line) or square root of scan rate (black line) plots for 1.5 μM (a, b) and 100 μM (c, d) TNP in aqueous 0.2 M KCl and 0.1 M PBS (pH 7.4) solution at PTPTCz-modified GC electrodes with scan rates of 0.01 Vs^{-1} – 0.40 Vs^{-1} .

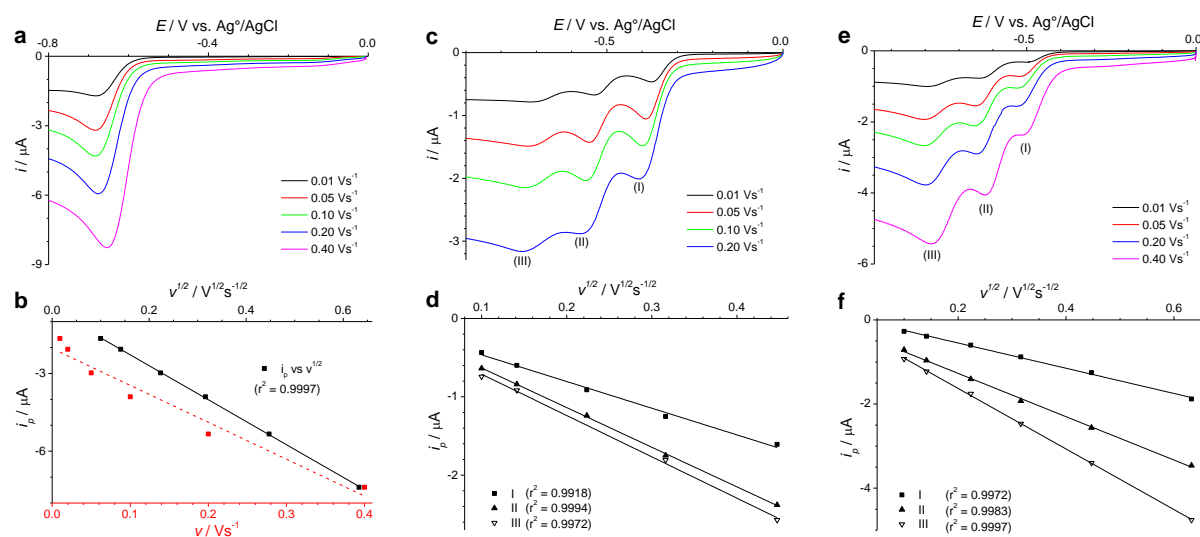


Figure 12. Linear scan voltammograms and cathodic peak current vs square root of scan rate plots for 100 μM NB (a, b), TNB (c, d) and TNP (e, f), respectively, in aqueous 0.2 M KCl and 0.1 M PBS (pH 7.4) solution on nonmodified, bare GC electrodes at scan rates from 0.01 Vs^{-1} to 0.40 Vs^{-1} .

controlled process. Regardless of the much higher concentration of the analytes (100 μM) in the experiments with nonmodified GC electrodes (concentrations for PTPTCz-modified GC electrodes $\leq 3 \mu\text{M}$) a higher peak current is observed for the modified electrodes for all nitroaromatic analytes.

2.2.6. Gas-Phase Nitroaromatic Analytes Detection by PSpCz Thin Films²

Regarding civil and environmental security, the detection of explosives in gas-phase is highly desirable.⁴³ Fluorescent polymers networks have shown to have potential application as luminescent sensor for traces of explosives.¹² In the previous sections, a direct correlation between the surface area of various MPN films and the current response to the electrochemical reduction of nitroaromatic analytes in aqueous systems was demonstrated using MPN-modified GC electrodes. Now, spirobifluorene-cored MPN films (PSpCz) are also used in the gas-phase detection of nitroaromatic explosives due to their inherent fluorescence and high BET surface area ($1297 \text{ m}^2\text{g}^{-1}$). Figure 13 shows 10 successive voltammetric cycles for the electrochemical polymerization of 0.5 mM SpCz in acetonitrile/dichloromethane (1:4) at ITO electrodes. PSpCz thin films with thickness of ca. 50 nm resulted by scanning in a potential range of 0 V – 0.98 V with a scan rate of 0.10 Vs^{-1} . The so-called nucleation loop with a crossing effect between the first anodic scan and the reverse sweep is observed during the first cycle. This phenomenon is usually related to a nucleation process of the polymer at the clean electrode.²⁷ Tapping mode AFM image shows a rather smooth morphology with R_q of 14 nm (see inset Figure 13).

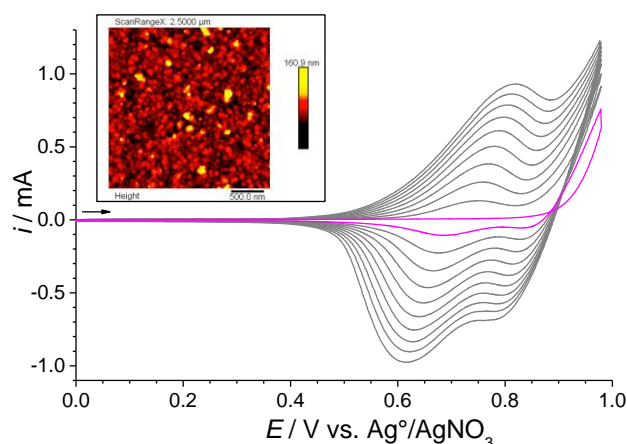


Figure 13. Ten successive cyclic voltammograms at ITO electrode for 0.5 mM SpCz in acetonitrile/dichloromethane (1:4) mixture and 0.1 M TBAP as supporting electrolyte, potential range: 0 V – 0.98 V, scan rate: 0.10 Vs^{-1} . The inset shows tapping mode AFM image of the MPN film.

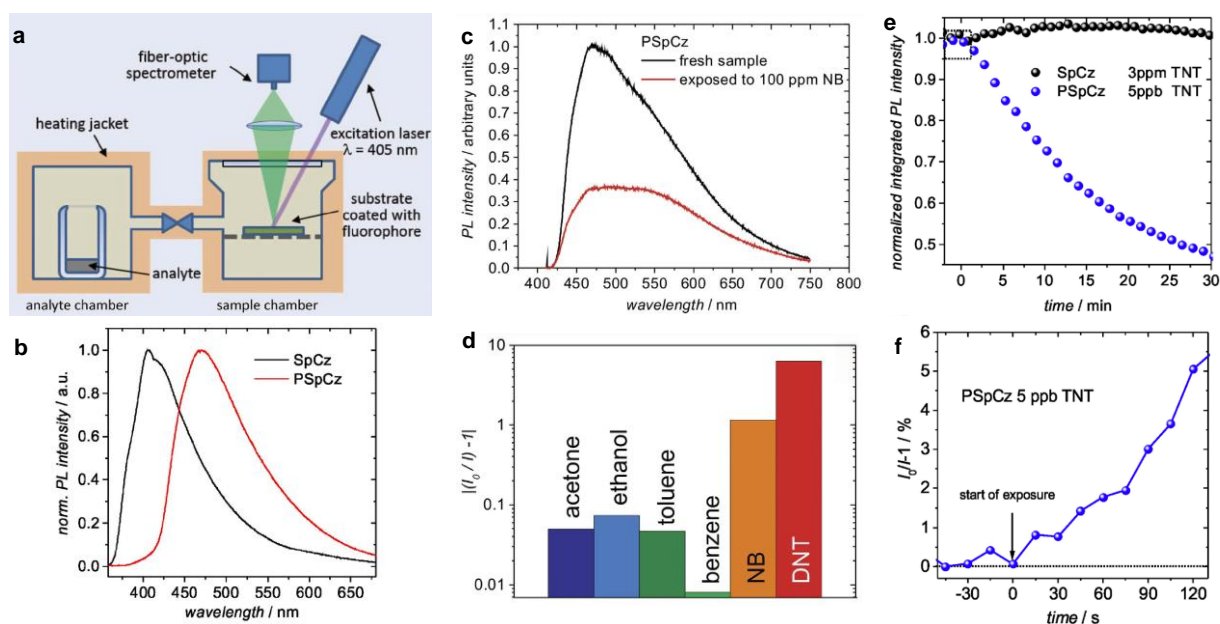


Figure 14. Setup for the characterization of the PL sensing upon controlled exposure concentrations of various analytes (a). PL spectra of the thermally evaporated SpCz film and the resulting electrogenerated MPN film (b). PL spectra of pristine PSpCz film and after exposure to 100 ppm NB for 150 s (c). Logarithmic quenching efficiency after exposure to 100 ppm of various analytes for 150 s (d). Integrated PL intensity (455 nm – 480 nm) for SpCz film (black dots) and PSpCz film (blue dots) to different levels of TNT (e). Quenching efficiency of PSpCz films exposed to 5 ppb at short time scales (f). Adapted from ².

Figure 14a depicts the setup used for a controlled exposition of various analytes to the PSpCz thin films. The analytes are placed in a separate chamber (analyte chamber) that is connected via a needle valve to a second chamber containing the PSpCz films on ITO (sample chamber). Either chamber can be separately heated. For comparison, thin films of SpCz monomer (thickness of also ca. 50 nm) were prepared by thermal evaporation. As expected, low BET surface area of only $0.88 \text{ m}^2\text{g}^{-1}$ was determined for nonporous monomer (SpCz) films. Photoluminescence (PL) spectra upon excitation at 355 nm for both type of films are shown in Figure 14b. A red-shifted PL peak centered at 472 nm is obtained for the PSpCz film if compared to the PL peak centered at 407 nm for the SpCz film. Figure 14c shows the PL quenching of PSpCz upon exposure to 100 ppm of NB for 150 s. PL intensity quenching of ca. 60 % is observed. The so-called quenching efficiency of the PSpCz films upon exposure to different analytes (e.g. acetone, ethanol, toluene, benzene, NB, and 2,4-dinitrotoluene – DNT) is shown Figure 14d in a logarithmic representation. Quenching efficiencies > 1 are found for electron-poor nitroaromatic analytes (NB and DNT), while for the rest of analytes only a slight effect on the PL is observed. A possible mechanism of PL quenching is an energy

transfer between the excited, electron-rich host and the electron-poor nitroaromatic quencher.⁴⁴ A higher quenching efficiency showed for the energy transfer from the LUMO level of PSpCz (-2.58 eV) to LUMO level of DNT (-3.22 eV) might be ascribed to a deeper LUMO level of DNT if compared to LUMO level of NB (-2.91 eV). Finally, gas-phase detection of 2,4,6-trinitrotoluene (TNT) at concentration of 5 ppb (room temperature level) was investigated for PSpCz films (see Figure 14e). PL intensity of the PSpCz films is quenched by ca. 50 % after 30 min by contact with TNT vapors. A clearly detectable quenching effect is even found after a few seconds (see Figure 14f). For comparison, PL quenching is not detectable for nonporous SpCz films at even much higher TNT concentration of 3 ppm. These results clearly demonstrate the importance of the microporosity/high surface area of the films that facilitates the interaction between the MPN surface and the quencher molecules.

2.3. Conclusions

In summary, electrochemical polymerization of a series of carbazole-based multifunctional monomers resulted in the generation of microporous polymer networks as thin films with high surface areas up to $1300 \text{ m}^2\text{g}^{-1}$. The observed porosity is directly related to the number of carbazole units of the monomers. MPN-modified glassy carbon electrodes were successfully used for the electrochemical detection of 1,3,5-trinitrobenzene as prototypical nitroaromatic analyte in aqueous solution, resulting in a distinct enhancement of the cathodic current response by up to 2 orders of magnitude for the best performing microporous polymer network. The electrochemical reduction of the nitroaromatic analytes was found to be an adsorption-controlled process for low scan rates but becomes diffusion-controlled for higher scan rates. These studies demonstrate a high application perspective of electropolymerized carbazole-based MPN films for the electrochemical sensing of nitroaromatic analytes. Additionally, the application potential of PSpCz films for the gas-phase sensing of nitroaromatic explosives was demonstrated, displaying high detection sensitivity up to TNT trace concentrations (5 ppb).

2.4. Experimental Section

2.4.1. Monomers and Bulk Polymers

4,4'-Di(carbazol-9-yl)-1,1'-biphenyl (CBP) (> 98.0 %) and tri[4-(carbazol-9-yl)phenyl]-amine (TCTA) (> 98.0 %) were purchased from TCI. 1,3,5-Tri(carbazol-9-yl)benzene (TCB) (97 %)

was purchased from Sigma-Aldrich. All other reagents and chemicals were purchased from commercial companies, unless otherwise stated. ^1H and ^{13}C NMR spectra were obtained on Bruker Avance 400 and III 600 machines. APLI mass spectra were recorded on a Bruker Daltonik micrOTOF system (KrF*-Laser ATLEX-SI, ATL Wermelskirchen). A Tousimis Samdri-795 system was used for washing the bulk polymers with supercritical carbon dioxide. Nitrogen and krypton adsorption-desorption isotherms were recorded on a BEL Japan Inc Belsorp-max system at 77 K. A maximum relative pressure of 0.6 was set for measurements with Kr gas. All samples were dried on a Belprep-vac II at 140 °C and ~ 2 Pa overnight prior to the gas sorption measurements.

2.4.1.1. Synthesis of 4,7-di[4-(carbazol-9-yl)phenyl]benzo[c][1,2,5]thiadiazole (CBPBT)

4,7-Di(4,4,5,5-tetramethyl-1,3,2-dioxaborolan-2-yl)benzo[c][1,2,5]thiadiazole (1.683 g, 4.12 mmol) and 9-(4-bromophenyl)carbazole (2.65 g, 8.24 mmol) were placed in a 250 mL round flask. Next, degassed toluene (15 mL), n-butanol (12 mL) and 20% aqueous Na_2CO_3 solution (20 mL) were added. After addition of tetrakis (triphenylphosphine)palladium(0) (0.124 g, 0.107 mmol) in toluene (15 mL), the mixture was refluxed under exclusion of light and argon atmosphere overnight. After cooling to room temperature, dichloromethane (50 mL) was added and the organic phase washed with three portions of aqueous 2 N HCl (each 50 mL). After removal of the solvents, the crude product was purified by column chromatography on silica, (eluent: hexane/chloroform 7:3). The product was isolated as yellow powder, yield: 1.7 g (67 %). ^1H NMR (600 MHz, $\text{C}_2\text{D}_2\text{Cl}_4$) δ : 8.39 (d, $J = 8.4$ Hz, 4H), 8.22 (d, $J = 7.8$ Hz, 4H), 8.05 (s, 2H), 7.83 (d, $J = 8.4$ Hz, 4H), 7.62 (d, $J = 8.2$ Hz, 4H), 7.53-7.50 (m, 4H), 7.39-7.37 (m, 4H); ^{13}C NMR (151 MHz, $\text{C}_2\text{D}_2\text{Cl}_4$) δ : 154.06, 140.88, 137.89, 136.10, 132.44, 130.57, 128.05, 126.84, 125.97, 123.52, 120.16, 120.11, 109.89; MS (APLI) 618.172 [618.188] (M^+).

2.4.1.2. Synthesis of 2,2',7,7'-tetra(carbazol-9-yl)-9,9'-spirobifluorene (SpCz)

2,2',7,7'-Tetrabromo-9,9'-spirobifluorene (2.00 g, 3.16 mmol), carbazole (2.55 g, 15.23 mmol), copper(I) iodide (2.90 g, 15.23 mmol), potassium carbonate (5.27 g, 38.14 mmol) and 2,2'-bipyridine (0.24 g, 1.53 mmol) were placed in a 100 mL round flask and carefully degassed. 1,2-Dichlorobenzene (50 mL) was added as solvent, and the mixture was stirred under argon atmosphere and exclusion of light at 180 °C for 3 days. The hot reaction mixture was filtered through celite and washed with hot toluene. After evaporation of the solvent, the crude product was purified by column chromatography on silica, (eluent: hexane/dichloromethane 6:3) and recrystallized from a hexane/dichloromethane mixture. The

product was isolated as white powder, yield: 1.81 g (83 %). ^1H NMR (600 MHz, $\text{C}_2\text{D}_2\text{Cl}_4$) δ : 8.16 (d, $J = 7.7$ Hz, 8H), 8.12 (d, $J = 8.1$ Hz, 4H), 7.70 (dd, $J = 8.0, 1.9$ Hz, 4H), 7.46-7.41 (m, 8H), 7.38-7.33 (m, 16H), 7.32 (d, $J = 1.8$ Hz, 4H); ^{13}C NMR (151 MHz, $\text{C}_2\text{D}_2\text{Cl}_4$) δ : 149.76, 140.57, 140.05, 137.27, 127.27, 126.00, 123.09, 122.47, 121.99, 120.34, 120.08, 109.40, 65.75; MS (APLI) 976.346 [976.357] (M^+).

2.4.1.3. Synthesis of tetra[4-(carbazol-9-yl)phenyl]methane (TPTCz)

Tetra(4-bromophenyl)methane (1.00 g, 1.58 mmol), carbazole (1.27 g, 7.56 mmol), copper(I) iodide (1.44 g, 7.56 mmol), potassium carbonate (2.62 g, 18.95 mmol) and 2,2'-bipyridine (0.12 g, 0.76 mmol) were placed in a 100 mL round flask and carefully degassed. 1,2-Dichlorobenzene (50 mL) was added, and the mixture was stirred under argon atmosphere and exclusion of light at 180 °C for 3 days. The hot reaction mixture was filtered through celite and washed with hot toluene. After evaporation of the solvent, the crude product was purified by column chromatography on silica, (eluent: hexane/chloroform 7:3) and recrystallized from a hexane/chloroform mixture. The product was isolated as slightly yellow powder, yield: 0.55 g (35 %). ^1H NMR (400 MHz, $\text{C}_2\text{D}_2\text{Cl}_4$) δ : 8.20 (d, $J = 7.7$ Hz, 8H), 7.77 (d, $J = 8.9$ Hz, 8H), 7.73 (d, $J = 8.9$ Hz, 8H), 7.63 (d, $J = 8.2$ Hz, 4H), 7.52-7.48 (m, 8H), 7.38-7.34 (m, 8H); ^{13}C NMR (101 MHz, $\text{C}_2\text{D}_2\text{Cl}_4$) δ : 144.92, 140.45, 135.82, 132.42, 126.03, 125.96, 123.19, 120.26, 120.13, 109.87, 64.42.; MS (APLI) 980.377 [980.388] (M^+).

2.4.1.4. Synthesis of bulk polymers

All monomers were chemically polymerized using the same methodology, which is described for CBP polymerization as following: CBP (300 mg, 0.619 mmol) was dissolved in anhydrous chloroform (30 mL) and transferred dropwise to a 250 mL round flask which contains a suspension of iron(III)chloride (603 mg, 3.71 mmol) in anhydrous chloroform (20 mL). The resulting mixture was stirred at room temperature for one day under argon atmosphere. After addition of methanol (100 mL), the mixture was stirred for one more hour. The resulting precipitate was collected by filtration and washed with methanol. The powder was vigorously treated with aqueous hydrochloric acid 37 % for 2 h, filtered and washed with water and methanol. After Soxhlet extraction with methanol and THF for 24 h, the product was finally treated with ethanol (p.a.) for three days and washed with supercritical carbon dioxide. PCBP was isolated as slightly yellow powder, yield: 231 mg (77 %), PCBPBT as yellow powder (78 %), PTCB as yellow powder (88 %), PTCTA as slightly yellow powder (28 %), PSpCz as slightly yellow powder (87 %), and PTPTCz as slightly yellow powder (95 %).

2.4.2. Electrochemical Studies

Acetonitrile, dichloromethane and chloroform (HPLC grade) were refluxed over phosphorus pentoxide for 3 h and distilled. Tetrabutylammonium perchlorate (TBAP, for electrochemical analysis, $\geq 99.0\%$), phosphate buffered saline (PBS, pH 7.4), nitrobenzene (NB, analytical standard) and 2,4,6-trinitrophenol (TNP, $\geq 98\%$, moistened with water) were purchased from Sigma-Aldrich. 1,3,5-Trinitrobenzene (TNB, neat) was purchased from Supelco. Potassium chloride (KCl, $\geq 99.5\%$, ACS) was purchased from Roth. Indium tin oxide-coated transparent electrodes on glass (ITO, $\leq 20\ \text{Ohm m}^{-2}$) were purchased from pgo. For electrochemical polymerization and characterization a Potentiostat/Galvanostat PAR VersaSTAT 4 in combination to a three-electrode cell was used. The AFM images were obtained with an atomic force microscope Bruker diInnova operated in tapping mode. The average surface roughness was extracted from the topography images. The thickness of the films was measured with a surface profilometer Veeco Dektak 150.

2.4.2.1. Electrochemical polymerization on Pt electrodes

5 mL of 0.5 mM solutions of the monomers were prepared in acetonitrile/dichloromethane (1:4) using 0.1 M TBAP as supporting electrolyte. The solutions were placed in a three-electrode cell under argon atmosphere at 25 °C. A platinum disc electrode (Pt, 1 mm diameter) was used as working electrode (WE); a platinum wire was used as counter electrode (CE). $\text{Ag}^\circ/\text{AgNO}_3$ (0.1 M AgNO_3 , 0.60 V vs NHE) was used as reference electrode (RE). Multiple cyclic voltammograms were recorded from 0 V to 1.2 V with a scan rate of 0.10 Vs^{-1} .

2.4.2.2. Electrochemical polymerization on glassy carbon (GC) electrodes and electrochemical sensing of TNB, NB and TNP

The above mentioned solutions of the monomers were placed in a three-electrode cell. Glassy carbon disc electrode (GC, 1 mm diameter) was used as working electrode (WE). Potentiostatic polymerization of a monomer was achieved by applying a potential of 1.1 V until an oxidative charge of 0.2 mC was accumulated. A potential of 0 V was applied after polymerization during 30 s in order to discharge the deposit. After rinsing the deposit with acetonitrile and dichloromethane, the MPN-modified GC electrodes were used as WE in a 10 mL of aqueous 0.2 M KCl and 0.1 M PBS under argon atmosphere at 25 °C. A platinum wire and $\text{Ag}^\circ/\text{AgCl}(\text{sat.})$ (NaCl 3 M, 0.21 V vs NHE) were used as CE and RE, respectively. After 5 min of stirring, prepotential of 0 V was applied for 30 s. Linear scan voltammograms were recorded from 0 V to -1 V with a scan rate of 0.01 Vs^{-1} . For 1,3,5-trinitrobenzene (TNB)

detection, 5 μL of 1 mM TNB solution in acetonitrile were added sequentially in order to adjust the TNB concentration from 0 μM to 3 μM . For nitrobenzene (NB) experiments, 6 μL of 5 mM NB in acetonitrile were added to obtain a 3 μM solution. For 2,4,6-trinitrophenol (TNP, picric acid) experiments, 150 μL of 100 μM TNP in water was added to obtain a 1.5 μM solution. Corresponding 100 μM solutions were obtained by adding 200 μL of 5 mM stock solutions.

2.4.2.3. Electrochemical polymerization on ITO electrodes

10 mL of the monomers solutions were placed in a three-electrode cell. ITO ($\sim 1.5 \times 1.2$ cm deposit area) on glass and a platinum gauze (2.5×1.2 cm area), separated by 1 cm, were used as WE and CE, respectively. $\text{Ag}^\circ/\text{AgNO}_3$ (0.1 M AgNO_3 , 0.60 V vs NHE) was used as RE. For krypton gas sorption isotherms, thick films were produced by applying an oxidative potential of 1 V (CBP, SpCz, TPTCz) or 1.1 V (CBPBT, TCB, TCTA) for 20 min. A potential of 0 V was applied after the polymerization for 60 s in order to discharge the deposits. After rinsing the deposits with acetonitrile and dichloromethane, they were dried for 20 min at 85 $^\circ\text{C}$. The collection of ca. 2 mg of material was necessary for reliable BET measurements. For thickness measurements, MPN films on ITO were prepared by applying a potential of 1.1 V until an oxidative charge density of 25.5 mC cm^{-2} was accumulated. After the films had been dedoped by applying a potential of 0 V for 60 s, they were rinsed with acetonitrile and dichloromethane and dried for 20 min at 85 $^\circ\text{C}$. Thin films of PSpCz for the gas-phase detection experiments were obtained applying 10 successive cyclic voltammograms from 0 V to 0.98 V with a scan rate of 0.10 Vs^{-1} .

2.5. References

- (1) Palma-Cando, A.; Scherf, U. *ACS Appl. Mater. Interfaces*. **2015**, *7*, 11127.
- (2) Raupke, A.; Palma-Cando, A.; Shkura, E.; Teckhausen, P.; Polywka, A.; Gornn, P.; Scherf, U.; Riedl, T. *Sci. Rep.* **2016**, *6*, 29118.
- (3) Dawson, R.; Stockel, E.; Holst, J. R.; Adams, D. J.; Cooper, A. I. *Energy Environ. Sci.* **2011**, *4*, 4239.
- (4) Fischer, S.; Schimanowitz, A.; Dawson, R.; Senkovska, I.; Kaskel, S.; Thomas, A. J. *Mater. Chem. A* **2014**, *2*, 11825.
- (5) Chen, Q.; Luo, M.; Hammershoj, P.; Zhou, D.; Han, Y.; Laursen, B. W.; Yan, C.-G.; Han, B.-H. *J. Am. Chem. Soc.* **2012**, *134*, 6084.
- (6) Zhang, X.; Lu, J.; Zhang, J. *Chem. Mater.* **2014**, *26*, 4023.

- (7) Zhang, Y.; A, S.; Zou, Y.; Luo, X.; Li, Z.; Xia, H.; Liu, X.; Mu, Y. *J. Mater. Chem. A* **2014**, *2*, 13422.
- (8) Zhao, Q.; Zhang, P.; Antonietti, M.; Yuan, J. *J. Am. Chem. Soc.* **2012**, *134*, 11852.
- (9) Zhang, K.; Kopetzki, D.; Seeberger, P. H.; Antonietti, M.; Vilela, F. *Angew. Chem. Int. Ed.* **2013**, *52*, 1432.
- (10) Schmidt, J.; Weber, J.; Epping, J. D.; Antonietti, M.; Thomas, A. *Adv. Mater.* **2009**, *21*, 702.
- (11) Bildirir, H.; Paraknowitsch, J. P.; Thomas, A. *Chem. Eur. J.* **2014**, *20*, 9543.
- (12) Liu, X.; Xu, Y.; Jiang, D. *J. Am. Chem. Soc.* **2012**, *134*, 8738.
- (13) Brutschy, M.; Schneider, M. W.; Mastalerz, M.; Waldvogel, S. R. *Adv. Mater.* **2012**, *24*, 6049.
- (14) Preis, E.; Widling, C.; Scherf, U.; Patil, S.; Brunklaus, G.; Schmidt, J.; Thomas, A. *Polym. Chem.* **2011**, *2*, 2186.
- (15) Luo, Y.; Zhang, S.; Ma, Y.; Wang, W.; Tan, B. *Polym. Chem.* **2013**, *4*, 1126.
- (16) Gu, C.; Chen, Y.; Zhang, Z.; Xue, S.; Sun, S.; Zhang, K.; Zhong, C.; Zhang, H.; Pan, Y.; Lv, Y.; Yang, Y.; Li, F.; Zhang, S.; Huang, F.; Ma, Y. *Adv. Mater.* **2013**, *25*, 3443.
- (17) Gu, C.; Chen, Y.; Zhang, Z.; Xue, S.; Sun, S.; Zhong, C.; Zhang, H.; Lv, Y.; Li, F.; Huang, F.; Ma, Y. *Adv. Energy Mater.* **2014**, *4*, 1301771.
- (18) Zhang, H.; Zhang, Y.; Gu, C.; Ma, Y. *Adv. Energy Mater.* **2015**.
- (19) Gu, C.; Huang, N.; Gao, J.; Xu, F.; Xu, Y.; Jiang, D. *Angew. Chem. Int. Ed.* **2014**, *53*, 4850.
- (20) Dong, W.; Fei, T.; Palma-Cando, A.; Scherf, U. *Polym. Chem.* **2014**, *5*, 4048.
- (21) Ma, H.; Yao, L.; Li, P.; Ablikim, O.; Cheng, Y.; Zhang, M. *Chem. Eur. J.* **2014**, *20*, 11655.
- (22) Wei, Y.; Chan, C. C.; Tian, J.; Jang, G. W.; Hsueh, K. F. *Chem. Mater.* **1991**, *3*, 888.
- (23) Dietrich, M.; Heinze, J.; Heywang, G.; Jonas, F. *J. Electroanal. Chem.* **1994**, *369*, 87.
- (24) Ribeiro, A. S.; da Silva, A. U.; Ribeiro, L. v. M. O.; da Silva, J. G.; Navarro, M.; Tonholo, J. *J. Electroanal. Chem.* **2005**, *580*, 313.
- (25) Yu, T.; Wu, X.; Lv, Y.; Liu, L.; Du, L.; Zhou, J.; Xie, Z.; Ma, Y. *J. Mater. Chem. C* **2014**, *2*, 4117.
- (26) Groenendaal, L.; Jonas, F.; Freitag, D.; Pielartzik, H.; Reynolds, J. R. *Adv. Mater.* **2000**, *12*, 481.
- (27) Heinze, J.; Frontana-Uribe, B. A.; Ludwigs, S. *Chem. Rev.* **2010**, *110*, 4724.

- (28) Argun, A. A.; Aubert, P.-H.; Thompson, B. C.; Schwendeman, I.; Gaupp, C. L.; Hwang, J.; Pinto, N. J.; Tanner, D. B.; MacDiarmid, A. G.; Reynolds, J. R. *Chem. Mater.* **2004**, *16*, 4401.
- (29) Kerszulis, J. A.; Amb, C. M.; Dyer, A. L.; Reynolds, J. R. *Macromolecules* **2014**, *47*, 5462.
- (30) Ambrose, J. F.; Nelson, R. F. *J. Electrochem. Soc.* **1968**, *115*, 1159.
- (31) Roncali, J.; Leriche, P.; Cravino, A. *Adv. Mater.* **2007**, *19*, 2045.
- (32) Yuan Chiu, K.; Xiang Su, T.; Hong Li, J.; Lin, T.-H.; Liou, G.-S.; Cheng, S.-H. *J. Electroanal. Chem.* **2005**, *575*, 95.
- (33) Sing, K. S. W. *Pure Appl. Chem.* **1985**, *57*, 603.
- (34) Sing, K. S. W.; Everett, D. H.; Haul, R. A. W.; Moscou, L.; Pierotti, R. A.; Rouquerol, J.; Siemieniewska, T. In *Handbook of Heterogeneous Catalysis*; Wiley-VCH Verlag GmbH & Co. KGaA: Weinheim, 2008.
- (35) Evans, S. A. G.; Elliott, J. M.; Andrews, L. M.; Bartlett, P. N.; Doyle, P. J.; Denuault, G. *Anal. Chem.* **2002**, *74*, 1322.
- (36) Ma, J.; Zhang, Y.; Zhang, X.; Zhu, G.; Liu, B.; Chen, J. *Talanta* **2012**, *88*, 696.
- (37) Qi, B.; Lin, F.; Bai, J.; Liu, L.; Guo, L. *Mater. Lett.* **2008**, *62*, 3670.
- (38) Laviron, E.; Meunier-Prest, R.; Vallat, A.; Roullier, L.; Lacasse, R. *J. Electroanal. Chem.* **1992**, *341*, 227.
- (39) Zhang, H.-X.; Cao, A.-M.; Hu, J.-S.; Wan, L.-J.; Lee, S.-T. *Anal. Chem.* **2006**, *78*, 1967.
- (40) Quan, Y.; Xue, Z.; Shi, H.; Zhou, X.; Du, J.; Liu, X.; Lu, X. *Analyst* **2012**, *137*, 944.
- (41) Xue, Z.; Lian, H.; Hu, C.; Feng, Y.; Zhang, F.; Liu, X.; Lu, X. *Aust. J. Chem.* **2014**, *67*, 796.
- (42) Bard, A. J.; Faulkner, L. R. *Electrochemical Methods: Fundamentals and Applications*; 2 ed.; John Wiley & Sons: New York, 1994.
- (43) Sun, X.; Wang, Y.; Lei, Y. *Chem. Soc. Rev.* **2015**, *44*, 8019.
- (44) Toal, S. J.; Trogler, W. C. *J. Mater. Chem.* **2006**, *16*, 2871.

Chapter 3

Electrogenerated MPNs from Tetra- and Octacarbazole-Based Monomers¹

A series of four tetra- or octacarbazolyl-substituted, tetraphenylmethane/silane monomers were oxidatively coupled into microporous polymer networks (MPNs). Chemical polymerization with iron(III) chloride gives bulk MPNs with BET surface areas (S_{BET}) of up to $1331 \text{ m}^2\text{g}^{-1}$ (for the octacarbazolyl-substituted tetraphenylmethane monomer). Slightly increased S_{BET} values result for the materials made from the octacarbazolyl monomers if compared to the tetracarbazolyl analogues, while the exchange of the central carbon by a silicon atom leads to decreased surface areas. The latter phenomenon might be related to electronic interactions of aromatic substituents through the silicon centers. This may cause a reduced reactivity of the carbazole after the initial oxidative couplings and finally a reduced cross-linking density of the resulting MPNs. Moreover, electrochemical oxidative coupling enables the formation of thin polymer films on the working electrode. These films also show high S_{BET} values that are only slightly reduced if compared to the corresponding bulk MPNs. Electrochemical quartz crystal microbalance measurements allow for an in-situ characterization of the electrochemical MPN generation. Finally, the electrochemical reduction of a series of nitroaromatic compounds (NACs) on MPN-modified glassy carbon electrodes was studied and applied for high sensitivity NACs detection up to the ppb range.

3.1. Introduction

Films of microporous polymer networks (MPNs) synthesized by electrochemical oxidative polymerization have been intensively studied during the last years due to their promising application potential in the organic electronics field.^{2,3} These type of electrogenerated thin films not only show the typical properties of microporous polymer materials such as high intrinsic surface, chemical resistance and thermal stability, but also the advantages of an electrochemical polymerization, among others, easy control of thickness and surface morphology of the deposits, catalyst-free deposition procedures and tunable electrical properties via in-situ doping/dedoping of the films.⁴ Jiang and co-workers reported the electrogeneration of MPN films from organoborane-cored tri-carbazolyl monomers and their use as charge extraction/injection interlayers of organic solar cells and organic light-emitting diodes.⁵ These thin interlayers show electron- or hole-selective charge transport in their pristine state or after doping, respectively. Müllen and co-workers synthesized pyrene-cored

multifunctional triphenylamine dendrimers for electrochemical polymerization into thin films.⁶ The films were applied as photoluminescence (PL) chemosensors for the detection of nitroexplosives and Fe³⁺ anions with good sensitivity and selectivity.

In this chapter, chemical and electrochemical oxidative polymerizations of four tetra- or octa-functional carbazolyl monomers with tetraphenylmethane or –silane cores are carried out. Bulk microporous polymer networks obtained by oxidative coupling with iron(III) chloride showed increased specific surface areas (S_{BET}) for the octacarbazolyl monomers if compared to the corresponding tetracarbazolyl monomers. Most probably, the increased number of carbazole groups leads to a higher cross-linked, rigidified networks, and therefore to higher surface areas. On the other hand, the networks made from tetraphenylmethane-cored monomers display higher microporosities if compared to the corresponding tetraphenylsilane-cored MPNs. This phenomenon might be related to the electronic interaction of aromatic substituents through silicon centers (so-called σ - π -conjugation) thus sequentially lowering the reactivity of carbazolyl groups after the initial (first, second or third) coupling steps. This may finally cause a lower cross-linking density and lower S_{BET} values. Nitrogen gas sorption isotherms, thermal stability and optical properties were determined for all bulk MPN materials. Electrochemical oxidative polymerization of the series of carbazolyl monomers and the ongoing doping/dedoping processes of the as-formed MPN films were followed up with the electrochemical quartz crystal microbalance (EQCM) method. Electropolymerization of the monomers leads to the formation of thin MPN films with slightly reduced S_{BET} values if compared to the corresponding chemically synthesized bulk materials. Finally, MPN-modified glassy carbon (GC) electrodes were fabricated and used for the electrochemical detection of different nitroaromatic compounds (NACs) in aqueous environment with high sensitivities up to 0.1 μM NACs (ppb range).

3.2. Results and Discussions

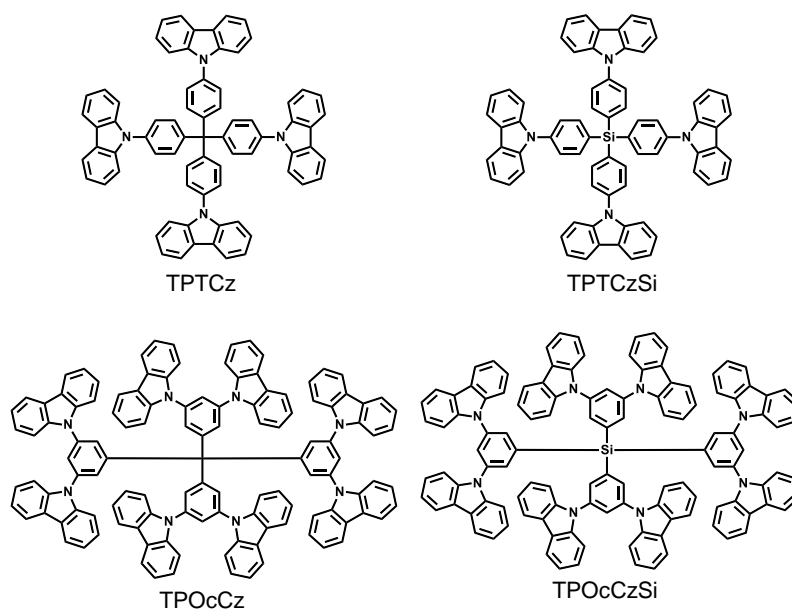
3.2.1. Synthesis of the Series of Monomers

The four multifunctional carbazolyl-substituted monomers were all synthesized following literature procedures (see Experimental Section for details). Tetra[4-(carbazol-9-yl)phenyl]methane (TPTCz) was synthesized in three steps with moderate yield: After formation of the tetraphenylmethane core by reaction of aniline with triphenylchloromethane, its bromination results in tetra(4-bromophenyl)methane. Finally, a fourfold Ullman-type

coupling with carbazole gave monomer TPTCz in 36 % yield. Tetra[3,5-di(carbazol-9-yl)phenyl]methane (TPOcCz) was obtained in a five step procedure. Nitration of tetraphenylmethane with fuming nitric acid followed by a Raney-nickel-catalyzed hydrazine reduction gave tetra(4-aminophenyl)methane in 72 % yield. Octabromination of the tetraamine with bromine and subsequent deamination yielded tetra(3,5-dibromophenyl)methane. Again, an eightfold Ullman-type coupling with carbazole delivered monomer TPOcCz in 29 % yield. The silicon-cored monomers tetra[4-(carbazol-9-yl)phenyl]silane (TPTCzSi) and tetra[3,5-di(carbazol-9-yl)phenyl]silane (TPOcCzSi) were synthesized in reductive coupling procedures of 9-(4-bromophenyl)-carbazole or 5-bromo-1,3-di(carbazol-9-yl)benzene with tetrachlorosilane with 72 % and 20 % yield, respectively.

3.2.2. Characterization of Chemically Synthesized Bulk Polymers

Oxidative coupling of the carbazole-based monomers with iron(III) chloride resulted in the formation of the bulk polymers in excellent yields (> 85 %), isolated as fine powdery materials. Thermogravimetric analysis of the polymers showed a good thermal stability under argon up to 450 °C (see Figure 1). Solid state UV-vis reflectance and photoluminescence (PL) spectra of the insoluble polymers are presented in Figure 2. PTPOcCz (made from the octacarbazolyl monomer TPOcCz) showed a red-shifted absorption onset if compared to PTPTCz (made from the tetracarbazolyl monomer TPTCz). In contrast, both silicon-cored MPNs PTPTCzSi and PTPOcCzSi displayed similar absorption spectra. PTPTCzSi showed a



Scheme 1. Chemical structures of the investigated carbazole-based monomers.

Chapter 3

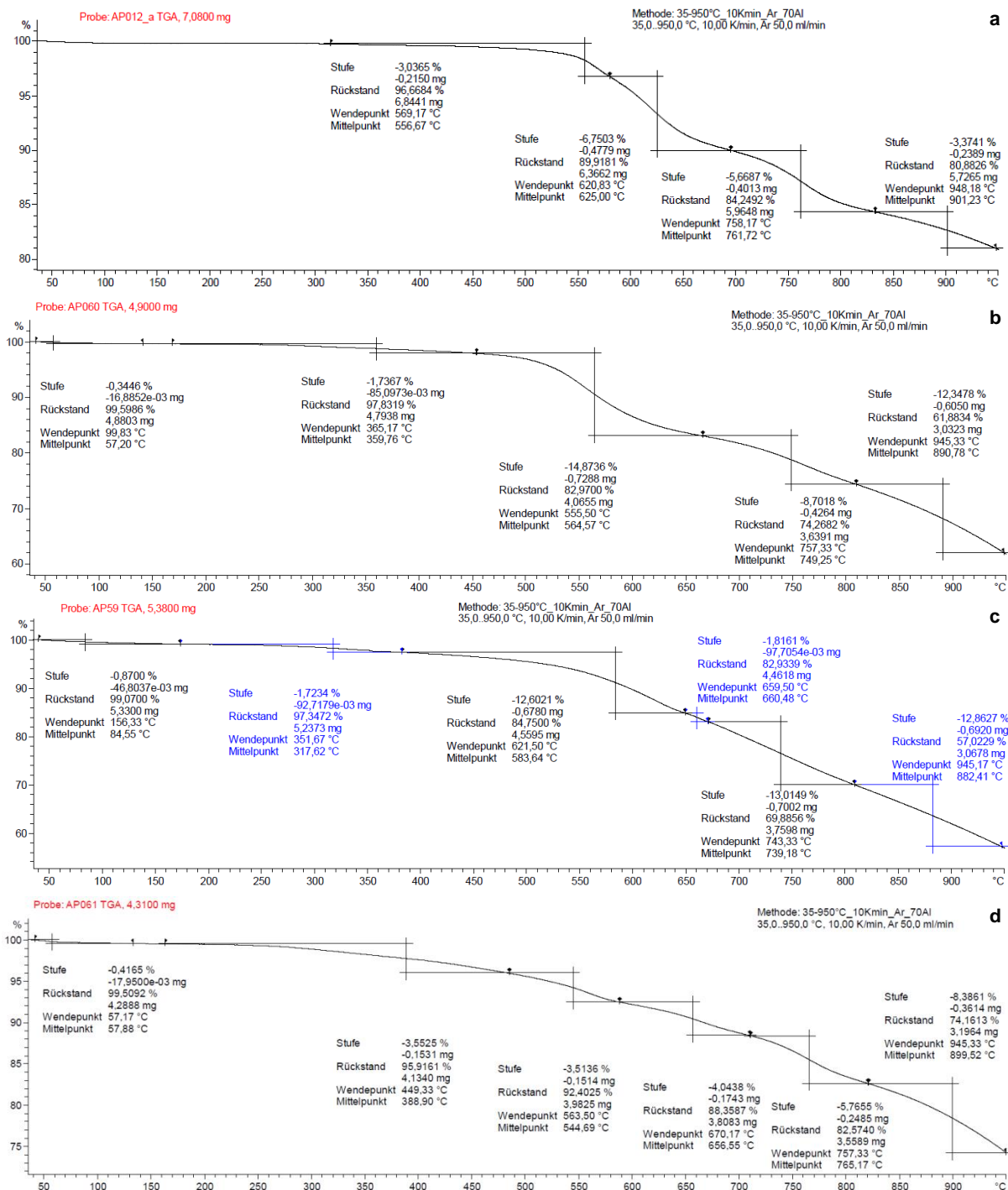


Figure 1. TGA curves of the bulk MPNs (FeCl_3 oxidation): PTPTCz (a), PTPTCzSi (b), PTPOcCz (c), and PTPOcCzSi (d).

remarkable intense photoluminescence. The PL maxima of the bulk MPNs are centered at 444 nm (PTPTCz), 473 nm (PTPTCzSi), 482 nm (PTPOcCz) and 471 nm (PTPOcCzSi). The optical spectra reflect the presence of N-arylated biscarbazole chromophores and are comparable to the spectra of similar networks.⁷

Electrogenerated MPNs from Tetra- and Octacarbazole-Based Monomers

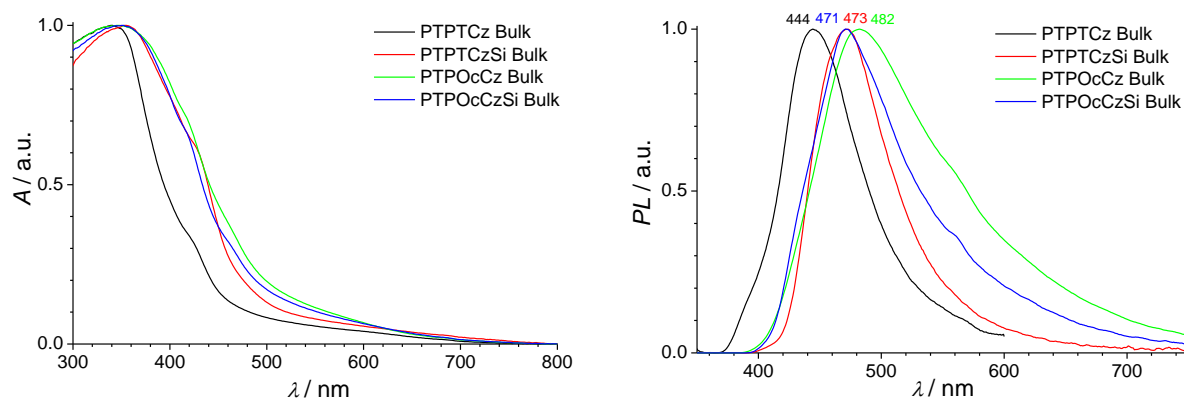


Figure 2. UV-vis (diffuse reflection) (a) and photoluminescence (b) spectra of the solid-state, bulk MPNs.

Specific surface areas of the bulk polymers were calculated by applying the Brunauer-Emmett-Teller equation to their respective nitrogen gas adsorption isotherms at 77 K (see Figure 3). A highly uptake of gas at low relative pressures (< 0.1) is characteristic of microporous materials.⁸ Pore sizes were determined from a nonlocal density functional theory (NLDFT) model resulting in average pore diameters of 0.91 nm – 1.38 nm.^{9,10} For PTPTCz, the additional gas uptake at high relative pressure (> 0.9) and the more pronounced hysteresis should be related to meso- and macroporosity (interparticular voids). Table 1 outlines the porosity data for the four bulk MPNs. Hereby, the two octacarbazolyl-based MPNs (PTPOcCz and PTPOcCzSi) show increased S_{BET} values if compared to the corresponding tetracarbazolyl-based MPNs (PTPTCz and PTPTCzSi). This phenomenon maybe related to an increased cross-linking density as result of the increased amount of reactive carbazolyl groups in the monomers. The S_{BET} value for PTPTCz well compares to published data for analogous MPNs made under similar conditions.^{11,12} PTPOcCz possesses the highest specific surface

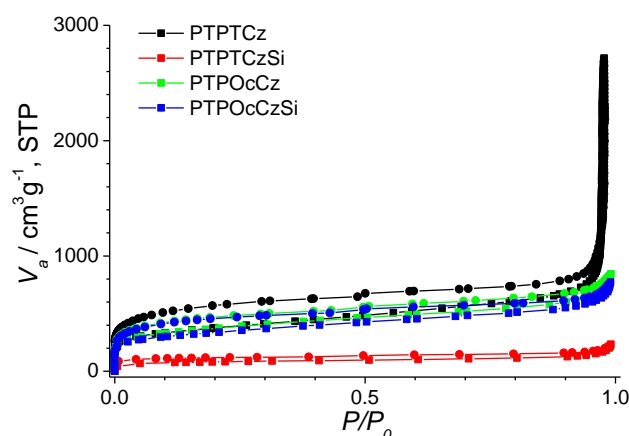


Figure 3. Nitrogen gas sorption isotherms of chemically synthesized bulk MPNs.

Table 1. Porosity data, gas uptake (at 298 K) and gas sorption selectivity of the four bulk MPNs synthesized by oxidative coupling with iron(III) chloride.

Polymer	S_{BET} [m^2g^{-1}]	Pore volume ^a	Gas uptake [%]				Selectivity ^c	
			CO_2	N_2	CH_4	H_2 ^b	CO_2/N_2	CO_2/CH_4
PTPTCz	1322	1.22	7.49	0.35	0.96	1.53	13.4	2.9
PTPTCzSi	294 (574) ^d	0.22	3.27	0.13	0.40	0.69	15.7	3.0
PTPOcCz	1331	1.00	8.47	0.43	1.03	1.52	12.4	3.0
PTPOcCzSi	1194	0.92	7.87	0.32	0.97	1.44	15.8	3.0

^a Determined at $P/P_0 = 0.95$; ^b Measured at 77 K; ^c Calculated by applying Henry's law;¹³

^d Obtained by applying the reaction conditions reported by Ren and co-workers¹⁴

area (S_{BET}) of 1331 m^2g^{-1} . On the other hand, both carbon-cored materials (PTPTCz and PTPOcCz) displayed an increased S_{BET} values in relation to the respective silicon-cored MPNs (PTPTCzSi and PTPOcCzSi). This phenomenon can be related to the electronic σ - π -interaction of aromatic substituents through the silicon centers thus sequentially decreasing the reactivity of the carbazolyl groups after the initial (first, second, third, etc.) coupling steps leading to a lower cross-linking density and lower S_{BET} values.¹⁵ This effect is more pronounced for the tetracarbazolyl-based MPN (PTPTCzSi) that displays a strikingly low S_{BET} value of 294 m^2g^{-1} . Ren and co-workers reported a much higher S_{BET} value of 1856 m^2g^{-1} for PTPTCzSi by applying harsher reaction conditions (higher temperature and pressure, and longer reaction time).¹⁴ When applying Ren's reaction conditions, a S_{BET} value of 574 m^2g^{-1} was found for the resulting MPN, still lower than the literature value. Microporous polymer networks are promising candidates for applications in gas storage and separation.^{16,17} The four MPNs are characterized by reasonably good CO_2 uptake capacities of up to 8.47% at 25 °C (see Figure 4) which is related to the polar character of the electron-rich carbazolyl-based MPN. The selectivities of gas adsorption by applying Henry's law for CO_2/N_2 and CO_2/CH_4 at 25 °C were 13.4 and 2.9 for PTPTCz, 15.7 and 3.0 for PTPTCzSi, 12.4 and 3.0 PTPOcCz, and 15.8 and 2.7 PTPOcCzSi, respectively.

3.2.3. Electrochemical Characterization of the Monomers and Polymers at Pt Disc Electrodes

Next, the corresponding MPN films were fabricated by electrochemical, oxidative coupling of the four monomers. In the experiments, 0.1 mM monomer solutions in acetonitrile/dichloromethane (1:4) were used together with tetrabutylammonium perchlorate (TBAP) as supporting electrolyte in a conventional three-electrode cell. Multiple cyclic voltammograms

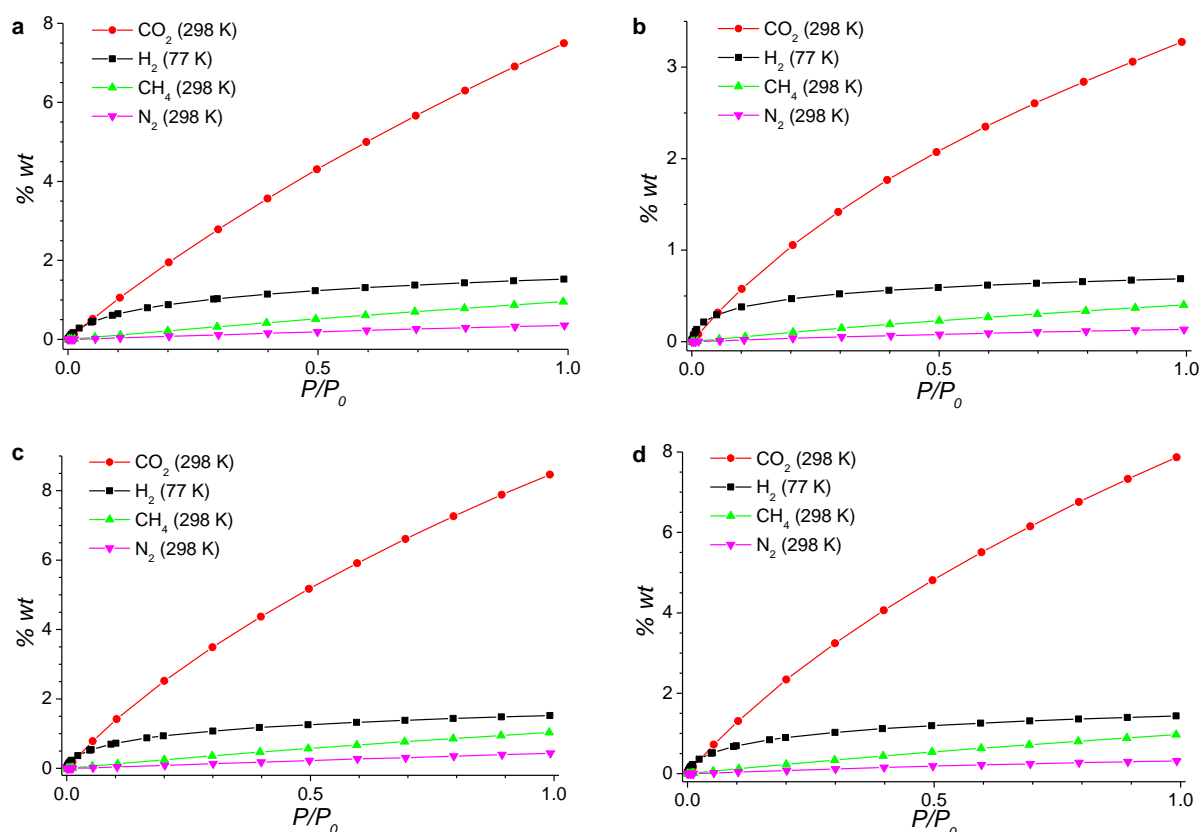


Figure 4. Gas adsorption isotherms for the bulk MPNs: PTPTCz (a), PTPTCzSi (b), PTPOcCz (c), and PTPOcCzSi (d).

were applied from -1.0 V to 1.1 V at a scan rate of 0.10 Vs⁻¹. Figure 5 shows the first anodic voltammograms during electropolymerization on Pt disc electrodes for all monomers. Herein, the first oxidation peaks are ascribed to the oxidation of carbazolyl groups into cation radicals followed by dimerization (radical coupling) and deprotonation of the coupled intermediates into 3,3'-dicarbazole linkages.¹⁸ Two important issues should be mentioned: (i) lower oxidation potentials are needed for both tetracarbazolyl monomers (TPTCz and TPTCzSi) if compared to the corresponding octacarbazolyl monomers (TPOcCz and TPOcCzSi). This may be related to the substitution pattern of the monomers: In the sterically demanding octacarbazolyl monomers a higher carbazolyl-phenyl distortion angle is expected. (ii) Higher oxidation current peaks are observed for the octacarbazolyl monomers in line with the double amount of electroactive carbazolyl groups. TPTCzSi showed a reduced peak current if compared to TPTCz probably caused by the low solubility of the monomer in the solvent mixture (0.1 mM concentration cannot be reached). Twenty successive cyclic voltammograms during polymerization of the monomers are depicted in Figure 6, where the successive cycling

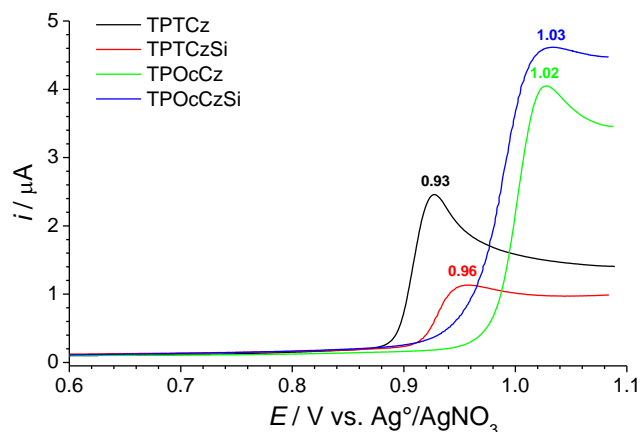


Figure 5. First anodic scan voltammograms for 0.1 mM solutions of the monomers and 0.1 M tetrabutylammonium perchlorate in acetonitrile/dichloromethane (1:4) at Pt disc electrodes. The voltammograms were recorded from 0 to 1.1 V with a scan rate of 0.10 V s^{-1} .

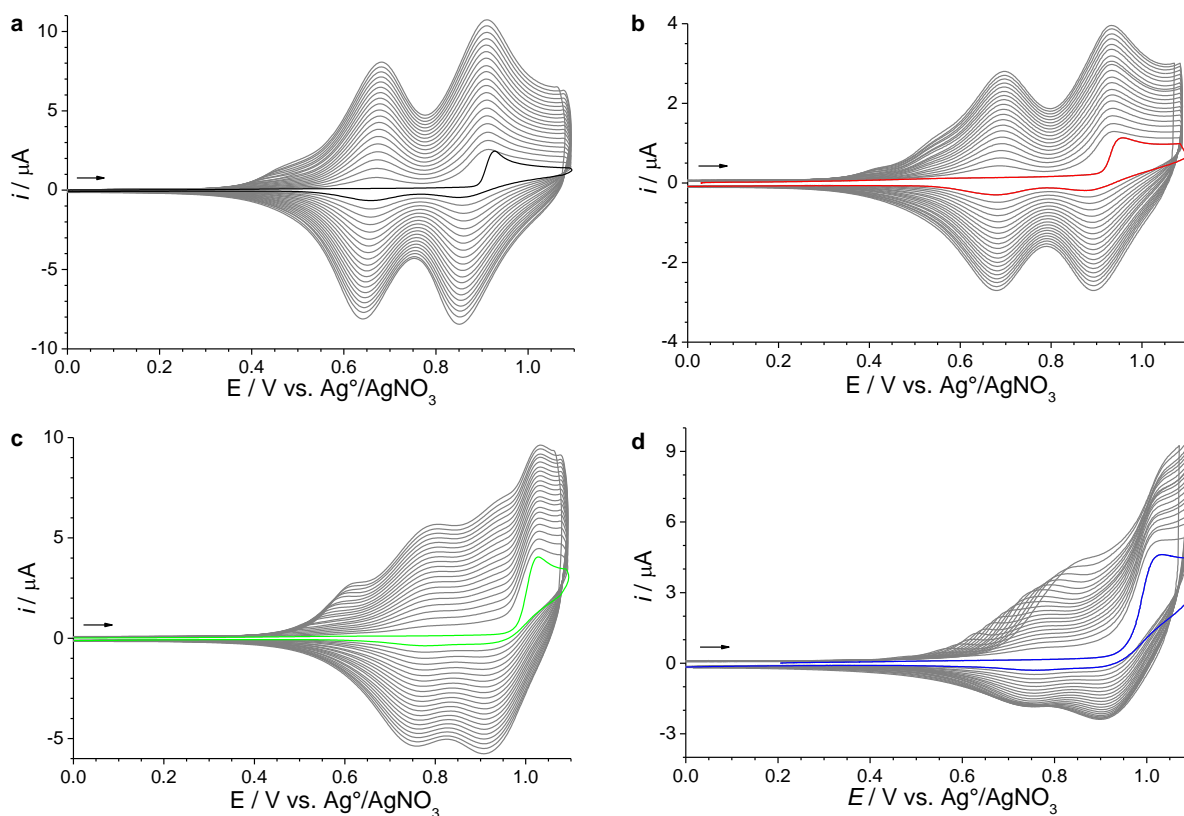


Figure 6. Twenty cyclic voltammograms at Pt disc electrodes for 0.1 mM solutions of TPTCz (a), TPTCzSi (b), TPOcCz (c) and TPOcCzSi (d) in acetonitrile/dichloromethane (1:4) mixtures and 0.1 M TBAP as supporting electrolyte. Cyclic voltammograms were recorded from -1.0 V to 1.1 V and scan rate of 0.10 V s^{-1} .

leads to a progressively increased current, thus reflecting the deposition and increasing thickness of the MPN films onto the electrode. In the case of both tetracarbazolyl monomers, two reversible peaks are clearly shown after the first cycle in the potential range of 0.5 V – 1.0 V. These peaks can be related to the doping/dedoping of the polymer film under formation of radical-cations (polarons) or dication (bipolarons).¹⁹ For the octacarbazolyl monomers, these peaks are still observed but they are less defined. Cyclic voltammograms at different scan rates (0.005 Vs⁻¹ – 0.20 Vs⁻¹) for the MPN deposits on Pt disc electrodes in monomer-free solutions (see Figure 7) show a linear relationship between peak current and scan rate characteristic of well-adhered polymer deposits where the current is not diffusion-controlled.²⁰

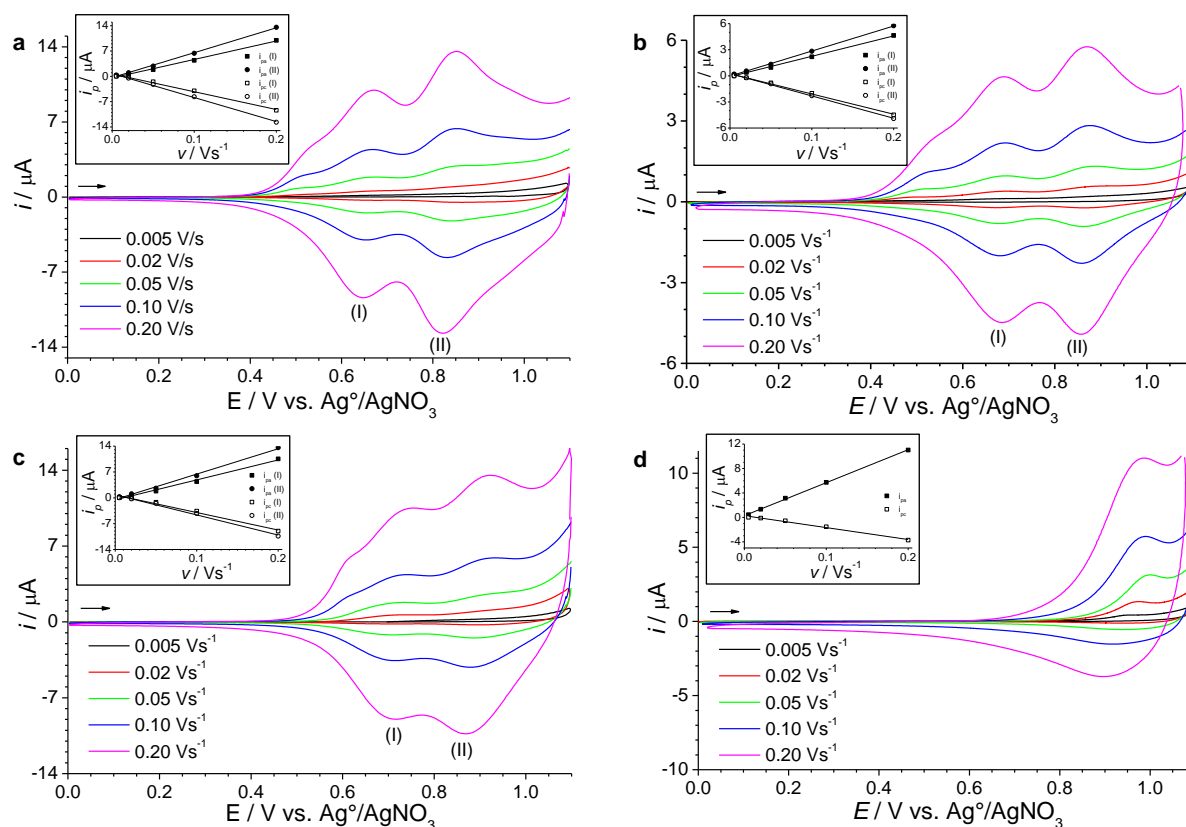


Figure 7. Cyclic voltammograms and linear dependence of peaks current and scan rate for deposits of PTPTCz (a, b), PTPTCzSi (c, d), PTPOCz (e, f) and PTPOCzSi (g, h), respectively, on Pt disc electrodes in monomer-free acetonitrile containing 0.1 M TBAP as supporting electrolyte. A potential range of 0 V – 1.1 V was used at different scan rates from 0.005 to 0.20 Vs⁻¹. The films were prepared as described in the caption of Figure 6.

3.2.4. Electrochemical Quartz Crystal Microbalance Studies of the Monomers and Polymers

The electrochemical quartz crystal microbalance (EQCM) technique, also called electrogravimetry, is a powerful method for the determination of very small mass changes (up to pg) at the electrode. The method can be coupled with simultaneous electrochemical measurements, e.g. cyclic voltammetry.²¹ The mass variations result from frequency changes (f) of a quartz crystal resonator. The frequency change is related to the mass variation by the Sauerbrey equation.²² A proportionality factor of 1.068 ng Hz^{-1} was used in the analysis of the experiments. Ten cyclic voltammograms of electropolymerization for the carbon-cored monomers (TPTCz and TPOcCz) at Pt/quartz electrodes were recorded under similar conditions as described in the previous section (see Figures 8a and 8d). The following features are worth mentioning: (i) During the first anodic scan, the frequency decrease starts at potentials of around 0.9 V corresponding to the oxidation of the electroactive carbazolyl units and subsequent deposition of the MPN films. (ii) As obvious in Figures 8b and 8e, the mass increase reflects the amount of MPN deposits on the Pt/quartz electrode during successive cycling. After the initial deposition during the first cycle, a constantly increasing mass is ob-

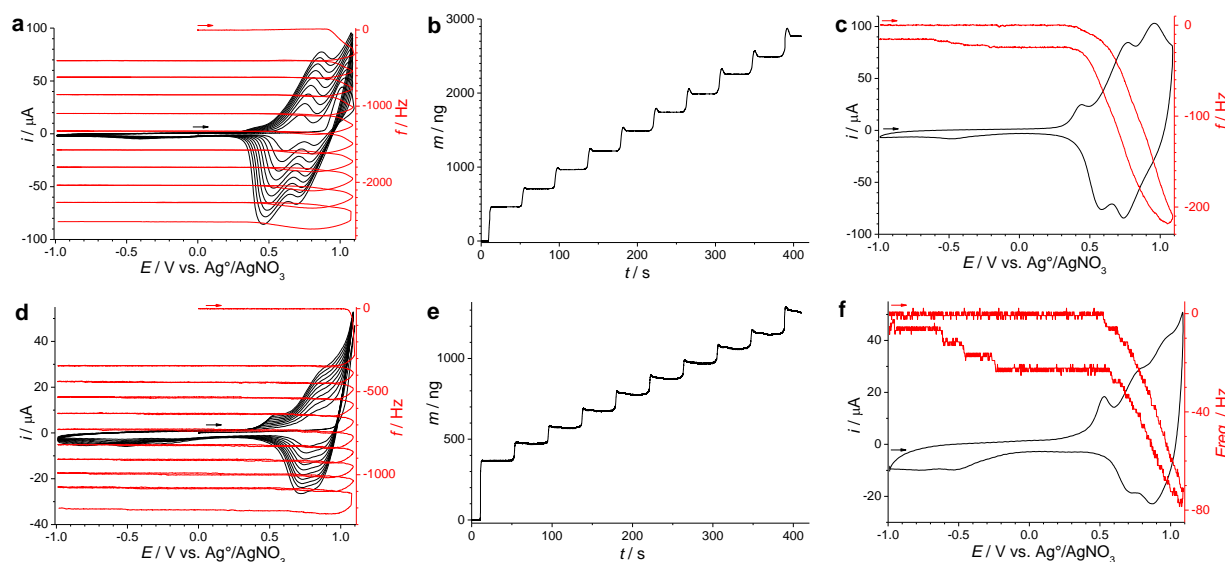


Figure 8. Ten cyclic voltammograms (black lines) and frequency changes (red lines), and mass accumulation in the electrochemical polymerization of 0.1 mM solutions of TPTCz (a, b) and TPOcCz (d, e), respectively, using 0.1 M TBAP in acetonitrile/dichloromethane (1:4) at Pt/quartz electrodes. Cyclic voltammograms (black lines) and frequency changes (red lines) for TPTCz (c) and TPOcCz (f) on Pt/quartz electrodes in a monomer-free solution of 0.1 M TBAP in acetonitrile. The cyclic voltammograms were recorded from -1.0 V to 1.1 V with a scan rate of 0.10 Vs^{-1} .

served pointing for a homogeneous film growth. (iii) Additionally, the mass plots clearly show gain and loss of mass at the beginning of each step which is related to uptake and release of counteranions (perchlorates) in doping/dedoping processes of the deposits thus reflecting the electroactivity of the material.²³ The amplitude of this effect increases with the number of cycles due to the increasing thickness of the film. Figures 8c and 8f depict cyclic voltammograms and frequency changes for MPN deposits in monomer-free solution (0.1 M TBAP in MeCN). The decreased frequency and increased mass during oxidation is related to a p-doping process with insertion of perchlorate counteranions into the MPN deposit, while during the following reduction, dedoping occurs as visible by an increased frequency due to the release of perchlorate counteranions into the solution. The hysteresis of the frequency scans and the slight mass increase at the turning point of the cycle should be related to the limited ion mobility and to an incomplete desorption of perchlorate anions due to ion trapping, respectively.²⁴ This phenomenon is more noticeable for TPOcCz than for TPTCz deposits. Similar results were obtained for the two silicon-cored monomers (see Figure 9).

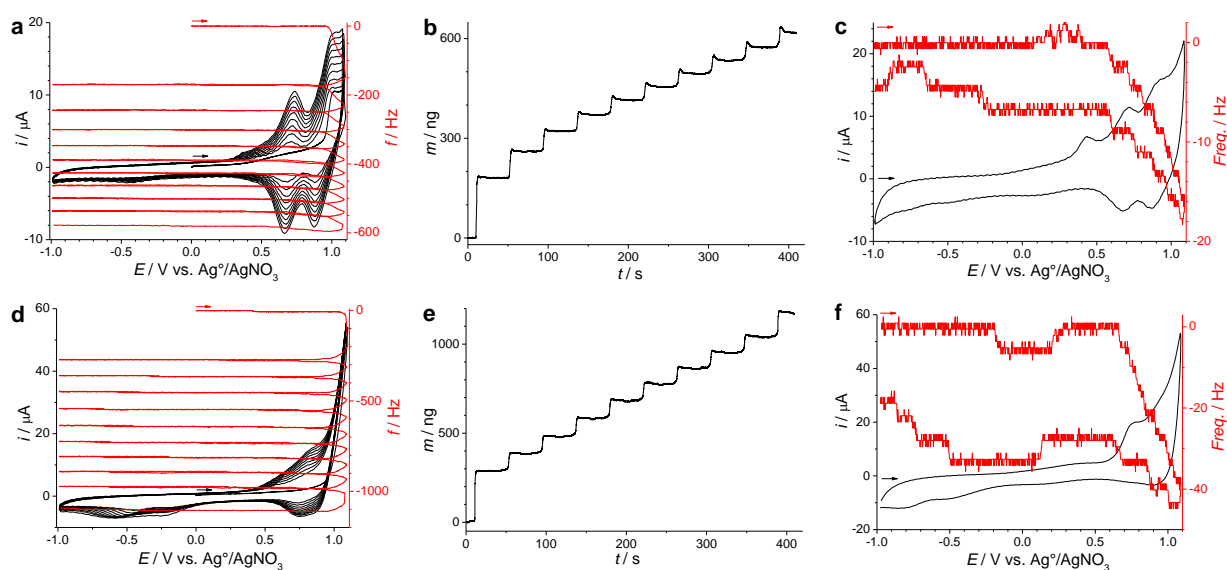


Figure 9. Ten cyclic voltammograms (black lines) and frequency changes (red lines), and mass accumulation in the electrochemical polymerization of 0.1 mM solutions of TPTCzSi (a, b) and TPOcCzSi (d, e), respectively, using 0.1 M TBAP in acetonitrile/dichloromethane (1:4) at Pt/quartz electrodes. Cyclic voltammograms (black lines) and frequency changes (red lines) for PTPTCzSi (c) and PTPOcCzSi (f) on Pt/quartz electrodes in a monomer-free solution of 0.1 M TBAP in acetonitrile. The cyclic voltammograms were recorded from -1.0 V to 1.1 V with a scan rate of 0.10 Vs⁻¹.

3.2.5. Porosity, Optical and Morphological Characterization of Electrogenerated MPN Films

Krypton adsorption isotherms at 77 K of thick films of the series of microporous polymer networks have been recorded and are shown in Figure 10a in the range of the relative pressure of 0 – 0.6. The free-standing, thick films were obtained by potentiostatic electrochemical polymerization of 0.5 mM monomer solutions in MeCN/DCM (1:4) applying an oxidative potential of 1.0 V (TPTCz and TPTCzSi) or 1.1 V (TPOcCz and TPOcCzSi) for 20 min. For comparison, nitrogen adsorption isotherms of their respective bulk polymers have been also recorded and are depicted in Figure 10b. Similar trends in the adsorption isotherms are observed for both series of polymers. First, a high gas uptake at low relative pressure (< 0.1) reflects once again the microporous nature of the films. Generally, slightly reduced specific surface areas were found for the films if compared to the bulk materials (see Table 2).

Moreover, the electrochemically accessible surface area (S_{EQCM}) of the MPN films were calculated by using the procedure describe by Ignaszac and co-workers.²⁵ Hereby, the S_{EQCM} values are related to the mass gain of the deposit during ion uptake (doping). In this case, perchlorate anions flow into the MPN deposits during oxidation as an equivalent to the positive charges formed during p-doping (see Figure 8c, 8f, 9c and 9f). As expected, much lower S_{EQCM} surface areas results if compared to the S_{BET} values (see Table 2). Nevertheless, similar trends are observed for both S_{BET} and S_{EQCM} with the highest values for PTPTCz and the lowest for PTPTCzSi films. The difference between both values might be explained as following: S_{BET} surface areas from gas sorption isotherms are based on physical sorption of

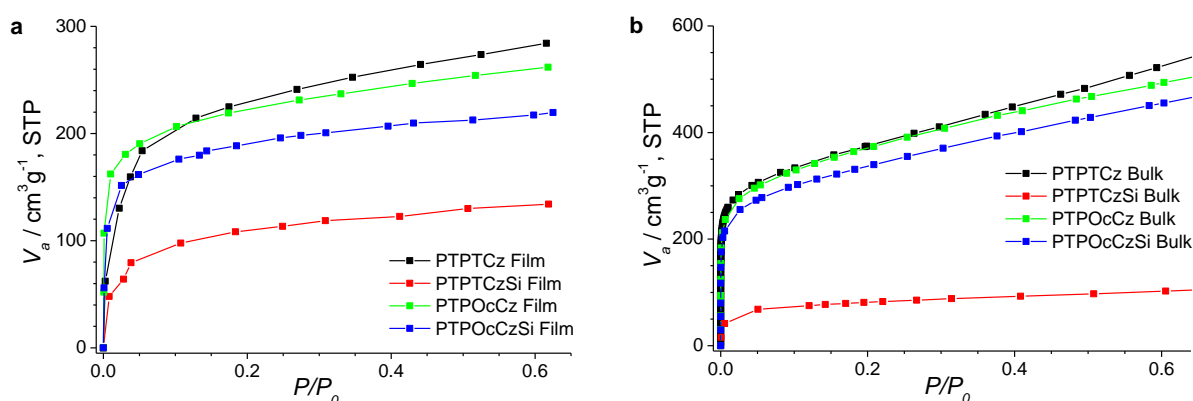


Figure 10. Adsorption isotherms of electropolymerized MPN films (a) and the corresponding bulk polymers synthesized by oxidative coupling with iron(III) chloride (b), using Kr or N_2 gas, respectively.

Table 2. Specific surface area obtained by using Kr gas adsorption isotherms and EQCM measurements of electrogenerated MPN films. All S_{BET} film measurements were carried out at least twice.

Films	S_{BET} [m ² g ⁻¹]	$S_{\text{EQCM}} (\text{ClO}_4^-)$ [m ² g ⁻¹]
PTPTCz	1106	92
PTPTCzSi	492	39
PTPOcCz	1027	46
PTPOcCzSi	872	44

gases in the bulk material, while S_{EQCM} surface areas from ionic uptake are based on electrostatic interactions between the charged material (oxidized or reduced) and the respective counterions. Basically, the latter technique is limited by the maximum doping level that is possible (often around 0.25 to 0.40)²⁶ thus reducing the calculated surface area.

FT-IR spectra of the series of bulk polymers and MPN films showed similar characteristic peaks in the range of 650 cm⁻¹ – 2000 cm⁻¹ (see Figure 11). Moreover, the emergence of a peak at ca. 800 cm⁻¹ (799 cm⁻¹ for the bulk polymers and 805 cm⁻¹ for the electrogenerated films) is usually attributed to the trisubstituted carbazole ring in both materials.^{27,28} Morphology studies of the MPN thin films were done by tapping mode AFM (see Figure 12). The films were prepared from 0.1 mM solutions of the monomers in MeCN/DCM (1:4) using 0.1 M TBAP as supporting electrolyte. Ten consecutive cyclic voltammograms in the potential range from -1.0 V to 1.0 V (TPTCz, TPTCzSi) or 1.1 V (TPOcCz, TPOcCzSi) were applied with a scan rate of 0.10 Vs⁻¹. Potentiodynamic electrochemical polymerization of the series of monomers on ITO resulted in the deposition of thin, smooth MPN thin films (one prerequisite for a potential application in organic electronic devices). The films show average surface roughness (Rq)/thickness of 3.6 nm/52 nm for PTPTCz, 6.7 nm/30 nm for PTPTCzSi, 4.2 nm/62 nm for PTPOcCz, and 4.8 nm/61 nm for PTPOcCzSi, respectively.

3.2.6. Electrochemical Reduction of Nitroaromatic Analytes at MPN-Modified Glassy Carbon Electrodes

In the previous Chapter,^{12,29} a correlation between the current response in the electrochemical reduction of 1,3,5-trinitrobenzene at MPN-modified glassy carbon (GC) electrodes and the specific surface area of the polymer deposit in aqueous solutions was demonstrated.^{11,26} Follo-

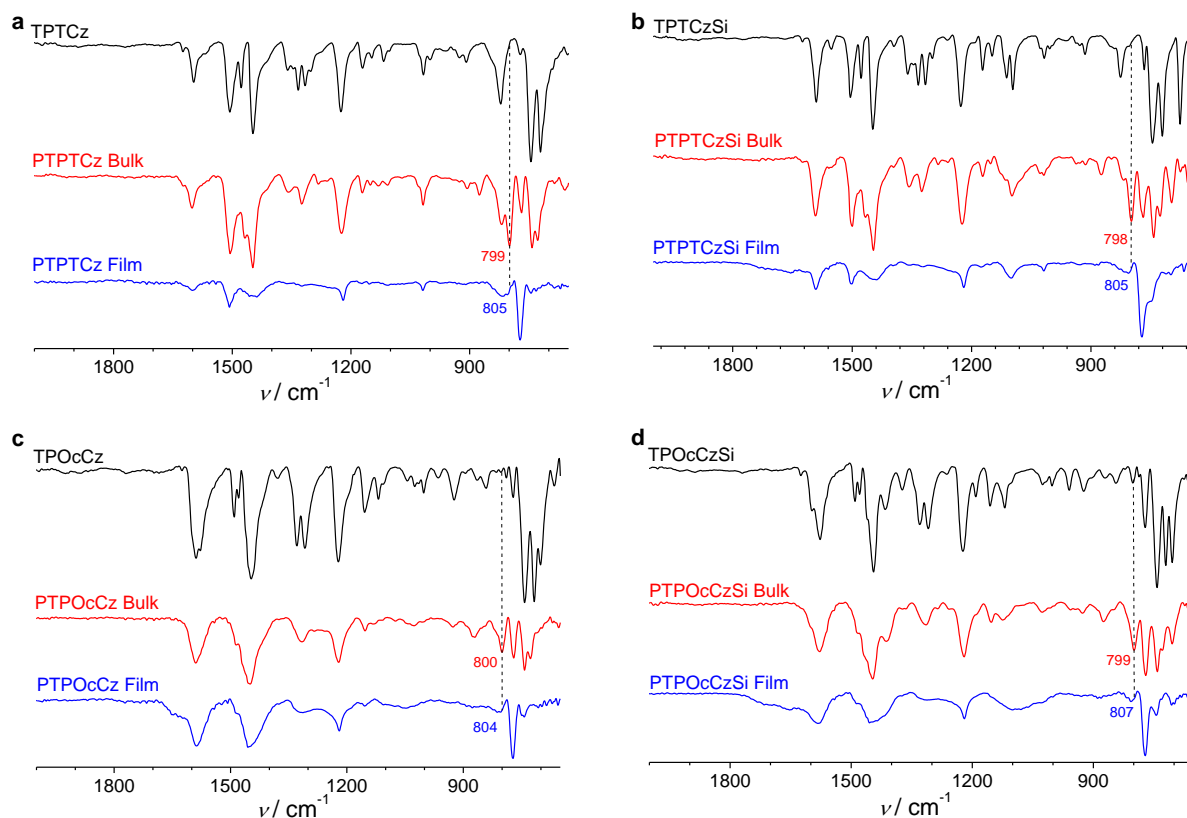


Figure 11. FT-IR spectra of the monomers: TPTCz (a), TPTCzSi (b), TPOcCz (c), TPOcCzSi (d) (black lines); the corresponding bulk MPNs (red lines), and the corresponding electrogenerated MPN films (blue lines).

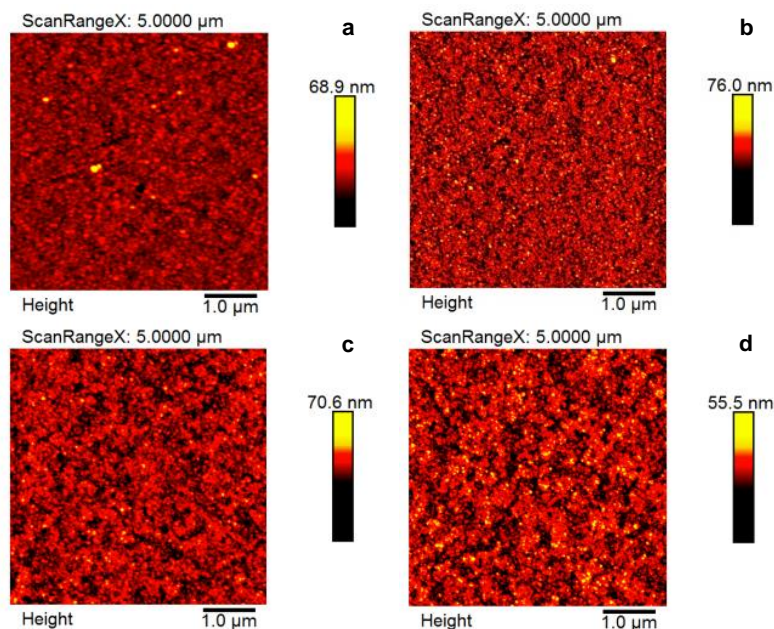


Figure 12. Tapping mode AFM images of MPN films on ITO: PTPTCz (a), PTPTCzSi (b), PTPOcCz (c), and PTPOcCzSi (d).

wing the same line, the electrochemical detection of various nitroaromatic analytes was carried out on GC electrodes modified with MPN films made from the herein described monomers. The MPN deposits were prepared by potentiostatic electrochemical polymerization of 0.1 mM monomer solutions in an acetonitrile/dichloromethane (1:4) mixture. An oxidative potential of 1.1 V was applied until an accumulative charge of 0.2 mC was reached (for all the materials). Next, linear scan voltammograms were recorded in buffered aqueous solutions (pH 7.4) containing 0.5 μM nitrobenzene (NB) within a potential range from 0 V to -1.0 V and scan rate of 0.01 Vs^{-1} (see Figure 13a). A single reduction peak is observed at a potential of -0.63 V to -0.65 V that is ascribed to the reduction of the nitro to hydroxylamine groups by uptake of four electrons.³⁰ Non-modified GC electrodes did not show any peak for the mentioned NB concentration again illustrating the increased sensitivity of the MPN-modified electrodes if compared to the bare GC electrode. This phenomenon might result from interfacial interactions between the electron-poor nitroaromatic compounds and the electron-rich dicarbazolyl groups of the microporous polymers.³¹ A clear correlation between the cathodic current in the reduction of NB and the S_{BET} values of the MPN structure

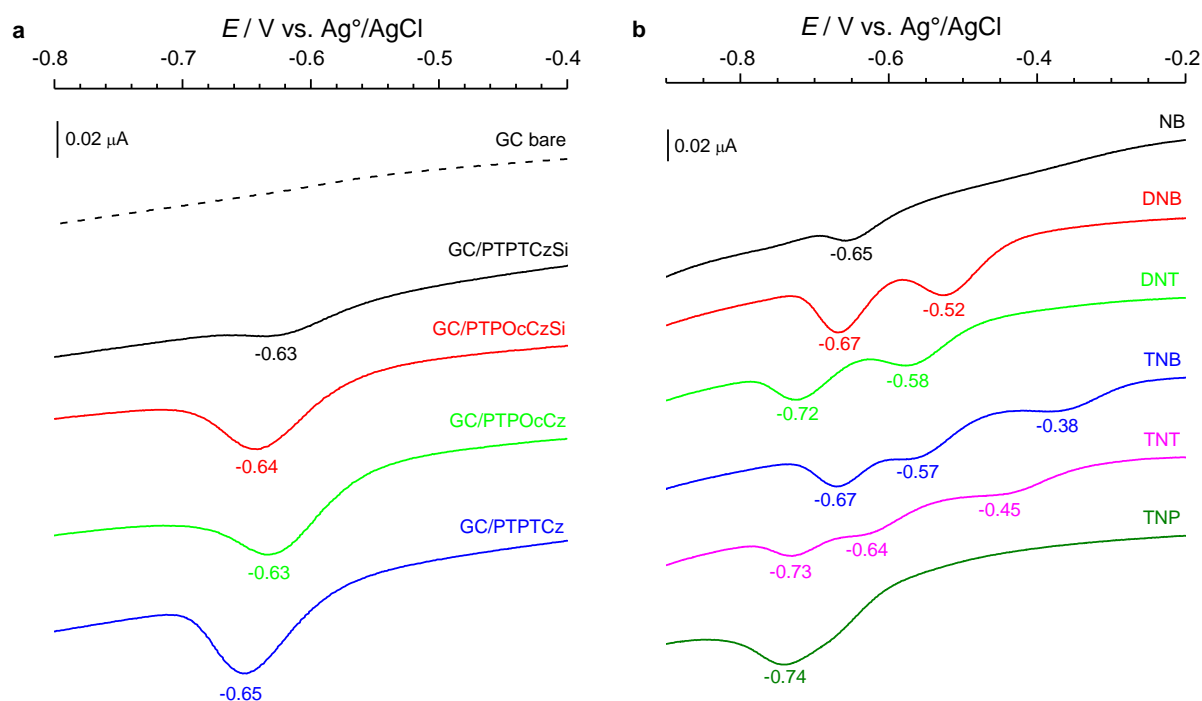


Figure 13. Linear scan voltammograms for the reduction of 0.5 μM NB at non-modified and MPN-modified GC electrodes (a), or for the reduction of 0.1 μM solutions of various, other nitroaromatic analytes at PTPTCz-modified GC electrodes (b), in buffered, aqueous solution (pH 7.4). LSVs were obtained with a scan rate of 0.01 V s^{-1} . The MPN deposits were prepared in MeCN/DCM (1:4) solution with an accumulative oxidation charge of 0.20 mC.

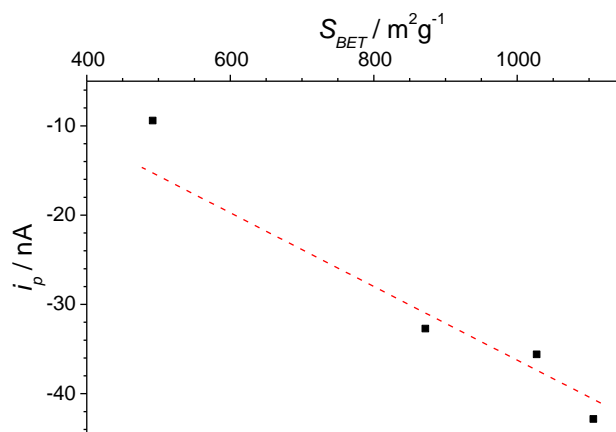


Figure 14. Dependence of the cathodic peak currents (after background correction) for the reduction of nitrobenzene at MPN-modified GC electrodes, on the specific surface areas (S_{BET}) of the polymer deposits.

that is used in the modification of GC electrodes was observed with the highest response for PTPTCz-modified GC electrodes (see Figure 14).

Finally, the sensitivity of the PTPTCz-modified GC electrodes was tested for lowered analyte concentrations of a series of mono-, di- and trinitroaromatic compounds. Figure 13b shows the LSVs for the reduction of 0.1 μM solutions of nitrobenzene (NB), 1,3-dinitrobenzene (DNB), 2,4-dinitrotoluene (DNT), 1,3,5-trinitrobenzene (TNB), 2,4,6-trinitrophenol (TNP) and 2,4,6-trinitrotoluene (TNT) at PTPTCz-modified GC electrodes. One, two or three reduction peaks were clearly observed even for low analyte concentrations (ppb range) corresponding to the reduction of one, two or three nitro-substituents, respectively. Strikingly, TNP only shows a single, broad peak. The reduction peak potential for NB was observed at -0.65 V, while DNB showed one reduction peak at similar potential (-0.67 V) and another one at a lower reduction potential of -0.52 V. Therefore, less energy is required for the initial interfacial charge-transfer between the electron-rich carbazolyl microporous polymer and the electron-poorer 1,3-dinitrobenzene if compared to nitrobenzene. As expected, TNB shows reduction peaks at -0.67 V, -0.57 V and an additional one at a lower reduction potential of -0.38 V. For DNT and TNT reduction peak potentials are found at -0.72 V and -0.58 V (DNT), and -0.73 V, -0.64 V and -0.45 V (TNT).

3.3. Conclusions

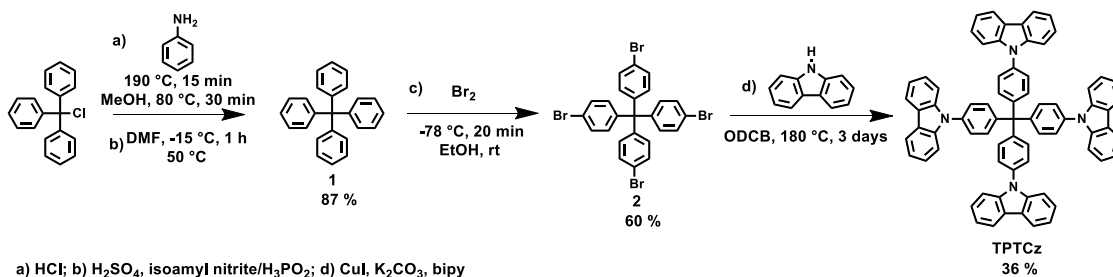
In summary, four carbon- or silicon-cored tetra- or octafunctional carbazolyl monomers were polymerized into microporous polymer networks by oxidative coupling, both chemical (FeCl_3) or electrochemical approach. The formation of MPNs (as powdery materials or homogeneous films) with high S_{BET} surface areas was observed for both methods. Hereby, the use of octacarbazolyl monomers resulted in MPNs with slightly increased surface areas in relation to the corresponding tetracarbazolyl polymers. On the other hand, silicon-cored monomers displayed the tendency to produce MPNs with reduced surface areas if compared to carbon-cored monomers. Electrochemical quartz microbalance (EQCM) studies showed stepwise deposition of the networks by potentiodynamic electropolymerization overlaid by doping/dedoping cycles. An expected reduced electrochemically accessible surface area (S_{EQCM}) was observed for all MPN films if compared to the S_{BET} values. Finally, MPN-modified GC electrodes were used for the electrochemical reduction of various nitroaromatic compounds (NACs) in aqueous environment up to analyte concentrations of 0.1 μM (ppb level).

3.4. Experimental Section

3.4.1. Monomers and Bulk Polymers

All reagents and chemicals were purchased from commercial companies, unless otherwise stated. ^1H and ^{13}C NMR spectra were obtained on a Bruker Avance 400 and III 600 machines. APLI mass spectra were recorded on a Bruker Daltronik micrOTOF system (KrF*-Laser ATLEX-SI, ATL Wermelskirchen), MALDI-TOF mass spectra on a Bruker Reflex TOF, and field desorption (FD) mass spectra on a VG Instruments ZAB2-SE-FPD. Thermogravimetric analyses were recorded under argon flow on a Mettler Toledo TGA/DSC1 STAR System. FT-IR and UV-vis spectra were recorded on a JASCO FT/IR-4200 and V-670, respectively. Photoluminescence spectra were obtained on a HORIBA Scientific FluoroMax-4 Spectrofluorometer. A Tousimis Samdri-795 system was used for washing the bulk polymers with supercritical carbon dioxide. Nitrogen and krypton adsorption-desorption isotherms were recorded on a BEL Japan Inc Belsorp-max system at 77 K. A maximum relative pressure of 0.6 was set for measurements with Kr gas. All samples were dried on a Belprep-vac II at 140 $^\circ\text{C}$ and ~ 2 Pa overnight prior to the gas sorption measurements. The data analysis was carried out with the software BELMaster Version 6.1.0.8. The average pore diameters were estimated from the pore distribution curves by applying a nonlocal density functional theory (NLDFT)

model. These curves are calculated by fitting theoretical adsorption isotherms (by using the integral isotherm equation) to the experimental isotherms in order to minimize errors.



3.4.1.1. Synthesis of tetraphenylmethane (1)

(Chloromethanetriyl)tribenzene (20 g, 71.7 mmol) and aniline (17.37 g, 187 mmol) were filled into a 500 mL round flask. The reaction mixture was slowly heated up to 190 °C under vigorous stirring. After 15 min, the reaction mixture was allowed to cool down to r.t. An aqueous solution of HCl 2M (80 mL) and methanol (120 mL) were added to the pulverized solid and the reaction mixture was heated to 80 °C for 30 min. After cooling down to r.t., the resulting solid was filtered off, washed with water and dried in vacuo (70 °C, 24 h). In a 1L round flask, the dry solid was suspended in DMF (200 mL) and cooled down to -15 °C. At this temperature, sulfuric acid 96% (22 mL) and isopentyl nitrite (17 mL) were added slowly and the resulting suspension was stirred for 1 h. Phosphinic acid 30% (60 mL) was added dropwise. Once the addition was completed, the reaction mixture was heated to 50 °C until the evolution of gas was ceased. Then, the solid was filtered off and washed twice with DMF, water and ethanol. The raw material was recrystallized from dichloromethane and dried in vacuo (70 °C, 24 h) to give white crystals, yield: 20 g (87 %). ¹H NMR (400 MHz, C₂D₂Cl₄) δ: 7.30-7.18 (m, 20H); ¹³C NMR (101 MHz, C₂D₂Cl₄) δ: 146.64, 130.97, 127.38, 125.72, 64.81.; MS (APLI) 320.146 [320.157] (M⁺).

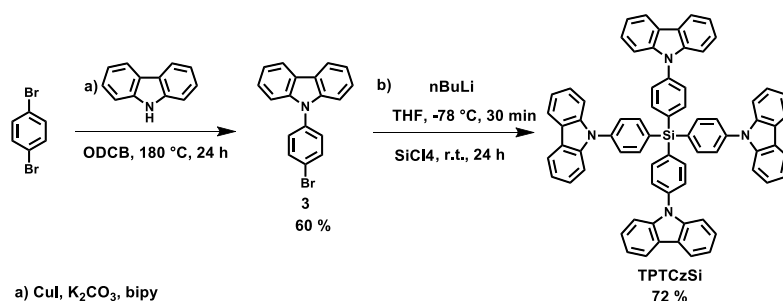
3.4.1.2. Synthesis of tetra(4-bromophenyl)methane (2)

To a 250 mL three-necked round-bottomed flask containing bromine (199 g, 1248 mmol), tetraphenylmethane (20 g, 62.4 mmol) was added in small portions under vigorous mechanical stirring at r.t. After the addition was completed, the resulting solution was stirred for 20 min and then cooled to -78 °C. At this temperature, ethanol (175 mL) was added slowly and the reaction mixture was allowed to warm up to r.t. overnight. Afterwards, the precipitate was filtered off and washed subsequently with saturated aqueous sodium hydrogensulfite solution and water. After drying in vacuo, the crude product was purified by

column chromatography on silica (eluent: hexane/dichloromethane 9.5:0.5) to give white crystals, yield: 25 g (60 %). ^1H NMR (600 MHz, $\text{C}_2\text{D}_2\text{Cl}_4$) δ : 7.42 (d, $J = 8.7$ Hz, 8H), 7.04 (d, $J = 8.7$ Hz, 8H); ^{13}C NMR (151 MHz, $\text{C}_2\text{D}_2\text{Cl}_4$) δ : 144.33, 132.15, 131.01, 120.53, 63.48.; MS (MALDI-TOF) 635.7 [635.8] (M^+).

3.4.1.3. Synthesis of tetra[4-(carbazol-9-yl)phenyl]methane (TPTCz)

Tetra(4-bromophenyl)methane (1.00 g, 1.58 mmol), carbazole (1.27 g, 7.56 mmol), copper(I) iodide (1.44 g, 7.56 mmol), potassium carbonate (2.62 g, 18.95 mmol) and 2,2'-bipyridine (0.12 g, 0.76 mmol) were placed in a 100 mL round flask and carefully degassed. 1,2-Dichlorobenzene (50 mL) was added, and the mixture was stirred under argon atmosphere and exclusion of light at 180 °C for 3 days. The hot reaction mixture was filtered through celite and washed with hot toluene. After evaporation of the solvent, the crude product was purified by column chromatography on silica, (eluent: hexane/chloroform 7:3) and recrystallized from a hexane/chloroform mixture. The product was isolated as slightly yellow powder, yield: 0.55 g (36 %). ^1H NMR (400 MHz, $\text{C}_2\text{D}_2\text{Cl}_4$) δ : 8.20 (d, $J = 7.7$ Hz, 8H), 7.77 (d, $J = 8.9$ Hz, 8H), 7.73 (d, $J = 8.9$ Hz, 8H), 7.63 (d, $J = 8.2$ Hz, 4H), 7.52-7.48 (m, 8H), 7.38-7.34 (m, 8H); ^{13}C NMR (101 MHz, $\text{C}_2\text{D}_2\text{Cl}_4$) δ : 144.92, 140.45, 135.82, 132.42, 126.03, 125.96, 123.19, 120.26, 120.13, 109.87, 64.42.; MS (APLI) 980.377 [980.388] (M^+).



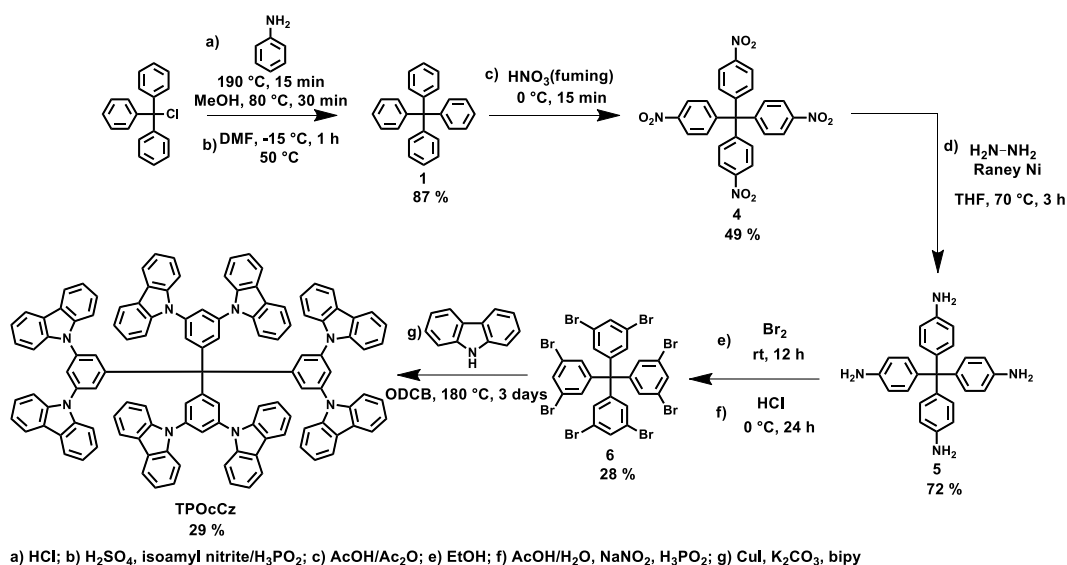
3.4.1.4. Synthesis of 9-(4-bromophenyl)-carbazole (3)

1,4-Dibromobenzene (14.11 g, 59.8 mmol), 9H-carbazole (5.00 g, 29.9 mmol), copper(I) iodide (0.57 g, 2.99 mmol), potassium carbonate (37.20 g, 269 mmol), 2,2'-bipyridine (1.21 g, 7.77 mmol) and o-dichlorobenzene (250 ml) were added under protective argon atmosphere and exclusion of light and stirred at 180 °C overnight. The hot reaction mixture was filtered over celite and washed with hot toluene. The residue was purified by silica gel column chromatography using hexane as the eluent to give a crystalline white solid, yield: 5.79 g (60 %) ^1H NMR (400 MHz, $\text{C}_2\text{D}_2\text{Cl}_4$) δ : 8.19-8.14 (m, 2H), 7.80-7.74 (m, 2H), 7.51-7.40 (m,

6H), 7.34 (ddd, $J = 7.99, 5.48, 1.36$ Hz, 2H); ^{13}C NMR (101 MHz, $\text{C}_2\text{D}_2\text{Cl}_4$) δ : 140.34, 136.49, 133.05, 128.44, 126.12, 123.15, 120.73, 120.28, 120.22, 109.53; MS (APLI) 321.007 [321.015] (M^+).

3.4.1.5. Synthesis of tetra[4-(carbazol-9-yl)phenyl]silane (TPTCzSi)

2.48 M n-BuLi in hexane (3.38 mL) was added dropwise to a solution of 9-(4-bromophenyl)-carbazole (3 g, 9.31 mmol) in dry THF (30 ml) at -78°C . After stirring for 1 h, tetrachlorosilane (0.32 g, 1.86 mmol) was added dropwise to the mixture. The mixture was allowed to warm up to r.t. and stirred overnight. The precipitate in the mother liquid was filtered and washed with water and dichloromethane to give a white solid, yield: 1.34 g (72 %). ^1H NMR (400 MHz, $\text{C}_2\text{D}_2\text{Cl}_4$) δ : 8.20 (d, $J = 7.65$ Hz, 8H), 8.10 (d, $J = 8.34$ Hz, 8H), 7.83 (d, $J = 8.33$ Hz, 8H), 7.66 (d, $J = 8.25$ Hz, 8H), 7.52-7.47 (m, 8H), 7.39-7.34 (m, 8H); ^{13}C NMR (101 MHz, $\text{C}_2\text{D}_2\text{Cl}_4$) δ : 140.31, 139.25, 137.91, 132.32, 126.22, 126.08, 123.30, 120.27, 109.92; MS (APLI) 996.356 [996.365] (M^+).



3.4.1.6. Synthesis of tetra(4-nitrophenyl)methane (4)

To 40 mL of fresh, fuming nitric acid (40 mL) maintained at 0°C , tetraphenylmethane (7.4 g, 23.09 mmol) was slowly added over 15 min followed by a mixture of acetic anhydride (12.5 mL) and acetic acid (25 mL) while maintaining the same temperature. Stirring was continued for another 15 min and the reaction mixture was diluted with acetic acid (50 mL) to precipitate the crude product, which was filtered off and washed with acetic acid (10 mL) to give a slightly orange solid, yield: 5.7 g (49 %). ^1H NMR (400 MHz, DMSO) δ : 8.26-8.21 (m,

8H), 7.63-7.58 (m, 8H); ^{13}C NMR (101 MHz, DMSO) δ : 150.99, 146.09, 131.46, 123.76, 65.25; MS (MALDI-TOF) 501.1 [500.1] (M^+).

3.4.1.7. Synthesis of tetra(4-aminophenyl)methane (5)

To tetra(4-nitrophenyl)methane (4.00 g, 7.99 mmol) in THF (250 mL), hydrazine monohydrate (5.00 g, 156 mmol) and Raney-nickel 50% (25 g) were added and refluxed at 70 °C for about 3 hours. The mixture was hot filtered and washed with ethanol. The solvent was evaporated and the residue was washed with ethanol and dried to give a white solid, yield: 2.2 g (72 %). ^1H NMR (600 MHz, DMSO) δ : 6.70-6.66 (m, 8H), 6.42-6.37 (m, 8H), 4.82 (s, 8H); ^{13}C NMR (101 MHz, DMSO) δ : 145.62, 135.83, 131.00, 112.55, 61.09; MS (MALDI-TOF) 379.4 [380.2] (M^+).

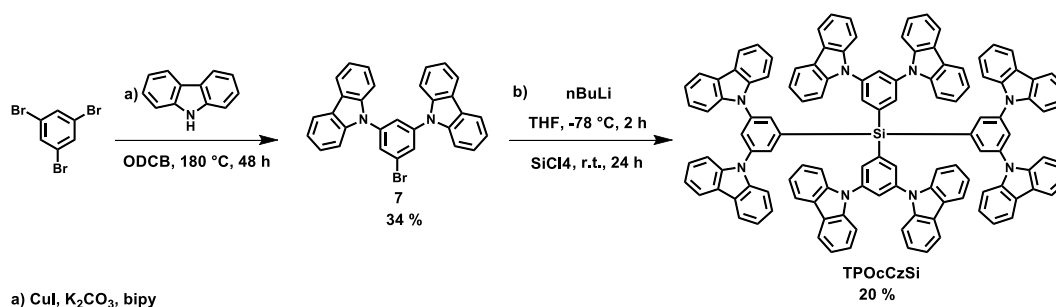
3.4.1.8. Synthesis of tetra(3,5-dibromophenyl)methane (6)

To a 100 mL round flask containing bromine (8.13 mL) at 0 °C, tetra(4-aminophenyl)methane (1.50 g, 3.94 mmol) was added in small portions under vigorous stirring. When the addition was completed, the resulting solution was stirred for 2 h at this temperature. Finally, chilled ethanol (50 mL) was slowly added and the reaction mixture was allowed to warm up to r.t. overnight. Afterwards, the precipitate was filtered off and washed subsequently with saturated aqueous sodium hydrogensulfite solution and water. After drying in vacuo, the violet solid was added in an ice-water cooled mixture of acetic acid (24 mL), water (10 mL) and concentrated HCl (3 mL), and then a solution of NaNO_2 in water (4 mL) was added dropwise. The reaction mixture was stirred for 30 min and then chilled solution of H_3PO_2 50% (25 mL) was added at 0 °C. After being stirred overnight at 0 °C, the reaction mixture was extracted with ethyl acetate. After drying over MgSO_4 and removal of the solvent, the crude product was purified by column chromatography on silica, (eluent: hexane/dichloromethane 9.5:0.5) to give a white solid, yield: 0.70 g (28 %). ^1H NMR (400 MHz, $\text{C}_2\text{D}_2\text{Cl}_4$) δ : 7.67 (t, $J = 1.64$ Hz, 4H), 7.18 (d, $J = 1.66$ Hz, 8H); ^{13}C NMR (151 MHz, $\text{C}_2\text{D}_2\text{Cl}_4$) δ : 146.84, 133.48, 131.79, 123.20, 63.32.; MS (FD) 950.5 [951.6] (M^+).

3.4.1.9. Synthesis of tetra[3,5-di(carbazol-9-yl)phenyl]methane (TPOcCz)

To a 100 mL two-necked round flask, tetra(3,5-dibromophenyl)methane (0.45 g, 0.473 mmol), 9H-carbazole (0.759 g, 4.54 mmol), copper(I) iodide (0.865 g, 4.54 mmol), potassium carbonate (1.569 g, 11.35 mmol) and 2,2'-bipyridine (0.071 g, 0.456 mmol) in *o*-dichlorobenzene (25 mL) were added under protective argon atmosphere and exclusion of light and were stirred at 180 °C during 3 days. The hot reaction mixture was filtered over celite and washed with hot toluene. The crude product was purified by column

chromatography on silica, (eluent: hexane/chloroform 7:3). Precipitation into ethanol from a dichloromethane solution gives a white solid, yield: 0.22 g (29 %). ^1H NMR (400 MHz, $\text{C}_2\text{D}_2\text{Cl}_4$) δ : 8.30 (d, $J = 1.3$ Hz, 8H), 8.14 (d, $J = 7.76$ Hz, 16H), 7.98 (t, $J = 1.3$ Hz, 4H), 7.24 (d, $J = 8.30$ Hz, 16H), 7.14 (t, $J = 7.55$ Hz, 16H), 6.33 (t, $J = 7.69$ Hz, 16H); ^{13}C NMR (101 MHz, $\text{C}_2\text{D}_2\text{Cl}_4$) δ : 149.34, 140.01, 139.61, 139.47, 126.32, 125.54, 123.34, 120.84, 120.39, 109.37, 67.22.; MS (APLI) 1641.547 [1641.623] (M^+).



3.4.1.10. Synthesis of 9,9'-(5-bromo-1,3-phenylene)bis(carbazole) (7)

To a 500 mL double-necked round flask, 1,3,5-tribromobenzene (10.00 g, 31.8 mmol), 9H-carbazole (10.62 g, 63.5 mmol), copper(I) iodide (12.10 g, 63.5 mmol), potassium carbonate (26.3 g, 191 mmol) and 2,2'-bipyridine (1.191 g, 7.62 mmol) in *o*-dichlorobenzene (250 ml) were added under protective argon atmosphere and exclusion of light and were stirred at 180 °C for 2 days. The hot reaction mixture was filtered over celite and washed with hot toluene. The residue was purified by silica gel column chromatography (eluent: hexane/dichloromethane 9:1). Recrystallization from ethanol/chloroform mixture gives white crystals, yield: 5.20 g (34 %) ^1H NMR (400 MHz, $\text{C}_2\text{D}_2\text{Cl}_4$) δ : 8.18 (d, $J = 7.69$ Hz, 4H), 8.09 (d, $J = 1.83$ Hz, 2H), 7.85 (t, $J = 1.81$, 1H), 7.59 (d, $J = 8.20$ Hz, 4H), 7.53-7.47 (m, 4H), 7.40-7.34 (m, 4H); ^{13}C NMR (101 MHz, $\text{C}_2\text{D}_2\text{Cl}_4$) δ : 140.05, 139.96, 134.27, 126.36, 124.32, 123.45, 120.72, 120.45, 109.54, 95.16; MS (APLI) 488.064 [488.073] (M^+).

3.4.1.11. Synthesis of tetra[3,5-di(carbazol-9-yl)phenyl]silane (TPOcCzSi)

2.48 M *n*-BuLi in hexane (1.86 mL) was added dropwise to a solution of 9,9'-(5-bromo-1,3-phenylene)bis(carbazole) (2.5 g, 5.13 mmol) in dry THF (30 ml) at -78°C . After stirring for 1 h, tetrachlorosilane (0.174 g, 1.03 mmol) was added dropwise to the mixture. The mixture was then allowed to warm up to r.t. and stirred overnight. After that, a saturated, aqueous NH_4Cl solution was added for stopping the reaction and the mixture was extracted with DCM. The combined organic solution was washed with water and dried over anhydrous Na_2SO_4 .

The crude product was purified by column chromatography on silica, (eluent: hexane/chloroform 7:3). Precipitation into ethanol from a dichloromethane solution gives a white solid, yield: 0.34 g (20 %). ^1H NMR (400 MHz, $\text{C}_2\text{D}_2\text{Cl}_4$) δ : 8.24 (d, $J = 1.88$ Hz, 8H), 8.13 (d, $J = 7.65$ Hz, 16H), 7.96 (t, $J = 1.75$, 1H), 7.27-7.20 (m, 32H), 6.99-6.91 (m, 16H); ^{13}C NMR (101 MHz, $\text{C}_2\text{D}_2\text{Cl}_4$) δ : 140.06, 139.88, 135.41, 132.62, 127.72, 126.29, 123.29, 120.59, 120.35, 109.09; MS (APLI) 1657.649 [1657.599] (M^+).

3.4.1.12. Synthesis of bulk polymers by oxidative coupling with FeCl_3

All monomers were chemically polymerized using the same methodology, here exemplarily described for the TPOcCz monomer: tetra[3,5-di(carbazol-9-yl)phenyl]methane (200 mg, 0.122 mmol) was dissolved in anhydrous chloroform (25 mL) and transferred dropwise to a 250 mL round flask which contains a suspension of iron(III)chloride (435 mg, 2.68 mmol) in anhydrous chloroform (25 mL). The resulting mixture was stirred at room temperature for one day under argon atmosphere. After addition of methanol (100 mL), the mixture was stirred for one more hour. The resulting precipitate was collected by filtration and washed with methanol. The powder was treated with aqueous hydrochloric acid (37 %) for 2 h, filtered off and washed with water and methanol. After Soxhlet extraction with methanol and THF for 24 h, the product was treated with ethanol (p.a.) for three days and finally washed with supercritical carbon dioxide. PTPOcCz was isolated as yellow powder, yield: 170 mg (85 %), PTPTCz as slightly yellow powder (95 %), PTPTCzSi as slightly yellow powder (87 %), and PTPOcCzSi as yellow powder (91 %).

3.4.2. Electrochemical Studies

Acetonitrile and dichloromethane (HPLC grade) were refluxed over calcium hydride and phosphorus pentoxide, respectively, for 3 h and distilled. Tetrabutylammonium perchlorate (TBAP, for electrochemical analysis, ≥ 99.0 %), phosphate buffered saline (PBS, pH 7.4), nitrobenzene (NB, analytical standard), 1,3-dinitrobenzene (DNB, analytical standard) and 2,4,6-trinitrophenol (TNP, $\geq 98\%$, moistened with water) were purchased from Sigma-Aldrich. 1,3,5-Trinitrobenzene (TNB, neat) was purchased from Supelco. Potassium chloride (KCl, ≥ 99.5 %, ACS) was purchased from Roth. Indium tin oxide-coated transparent electrodes on glass (ITO, ≤ 20 Ohm m^{-2}) were purchased from pgo. For electrochemical polymerization and characterization, an electrochemical workstation PAR VersaSTAT 4 was connected to a QCM922A oscillator (for EQCM experiments) and used in combination to a three-electrode cell. The AFM images were obtained with an atomic force microscope Bruker

diInnova operated in tapping mode. The average surface roughness and thickness of the films were extracted from the topography images.

3.4.2.1. Electrochemical polymerization and characterization on Pt disc and Pt/quartz crystal electrodes

10 mL of 0.1 mM solutions of the monomers were prepared in acetonitrile/dichloromethane (1:4) using 0.1 M TBAP as supporting electrolyte. The solutions were placed in a three-electrode cell under argon atmosphere at 25 °C. A platinum disc electrode (Pt, 1 mm diameter) or platinum sputtered quartz crystal electrode (5 mm diameter; nominal frequency 9.00 MHz \pm 30 kHz) was used as working electrode (WE); a platinum wire was used as counter electrode (CE). Ag⁰/AgNO₃ (0.1 M AgNO₃, 0.60 V vs NHE) was used as reference electrode (RE). Multiple cyclic voltammograms were repeatedly recorded in a potential range 0 – 1.1 V with a scan rate of 0.1 Vs⁻¹. The resulting deposits on Pt were placed as WE in 0.1 M solutions of TBAP in acetonitrile. Multiple cyclic voltammograms at different scan rates from 0.005 to 0.20 Vs⁻¹ were recorded in the potential range 0 – 1.1 V.

3.4.2.2. Electrochemical polymerization on ITO electrodes for porosity measurements and morphological characterization

10 mL of the monomers solutions were placed in a three-electrode cell. ITO (~ 1.5x1.2 cm deposit area) on glass and a platinum gauze (2.5x1.2 cm area), separated by 1 cm, were used as WE and CE, respectively; Ag⁰/AgNO₃ as RE. For krypton gas sorption measurements, thick films were produced by applying an oxidative potential of 1.0 V (TPTCz and TPTCzSi) or 1.1 V (TPOcCz and TPTOcCzSi) for 20 min. A potential of -1.0 V was applied after the electropolymerization for 60 s in order to dedoped the deposits. After rinsing the deposits with acetonitrile and dichloromethane, they were dried for 20 min at 100 °C. The collection of ca. 2 mg of material was necessary for reliable BET measurements. For morphological characterization, MPN films on ITO were prepared by applying ten cyclic voltammograms in the potential range of -1.0 V to 1.0 V (tetracarbazolyl monomers) or -1.0 V to 1.1 V (octacarbazolyl monomers) at scan rate of 0.01 Vs⁻¹. After rinsing the films with acetonitrile and dichloromethane, they were dried for 20 min at 100 °C.

3.4.2.3. Electrochemical polymerization on glassy carbon (GC) electrodes and electrochemical sensing of TNB

10 mL of a 0.1 mM solution of the monomers were placed in a three-electrode cell under argon atmosphere at 25 °C. A glassy carbon disc electrode (GC, 1 mm diameter) was used as working electrode (WE); a platinum wire as counter electrode (CE); and Ag⁰/AgNO₃ as

reference electrode (RE). Potentiostatic polymerization of the monomers was achieved by applying a potential of polymerization of 1.1 V until oxidative charge accumulation of 0.20 mC. A potential of -1.0 V was applied after polymerization during 60 s in order to discharge the deposits. After rinsing the deposits with acetonitrile and dichloromethane, the MPN-modified GC electrodes were used as WE in 10 mL solution of aqueous 0.2 M KCl and 0.1 M PBS under argon atmosphere at 25 °C. A platinum wire and Ag⁰/AgCl(sat.) (NaCl 3M, 0.21 V vs NHE) were used as CE and RE, respectively. After 5 min of stirring, a prepotential of 0 V was applied for 30 s. Linear scan voltammograms were recorded from 0 to -1 V with a scan rate of 0.01 Vs⁻¹. For detection of nitroaromatic compounds, aliquots from 100 μM stock solutions in acetonitrile were added to the buffered aqueous solutions in order to adjust the NACs concentration.

3.5. References

- (1) Palma-Cando, A.; Preis, E.; Scherf, U. *Macromolecules* **2016**, DOI: 10.1021/acs.macromol.6b02025.
- (2) Gu, C.; Huang, N.; Chen, Y.; Qin, L.; Xu, H.; Zhang, S.; Li, F.; Ma, Y.; Jiang, D. *Angew. Chem.* **2015**, *127*, 13798.
- (3) Räupe, A.; Palma-Cando, A.; Shkura, E.; Teckhausen, P.; Polywka, A.; Görrn, P.; Scherf, U.; Riedl, T. *Sci. Rep.* **2016**, *6*, 29118.
- (4) Palma-Cando, A.; Scherf, U. *Macromol. Chem. Phys.* **2016**, *217*, 827.
- (5) Gu, C.; Huang, N.; Chen, Y.; Zhang, H.; Zhang, S.; Li, F.; Ma, Y.; Jiang, D. *Angew. Chem. Int. Ed.* **2016**, *128*, 3101.
- (6) Ma, H.; Li, F.; Li, P.; Wang, H.; Zhang, M.; Zhang, G.; Baumgarten, M.; Müllen, K. *Adv. Funct. Mater.* **2016**, *26*, 2025.
- (7) Chen, Q.; Liu, D.-P.; Zhu, J.-H.; Han, B.-H. *Macromolecules* **2014**, *47*, 5926.
- (8) Sing, K. S. W. *Pure Appl. Chem.* **1985**, *57*, 603.
- (9) Lastoskie, C.; Gubbins, K. E.; Quirke, N. *J. Phys. Chem.* **1993**, *97*, 4786.
- (10) Olivier, J. P. *J. Porous Mater.* **1995**, *2*, 9.
- (11) Chen, Q.; Liu, D.-P.; Luo, M.; Feng, L.-J.; Zhao, Y.-C.; Han, B.-H. *Small* **2014**, *10*, 308.
- (12) Palma-Cando, A.; Scherf, U. *ACS Appl. Mater. Interfaces.* **2015**, *7*, 11127.
- (13) Preis, E.; Dong, W.; Brunklaus, G.; Scherf, U. *J. Mater. Chem. C* **2015**, *3*, 1582.

Chapter 3

- (14) Jiang, F.; Sun, J.; Yang, R.; Qiao, S.; An, Z.; Huang, J.; Mao, H.; Chen, G.; Ren, Y. *New J. Chem.* **2016**, *40*, 4969.
- (15) Traylor, T. G.; Hanstein, W. G.; Berwin, H. J. *J. Am. Chem. Soc.* **1970**, *92*, 7476.
- (16) Sekizkardes, A. K.; Culp, J. T.; Islamoglu, T.; Marti, A.; Hopkinson, D.; Myers, C.; El-Kaderi, H. M.; Nulwala, H. B. *Chem. Commun.* **2015**, *51*, 13393.
- (17) Qiao, S.; Du, Z.; Yang, R. *J. Mater. Chem. A* **2014**, *2*, 1877.
- (18) Ambrose, J. F.; Nelson, R. F. *J. Electrochem. Soc.* **1968**, *115*, 1159.
- (19) Brédas, J. L.; Street, G. B. *Acc. Chem. Res.* **1985**, *18*, 309.
- (20) Lin, K.; Ming, S.; Zhen, S.; Zhao, Y.; Lu, B.; Xu, J. *Polym. Chem.* **2015**, *6*, 4575.
- (21) Inzelt, G. In *Electrochemical Dictionary*; 1 ed.; Bard, A. J., Inzelt, G., Scholz, F., Eds.; Springer: Berlin, 2008, p 723.
- (22) Sauerbrey, G. *J. Physik* **1959**, *155*, 206.
- (23) Fulghum, T.; Karim, S. M. A.; Baba, A.; Taranekar, P.; Nakai, T.; Masuda, T.; Advincula, R. C. *Macromolecules* **2006**, *39*, 1467.
- (24) Weidlich, C.; Mangold, K. M.; Jüttner, K. *Electrochim. Acta* **2005**, *50*, 1547.
- (25) Mosch, H. L. K. S.; Akintola, O.; Plass, W.; Höppener, S.; Schubert, U. S.; Ignaszak, A. *Langmuir* **2016**, *32*, 4440.
- (26) Heinze, J.; Frontana-Urbe, B. A.; Ludwigs, S. *Chem. Rev.* **2010**, *110*, 4724.
- (27) Zhang, X.; Lu, J.; Zhang, J. *Chem. Mater.* **2014**, *26*, 4023.
- (28) Zhang, H.; Zhang, Y.; Gu, C.; Ma, Y. *Adv. Energy Mater.* **2015**, *5*, 1402175.
- (29) Palma-Cando, A.; Brunklaus, G.; Scherf, U. *Macromolecules* **2015**, *48*, 6816.
- (30) Laviron, E.; Meunier-Prest, R.; Vallat, A.; Roullier, L.; Lacasse, R. *J. Electroanal. Chem.* **1992**, *341*, 227.
- (31) Shamsipur, M.; Tabrizi, M. A.; Mahkam, M.; Aboudi, J. *Electroanalysis* **2015**, *27*, 1466.

Chapter 4

Electrogenerated MPNs from Tetrathiophene-based Monomers¹

Four thiophene-based monomers were synthesized by Stille- or Suzuki-type couplings followed by chemical or electrochemical polymerization into microporous polymer networks (MPNs) with high BET surface areas (S_{BET}). Similar S_{BET} values of up to 2020 and 2135 m^2g^{-1} were determined for tetraphenylmethane-cored bulk MPN powders and thin films, respectively. Electrochemical polymerization in boron trifluoride diethyletherate/dichloromethane mixtures allowed for the generation of MPN films with optimized porosity. Moreover, an interesting effect of boron trifluoride on the connectivity of the monomeric units during electropolymerization was observed for 3-thienyl-based monomers. Finally, the electrochemical reduction of 1,3,5-trinitrobenzene at MPN-modified glassy carbon (GC) electrodes showed increased cathodic responses compared to nonmodified GC electrodes due to interaction between electron-deficient nitroaromatic analyte and electron-rich MPN film. The influence of the specific surface area of MPNs on the electrochemical response was also studied for this class of materials.

4.1. Introduction

Microporous polymer networks (MPNs) have attracted enormous attention in the materials science community due to their promising properties: high surface area, well-distributed porosity, chemical and thermal resistance, possible incorporation of various functional groups, among others. Hence, MPNs promise a high application potential in gas capture and separation,²⁻⁷ catalysis,⁸⁻¹² organic electronic devices¹³⁻¹⁵ and sensors.¹⁶⁻¹⁸ Up to now, the highest BET surface area (S_{BET}) for a MPN material (6461 m^2g^{-1}) was reported by Zhou and co-workers¹⁹ for a network composed of interconnected tetraphenylsilane cores. However, synthesis of MPNs with surface areas of $> 2000 \text{ m}^2\text{g}^{-1}$ is still a challenge.²⁰ Thiophene-based MPNs are especially interesting due to their possible applications in electronic devices and for gas storage. Yu and co-workers²¹ reported thiophene-based MPNs for H_2 storage with S_{BET} of 971 m^2g^{-1} and H_2 uptake of 3.6 %wt at 77 K. Thomas and co-workers²² synthesized thienylene-arylene networks with S_{BET} of 1060 m^2g^{-1} . Nevertheless, these materials have been obtained as insoluble powders. Processing MPNs into thin films or layers is a major challenge towards many practical applications. A way to overcome the processing problems is an electrochemical polymerization of multifunctional monomers on a suited substrate. Until now,

mostly carbazole-based monomers have been electropolymerized due to their low oxidation potential. Ma and co-workers reported carbazole-based MPNs for use as charge injecting/extracting interlayers in OLEDs,²³ OPV devices,²⁴ and supercapacitors.²⁵ Jiang and co-workers reported MPN-based thin films with high S_{BET} values of up to $2190 \text{ m}^2\text{g}^{-1}$ (determined by Kr adsorption/desorption) for application in sensors^{26,27} or for the creation of energy transfer cascades.²⁸ In Chapter 2 and 3,^{29,30} a direct relation between the number of carbazole moieties in the monomer and the obtained S_{BET} of electrogenerated MPN films was described, as well as the use of the MPN films as electrochemical sensors for nitroaromatic analytes. On the other hand, the electrochemical polymerization of multifunctional thiophene monomers was first reported by Roncali and co-workers.³¹ The obtained 3D structures can show an increased electrical conductivity as demonstrated by Müllen and Heinze³² comparing 3D networks with weakly interacting aggregates of isolated terthiophene-substituted phenylene dendrimers. Thomas and co-workers³³ synthesized dithienothiophene-based microporous polymer films with interesting electrochromic properties by electropolymerization. In the electropolymerization of thiophene-based monomers, it has been shown that the necessary polymerization potential can be strongly reduced by adding boron trifluoride diethyletherate (BFEE) due to interactions between thiophene rings and boron trifluoride.³⁴⁻³⁷ Moreover, the mechanical and electrical properties of the resulting films were improved by using BFEE as additive.

In this Chapter, four tetrathienyl-substituted rigid monomers were synthesized in Stille- or Suzuki-type coupling reactions. Microporous polymer networks were obtained as powders by oxidative polymerization of the monomers with iron(III) chloride showing specific surface areas (S_{BET}) of up to $2020 \text{ m}^2\text{g}^{-1}$ from nitrogen gas sorption measurements. Optical and thermal properties as well as the gas sorption behavior are provided for these bulk MPNs. Corresponding, electrochemically generated MPN films were produced in boron trifluoride diethyletherate/dichloromethane mixtures showing S_{BET} values of up to $2135 \text{ m}^2\text{g}^{-1}$ (calculated from krypton gas adsorption/desorption). The MPN films produced in presence of boron trifluoride exhibit higher specific surface areas and a more defined electrochemical behavior if compared to the corresponding networks made in absence of boron trifluoride probably due to the exclusive formation of bithiophene connections. The thin films of the MPNs show a rather low surface roughness of only 3 nm – 5 nm for film thicknesses of 30 nm – 50 nm. Electrochemical reduction of 1,3,5-trinitrobenzene at glassy carbon electrodes

modified with the thiophene-based MPNs clearly indicates a direct relationship between specific surface area and current response via an adsorption-controlled interaction of the electron-poor nitroaromatic compound and the electron-rich thiophene-based MPN.

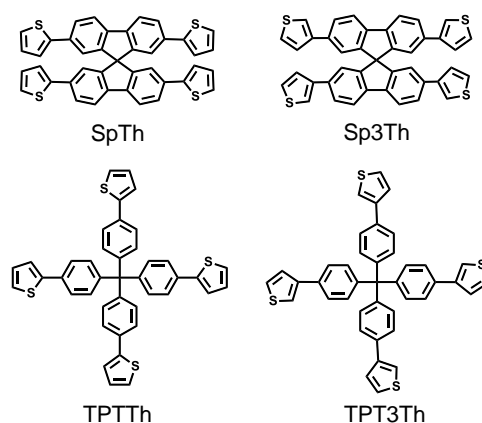
4.2. Results and Discussions

4.2.1. Synthesis of the Series of Monomers

Synthesis of tetrasubstituted thiophene-based monomers was carried out following literature procedures (see Experimental Section for details). Scheme 1 shows the chemical structures of the series of thiophene-based monomers studied. 2,2',7,7'-tetra(thien-2-yl)-9,9'-spirobifluorene (SpTh) and tetra[4-(thien-2-yl)phenyl]methane (TPTTh) were obtained by Stille-type coupling between 2,2',7,7'-tetrabromo-9,9'-spirobifluorene or tetra(4-bromophenyl)methane with tributyl(thien-2-yl)stannane. The corresponding 2,2',7,7'-tetra(thien-3-yl)-9,9'-spirobifluorene (Sp3Th) and tetra[4-(thien-3-yl)phenyl]methane (TPT3Th) monomers were synthesized by Suzuki-type coupling with thien-3-yl boronic acid.

4.2.2. Characterization of Chemically Synthesized Bulk Polymers

Oxidative chemical polymerization of the four monomers was carried out with iron(III) chloride in chloroform at room temperature to produce microporous polymers networks (MPNs) in high yields. Thermogravimetric analysis of all MPNs shows good stability up to 450 °C under argon (see Figure 1). Solid state $^{13}\text{C}\{^1\text{H}\}$ cross-polarization magic-angle spinning (CPMAS) spectra of the MPNs are depicted in Figure 2. All spectra well agree with the proposed chemical structures (insets). Peaks at ca. 65 ppm are attributed to the tetrasubstituted aliphatic carbons. Signals from 115 to 135 nm were related to protonated ben-



Scheme 1. Chemical structures of the investigated thiophene-based monomers.

Chapter 4

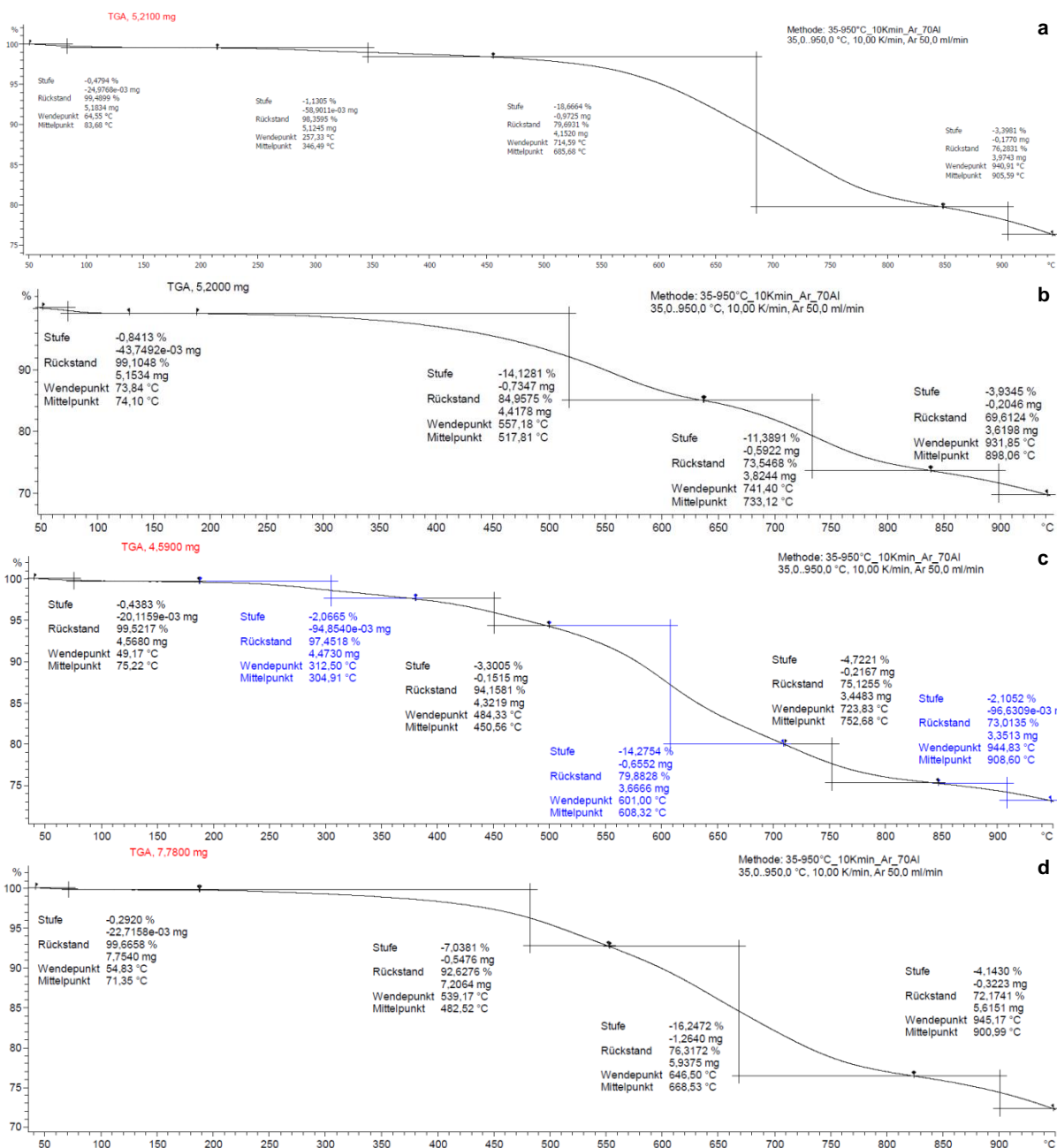


Figure 1. TGA plots of the bulk MPNs (made by FeCl_3 oxidation): PSpTh (a), PSp3Th (b), PTPTTh (c) and PTPT3Th (d).

zene and thiophene carbons, while signals at low field from 135 to 155 nm reflect nonprotonated aromatic carbons. UV-vis (diffuse reflection) and photoluminescence (PL) spectra are shown in Figure 3. The bulk polymers show broad PL bands with peak maxima at 524 nm (PTPTTh), 547 nm (PSpTh), 581 nm (PSp3Th), and 616 nm (PTPT3Th).

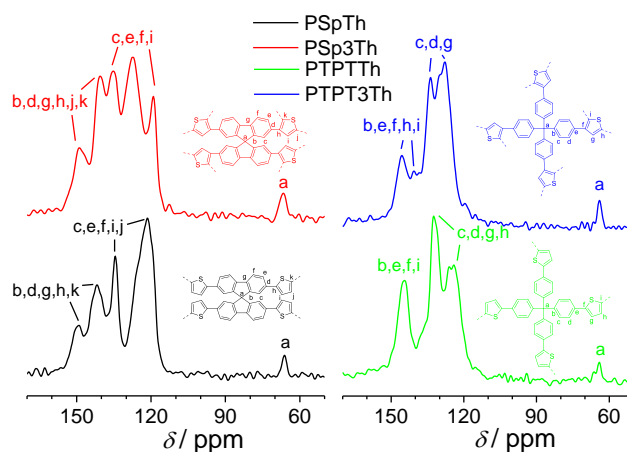


Figure 2. $^{13}\text{C}\{^1\text{H}\}$ CPMAS NMR spectra of bulk polymers.

The specific surface area of porous materials is usually determined by applying the Brunauer-Emmett-Teller (BET) equation to gas sorption isotherms at different temperatures.³⁸⁻⁴⁰ Figure 4 shows nitrogen adsorption/desorption isotherms for all bulk polymers. A combination of type I and II isotherms, according to the IUPAC,⁴¹ is observed for the MPNs as typical signature of microporous materials. Fast increase of volume of sorbate at relatively high pressure (> 0.9) is assigned to interparticular porosity (meso- and macropores).⁴² The specific surface areas were calculated by the BET equation (S_{BET}) and are listed in Table 1. A remarkably high S_{BET} of $2020 \text{ m}^2 \text{ g}^{-1}$, to the best of our knowledge the highest for thiophene-based MPNs, was obtained for PTPTTh which might be related to the presence of a largely continuous porous network. The latter assumption is supported by comparing S_{BET} values of the two MPNs made from 2-thienyl-substituted monomers that can only form bithiophene bridges in the oxidative coupling (SpTh and TPTTh in Scheme 1), with the values for the two MPNs made from 3-thienyl-substituted monomers that are able to form multiple linkages in 2- and 5-positions of the thiophene rings (Sp3Th and TPT3Th in Scheme 1). For both core

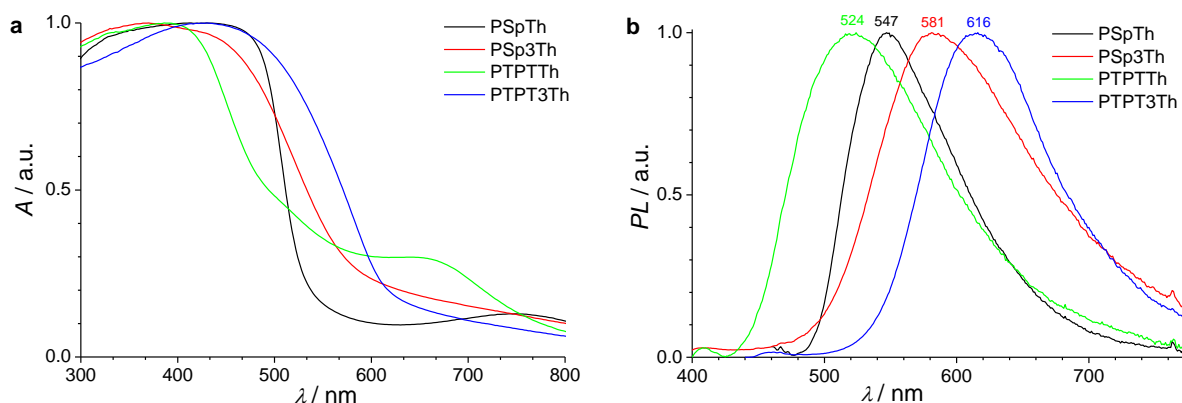


Figure 3. UV-vis (diffuse reflection mode) (a) and PL (b) spectra of the bulk polymers.

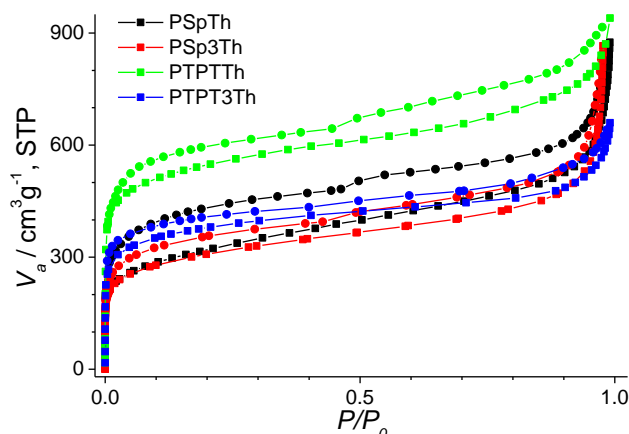


Figure 4. Nitrogen gas sorption isotherms of chemically synthesized MPN bulk polymers (oxidation with FeCl_3).

units, the S_{BET} values for the condensation products of the 2-thienyl-substituted monomers, PSpTh ($1153 \text{ m}^2\text{g}^{-1}$) and PTPTTh ($2020 \text{ m}^2\text{g}^{-1}$) are higher compared to PSp3Th ($1102 \text{ m}^2\text{g}^{-1}$) and PTPT3Th ($1390 \text{ m}^2\text{g}^{-1}$) made from 3-thienyl-substituted monomers. The effect is much more pronounced for tetraphenylmethane-cored MPNs (PTPTTh and PTPT3Th); their specific surface areas are generally higher as those of the corresponding spirobifluorene-cored MPNs (PSpTh and PSp3Th). The tetraphenylmethane-cored MPNs are characterized by a high structural symmetry, which may cause a more regular porosity and increased specific surface area of the MPNs.

MPNs possessing high specific surface areas might find applications in gas storage and separation (see Figure 5). The pore volumes of the materials are in the range of $0.82 - 1.22 \text{ cm}^3\text{g}^{-1}$ (see Table 1). Generally, higher gas uptakes for H_2 , N_2 , CH_4 and CO_2 are obtained for the tetraphenylmethane-cored MPNs. This difference can be partially related to different pore sizes of the materials which have been calculated from a non-local density functional theory (NLDFT) model resulting in pore diameters of ca. 1.43 nm for the tetraphenylmethane-cored MPNs and reduced pore diameters of ca. 0.40 nm for the spirobifluorene-cored MPNs. The selectivities of gas adsorption by applying Henry's law for CO_2/N_2 and CO_2/CH_4 at 298 K were 12.1 and 2.8 (SpTh), 11.5 and 2.6 (Sp3Th), 6.6 and 2.4 (PTPTTh), and 10.5 and 2.6 (PTPT3Th), respectively. Strikingly, the increased S_{BET} value of PTPTTh ($2020 \text{ m}^2\text{g}^{-1}$) leads to a reduced CO_2/N_2 selectivity (6.6) that is caused by an increased nitrogen uptake.

Electrogenerated MPNs from Tetrathiophene-Based Monomers

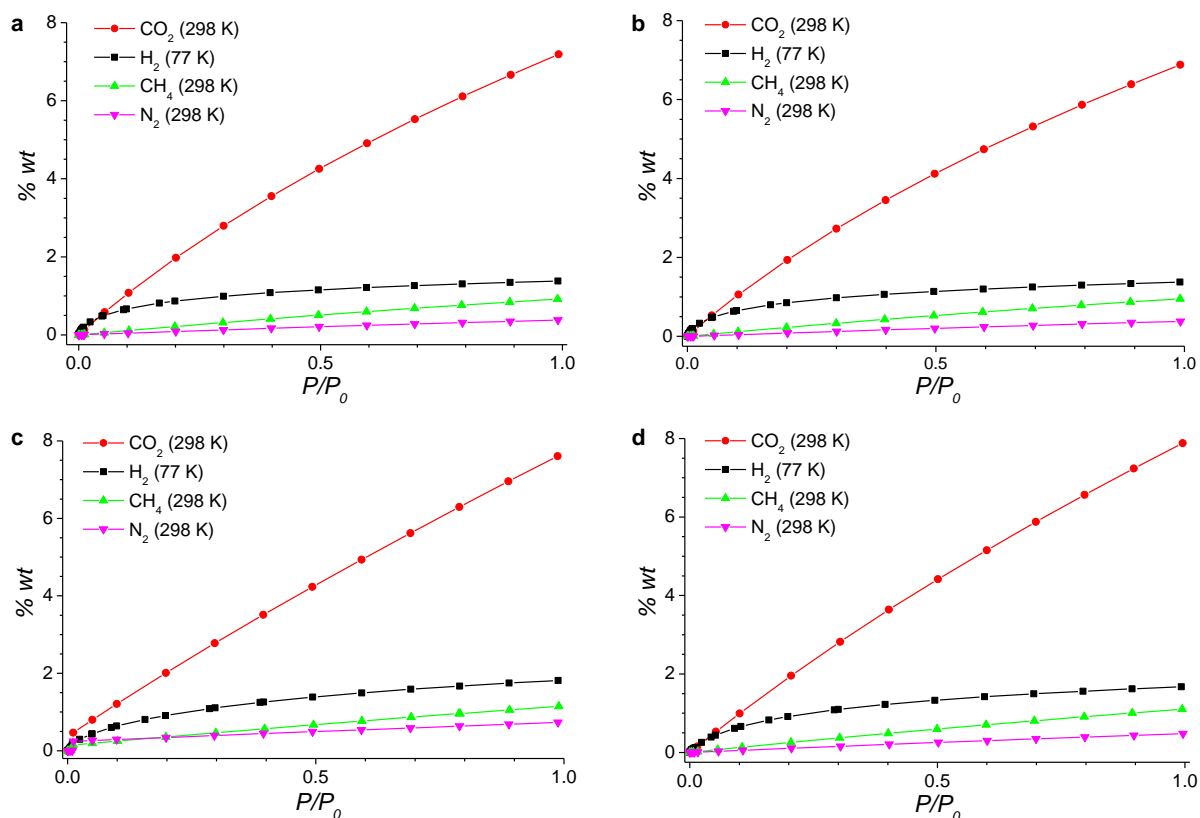


Figure 5. Gas adsorption isotherms for the bulk polymers: PSpTh (a), PSp3Th (b), PTPTTh (c) and PTPT3Th (d).

4.2.3. Electrochemical Characterization of the Monomers and Polymers at Pt Disc Electrodes

Electrochemical, oxidative polymerization is a proper technique for producing uniform thin films of MPNs on various electrodes in monomer/electrolyte mixtures.^{43,44} Several advantages over chemical polymerization exist, among others, a metal- and catalyst-free reaction, short reaction times, simultaneous film formation and deposition, simple doping and dedoping, and the possibility of in-situ characterization. Electrochemical polymerization of mostly bifunctional thiophene monomers into linear polymers has been extensively reported in relation to potential applications in the field of organic electronics (especially electrochromic devices).⁴⁵⁻⁴⁸ Only a few examples for the electrosynthesis of three-dimensional, conjugated polymer networks have been described, e.g. based on twisted bithiophene monomers with four 3,4-ethylenedioxythiophene (EDOT) substituents by Roncali and co-workers^{49,50} or Reynolds and co-workers.⁵¹

Table 1. Porosity data, gas uptake (at 298 K) and selectivity of chemically synthesized bulk MPNs.

Polymer	S_{BET} [m^2g^{-1}]	Pore volume ^a [cm^3g^{-1}]	Gas uptake [%]				Selectivity ^c	
			CO_2	N_2	CH_4	H_2 ^b	CO_2/N_2	CO_2/CH_4
PSpTh	1153	0.90	7.19	0.38	0.92	1.38	12.1	2.8
PSp3Th	1102	0.85	6.88	0.38	0.95	1.37	11.5	2.6
PTPTh	2020	1.22	7.61	0.73	1.15	1.81	6.6	2.4
PTPT3Th	1390	0.82	7.88	0.48	1.10	1.67	10.5	2.6

^a Determined at $P/P_0 = 0.95$; ^b Measured at 77 K; ^c Calculated by applying Henry's law^{16,52}

Herein, diluted solutions (0.1 mM) of the four thiophene-based monomers containing tetrabutylammonium tetrafluoroborate (TBABF₄) in either pure dichloromethane (DCM) or in a mixture of BFEE/DCM (1:4) were first potentiodynamically electropolymerized at platinum disc electrodes. Figure 6 shows the first anodic scan voltammograms for the electropolymerization of the monomers in DCM and BFEE/DCM (1:4). Two important issues should be mentioned: first, the onsets of the oxidation potential waves for the spirobifluorene-cored monomers are lower than the ones for the tetraphenylmethane-cored monomers (see Table 2). A more extended π -conjugated system in the spirobifluorene-cored monomers should cause the decreased oxidation potential. Second, the onset of the oxidation potential waves for all monomers is decreased by addition of BFEE (see Table 2). This phenomenon has been partially explained by a reduced aromaticity of thiophene rings in the presence of a Lewis acid.³⁶ Hereby, an interaction between the lone pair of the sulfur atom and boron tri-

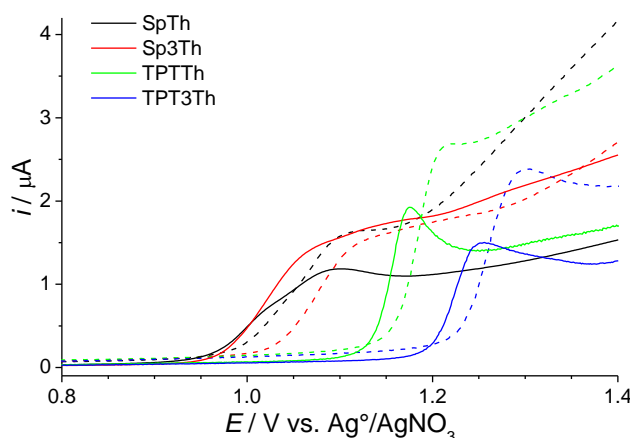


Figure 6. First anodic scan voltammograms for 0.1 mM solutions of the monomers and 0.1 M TBABF₄ in DCM (dashed lines) and BFEE/DCM (1:4) (solid lines) at Pt disc electrodes, the voltammograms were recorded from 0 V to 1.4 V with a scan rate of 0.10 V s⁻¹.

Table 2. Onset potential for electrochemical polymerization of thiophene-based monomers in dichloromethane and BFEE/DCM (1:4) solutions.

Monomer	E_{onset} [V] vs $\text{Ag}^{\circ}/\text{AgNO}_3$		ΔE [mV]
	DCM	BFEE/DCM	
SpTh	0.99	0.96	30
Sp3Th	1.04	0.98	60
TPTTh	1.16	1.11	50
TPT3Th	1.23	1.20	30

fluoride leads to this decreased aromaticity, thus causing the diminished oxidation potential. Cyclic voltammograms for electropolymerization of the monomer solutions in DCM and BFEE/DCM (1:4) at Pt disc electrodes are shown in Figure 7. Repeated scans allowed the consecutive deposition of MPN films on the electrode under observation of progressively increasing anodic and cathodic currents.⁵³ For SpTh and TPTTh monomers, a quite reversible redox behavior was observed for the deposited MPNs made in presence of boron trifluoride

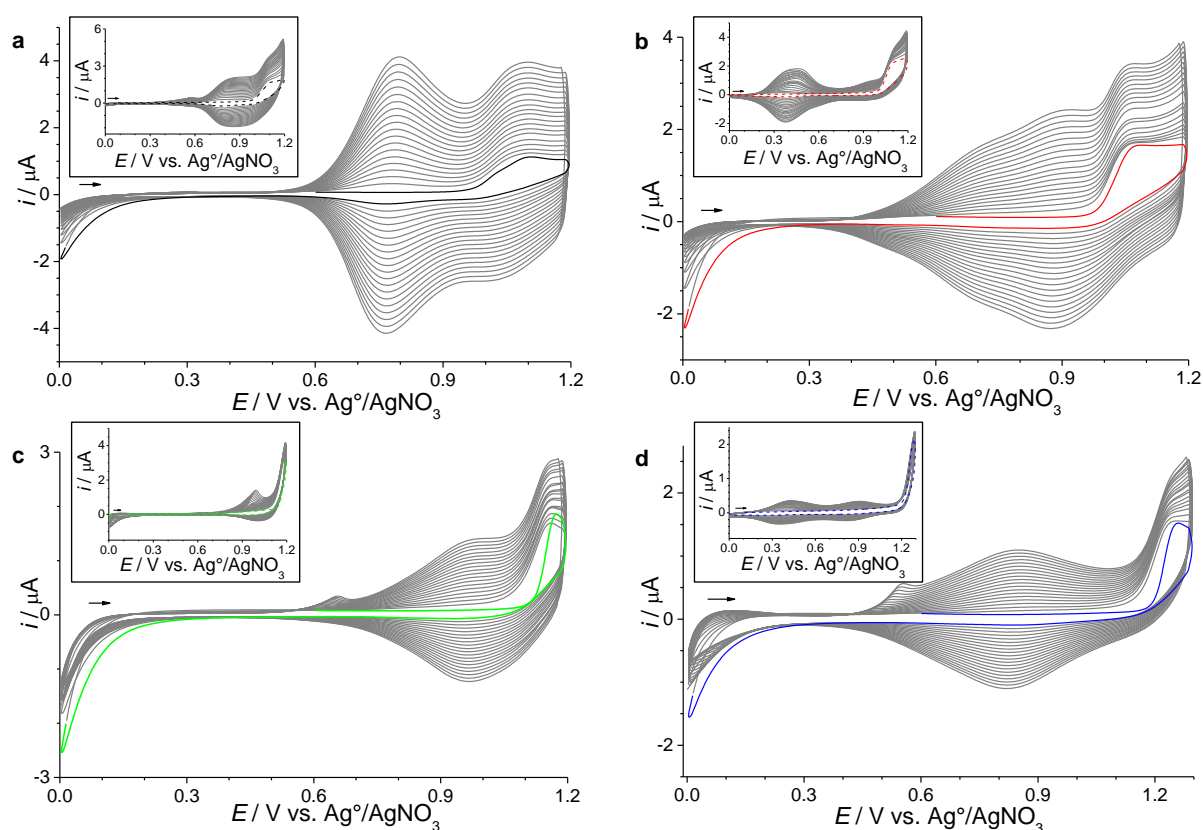
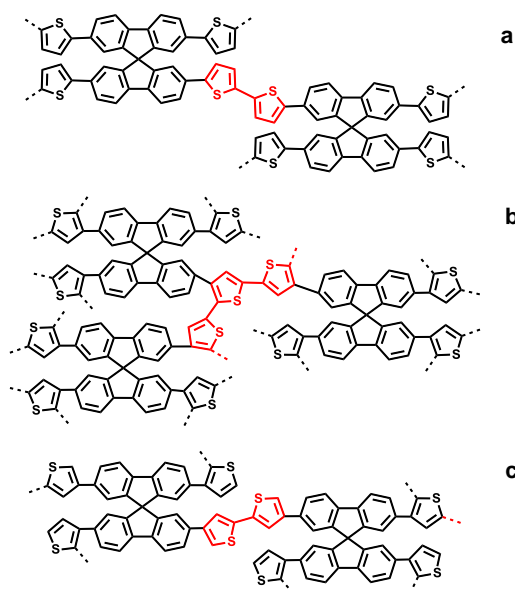


Figure 7. Twenty consecutive cyclic voltammograms at Pt disc electrodes for 0.1 mM SpTh (a), Sp3Th (b), TPTTh (c); potential range: 0 V to 1.2 V, and TPT3Th (d); potential range: 0 V to 1.3 V, and 0.1 M TBABF₄ in BFEE/DCM (1:4) mixtures. The scan rate was 0.10 Vs⁻¹. The insets show twenty consecutive cyclic voltammograms for the corresponding monomers in DCM solutions.

between 0.6 V and 1.1 V. The observed redox response is assigned to the formation of 2,2'-bithiophene bridges (see Scheme 2a). When comparing the voltammograms of electropolymerization with and without boron trifluoride for the 3-thienyl-substituted monomers (Sp3Th and TPT3Th), the occurrence of an additional redox peak at lower oxidation potential between 0.2 V and 0.6 V is observed for the polymerization of monomer solutions in DCM (without BFEE) that can be ascribed to the formation of branched oligothiophene connections via linking 2- and 5-positions of the 3-thienyl substituents (see Scheme 2b).⁴³ In contrast, cyclic voltammograms for electropolymerization of the same monomers in presence of boron trifluoride showed a complete disappearance of these peaks. The observed behavior may indicate that the coupling reaction is limited, in presence of boron trifluoride, to a dimerization of 3-thienyl substituents as a result of an interaction between Lewis acid and thiophene rings (see Scheme 2c). Cyclic voltammograms for the resulting MPN deposits on Pt disc electrodes in monomer-free DCM solutions are shown in Figure 8 at different scan rates from 0.005 Vs⁻¹ to 0.20 Vs⁻¹. A linear relationship between peak current and scan rate was observed for all deposits, a characteristic behavior of electroactive materials deposited on an electrode where the current is not diffusion-controlled.⁵⁴



Scheme 2. Idealized chemical structures of PSp3Th (a), PSp3Th prepared in DCM (b), and PSp3Th prepared in BFEE/DCM (c).

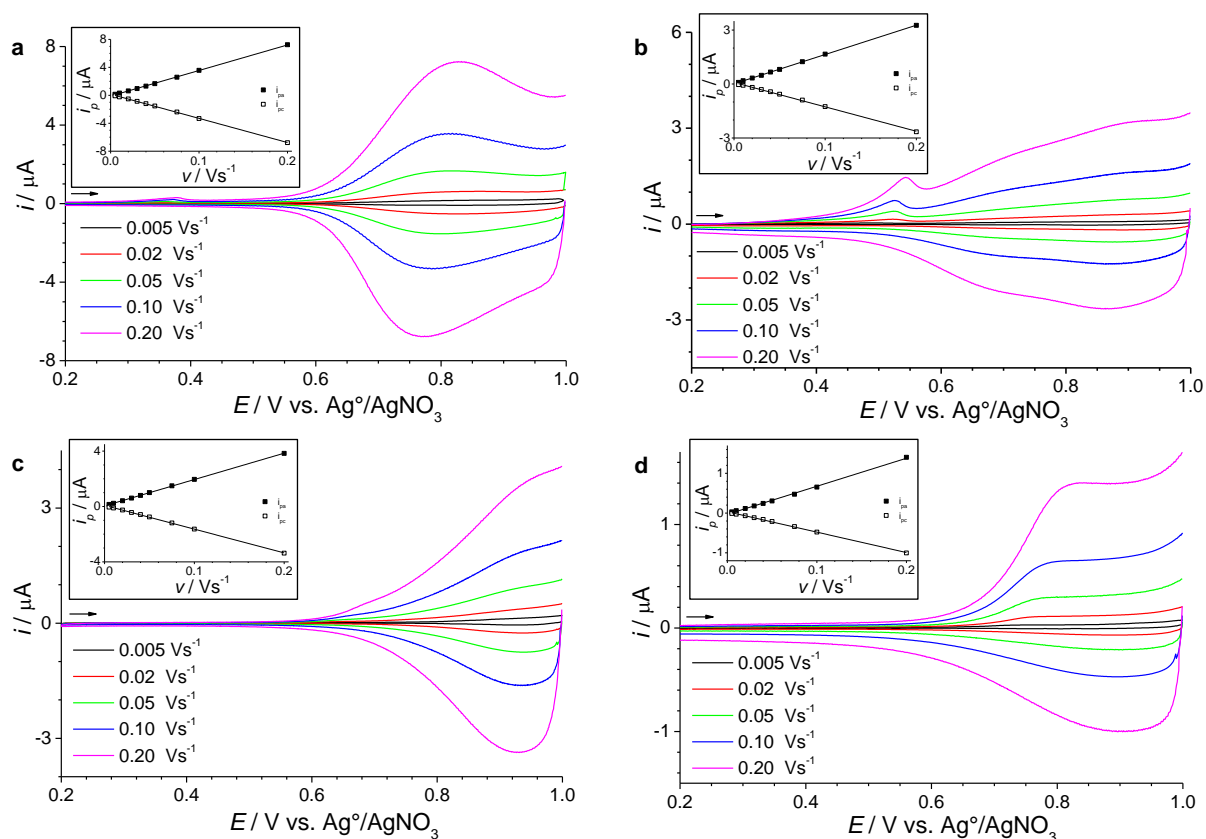


Figure 8. Cyclic voltammograms for PSpTh (a), PSp3Th (b), PTPTTh (c) and PTPT3Th (d) on Pt disc electrodes within the potential range of 0 V – 1 V at various scan rates from 0.005 to 0.20 Vs^{-1} , in monomer-free DCM containing 0.1 M TBABF₄. The films were prepared in BFEE/DCM (1:4) as described in the caption of Figure 7. The insets show the corresponding peak current vs scan rate plots.

4.2.4. Porosity, Optical and Morphological Characterization of Electrogenerated MPN Films

Potentiostatic electrochemical polymerization of 0.5 mM monomer solution in DCM with or without BFEE for twenty minute yielded thick, free-standing films which were collected in their dedoped state for the determination of the specific surface area by adsorption/desorption experiments. Around 2 mg of the materials were required for a reliable determination in krypton sorption experiments at 77 K. Krypton gas has a low saturation pressure of 2.5 torr at 77 K which is essential for a precise characterization of only small amounts of porous materials.²⁶ Figure 9 shows the adsorption isotherms in the P/P_0 range 0 – 0.6 using Kr gas at 77 K for all of the thiophene-based MPNs. Similar shapes of the isotherms were observed for all films, regardless the polymerization conditions (with or without BFEE). Alike their chemically synthesized counterparts, at low relative pressure (0 – 0.1) a quick uptake of sorbate gas (N_2 or Kr) was observed which is an indication of permanent microporous mate-

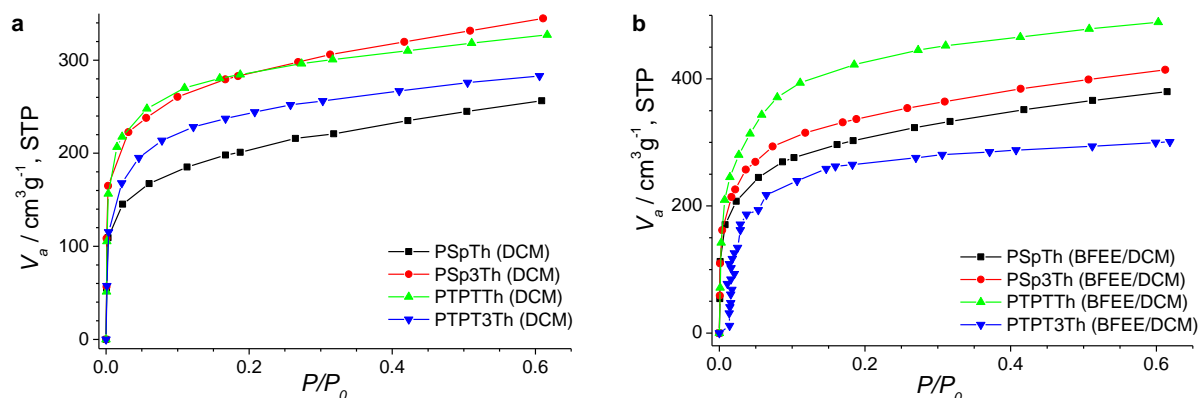


Figure 9. Kr gas adsorption isotherms of electropolymerized MPN films prepared in DCM (a) and BFEE/DCM mixtures (b).

rials.⁵⁵ Concerning the S_{BET} values determined by applying the BET equation, higher values were obtained for MPN deposits produced in the presence of boron trifluoride (see Table 3). For PSpTh and PTPTTh, S_{BET} values of 815 and 1258 m^2g^{-1} , respectively, were obtained for deposits produced in absence of boron trifluoride. These values are much lower compared to their corresponding chemically synthesized counterparts (PSpTh: 1153 m^2g^{-1} and PTPTTh: 2020 m^2g^{-1}). The reduced microporosity could be possibly explained by an incomplete crosslinking of thienyl groups or an overoxidation of the materials at the applied potential of 1.2 V. The addition of BFEE to the polymerization solution led to a significantly increased microporosity with S_{BET} values of 1240 and 2135 m^2g^{-1} for PSpTh and PTPTTh, respectively. This means, that the addition of boron trifluoride not only decreases the necessary oxidation potential for polymerization but allows for the formation of deposits with increased microporosity. Hereby, BF_3 -derived anionic species may act as stabilizing counterions during

Table 3. Calculated BET surface areas of electropolymerized MPN films, prepared in DCM and BFEE/DCM (1:4), by using Kr gas sorption. All S_{BET} film measurements were carried four times. Optical and electrochemical data of the MPN films prepared in BFEE/DCM (1:4).

MPN films	S_{BET} [m^2g^{-1}]		$E_{\text{g}}^{\text{opt } a}$ [eV]	HOMO ^{elec} ^b [eV]	LUMO ^c [eV]
	DCM	BFEE/DCM			
PSpTh	815	1240	-2.72	-5.61	-2.89
PSp3Th	1099	1576	-2.74	-5.43	-2.69
PTPTTh	1258	2135	-2.89	-5.72	-2.83
PTPT3Th	927	1114	-2.73	-5.65	-2.92

^a Determined from the onset of the absorption band; ^b Taken from the onset of the oxidation wave in monomer-free solution at 0.10 Vs^{-1} (see Figure 8); ^c Calculated from the HOMO level by subtracting optical band gap.

electropolymerization.⁵⁶ Moreover, a S_{BET} value of $1576 \text{ m}^2\text{g}^{-1}$ was obtained for PSp3Th films produced in presence of boron trifluoride. In this case, the obtained specific surface area is higher than the one obtained for the corresponding chemically synthesized polymer ($1102 \text{ m}^2\text{g}^{-1}$), possibly related to the preferred formation of bithiophene bridges during the electropolymerization in the presence of boron trifluoride (see Scheme 2). However, this behavior was not observed for PTPT3Th, where the S_{BET} value of $1114 \text{ m}^2\text{g}^{-1}$ for the electrosynthesized film produced in presence of boron trifluoride was slightly lower than that for the chemically made bulk polymer ($1390 \text{ m}^2\text{g}^{-1}$), possibly related to the high oxidation potential of 1.3 V that is required in this case (see Figure 7).

FTIR spectra of monomers, bulk polymers and MPN films are shown in Figure 10. For the 2-thienyl-based monomers SpTh and TPTTh, peaks at 690 and 699 cm^{-1} , respectively, were attributed to out-of-plane CH bending vibrations of mono-substituted thiophene rings.⁵⁷ Disappearance of these signals and the occurrence of new bands at 792 and 814 cm^{-1} for PSpTh and 796 and 815 cm^{-1} for PTPTTh reflect the formation of 2,5'-disubstituted bithiophene bridges in the microporous bulk materials or films.²¹ Accordingly, the polymers made from 3-thienyl-substituted monomers showed the disappearance of characteristic peaks for the corresponding monomers at 774 cm^{-1} (Sp3Th) and 773 cm^{-1} (TPT3Th),⁵⁸ and the occurrence of a new peak at about 817 cm^{-1} (PSp3Th) and 816 cm^{-1} (PTPT3Th) for 2,3,5-trisubstituted thiophene rings for the bulk polymers and MPN films produced in pure DCM. As expected, MPN films produced in the presence of boron trifluoride exhibited FTIR spectra quite similar to those of the corresponding counterparts made from 2-thienyl-substituted monomers. Here, the presence of two bands at 801 and 818 cm^{-1} for PSp3Th, and 800 and 814 cm^{-1} for PTPT3Th, may indicate the restriction of electropolymerization to the formation of bithiophene linkers. The broad band between 1000 and 1150 cm^{-1} may be related to the presence of some remaining BF_3 -based counteranionic species as impurities of the MPN films.⁵⁹ Further characterization experiments of MPN films were carried out with the materials produced in the presence of boron trifluoride. Absorption and PL spectra for the thiophene-based monomers in chloroform and the corresponding MPN thin films produced by potentiodynamic electropolymerization in the presence of boron trifluoride are shown in Figure 11. Red shifted long wavelength π - π^* transition bands for the MPN films if compared to the corresponding monomers indicate the presence of more extended π -conjugated seg-

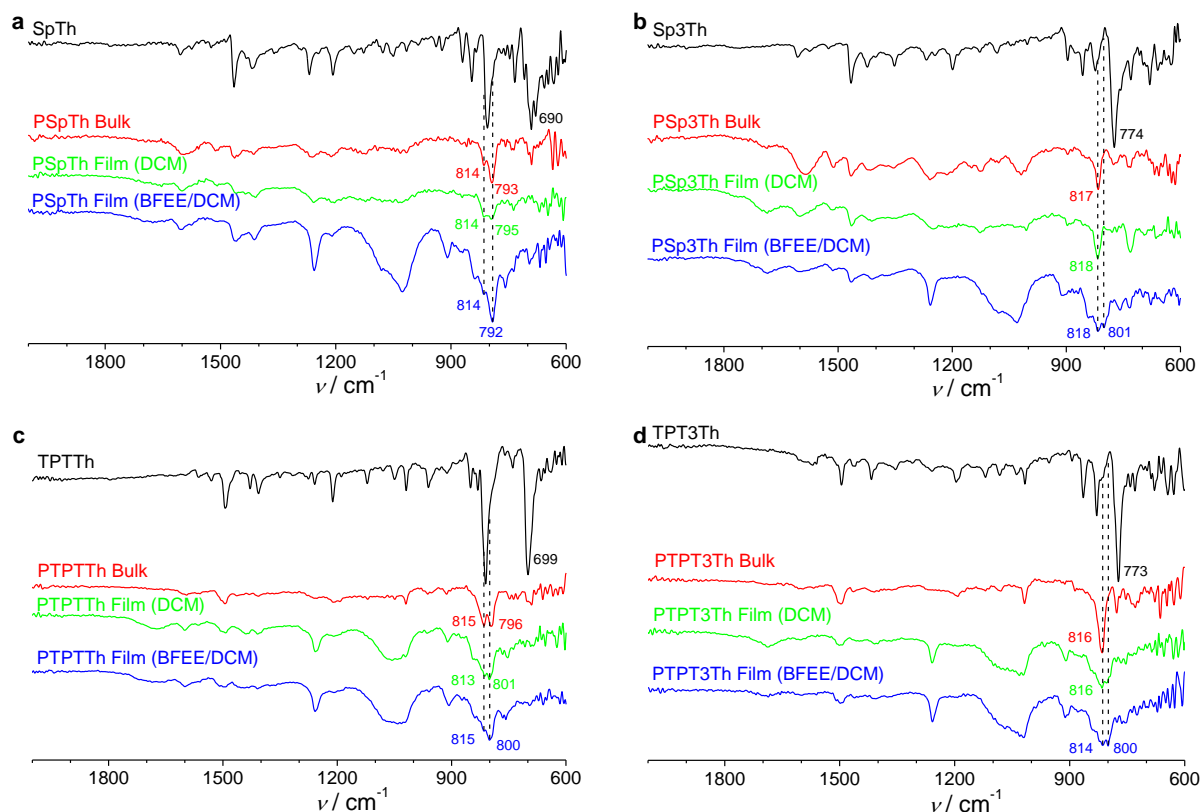


Figure 10. FT-IR spectra of monomers SpTh (a), Sp3Th (b), TPTTh (c) and TPT3Th (d) (black lines); the resulting bulk polymers (red lines); the resulting MPN films prepared by electropolymerization in pure DCM (green lines); and the resulting MPN films prepared by electropolymerization in BFEE/DCM (1:4) (blue lines).

ments in the polymer networks. As the bulk polymers, MPN films on ITO are photoluminescent and might be interesting for applications in chemical sensors.^{60,61} The surface microstructure of the thiophene-based MPN thin films was studied by tapping mode AFM. The films were prepared from a 0.1 mM solution of the monomers in BFEE/DCM (1:4) using 0.1 M TBAP as supporting electrolyte. Ten consecutive cyclic voltammograms in the potential range from 0 V to 1.2 V (SpTh, Sp3Th, TPTTh) or 1.3 V (TPT3Th) were applied with a scan rate of 0.1 Vs⁻¹. A very smooth surface topology was observed for all MPN thin films (see Figure 12) with average surface roughness (Rq) and thickness of 2.5 nm/50.3 nm for PSpTh, 3.6 nm/51.6 nm for PSp3Th, 3.5 nm/44.4 nm for PTPTTh, and 5.3 nm/32.8 nm for PTPT3Th, respectively. Such morphological properties are beneficial for a possible application in organic electronics (e.g. OLED, OFET, OPV) where the availability of high quality, uniform and smooth films is often required.

Electrogenerated MPNs from Tetrathiophene-Based Monomers

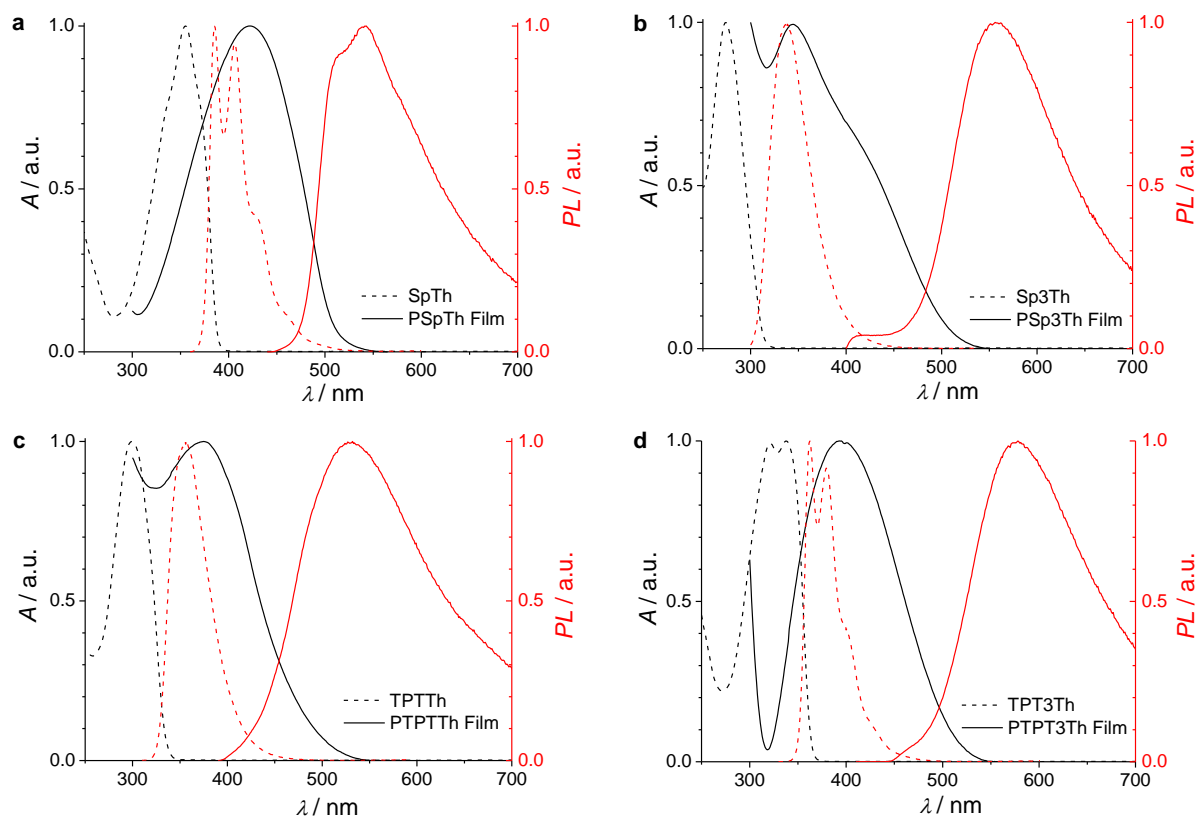


Figure 11. Absorption (black lines) and photoluminescence (red lines) spectra of monomers SpTh (a), Sp3Th (b), TPTTh (c) and TPT3Th (d) in chloroform (dashed lines) and the resulting MPN films prepared in BFEE/DCM (1:4) (solid lines).

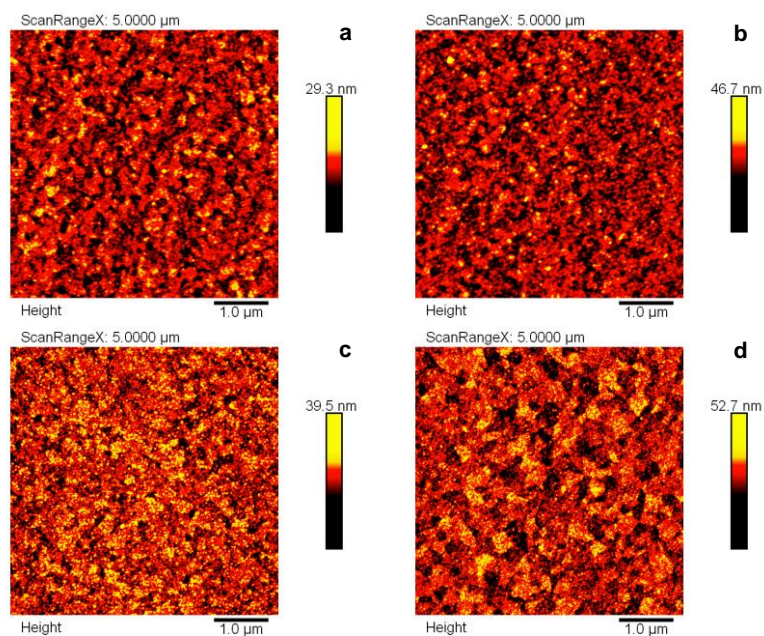


Figure 12. Tapping mode AFM images of MPN thin films on ITO of PSpTh (a), PSp3Th (b), PTPTTh (c) and PTPT3Th (d).

4.2.5. Electrochemical Reduction of 1,3,5-Trinitrobenzene at PTPTTh-Modified Glassy Carbon Electrodes

In Chapter 2,²⁹ a nice correlation between the current response in the electrochemical reduction of a “prototypical” nitroaromatic analyte, 1,3,5-trinitrobenzene (TNB), and the specific surface area of glassy carbon (GC) electrodes modified with carbazole-based MPN coatings was found. Following this line, PTPTTh-modified GC electrodes were also produced by applying a potential of 1.2 V until a polymerization charge of 0.2 mC was accumulated, both in DCM and BFEE/DCM. These modified electrodes were used as working electrode in the reductive electrochemical detection of TNB in aqueous 0.2 M KCl/0.1 M phosphate buffer solution (pH 7.4). Figure 13 shows linear scan voltammograms (LSV) in response to 0.5 μM TNB, after background correction, for non- and PTPTTh-modified GC electrodes. Three cathodic peaks are observed for reduction of the three nitro groups of TNB to hydroxylamine groups.⁶² Peaks at about -0.31 V (I), -0.47 V (II) and -0.65 V (III) were observed in accordance with literature results.⁶³ A much increased current response was observed for PTPTTh-modified GC electrodes if compared to the bare, nonmodified GC electrode. This phenomenon is most probably driven by strong interactions at the surface of the microporous materials with their high specific surface area. Such behavior has been related to the formation of charge-transfer complexes (Jack-Meisenheimer complexes) between electron-rich (e.g. amines, carbazoles, thiophenes) and electron-poor structural units (e.g. nitroaromatic analytes) by decreasing the interfacial charge-transfer resistance.⁶⁴ The influence of the surfa-

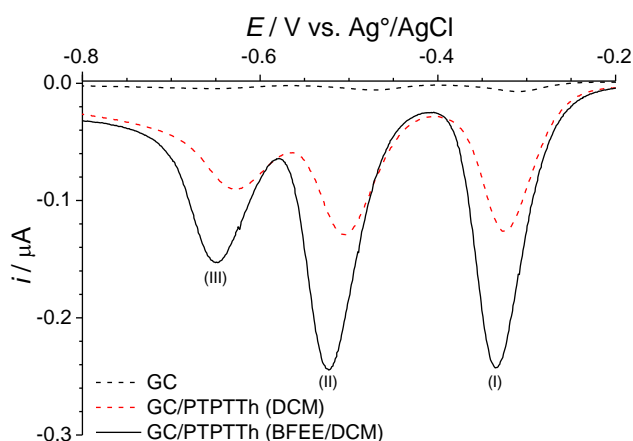


Figure 13. Linear scan voltammograms for the reduction of 0.5 μM TNB in aqueous 0.2 M KCl and 0.1 M PBS solution at nonmodified, and PTPTTh-modified GC electrodes prepared in DCM and BFEE/DCM (1:4) solutions for an accumulated oxidation charge of 0.20 mC during electropolymerization. LSVs were obtained with a scan rate of 0.01 Vs^{-1} .

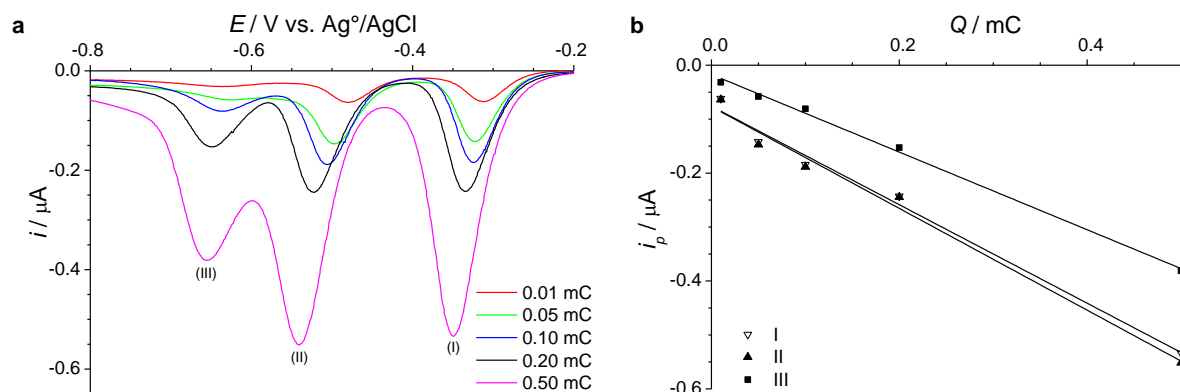


Figure 14. Linear scan voltammograms for the reduction of 0.5 μ M TNB in aqueous 0.2 M KCl and 0.1 M PBS solution at PTPTTh-modified GC electrodes prepared in BFEE/DCM (1:4) solution for accumulated oxidation charges from 0.01 mC to 0.50 mC during electropolymerization in BFEE/DCM (1:4) solution (a), and plot of TNB reduction peaks current versus accumulated oxidation charge during electropolymerization (b). LSVs were obtained with a scan rate of 0.01 Vs^{-1} .

ce area is clearly demonstrated by comparing the TNB reduction response of two PTPTTh-modified GC electrodes, whereby the electrode coating are made with and without BFEE as additive. The charge ratio in the reduction of TNB of 1.5 corresponds nicely to the S_{BET} ratio of 1.7 for the two materials (see Table 3). Linear scan voltammograms of the reduction of 0.5 μ M aqueous TNB solution depicted in Figure 14a for different thicknesses of the PTPTTh deposits on GC electrodes (produced in presence of boron trifluoride by varying the accumulative oxidation charge during polymerization). Similar three reduction peaks were observed with slight negative shifts of the potential for increasing thickness. A plot of reduction current response versus the accumulated charge during fabrication of the PTPTTh films (as an indirect measure of the film thickness) demonstrates a linear relationship and support the assumption of a strong interaction of the nitroaromatic analytes with the surface of the microporous deposits (see Figure 14b).

Finally, the detection range in the electrochemical reduction of TNB in aqueous solutions was tested as an orienting experiment for different TNB concentrations (0.5 μ M – 3.0 μ M) at PTPTTh-modified GC electrodes (see Figure 15a). For a nonmodified GC electrode, a linear relation between current response and concentration is observed in the studied concentration range indicating that the process is diffusion-controlled. For the PTPTTh-modified GC electrodes, the current response shows a turning saturation point for a concentration of ca. 1.5 μ M TNB (see Figure 15b). This phenomenon may be related to an adsorption-controlled pro-

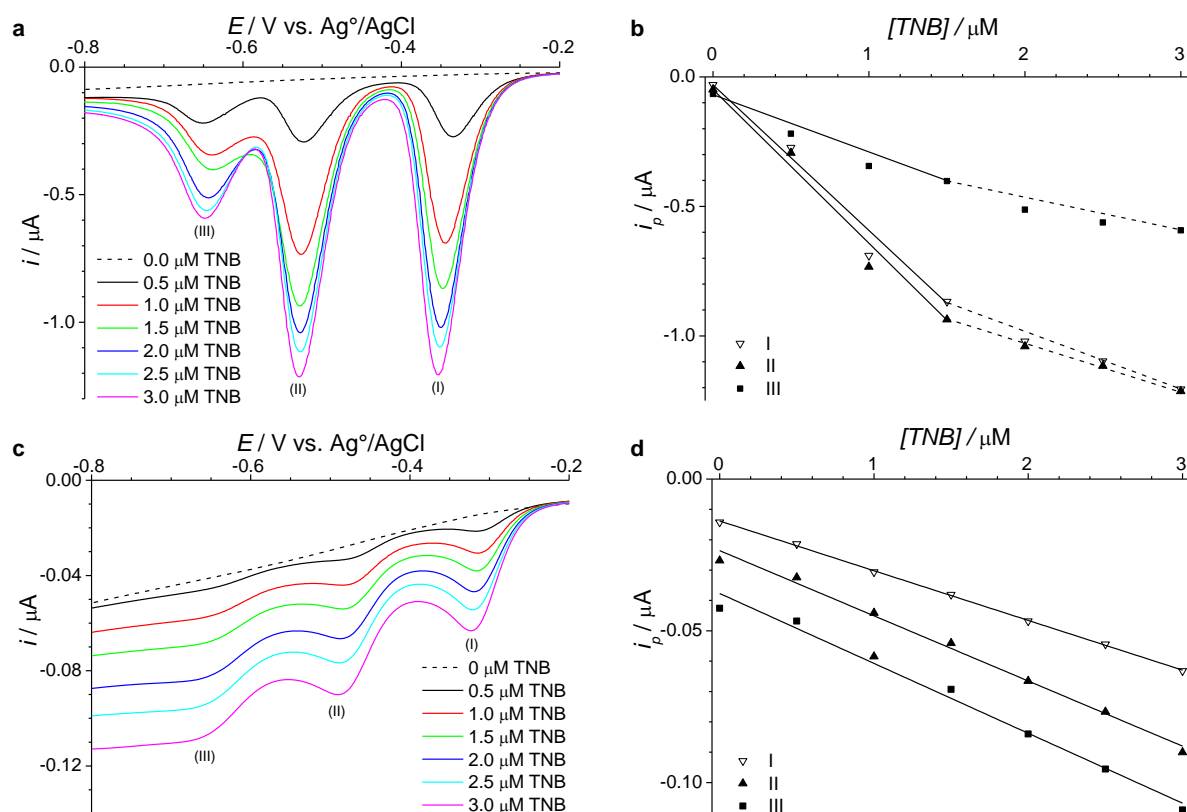


Figure 15. Linear scan voltammograms and reduction peaks current vs TNB concentration plots for the reduction of 0 μM – 3 μM TNB in aqueous 0.2 M KCl and 0.1 M PBS solutions at PTPTh-modified (a, b) and nonmodified (c, d) GC electrodes, respectively, with a scan rate of 0.01 V s^{-1} .

cess at low scan rate applied of 0.01 V s^{-1} as described for carbazole-based MPN films in Chapter 2.²⁹

4.3. Conclusions

To sum up, a series of tetrafunctional thiophene-based monomers was chemically and electrochemically polymerized resulting in microporous polymer networks with high specific surface areas of up to $2020 \text{ m}^2 \text{ g}^{-1}$ for powdery bulk materials and $2135 \text{ m}^2 \text{ g}^{-1}$ for thin films. All materials showed a good thermal stability and were PL-active. Electrochemical polymerization in boron trifluoride diethyletherate/dichloromethane mixtures generally produced MPN films with higher surface area and a more defined electrochemical behavior if compared to the ones made in pure DCM. Different coupling patterns have been observed for 3-thienyl-substituted monomers in the presence or absence of boron trifluoride as additive: In the presence of BFEE the preferred formation of bithiophene bridges was observed, thus

enhancing the microporosity of the materials. Favorably, thin MPN films were characterized by a pretty smooth morphology with a low average surface roughness < 5.3 nm. The aqueous electrochemical reduction of TNB at nonmodified and PTPTTh-modified GC electrodes showed a much increased cathodic current response for the modified electrodes, most probably driven by interactions of electron-poor nitroaromatic analyte molecules and the electron-rich thiophene-based MPN films with their high surface area.

4.4. Experimental Section

4.4.1. Monomers and Bulk Polymers

All reagents and chemicals were purchased from commercial companies, unless otherwise stated. ^1H and ^{13}C NMR spectra were obtained on a Bruker Avance III 600 machine. APLI mass spectra were recorded on a Bruker Daltronik micrOTOF system (KrF*-Laser ATLEX-SI, ATL Wermelskirchen). Elemental analyses were obtained on a Perkin Elmer 240 B. Thermogravimetric analyses were recorded under argon flow on a Mettler Toledo TGA/DSC1 STAR System. Solid state $^{13}\text{C}\{^1\text{H}\}$ cross-polarization magic-angle spinning (CPMAS) spectra were measured at 50.33 MHz using a Bruker AVANCE III 200 NMR spectrometer with a contact time of 2.5 ms, averaging 32768 transients at a relaxation delay of 2 s. All experiments were carried out at room temperature using a standard Bruker 2.5 mm double resonance MAS probe spinning at 20 kHz, typical $\pi/2$ -pulse lengths of 2.5 μs and SPINAL64 proton decoupling (200.15 MHz; $10\pi/12$ pulse set to 4.2 μs) at rather modest power levels of 46.5 Watt (^{13}C) and 19 Watt (^1H), respectively. The ^{13}C spectra were referenced with respect to tetramethylsilane (TMS) using solid adamantane as secondary standard (29.46 ppm for ^{13}C). FT-IR and UV-vis spectra were recorded on a JASCO FT-IR-4200 and V-670, respectively. Photoluminescence spectra were obtained on a HORIBA Scientific FluoroMax-4 Spectrofluorometer. A Tousimis Samdri-795 system was used for washing the bulk polymers with supercritical carbon dioxide. Nitrogen and krypton adsorption-desorption isotherms were recorded on a BEL Japan Inc Belsorp-max system at 77 K. A maximum relative pressure of 0.6 was set for measurements with Kr gas. All samples were dried on a Belprep-vac II at 140 $^{\circ}\text{C}$ and ~ 2 Pa overnight prior to the gas sorption measurements.

4.4.1.1. Synthesis of 2,2',7,7'-tetra(thien-2-yl)-9,9'-spirobifluorene (SpTh)

2,2',7,7'-Tetrabromo-9,9'-spirobifluorene (1.00 g, 1.58 mmol) and tributyl(thien-2-yl)stannane (2.36 g, 6.33 mmol) were placed in a 20 mL microwave vial and carefully degassed. Dry

toluene (20 mL) and tetrakis(triphenylphosphine)palladium(0) (0.09 g, 0.08 mmol) were added as solvent and catalyst, respectively. The mixture was stirred under argon atmosphere and exclusion of light at 140 °C for 2 hours. After evaporation of the solvent, the crude product was purified by column chromatography on silica (eluent: hexane/dichloromethane 7:3) and recrystallized from a chloroform/ethanol mixture. The product was isolated as yellow crystals, yield: 0.65 g (64 %). ¹H NMR (600 MHz, C₂D₂Cl₄) δ: 7.89 (d, *J* = 7.9 Hz, 4H), 7.68 (dd, *J* = 8.0, 1.7 Hz, 4H), 7.20 (dd, *J* = 5.0, 1.1 Hz, 4H), 7.18 (dd, *J* = 3.7, 1.1 Hz, 4H), 7.01 (d, *J* = 1.4 Hz, 4H), 6.97 (dd, *J* = 5.0, 3.7 Hz, 4H); ¹³C NMR (151 MHz, C₂D₂Cl₄) δ: 149.16, 143.84, 140.48, 133.96, 127.92, 125.96, 124.76, 123.34, 121.11, 120.54, 65.75; MS (APLI) 644.046 [644.076] (M⁺). Elem. Anal. for C₄₁H₂₄S₄, found: C 76.03, H 3.39, S 20.4; calc: C 76.36, H 3.75, S 19.89.

4.4.1.2. Synthesis of 2,2',7,7'-tetra(thien-3-yl)-9,9'-spirobifluorene (Sp3Th)

2,2',7,7'-Tetrabromo-9,9'-spirobifluorene (2.00 g, 3.16 mmol), thien-3-ylboronic acid (1.66 g, 13.0 mmol), and sodium carbonate (3.00 g, 28.3 mmol) were placed in a 250 mL two-necked round flask and carefully degassed. Toluene (35 mL), n-butanol (20 mL) and water (15 mL) were added as degassed solvents. Tetrakis(triphenylphosphine)palladium (0) (0.18 g, 0.16 mmol) in toluene (10 mL) was added and the mixture was stirred under argon atmosphere and exclusion of light under reflux for 24 hours. After cooling down the mixture to rt, chloroform (50 mL) was added and the resulting organic phase was washed 5 times with aqueous 2 N HCl. The collected organic phases were dried with MgSO₄. After solvent evaporation, the crude product was purified by column chromatography on silica (eluent: hexane/dichloromethane 7:3) and recrystallized from chloroform. The product was isolated as white powder, yield: 1.19 g (58 %). ¹H NMR (600 MHz, THF-d₈) δ: 7.96 (d, *J* = 8.0 Hz, 4H), 7.72 (dd, *J* = 8.0, 1.6 Hz, 4H), 7.46 (dd, *J* = 2.9, 1.4 Hz, 4H), 7.30 (dd, *J* = 5.1, 2.9 Hz, 4H), 7.27 (dd, *J* = 5.1, 1.3 Hz, 4H), 7.06 (d, *J* = 1.4 Hz, 4H); ¹³C NMR (151 MHz, THF-d₈) δ: 150.86, 142.89, 141.54, 136.79, 127.15, 127.01, 126.66, 122.49, 121.26, 79.48; MS (APLI) 644.053 [644.076] (M⁺). Elem. Anal. for C₄₁H₂₄S₄, found: C 76.01, H 3.50, S 20.07; calc: C 76.36, H 3.75, S 19.89.

4.4.1.3. Synthesis of tetra[4-(thien-2-yl)phenyl]methane (TPTTh)

Tetra(4-bromophenyl)methane (1.00 g, 1.57 mmol) and tributyl(thien-2-yl)stannane (2.93 g, 7.86 mmol) were placed in a 20 mL microwave vial and carefully degassed. Dry THF (10 mL), toluene (10 mL) and tetrakis(triphenylphosphine)palladium (0) (0.18 g, 0.16 mmol) were added as solvents and catalyst, respectively. The mixture was stirred under argon

atmosphere and exclusion of light at 140 °C for 24 hours. After evaporation of the solvent, the crude product was purified by column chromatography on silica, (eluent: hexane/dichloromethane 8:2). The product was isolated as white powder, yield: 0.18 g (18 %). ^1H NMR (600 MHz, $\text{C}_2\text{D}_2\text{Cl}_4$) δ : 7.56 (d, $J = 8.5$ Hz, 8H), 7.35 (dd, $J = 3.6, 0.9$ Hz, 4H), 7.30 (m, 12H), 7.10 (dd, $J = 5.0, 3.6$ Hz, 4H); MS (APLI) 648.102 [648.107] (M^+). Elem. Anal. for $\text{C}_{41}\text{H}_{28}\text{S}_4$, found: C 75.89, H 4.35, S 19.77; calc: C 75.49, H 4.46, S 19.92.

4.4.1.4. Synthesis of tetra[4-(thien-3-yl)phenyl]methane (TPT3Th)

Tetra(4-bromophenyl)methane (2.00 g, 3.14 mmol), thien-3-ylboronic acid (1.66 g, 13.0 mmol), and sodium carbonate (3.00 g, 28.3 mmol) were placed in a 250 mL two-necked round flask and carefully degassed. Toluene (35 mL), n-butanol (20 mL) and water (15 mL) were added as degasified solvents. Tetrakis(triphenylphosphine)palladium (0) (0.18 g, 0.16 mmol) in toluene (10 mL) was added and the mixture was stirred under argon atmosphere and exclusion of light under reflux for 24 hours. After cooling down the aqueous mixture to rt, chloroform (50 mL) was added and the resulting organic phase was washed 5 times with aqueous 2N HCl. The collected organic phases were dried with MgSO_4 . After solvent evaporation, the crude product was purified by column chromatography on silica (eluent: hexane/dichloromethane 7:2) and recrystallized from hexane/chloroform mixture. The product was isolated as white powder, yield: 0.40 g (20 %). ^1H NMR (600 MHz, THF- d_8) δ : 7.58 (m, 12H), 7.43 (m, 8H), 7.33 (m, 8H); ^{13}C NMR (101 MHz, THF- d_8) δ 146.67, 142.89, 134.80, 132.48, 127.13, 126.98, 126.45, 121.17, 65.34; MS (APLI) 648.107 [648.107] (M^+). Ele. Anal. for $\text{C}_{41}\text{H}_{28}\text{S}_4$, found: C 75.89, H 4.18, S 20.03; calc: C 75.89, H 4.35, S 19.77.

4.4.1.5. Synthesis of bulk polymers by oxidative coupling with FeCl_3

All monomers were chemically polymerized using the same methodology, which is here described for the SpTh monomer: 2,2',7,7'-Tetra(thien-2-yl)-9,9'-spirobifluorene (300 mg, 0.47 mmol) was dissolved in anhydrous chloroform (30 mL) and transferred dropwise to a 250 mL round flask which contains a suspension of iron(III)chloride (415 mg, 2.56 mmol) in anhydrous chloroform (20 mL). The resulting mixture was stirred at room temperature for one day under argon atmosphere. After addition of methanol (100 mL), the mixture was stirred for one more hour. The resulting precipitate was collected by filtration and washed with methanol. The powder was treated with aqueous hydrochloric acid (37 %) for 2 h, filtered off and washed with water and methanol. After Soxhlet extraction with methanol and THF for 24 h, the product was treated with ethanol (p.a.) for three days and finally washed with supercritical carbon dioxide. PSpTh was isolated as yellow powder, yield: 261 mg (84 %),

PSp3Th as slightly orange powder (92 %), PTPTTh as slightly green powder (45 %), and PTPT3Th as orange powder (99 %).

4.4.2. Electrochemical Studies

Dichloromethane (HPLC grade) was refluxed over phosphorus pentoxide for 3 h and distilled. Tetrabutylammonium tetrafluoroborate (TBABF₄, ≥ 99 %) was purchased from Alfa Aesar; boron trifluoride diethyletherate (BFEE, ≥ 46.5 % BF₃) and phosphate buffered saline (PBS, pH 7.4) from Sigma-Aldrich; 1,3,5-trinitrobenzene (TNB, neat) from Supelco; and potassium chloride (KCl, ≥ 99.5 %, ACS) from Roth. Indium tin oxide-coated transparent electrodes on glass (ITO, ≤ 20 Ohm m⁻²) were purchased from pgo. For electrochemical polymerization and characterization a Potentiostat/Galvanostat PAR VersaSTAT 4 was used with a three-electrode cell. The AFM images were recorded on an atomic force microscope Bruker diInnova operated in tapping mode. The average surface roughness values were extracted from the topography images. The thickness of the films was measured with a surface profilometer Veeco Dektak 150.

4.4.2.1. Electrochemical polymerization and characterization on Pt electrodes

10 mL of 0.1 mM solutions of the monomers were prepared in dichloromethane or BFEE/DCM (1:4) using 0.1 M TBABF₄ as supporting electrolyte. The solutions were placed in a three-electrode cell under argon atmosphere at 25 °C. A platinum disc electrode (Pt, 1 mm diameter) was used as working electrode (WE); a platinum wire as counter electrode (CE); and Ag⁰/AgNO₃ (0.01 M AgNO₃/0.1 M TBAP in acetonitrile, 0.53 V vs. NHE) as reference electrode (RE). For Figure 7, twenty cyclic voltammograms were repeatedly recorded in a potential range 0 – 1.2 V for SpTh, Sp3Th and TPTTh, and 0 – 1.3 V for TPT3Th with a scan rate of 0.1 Vs⁻¹. For recording CVs of the resulting products, the deposits on Pt disc electrodes were placed as WE in a monomer-free 0.1 M solutions of TBABF₄ in dichloromethane. Cyclic voltammograms at different scan rates from 0.005 to 0.20 Vs⁻¹ were recorded in the potential range 0 – 1.0 V (Figure 8).

4.4.2.2. Electrochemical polymerization on ITO electrodes for porosity measurements, as well as for optical, and morphological characterization

10 mL of the monomers solutions were placed in a three-electrode cell. ITO (~ 1.5x1.2 cm deposit area) on glass and a platinum gauze (2.5x1.2 cm area), separated by 1 cm, were used as WE and CE, respectively; Ag⁰/AgNO₃ as RE. For krypton gas sorption measurements, thick films were produced by applying an oxidative potential of 1.2 V (SpTh, Sp3Th and

TPTTh) or 1.3 V (TPT3Th) for 20 min. A potential of 0 V was applied after the electropolymerization for 60 s in order to discharge (dedoped) the deposits. After rinsing the deposits with acetonitrile and dichloromethane, they were dried for 20 min at 100 °C. The collection of ca. 2 mg of material was necessary for reliable BET measurements. For optical and thickness measurements, MPN films on ITO were prepared by applying ten cyclic voltammograms in the same potential range as the used for Pt disc electrodes. After rinsing the films with acetonitrile and dichloromethane, they were dried for 20 min at 100 °C.

4.4.2.3. Electrochemical polymerization of TPTTh on glassy carbon (GC) electrodes and electrochemical sensing of TNB.

10 mL of a 0.1 mM TPTTh solution were prepared in dichloromethane or BFEE/DCM (1:4) using 0.1 M TBABF₄ as supporting electrolyte. The solutions were placed in a three-electrode cell under argon atmosphere at 25 °C. A glassy carbon disc electrode (GC, 1 mm diameter) was used as working electrode (WE); a platinum wire as counter electrode (CE); and Ag⁰/AgNO₃ as reference electrode (RE). Potentiostatic polymerization of TPTTh was achieved by applying a potential of polymerization of 1.2 V until the required oxidative charge (0.01 – 0.50 mC) was accumulated. A potential of 0 V was applied after polymerization during 30 s in order to discharge (dedope) the deposits. After rinsing the deposits with acetonitrile and dichloromethane, the MPN-modified GC electrodes were used as WE in a 10 mL of aqueous 0.2 M KCl and 0.1 M PBS under argon atmosphere at 25 °C. A platinum wire and Ag⁰/AgCl(sat.) (NaCl 3 M, 0.21 V vs NHE) were used as CE and RE, respectively. After 5 min of stirring, a prepotential of 0 V was applied for 30 s. Linear scan voltammograms were recorded from 0 V to –1 V with a scan rate of 0.01 Vs⁻¹. For 1,3,5-trinitrobenzene (TNB) detection, 5 µL of 1 mM TNB solution in acetonitrile were added sequentially in order to adjust the TNB concentration from 0 µM to 3 µM.

4.5. References

- (1) Palma-Cando, A.; Brunklaus, G.; Scherf, U. *Macromolecules* **2015**, *48*, 6816.
- (2) Chen, Q.; Liu, D.-P.; Luo, M.; Feng, L.-J.; Zhao, Y.-C.; Han, B.-H. *Small* **2014**, *10*, 308.
- (3) Fischer, S.; Schimanowitz, A.; Dawson, R.; Senkovska, I.; Kaskel, S.; Thomas, A. *J. Mater. Chem. A* **2014**, *2*, 11825.
- (4) Chen, Q.; Liu, D.-P.; Zhu, J.-H.; Han, B.-H. *Macromolecules* **2014**, *47*, 5926.

- (5) Chen, Q.; Luo, M.; Hammershøj, P.; Zhou, D.; Han, Y.; Laursen, B. W.; Yan, C.-G.; Han, B.-H. *J. Am. Chem. Soc.* **2012**, *134*, 6084.
- (6) Sekizkardes, A. K.; Altarawneh, S.; Kahveci, Z.; İslamoğlu, T.; El-Kaderi, H. M. *Macromolecules* **2014**, *47*, 8328.
- (7) Sekizkardes, A. K.; Culp, J. T.; Islamoglu, T.; Marti, A.; Hopkinson, D.; Myers, C.; El-Kaderi, H. M.; Nulwala, H. B. *Chem. Commun.* **2015**, *51*, 13393.
- (8) Zhang, Y.; A, S.; Zou, Y.; Luo, X.; Li, Z.; Xia, H.; Liu, X.; Mu, Y. *J. Mater. Chem. A* **2014**, *2*, 13422.
- (9) Zhao, Q.; Zhang, P.; Antonietti, M.; Yuan, J. *J. Am. Chem. Soc.* **2012**, *134*, 11852.
- (10) Rose, M. *ChemCatChem* **2014**, *6*, 1166.
- (11) Bleschke, C.; Schmidt, J.; Kundu, D. S.; Blechert, S.; Thomas, A. *Adv. Synth. Catal.* **2011**, *353*, 3101.
- (12) Kundu, D. S.; Schmidt, J.; Bleschke, C.; Thomas, A.; Blechert, S. *Angew. Chem. Int. Ed.* **2012**, *51*, 5456.
- (13) Akiyama, T.; Matsushita, M.; Kakutani, K.; Yamada, S.; Takechi, K.; Shiga, T.; Motohiro, T.; Nakayama, H.; Kohama, K. *Jpn. J. Appl. Phys.* **2005**, *44*, 2799.
- (14) Roncali, J.; Leriche, P.; Cravino, A. *Adv. Mater.* **2007**, *19*, 2045.
- (15) Xu, Y.; Jin, S.; Xu, H.; Nagai, A.; Jiang, D. *Chem. Soc. Rev.* **2013**, *42*, 8012.
- (16) Preis, E.; Dong, W.; Brunklaus, G.; Scherf, U. *J. Mater. Chem. C* **2015**, *3*, 1582.
- (17) Zhang, K.; Kopetzki, D.; Seeberger, P. H.; Antonietti, M.; Vilela, F. *Angew. Chem. Int. Ed.* **2013**, *52*, 1432.
- (18) Liu, X.; Xu, Y.; Jiang, D. *J. Am. Chem. Soc.* **2012**, *134*, 8738.
- (19) Yuan, D.; Lu, W.; Zhao, D.; Zhou, H.-C. *Adv. Mater.* **2011**, *23*, 3723.
- (20) Dawson, R.; Stockel, E.; Holst, J. R.; Adams, D. J.; Cooper, A. I. *Energy Environ. Sci.* **2011**, *4*, 4239.
- (21) Yuan, S.; Kirklin, S.; Dorney, B.; Liu, D.-J.; Yu, L. *Macromolecules* **2009**, *42*, 1554.
- (22) Schmidt, J.; Weber, J.; Epping, J. D.; Antonietti, M.; Thomas, A. *Adv. Mater.* **2009**, *21*, 702.
- (23) Gu, C.; Chen, Y.; Zhang, Z.; Xue, S.; Sun, S.; Zhang, K.; Zhong, C.; Zhang, H.; Pan, Y.; Lv, Y.; Yang, Y.; Li, F.; Zhang, S.; Huang, F.; Ma, Y. *Adv. Mater.* **2013**, *25*, 3443.
- (24) Gu, C.; Chen, Y.; Zhang, Z.; Xue, S.; Sun, S.; Zhong, C.; Zhang, H.; Lv, Y.; Li, F.; Huang, F.; Ma, Y. *Adv. Energy Mater.* **2014**, *4*, 1301771.
- (25) Zhang, H.; Zhang, Y.; Gu, C.; Ma, Y. *Adv. Energy Mater.* **2015**, *5*, 1402175.

- (26) Gu, C.; Huang, N.; Gao, J.; Xu, F.; Xu, Y.; Jiang, D. *Angew. Chem. Int. Ed.* **2014**, *53*, 4850.
- (27) Gu, C.; Huang, N.; Wu, Y.; Xu, H.; Jiang, D. *Angew. Chem. Int. Ed.* **2015**, *54*, 11540.
- (28) Gu, C.; Huang, N.; Xu, F.; Gao, J.; Jiang, D. *Sci. Rep.* **2015**, *5*, 8867.
- (29) Palma-Cando, A.; Scherf, U. *ACS Appl. Mater. Interfaces.* **2015**, *7*, 11127.
- (30) Palma-Cando, A.; Preis, E.; Scherf, U. *Macromolecules* **2016**, DOI: 10.1021/acs.macromol.6b02025.
- (31) Roncali, J.; Thobie-Gautier, C.; Brisset, H.; Favart, J.-F.; Guy, A. *J. Electroanal. Chem.* **1995**, *381*, 257.
- (32) John, H.; Bauer, R.; Espindola, P.; Sonar, P.; Heinze, J.; Müllen, K. *Angew. Chem. Int. Ed.* **2005**, *44*, 2447.
- (33) Bildirir, H.; Osken, I.; Ozturk, T.; Thomas, A. *Chem. Eur. J.* **2015**, *21*, 9306
- (34) Shi, G.; Jin, S.; Xue, G.; Li, C. *Science* **1995**, *267*, 994.
- (35) Jin, S.; Xue, G. *Macromolecules* **1997**, *30*, 5753.
- (36) Shi, G.; Li, C.; Liang, Y. *Adv. Mater.* **1999**, *11*, 1145.
- (37) Wang, X.; Yue, R.; Lu, B.; Wei, Z.; Xu, J. *J. Mater. Sci.* **2010**, *45*, 1963.
- (38) Jiang, J.-X.; Su, F.; Trewin, A.; Wood, C. D.; Campbell, N. L.; Niu, H.; Dickinson, C.; Ganin, A. Y.; Rosseinsky, M. J.; Khimyak, Y. Z.; Cooper, A. I. *Angew. Chem.* **2007**, *119*, 8728.
- (39) Ben, T.; Ren, H.; Ma, S.; Cao, D.; Lan, J.; Jing, X.; Wang, W.; Xu, J.; Deng, F.; Simmons, J. M.; Qiu, S.; Zhu, G. *Angew. Chem.* **2009**, *121*, 9621.
- (40) Preis, E.; Widling, C.; Scherf, U.; Patil, S.; Brunklaus, G.; Schmidt, J.; Thomas, A. *Polym. Chem.* **2011**, *2*, 2186.
- (41) Sing, K. S. W. *Pure Appl. Chem.* **1985**, *57*, 603.
- (42) Qiao, S.; Du, Z.; Yang, R. *J. Mater. Chem. A* **2014**, *2*, 1877.
- (43) Heinze, J.; Frontana-Uribe, B. A.; Ludwigs, S. *Chem. Rev.* **2010**, *110*, 4724.
- (44) Palma-Cando, A. U.; Frontana-Uribe, B. A.; Maldonado, J. L.; Hernández, M. R. *Procedia Chem.* **2014**, *12*, 92.
- (45) Argun, A. A.; Aubert, P.-H.; Thompson, B. C.; Schwendeman, I.; Gaupp, C. L.; Hwang, J.; Pinto, N. J.; Tanner, D. B.; MacDiarmid, A. G.; Reynolds, J. R. *Chem. Mater.* **2004**, *16*, 4401.
- (46) Zotti, G.; Zecchin, S.; Schiavon, G.; Louwet, F.; Groenendaal, L.; Crispin, X.; Osikowicz, W.; Salaneck, W.; Fahlman, M. *Macromolecules* **2003**, *36*, 3337.

- (47) Ma, W.; Yang, C.; Gong, X.; Lee, K.; Heeger, A. J. *Adv. Funct. Mater.* **2005**, *15*, 1617.
- (48) Zhang, H.; Azimi, H.; Hou, Y.; Ameri, T.; Przybilla, T.; Spiecker, E.; Kraft, M.; Scherf, U.; Brabec, C. J. *Chem. Mater.* **2014**, *26*, 5190.
- (49) Piron, F.; Leriche, P.; Mabon, G.; Grosu, I.; Roncali, J. *Electrochem. Commun.* **2008**, *10*, 1427.
- (50) Piron, F.; Leriche, P.; Grosu, I.; Roncali, J. *J. Mater. Chem.* **2010**, *20*, 10260.
- (51) Reeves, B. D.; Thompson, B. C.; Abboud, K. A.; Smart, B. E.; Reynolds, J. R. *Adv. Mater.* **2002**, *14*, 717.
- (52) Yan, Q.; Lin, Y.; Kong, C.; Chen, L. *Chem. Commun.* **2013**, *49*, 6873.
- (53) Kumar, A.; Welsh, D. M.; Morvant, M. C.; Piroux, F.; Abboud, K. A.; Reynolds, J. R. *Chem. Mater.* **1998**, *10*, 896.
- (54) Wei, Y.; Chan, C. C.; Tian, J.; Jang, G. W.; Hsueh, K. F. *Chem. Mater.* **1991**, *3*, 888.
- (55) Jiang, M.-Y.; Wang, Q.; Chen, Q.; Hu, X.-M.; Ren, X.-L.; Li, Z.-H.; Han, B.-H. *Polymer* **2013**, *54*, 2952.
- (56) Alkan, S.; Cutler, C. A.; Reynolds, J. R. *Adv. Funct. Mater.* **2003**, *13*, 331.
- (57) Wang, B.; Zhao, J.; Cui, C.; Liu, J.; He, Q. *Sol. Energy Mater. Sol. Cells* **2012**, *98*, 161.
- (58) Rosatzin, H. *Spectrochim. Acta* **1963**, *19*, 1107.
- (59) Latonen, R.-M.; Kvarnström, C.; Ivaska, A. *J. Electroanal. Chem.* **2001**, *512*, 36.
- (60) Dong, W.; Fei, T.; Palma-Cando, A.; Scherf, U. *Polym. Chem.* **2014**, *5*, 4048.
- (61) Ma, H.; Yao, L.; Li, P.; Ablikim, O.; Cheng, Y.; Zhang, M. *Chem. Eur. J.* **2014**, *20*, 11655.
- (62) Laviron, E.; Meunier-Prest, R.; Vallat, A.; Roullier, L.; Lacasse, R. *J. Electroanal. Chem.* **1992**, *341*, 227.
- (63) Zhang, H.-X.; Cao, A.-M.; Hu, J.-S.; Wan, L.-J.; Lee, S.-T. *Anal. Chem.* **2006**, *78*, 1967.
- (64) Shamsipur, M.; Tabrizi, M. A.; Mahkam, M.; Aboudi, J. *Electroanalysis* **2015**, *27*, 1466.

Chapter 5

Electrogenerated MPNs from Tetraphenylethene-Cored Multifunctional Monomers¹

A series of novel microporous polymer networks (MPNs) were prepared from tetraphenylethene (TPE)-cored, multifunctional carbazole- or thiophene-based monomers by using chemical and electrochemical oxidative coupling methods. Octafunctional monomers lead to MPNs with high degree of cross-linking and optimized specific surface areas (S_{BET}) of up to $2200 \text{ m}^2\text{g}^{-1}$. Aggregation-induced emission (AIE) activity of the monomers is demonstrated. The MPN films were tested for application in the chemical sensing of nitroaromatic analytes by fluorescence quenching.

5.1. Introduction

Microporous polymer networks (MPNs) are covalently bonded and highly crosslinked materials which show permanent microporosity and high surface areas.² Chemical structure of the core as well as number and size of the linkers in the monomeric building blocks (tectons) play a significant role for the resulting properties of the MPNs, e.g. the specific surface area (S_{BET}).^{3,4} However, the generation of MPN films is still challenging. Thin MPN films are achievable by electrochemical, oxidative coupling of electroactive, multifunctional monomers.⁵ Usually carbazolyl or thienyl groups are used due to the low oxidative potentials required for oxidation and consecutive coupling/dimerization.^{6,7} In Chapter 2,⁸ it was shown that the number of carbazolyl linkers in the monomers (two, three or four) strongly influence the porosity of the resulting MPN films. Increasing the number of reactive groups leads to a higher cross-linking density and rigidity, and therefore to an enhanced surface area. In Chapter 3,⁹ it was studied how a further increase of the number of carbazolyl units (up to eight carbazolyls around a tetraphenylmethane core) impact on the microporosity of the resulting MPNs. Hereby, almost similar S_{BET} values resulted for either tetra- or octacarbazole-based MPNs, probably related to incomplete cross-linking caused by steric hindrance. This drawback may be overcome by introduction of additional spacers between core and linker units.

The study of aggregation-induced emission (AIE) phenomena have received enormous response from the scientific community since first report by Tang and co-workers in 2001.¹⁰

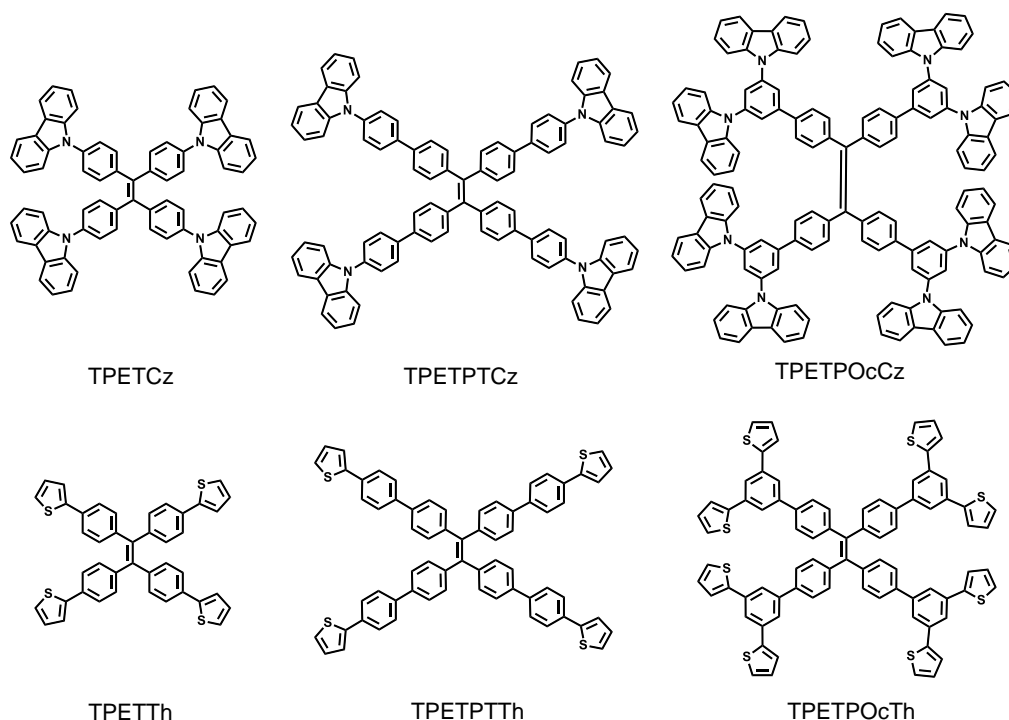
The main cause for the AIE effect is the restriction of intramolecular rotations and vibrations.¹¹ Based on this mechanism, many different propeller-shaped small molecules¹² and polymers¹³ have been synthesized, with the tetraphenylethene (TPE) core as the most prominent structural motif. AIE luminogens are connected to numerous potential applications as biological probes, for cell imaging, in organic light-emitting diodes and chemical sensors, among others.¹⁴ By connecting MPN films and AIE approaches, Jiang and co-workers studied electrogenerated MPN films made from carbazolyl-substituted TPE-cored monomers for use as chemical sensors for nitroaromatic explosives.¹⁵

In this Chapter, a series of six TPE-cored monomers were synthesized containing four or eight electroactive carbazolyl or thienyl substituents. AIE activity of the monomers as well as the porosity of the corresponding MPNs were studied in relation to structure and number of electroactive groups and the presence of additional 1,4-phenylene linkers. Bulk polymers as well as MPN films (obtained by chemical or electrochemical oxidative coupling, respectively) show high specific BET surface areas of up to 2200 m²g⁻¹. Whereas the AIE-active monomers show high photoluminescence quantum yields of up to 83 % in aggregated state, the corresponding electrogenerated MPN films are less emissive but show high sensitivity up to the ppm level in chemosensing experiments towards nitroaromatic analytes.

5.2. Results and Discussions

5.2.1. Synthesis of the Series of Monomers

The synthesis of the series of six TPE-cored monomers followed literature reports (see the Experimental Section for details). Scheme 1 presents the chemical structures of the monomers. The first pair of monomers have four functionalities (carbazolyl or thienyl) around the TPE core (TPETCz and TPETTh); the second pair of monomers with four groups contain additional 1,4-phenylene linkers (TPETPTCz and TPETPTTh); and the third pair of monomers with eight functionalities hold additional 1,3,5-phenylene linkers (TPETPOcCz and TPETPOcTh). 1,1,2,2-Tetra[4-(carbazol-9-yl)phenyl]ethene (TPETCz) was synthesized from bis[4-(carbazol-9-yl)phenyl]methanone (made by reaction of bis(4-fluorophenyl)methanone and carbazole) in a McMurry-type reductive coupling in 80 % yield. The intermediate of 1,1,2,2-tetra[4-(4,4,5,5-tetramethyl-1,3,2-dioxaborolan-2-yl)phenyl]ethene that was used for the generation of the other five monomers was synthesized by tetrabromination of tetraphenylethene followed by a Miyaura borylation. 1,1,2,2-Tetra[4



Scheme 1. Chemical structures of the six investigated carbazolyl- (top) and thienyl-substituted (bottom) monomers.

-(thiophen-2-yl)phenyl]ethene (TPETTh), 1,1,2,2-Tetra[4'-(carbazol-9-yl)-(1,1'-biphenyl)-4-yl]ethene (TPETPTCz), 1,1,2,2-tetra[4'-(thiophen-2-yl)-(1,1'-biphenyl)-4-yl]ethene (TPETPTTh), 1,1,2,2-tetra[3',5'-di(carbazol-9-yl)-(1,1'-biphenyl)-4-yl]ethene (TPETPOcCz), and 1,1,2,2-tetra[3',5'-di(thiophen-2-yl)-(1,1'-biphenyl)-4-yl]ethene (TPETPOcTh) were generated in Suzuki-type cross-couplings of the TPE intermediate with 2-bromothiophene, 9-(4-bromophenyl)-carbazole, 2-(4-bromophenyl)thiophene, 9,9'-(5-bromo-1,3-phenylene)bis(carbazole), or 2,2'-(5-bromo-1,3-phenylene)dithiophene, respectively, with good to moderate yields.

5.2.2. Characterization of Chemically Synthesized Bulk Polymers

The bulk polymer networks were generated as powdery materials by chemical oxidative coupling of the monomers with iron(III) chloride in chloroform. After washing and drying, the fine powders were obtained in good to excellent yields (73 % – 99 %). Thermogravimetric analysis of the polymer networks shows good thermal stability under argon up to 400 °C (see Figure 1 and 2). Nitrogen gas adsorption isotherms recorded at 77 K reveal microporosity for all bulk polymers, as documented in a rapid gas uptake at low relative pressures of < 0.1 (see Figure 3).¹⁶ The average pore diameters were calculated based on the nonlocal density func-

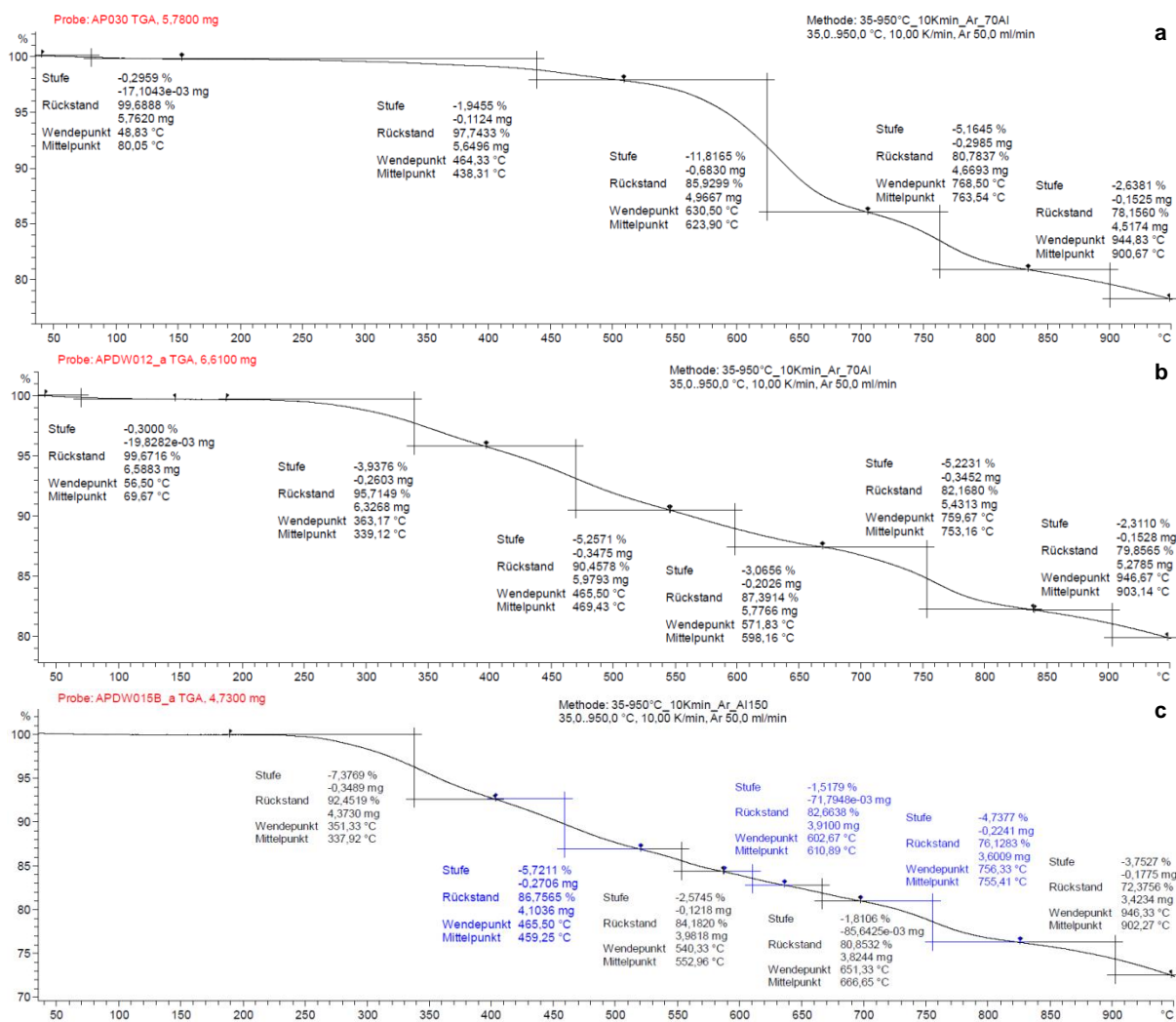


Figure 1. TGA plots of the bulk MPNs (made by FeCl_3 oxidation): PTPETCz (a), PTPETPTCz (b), and PTPETPOcZ (c).

tional theory (NLDFT) model to be 0.40 nm – 1.43 nm. On the other hand, significant gas adsorption also at high relative pressures (> 0.9) and the apparent hysteresis between the adsorption and desorption for all materials reflect the presence of additional meso- and macropores.¹⁷ Table 1 lists the calculated S_{BET} of the bulk polymers by applying the Brunauer-Emmett-Teller equation to the corresponding N_2 adsorption isotherms. The following points should be mentioned: i) PTPETCz and PTPETTh show very similar S_{BET} values of $1097 \text{ m}^2\text{g}^{-1}$ and $1085 \text{ m}^2\text{g}^{-1}$, respectively, both structures contain tectons with four carbazolyl or thienyl linkers around TPE cores. When an additional 1,4-phenylene spacer is introduced to the tectons, similarly reduced S_{BET} values are observed for PTPETPTCz ($1039 \text{ m}^2\text{g}^{-1}$) and PTPETPTTh ($956 \text{ m}^2\text{g}^{-1}$). This phenomenon might be explained by the formation of intercalated networks due to an increase of the pore diameter.¹⁸ ii) Remarkably high S_{BET}

Electrogenerated MPNs from Tetraphenylethene-Cored Multifunctional Monomers

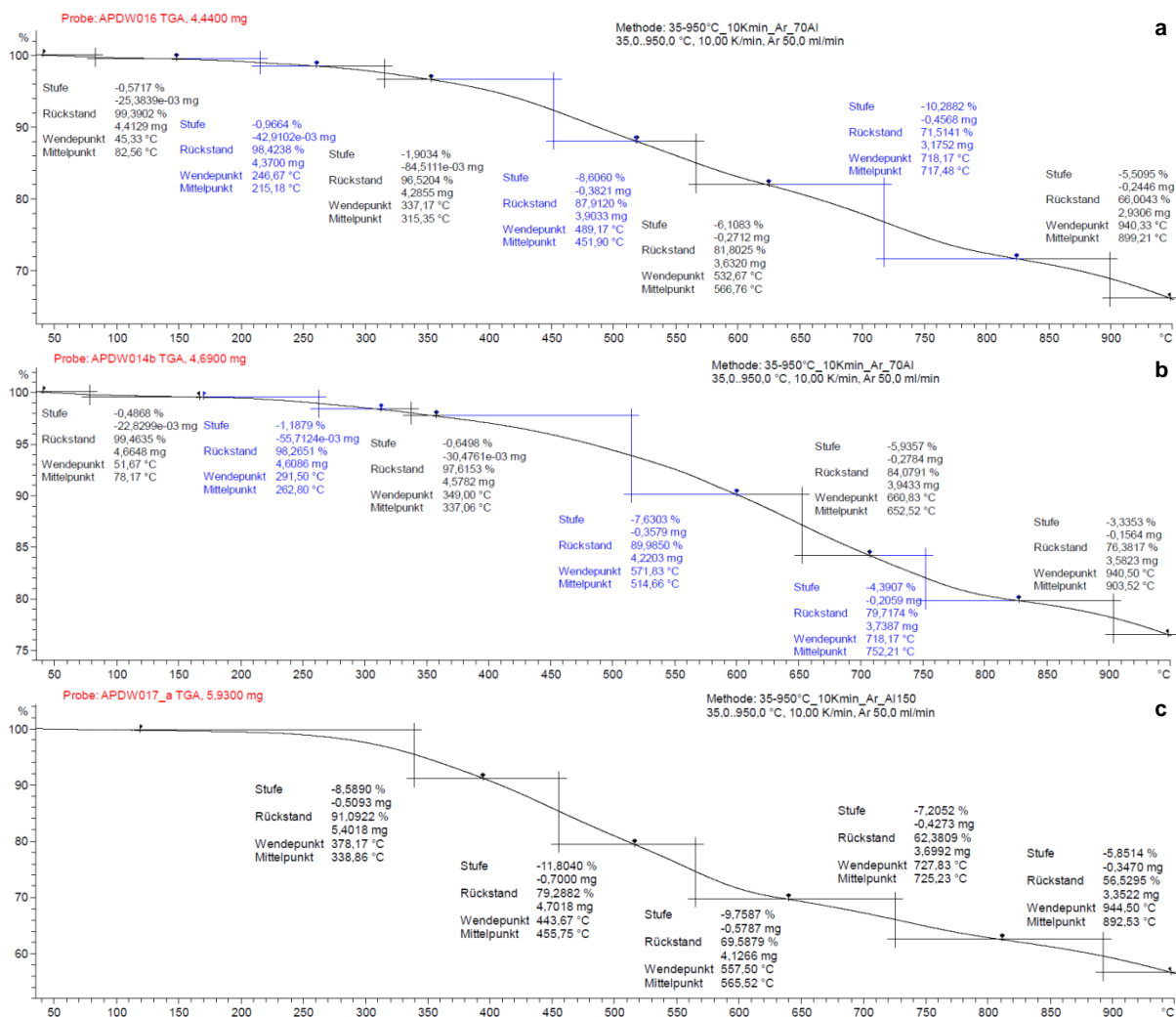


Figure 2. TGA plots of the bulk MPNs (made by FeCl₃ oxidation): PTPETTh (a), PTPETPTTh (b), and PTPETPOcTh (c).

values were found for PTPETPOcCz (2203 m²g⁻¹) and PTPETPOcTh (1767 m²g⁻¹) made from octafunctionalized monomers. Both tectons contain 1,3,5-trisubstituted phenylene linkers for attachment of the functional groups. The increased porosity might be related to the higher number of the reactive sites leading to higher cross-linking densities and increased rigidity. Possibly, the 1,3,5-trisubstituted spacer may also decrease the probability of chain intercalation. Please note that in Chapter 3,⁹ quite similar S_{BET} values were found for tetra- or octacarbazolyl substituents around a tetraphenylmethane core (1322 m²g⁻¹ and 1331 m²g⁻¹, respectively), thus illustrating the role of tectons' structure. iii) As a tendency, higher S_{BET} values were calculated for carbazole-based in relation to corresponding, structurally similar thiophene-based MPNs. Hereby, the increased size of the carbazolyl group may possibly play

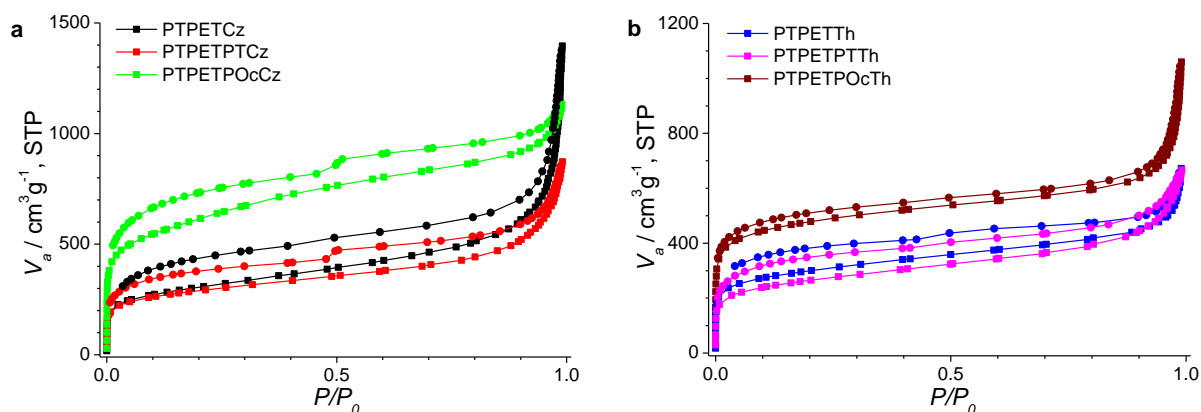


Figure 3. Nitrogen gas sorption isotherms of chemically synthesized carbazole-based (a), and thiophene-based (b) bulk MPNs.

a role. Due to the high microporosity and the polar character of the MPNs, they may find applications in gas storage and separation.^{19,20} CO₂ uptake capacities in the range of 5.33 % – 8.95 % at 25 °C and 1 bar were calculated for the chemically synthesized powdery networks (see Figure 4 and Table 2). By applying Henry’s law, maximum for CO₂/N₂ and CO₂/CH₄ gas adsorption selectivities of 13.0 and 2.8, respectively, are observed for PTPETPOcCz.

5.2.3. Electrochemical Characterization of the Monomers and Polymers at Pt Disc Electrodes

Electrochemical oxidative polymerization is a powerful technique that allows for a well-controlled deposition of polymer films on suitable electrodes from a monomer solution.²¹

Table 1. Calculated specific surface areas (S_{BET}) of chemically synthesized bulk polymers as well as of electrogenerated MPN films using N₂ and Kr gas sorption, respectively, and oxidation peak potentials (E_{p}^{ox}) of the corresponding monomers (observed during the first anodic scan).

Polymer	S_{BET} Bulk [m ² g ⁻¹]	S_{BET} Film [m ² g ⁻¹]	E_{p}^{ox} [V vs. Ag ^o /AgNO ₃]
PTPETCz	1097	979	0.89, 1.06
PTPETPTCz	1039	874	0.99
PTPETPOcCz	2203	2170	1.03
PTPETTh	1085	433	0.89, 1.36
PTPETPTTh	956	– ^a	1.06
PTPETPOcTh	1767	1634	1.12

^a not determined

Electrogenerated MPNs from Tetraphenylethene-Cored Multifunctional Monomers

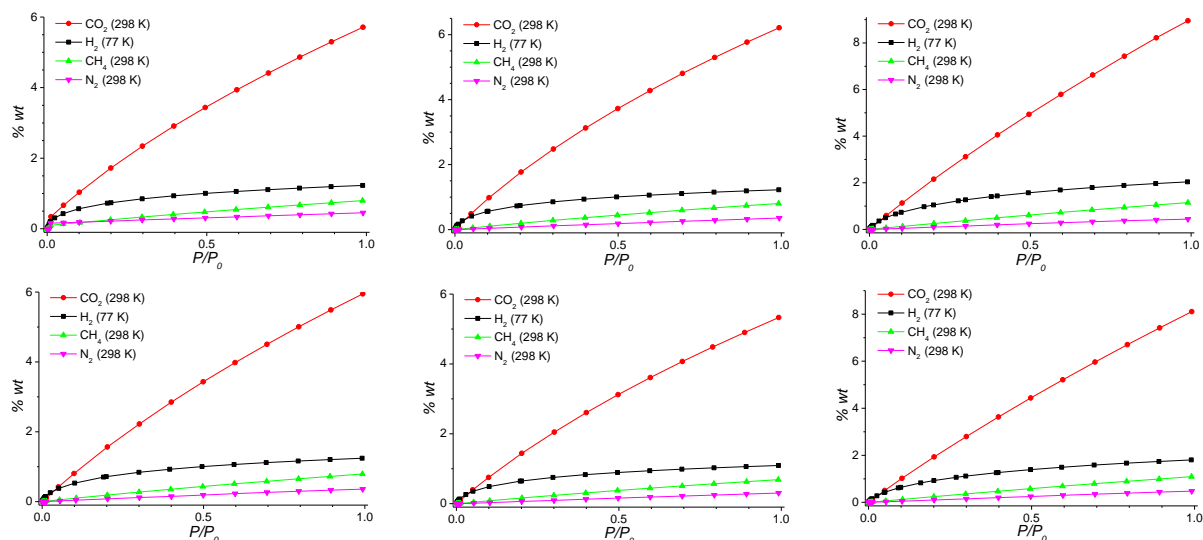


Figure 4. Gas adsorption isotherms for the bulk MPNs for PTPETCz (a), PTPETTh (b), PTPETPTCz (c), PTPETPTTh (d), PTPETPOcCz (e), and PTPETPOcTh (f).

Hereby, for the carbazole-based monomers diluted 0.1 mM solutions in dichloromethane were used together with 0.1 M tetrabutylammonium tetrafluoroborate (TBABF₄) as supporting electrolyte. For the thiophene-based monomers, addition of 20 % (V/V) boron trifluoride diethyletherate (BFEE) allows for an optimum polymerization into MPN films. As shown in Chapter 4,²² BFEE mainly decreases the required oxidation potential for electrochemical coupling resulting in boosted BET surface areas of the MPN films. Figure 5 shows the first anodic scan voltammograms for polymerization at Pt working electrodes for the carbazole-based (Figure 5a) and thiophene-based (Figure 5b) monomers. TPETCz and TPETTh show the presence of two oxidation peaks (see also Table 1). For both monomers, the reversible peaks at around 0.89 V (see insets of Figure S5a and S5b) might be related to the formation of

Table 2. Porosity data, gas uptake (at 298 K) and gas sorption selectivities of the six bulk MPNs synthesized by oxidative coupling with iron(III) chloride.

Polymer	Pore volume ^a [cm ³ g ⁻¹]	Gas uptake [%]				Selectivity ^c	
		CO ₂	N ₂	CH ₄	H ₂ ^b	CO ₂ /N ₂	CO ₂ /CH ₄
PTPETCz	1.13	5.71	1.23	0.80	0.45	8.0	2.6
PTPETPTCz	0.95	6.21	1.22	0.80	0.36	11.1	2.8
PTPETPOcCz	1.51	8.95	2.04	1.15	0.44	13.0	2.8
PTPETTh	0.75	5.95	1.24	0.79	0.36	10.6	2.7
PTPETPTTh	0.78	5.33	1.09	0.68	0.30	11.2	2.8
PTPETPOcTh	1.08	8.11	1.80	1.09	0.48	10.8	2.7

^a Determined at $P/P_0 = 0.95$; ^b Measured at 77 K; ^c Calculated by applying Henry's law.¹⁷

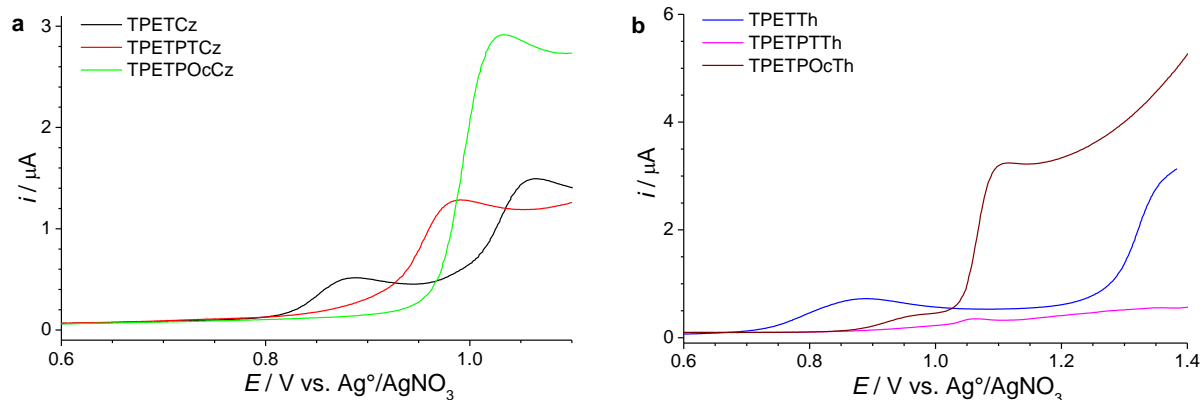


Figure 5. First anodic scan voltammograms at Pt disc electrodes for 0.1 mM monomer solutions in dichloromethane (for carbazolyl monomers) (a) or in BFEE/dichloromethane (1:4, for thienyl monomers) (b), with 0.1 M TBABF₄ as supporting electrolyte. The voltammograms were recorded with a scan rate of 0.10 Vs⁻¹.

stable, conjugated radical cations as reported for 1,4-dicarbazolyl-substituted phenylene monomers.²³ At higher potentials of 1.06 V and 1.36 V, respectively, the second irreversible oxidation peaks are observed for these carbazole- or thiophene-based monomers. These peaks should be related to the dimerization/cross-linking and deposition of the MPN films as reflected by the gradual current increase during multiple cycling (see Figure 6a and 6b). TPETPTCz and TPETPTTh exhibit single oxidation peaks at around 0.99 V and 1.06 V, respectively, for the electrochemical coupling reaction (see Figure 6c and 6d). The observed lower current for TPETPTTh stems from the low solubility of this monomer (monomer concentration < 0.1 mM). Finally, for the coupling of TPETPOcCz and TPETPOcTh slightly higher oxidation potentials of 1.03 V and 1.12 V, respectively, are needed if compared to the corresponding tetrasubstituted monomers (see Figure 6e and 6f). Moreover, the observed higher oxidation current peaks for the octasubstituted monomers reflect the doubled amount of electroactive groups in the tectons. Cyclic voltammograms of the electrogenerated films in monomer-free solutions at different scan rates from 0.005 Vs⁻¹ to 0.20 Vs⁻¹ exhibit two reversible peaks for carbazole-based and one reversible peak for thiophene-based MPNs (potential range of 0.5 V – 1.1 V, see Figure 7). These peaks are related to charging/discharging processes in conducting polymer films via reversible formation of radical cations and/or dications.²⁴ Additionally, the observed linear relation between peak currents and scan rate documents the formation of well-adhered deposits where the electron transfer is not a diffusion-controlled process (see insets of Figure 7).

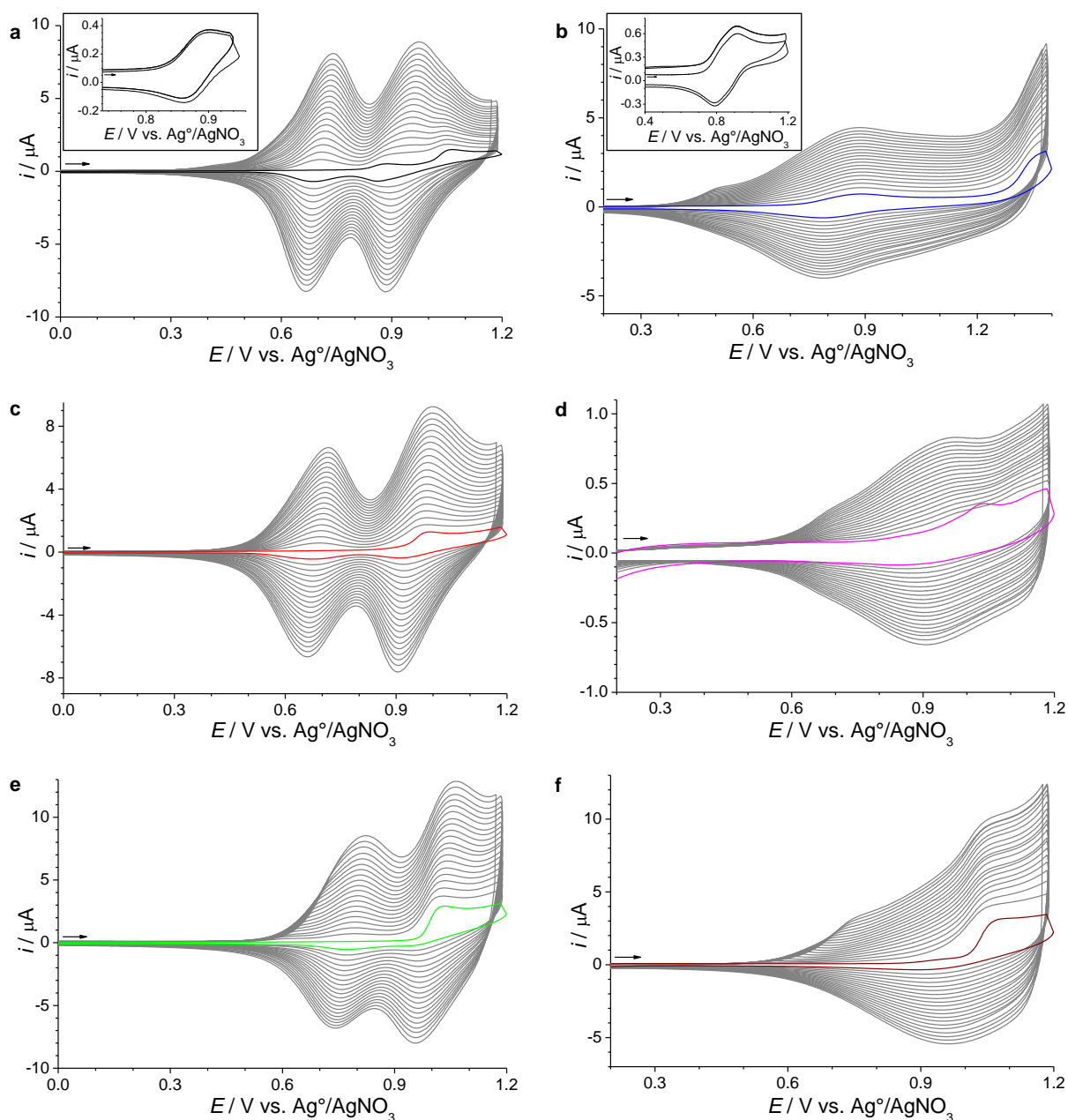


Figure 6. Twenty cyclic voltammograms at Pt disc electrodes for 0.1 mM solutions of TPETCz (a), TPETTh (b), TPETPTCz (c), TPETPTTh (d), TPETPOcCz (e), and TPETPOcTh (f) in dichloromethane for the carbazole-based monomers or in BFEE/dichloromethane (1:4) mixtures for the thiophene-based monomers. 0.1 M TBABF₄ was used as supporting electrolyte. Cyclic voltammograms were recorded from -1.0 V to 1.2 V (a,c,e), 0 V to 1.4 V (b), or 0 V to 1.2 V (d, f) with a scan rate of 0.10 Vs⁻¹. The insets show the cyclic voltammograms in a narrower potential window for the reversible peaks for TPETCz (a) and TPETTh (b).

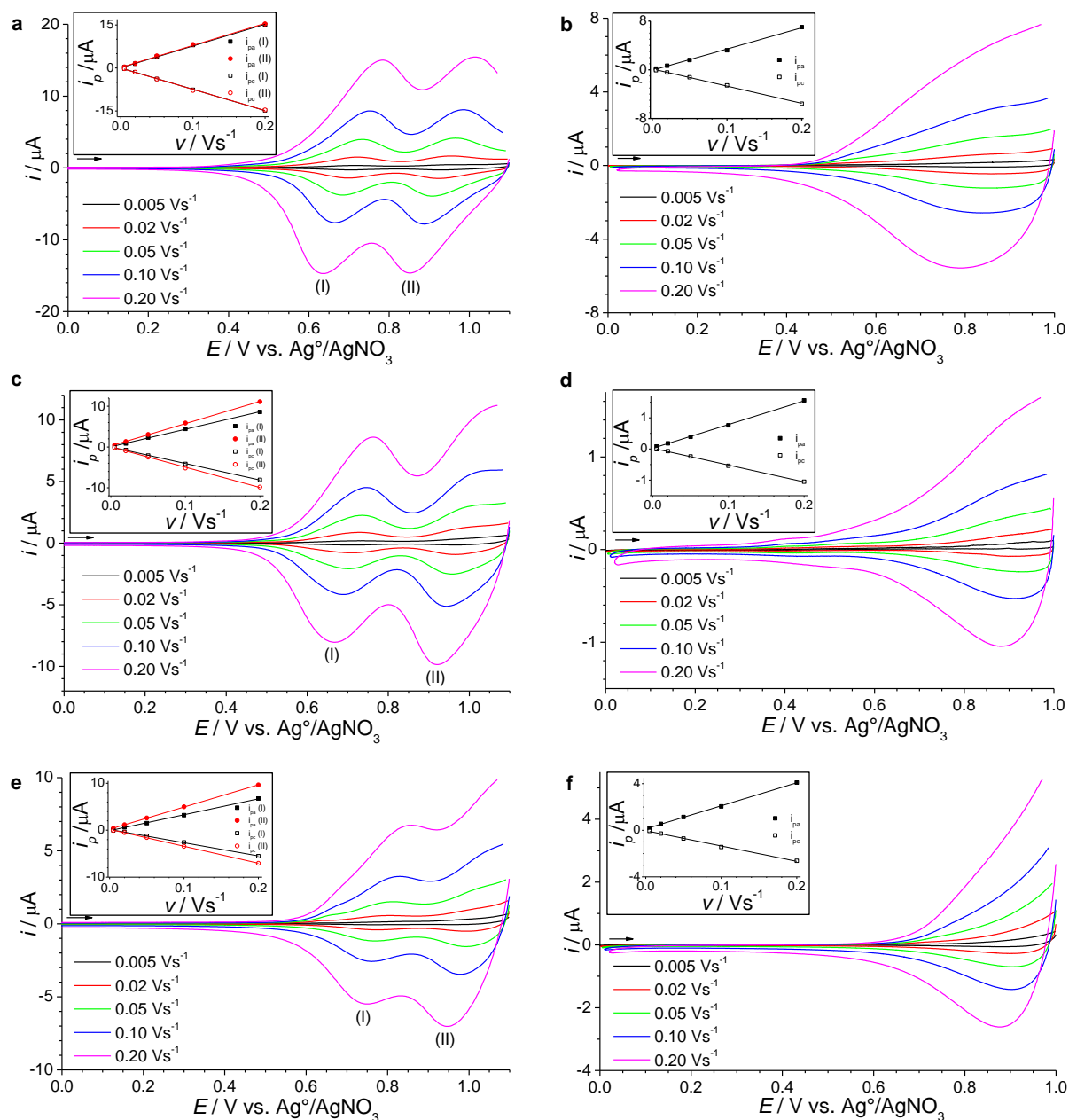


Figure 7. Cyclic voltammograms for PTPETCz (a), PTPETTh (b), PTPETPTCz (c), PTPETPTTh (d), PTPETPOcCz (e), and PTPETPOcTh (f) deposits on Pt disc electrodes in monomer-free dichloromethane containing 0.1 M TBABF₄ as supporting electrolyte. CVs were recorded from 0 V to 1.1 V (a,c,e) or 1.0 V (b,d,f) at different scan rates from 0.005 to 0.20 Vs^{-1} . The films were prepared as described in the caption of Figure 6. The insets demonstrate the linear dependence of peaks current and scan rate.

5.2.4. Porosity Characterization of Electrogenerated MPN Films

Especially potentiostatic oxidative polymerization allows for the formation of thicker, free-standing MPN when increasing the monomer concentration to 0.5 mM. After repeated washing and drying of the films, they were used to extract the corresponding krypton gas sorption data (77 K, relative pressure of 0 – 0.6). As shown in the representative sorption isotherms of Figure 8a. A fast krypton uptake at low relative pressures of < 0.1 again documents microporosity (see Figure 8b for nitrogen uptake in corresponding bulk polymers). Slightly reduced S_{BET} values are observed for most of the electrogenerated MPN films if compared to the corresponding bulk polymers (see Table 1). Strikingly, electrogenerated PTPETTh films display a dramatically lowered S_{BET} value of $433 \text{ m}^2\text{g}^{-1}$ ($1085 \text{ m}^2\text{g}^{-1}$ for the corresponding bulk polymer). This finding can be related to the relatively high oxidation potential of 1.4 V necessary for film deposition probably resulting in overoxidation and occurrence of side reactions. The S_{BET} value of PTPETPTTh films was not determined by krypton adsorption measurements due to the poor monomer solubility leading to the formation of only thin deposits.

5.2.5. Optical Characterization of the AIE-active Monomers in Solution and Solid State.

Organic materials with high solid state photoluminescent (PL) are of increasing importance for many potential applications, e.g. in electronic devices or sensors. One concept towards this goal, the so-called aggregation-induced emission (AIE) of small molecules and polymers has been intensely studied during the last 15 years; especially, materials based on the tetra-

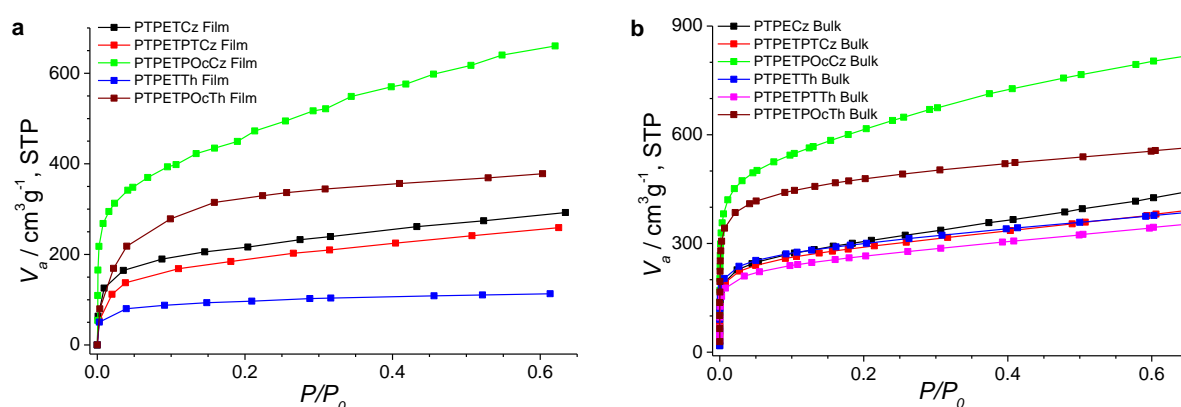


Figure 8. Adsorption isotherms of electropolymerized MPN films (a), and corresponding bulk polymers synthesized by oxidative coupling with iron(III) chloride (b), using Kr or N_2 gas, respectively.

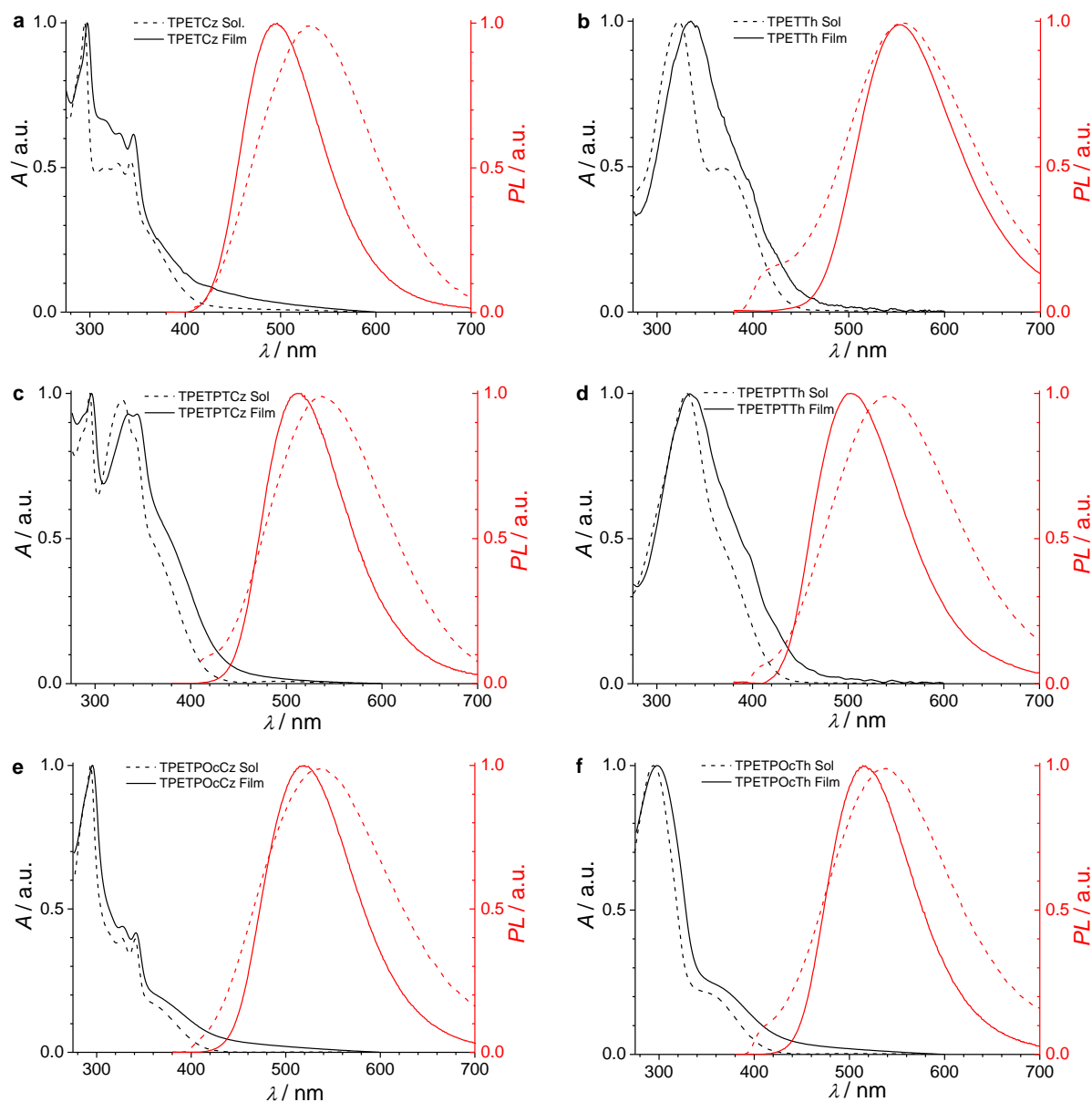


Figure 9. Absorption (black lines) and photoluminescence (red lines) spectra of the monomers: TPETCz (a), TPETTh (b), TPETPTCz (c), TPETPTTh (d), TPETPOcCz (e), and TPETPOcTh (f) in diluted chloroform solutions (dashed lines) and in the solid state (films) on quartz, solid lines).

phenylethylene motif have been extensively investigated.²⁵ Herein, AIE properties of the TPE-cored monomers were studied due to a good synthetic accessibility and favorable optical properties. Subsequently, the use of MPN films made from these monomers was explored for the chemical detection of nitroaromatic analytes. The optical spectra of the monomers are depicted in Figure 9. Red-shifted absorption spectra are observed for the monomers films in relation to their corresponding solutions in chloroform. Photoluminescence spectra show solid

Table 3. Photoluminescent data (upon excitation at 340 nm) for the series of monomers in diluted chloroform solutions and as thin films on quartz.

Monomer	PL λ_{\max}	PL-QY	PL-QY
	Film [nm]	Sol. [%]	Film [%]
TPETCz	497	1.3	83
TPETPTCz	512	5.8	56
TPETPOcCz	520	2.9	73
TPETTh	553	0.8	7
TPETPTTh	503	2.5	4
TPETPOcTh	514	1.7	38

state PL maxima between 497 nm for TPETCz and 553 nm for TPETTh (see Table 3 and Figure 10). The corresponding photoluminescence quantum yields (PL-QYs) in solution and in solid state are summarized in Table 3. Please notice: i) For all monomers, the transition from solution to the solid state leads to up to 63 times increased PL-QYs (for TPETCz) due to the AIE effect. ii) The carbazole-based monomers generally display higher PL-QYs if compared to the corresponding thiophene-based counterparts.

For completion, the AIE effect was also investigated in solvent/non-solvent mixtures. As an example, Figure 11a shows PL spectra of 0.01 mM TPETPOcCz in THF/water mixtures with an increasing non-solvent fraction (0 % to 90 % water). The low PL intensity for water contents < 30 % (see Figure 11b) rapidly increases and reaches a maximum for 90 % water, with a 67-fold increase if compared to the THF solution. The aggregated state is expected to restrict intramolecular rotations and to block non-radioactive deactivation channels thus lea-

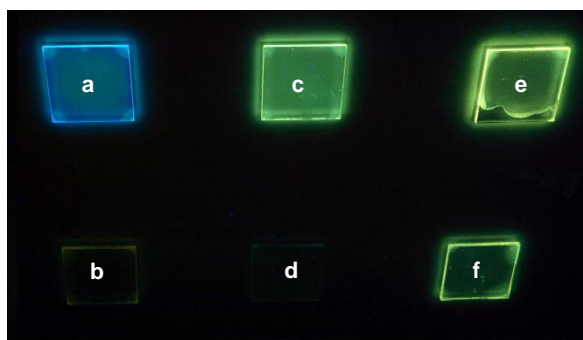


Figure 10. Photographs of monomer films of TPETCz (a), TPETTh (b), TPETPTCz (c), TPETPTTh (d), TPETPOcCz (e), and TPETPOcTh (f) on quartz plates upon excitation at 364 nm with an UV lamp.

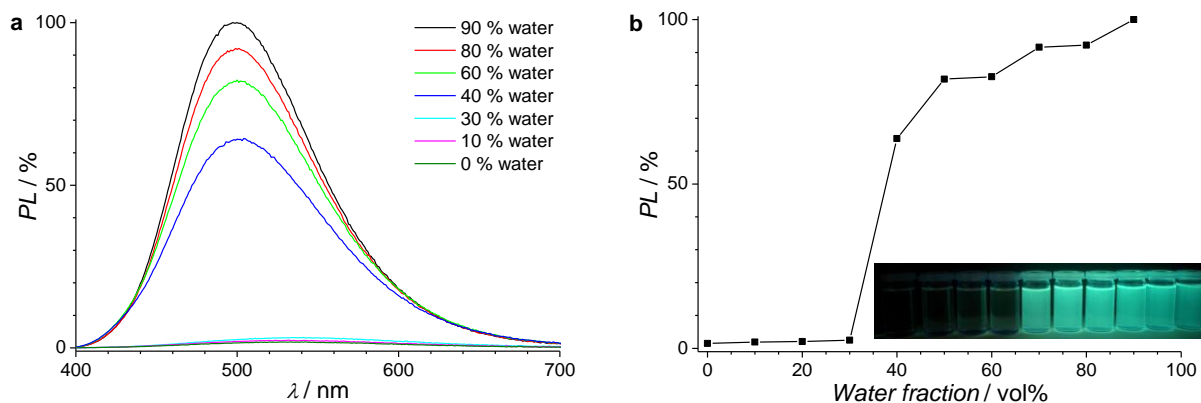


Figure 11. Photoluminescence spectra (a) and photoluminescence intensity at 497 nm (b) of 0.01 mM TPETPOcCz in THF/water mixtures upon excitation at 340 nm.

ding to a strong PL increase.²⁶ To finish up the monomer section, the PL quenching properties of aggregated TPETPOcCz dispersions in THF/water (1:9) caused by a prototypical nitroaromatic analyte, 1,3,5-trinitrobenzene (TNB) were explored. A progressive decrease of the PL intensity was obtained by adding TNB at the ppm level (0 ppm – 26 ppm, see Figure 12a). A possible mechanism of PL quenching may be energy transfer between the excited, electron-rich host and the electron-deficient nitroaromatic quencher.²⁷ A Stern-Volmer analysis displays an upward bended plot at high TNB concentrations thus pointing for amplified PL quenching (see Figure 12b).²⁸ Three quenching constants (K_{SV}) were calculated depending on the TNB concentration: $6.78\text{E}4 \text{ M}^{-1}$ below 30 μM , $1.52\text{E}5 \text{ M}^{-1}$ between 30 μM and 105 μM , and $2.53\text{E}5 \text{ M}^{-1}$ between 105 μM and 120 μM .

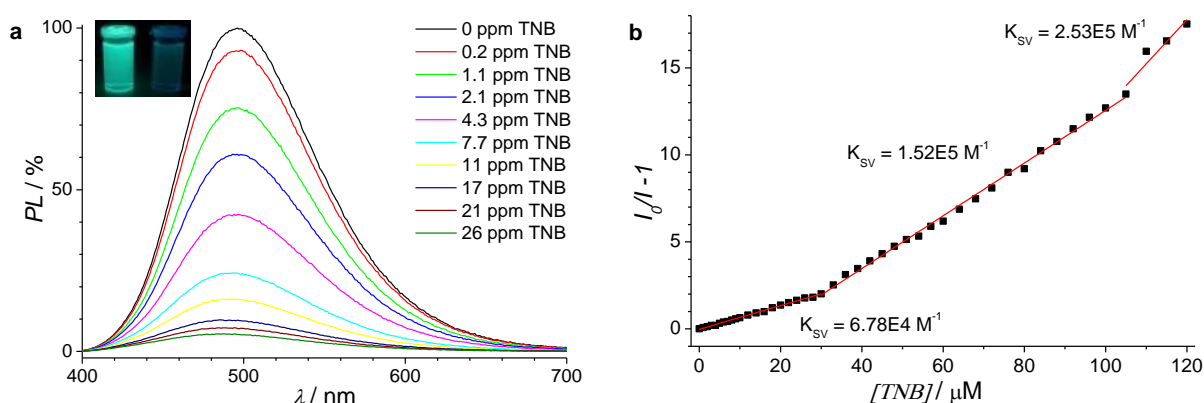


Figure 12. Photoluminescence spectra (a) of a 0.01 mM TPETPOcCz dispersion in THF/water (1:9) upon excitation at 340 nm, and Stern-Volmer plot of the PL intensity at 497 nm (b) by addition of different amounts of TNB.

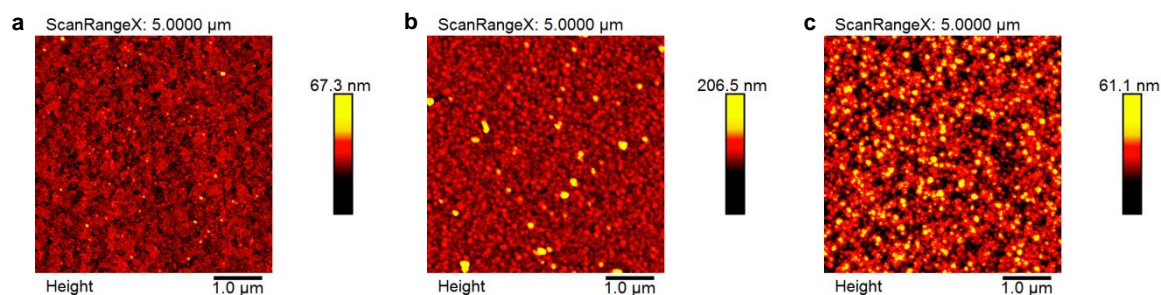


Figure 13. Tapping mode AFM images of MPN films on ITO: PTPETCz (a), PTPETPTCz (b), and PTPETPOcCz (c).

5.2.6. Optical and Morphological Characterization of Electrogenerated AIE-active MPN Films

As previously mentioned, the electrogenerated MPN films are also characterized by an intense PL, especially the carbazole-based materials. Therefore, the optical properties of the carbazolyl MPN films were also studied. The presence of high permanent microporosity and intense PL should provide a unique combination of properties, especially, for the PL quenching applications. Towards this end, MPN films were electrochemically prepared from a 0.1 mM solution of the carbazolyl monomers in dichloromethane using 0.1 M TBABF₄ as supporting electrolyte. Ten consecutive voltammetric cycles in the range from -1.0 V to 1.1 V were applied with a scan rate of 0.10 Vs⁻¹. Tapping mode AFM images of the films show a smooth topology (see Figure 13) with an average roughness (Rq) of 4 nm – 13 nm at thicknesses of 25 nm – 75 nm (see Table 4). The absorption spectra of the MPN films display long wavelength absorption maxima at ca. 350 nm (see Figure 14a).¹⁵ Upon excitation at 340 nm, these MPN thin films emit green-yellowish light with PL maxima centered at 527 nm for PTPETCz, 542 nm for PTPETPTCz, and 529 nm for PTPETPOcCz (see Figure 14b). Moderately high PL-QY values of 3.9 % (PTPETCz), 11.5 % (PTPETPTCz), and 3.1 % (PTPETPOcCz) were found, with the values still higher than the ones of the corresponding

Table 4. Average roughness, thicknesses and PL-QYs for excitation at 340 nm of electrogenerated carbazole-based MPN films on ITO.

MPN films	Rq (nm)	Thickness (nm)	PL λ_{\max} Film [nm]	PL-QY Film [%]
PTPETCz	4.0	25	527	3.9
PTPETPTCz	13.0	50	542	11.5
PTPETPOcCz	7.7	75	529	3.1

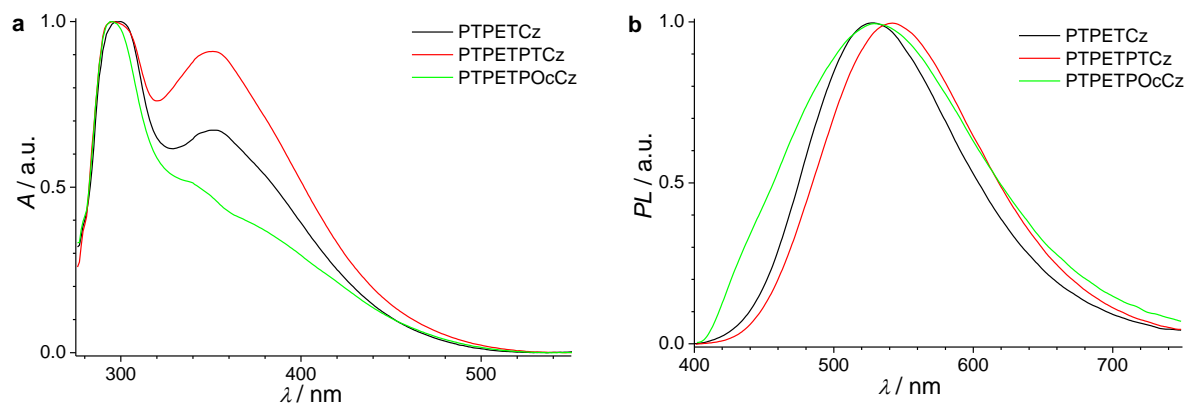


Figure 14. Absorption (a) and photoluminescence (b) spectra of the carbazole-based MPN films on ITO.

monomers in chloroform solutions. As shown in Chapter 2,²⁹ MPN films are better suited than the corresponding monomer films for the chemical detection of low concentrations of nitroaromatic analytes thus demonstrating the added value of the microporosity on sensing applications. Therefore, the potential of electrogenerated PTPETPOcCz films for the chemical sensing of nitroaromatic compounds was explored. Figure 15a illustrates the PL quenching upon contacting these MPN films with 100 ppm solutions of 4-nitrophenol (NP), 2,4,6-trinitrophenol (TNP), nitrobenzene (NB), 1,3-dinitrobenzene (DNB), 1,3,5-trinitrobenzene (TNB), 4-nitrotoluene (NT), 2,6-dinitrotoluene (DNT), and 2,4,6-trinitrotoluene (TNT) in acetonitrile for 1 min. The PL quenching correlates well to the number of nitro groups in the analyte, with a maximum PL quenching of 77 % for TNB. Assuming excited state energy

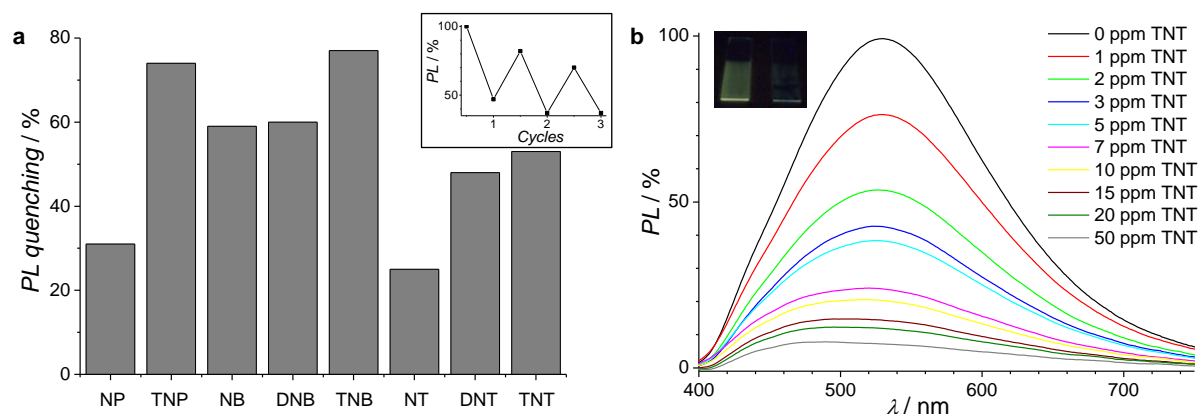


Figure 15. PL quenching of PTPETPOcCz thin films (upon excitation at 340 nm) after contacting with 100 ppm solutions of various nitroaromatic analytes in acetonitrile for 1 min (a), and PL spectra of PTPETPOcCz thin films after contacting with TNT solutions of different concentrations (b). The inset illustrates the reusability of the films after use in the detection of TNT and subsequent recycling.

transfer between electron-rich MPN film and electron-deficient quencher, this trend may be easily rationalized. Finally, PTPETPOcCz thin films were tested for the detection limit towards TNT due its importance to public health and security as well as for the environment.³⁰ Figure 15b displays a progressively decreased PL intensity for low ppm concentrations with a clearly detectable quenching already for 1 ppm TNT. PTPETPOcCz films also show good reusability after removal of the analyte by washing with acetonitrile and drying at reduced pressure at 100 °C (see inset of Figure 15a).

5.3. Conclusions

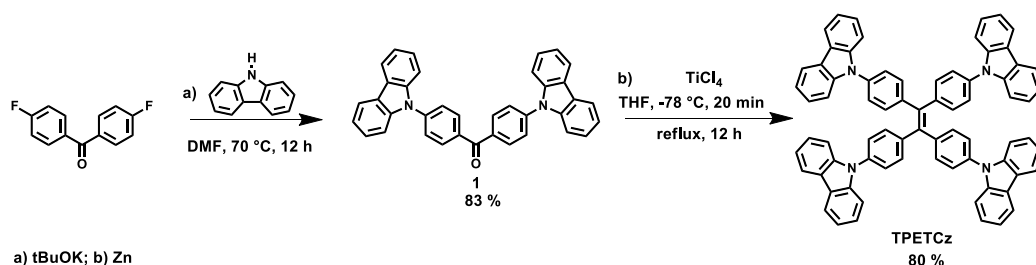
To sum up, a series of six tetraphenylethene-cored, carbazole- or thiophene-based monomers was synthesized and used in the generation of corresponding microporous polymers networks by chemical or electrochemical oxidative coupling. All polymers showed high microporosity with BET surface areas of up to 2203 m²g⁻¹. The monomers displayed the expected AIE activity especially for the carbazole-based monomers. Thin MPN films produced by electrochemical coupling were used for PL quenching-based sensing of nitroaromatic explosives reacting to low level of ca. 1 ppm for TNT.

5.4. Experimental Section

5.4.1. Monomers and bulk polymers

All reagents and chemicals were purchased from commercial suppliers, unless otherwise stated. ¹H and ¹³C NMR spectra were obtained on Bruker Avance 400 and III 600 machines. APLI mass spectra were recorded on a Bruker Daltronik micrOTOF system (KrF*-Laser ATLEX-SI, ATL Wermelskirchen), MALDI-TOF mass spectra on a Bruker Reflex TOF, and field desorption (FD) mass spectra on a VG Instruments ZAB2-SE-FPD. Thermogravimetric analyses were carried out under argon flow on a Mettler Toledo TGA/DSC1 STAR System. UV-vis spectra were recorded on a JASCO V-670. Photoluminescence spectra were obtained on a HORIBA Scientific FluoroMax-4 Spectrofluorometer connected to a Quanta-Phi integrating sphere for determination of PL quantum yields. A Tousimis Samdri-795 system was used for washing the bulk polymers with supercritical carbon dioxide. Nitrogen and krypton adsorption-desorption isotherms were recorded on a BEL Japan Inc Belsorp-max system at 77 K. A maximum relative pressure of 0.6 was set for measurements with Kr gas.

All samples were dried on a Belprep-vac II at 140 °C and ~ 2 Pa overnight prior to the gas sorption measurements.

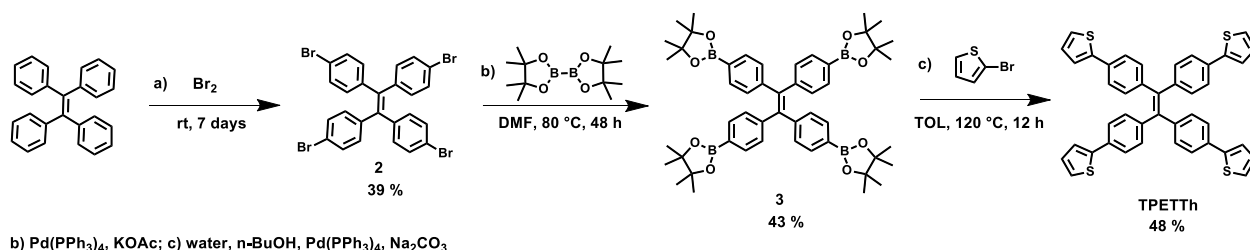


5.4.1.1. Synthesis of bis[4-(carbazol-9-yl)phenyl]methanone (1)

In a 100 mL round flask, carbazole (3.07 g, 18.33 mmol) was dissolved in anhydrous DMF (30 mL). After adding potassium tert-butoxide (2.16 g, 19.25 mmol), the mixture was heated up to 70 °C for 10 min and then bis(4-fluorophenyl)methanone (2.00 g, 9.17 mmol) in DMF (20 mL) were added. The mixture was stirred for additional 12 h. After cooling down to room temperature, the crude was poured into ice-water, filtered and recrystallized from acetone to give a yellow product, yield: 3.89 g (83 %). ^1H NMR (400 MHz, $\text{C}_2\text{D}_2\text{Cl}_4$) δ : 8.24-8.18 (m, 8H), 7.84 (d, $J = 8.50$ Hz, 4H), 7.63 (d, $J = 8.23$ Hz, 4H), 7.55-7.48 (m, 4H), 7.42-7.36 (m, 4H); ^{13}C NMR (101 MHz, $\text{C}_2\text{D}_2\text{Cl}_4$) δ : 194.38, 141.60, 140.00, 135.53, 131.82, 126.30, 126.20, 123.56, 120.68, 120.39, 109.80; MS (APLI) 512.171 [512.189] (M^+).

5.4.1.2. Synthesis of 1,1,2,2-tetra[4-(carbazol-9-yl)phenyl]ethene (TPETCz)

To a solution of bis[4-(carbazol-9-yl)phenyl]methanone (1.50 g, 2.93 mmol) in dry THF (50 mL), zinc dust (0.46 g, 7.03 mmol) was added followed by the addition of titanium(IV) chloride (0.67 g, 3.52 mmol) after cooling to -78 °C. After stirring for 20 min under argon, the reaction mixture was warmed up to room temperature and then heated up to reflux for 12 h. Next, the reaction mixture was cooled to room temperature and poured into water. The organic layer was extracted with dichloromethane and the combined organic layers were washed with brine and water, and finally dried over magnesium sulfate. After solvent evaporation, the residue was washed with dichloromethane resulting in a white solid, yield: 1.16 g (80 %). ^1H NMR (400 MHz, $\text{C}_2\text{D}_2\text{Cl}_4$) δ : 8.21-8.15 (m, 8H), 7.60-7.53 (m, 16H), 7.49 (d, $J = 8.05$ Hz, 8H), 7.42-7.36 (m, 8H), 7.35-7.29 (m, 8H); ^{13}C NMR (101 MHz, $\text{C}_2\text{D}_2\text{Cl}_4$) δ : 141.85, 140.99, 140.48, 136.14, 132.81, 126.23, 126.10, 123.12, 120.23, 120.05, 109.68; MS (MALDI TOF) 992.3 [992.4] (M^+).



5.4.1.3. Synthesis of 1,1,2,2-tetra(4-bromophenyl)ethene (2)

An evaporation plate with 1,1,2,2-tetraphenylethene (20 g, 60.20 mmol) and bromine (10 mL) was placed in a slightly open desiccator for 7 days (bromine was refilled whenever needed). The brownish product was recrystallized from a dichloromethane/methanol (2:1) mixture to give a white solid, yield: 15.17 g (39 %). ¹H NMR (400 MHz, C₂D₂Cl₄): δ 7.29 (d, *J* = 8.5 Hz, 8H), 6.86 (d, *J* = 8.5 Hz, 8H); ¹³C NMR (101 MHz, C₂D₂Cl₄): δ 141.3, 139.4, 132.6, 131.1, 121.0; MS (APLI) 647.781 [647.795] (M⁺).

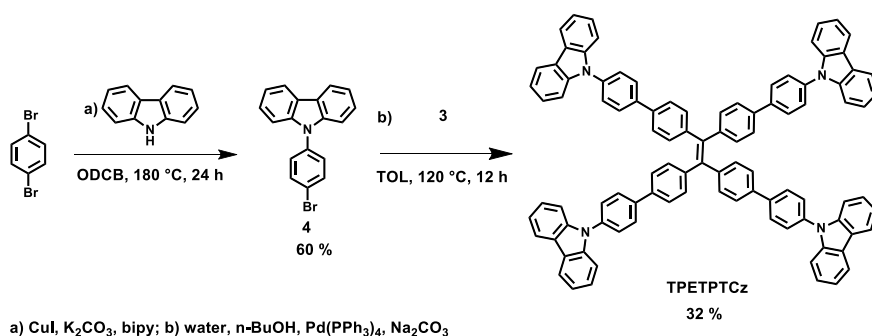
5.4.1.4. Synthesis of 1,1,2,2-tetra[4-(4,4,5,5-tetramethyl-1,3,2-dioxaborolan-2-yl)phenyl]ethene (3)

1,1,2,2-Tetra(4-bromophenyl)ethene (7.00 g, 10.80 mmol), potassium acetate (8.48 g, 86.0 mmol), bis(pinacolato)diboron (12.07 g, 47.5 mmol) and anhydrous DMF (90 mL) were placed in a two-necked round bottom flask under argon atmosphere and stirred for 15 minutes. After addition of tetrakis(triphenylphosphine)palladium(0) (0.62 g, 0.54 mmol) in DMF (10 mL), the mixture was stirred under exclusion of light at 100 °C for 48 hours. After cooling to room temperature, the mixture was quenched with water and extracted with dichloromethane. The combined organic layers were dried over anhydrous magnesium sulfate. The solvent was evaporated and the residue was recrystallized from a mixture of ethanol/dichloromethane to give a light yellow solid, yield: 3.90 g (43 %) ¹H NMR (600 MHz, C₂D₂Cl₄): δ 7.58-7.50 (m, 8H), 7.07-6.98 (m, 8H), 1.37 (s, 48H); ¹³C NMR (141 MHz, C₂D₂Cl₄): δ 146.0, 141.2, 134.0, 130.3, 83.6, 24.8; MS (APLI) 834.472 [836.500] (M⁺).

5.4.1.5. Synthesis of 1,1,2,2-tetra[4-(thiophen-2-yl)phenyl]ethene (TPETTh)

1,1,2,2-Tetra[4-(4,4,5,5-tetramethyl-1,3,2-dioxaborolan-2-yl)phenyl]ethene (2.00 g, 2.39 mmol), 2-bromothiophene (1.72 g, 10.52 mmol), sodium carbonate (2.28 g, 21.5 mmol), anhydrous toluene (20 mL), degasified butanol (12 mL) and degasified water (15 mL) were added to a two-necked round flask under argon atmosphere. After heating up to 80 °C, tetrakis(triphenylphosphine)palladium(0) (0.28 g, 0.24 mmol) in toluene (10 mL) was added to the mixture and refluxed under exclusion of light at 120 °C for 10 h. After cooling down to

room temperature, the crude product was diluted with chloroform and washed with aqueous 2 N HCl. The organic phase was dried over anhydrous magnesium sulfate and the solvent was removed by evaporation. The residue was purified by silica gel column chromatography (eluent: hexane/dichloromethane in a gradient from 6:1 to 4:1) to give a yellow solid, yield: 0.76 g (48 %). ^1H NMR (400 MHz, $\text{C}_2\text{D}_2\text{Cl}_4$): δ 7.38 (d, $J = 8.4$ Hz, 8H), 7.28 (dd, $J = 3.6$, 1.0 Hz, 8H), 7.24 (dd, $J = 5.1$, 1.0 Hz, 8H), 7.07 (d, $J = 8.4$ Hz, 8H), 7.04 (dd, $J = 5.1$, 3.6 Hz, 8H); ^{13}C NMR (101 MHz, $\text{C}_2\text{D}_2\text{Cl}_4$): δ 144.3, 143.0, 140.4, 132.6, 132.3, 128.5, 125.4, 125.2, 123.4; MS (APLI) 660.096 [660.107] (M^+).



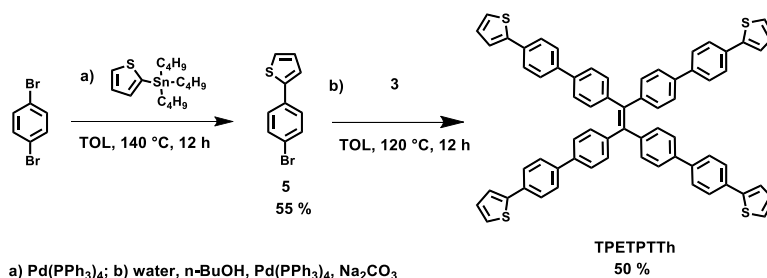
5.4.1.6. Synthesis of 9-(4-bromophenyl)-carbazole (4)

1,4-Dibromobenzene (14.11 g, 59.8 mmol), carbazole (5.00 g, 29.9 mmol), copper(I)iodide (0.57 g, 2.99 mmol), potassium carbonate (37.2 g, 269 mmol), 2,2'-bipyridine (1.21 g, 7.77 mmol) and o-dichlorobenzene (70 mL) were added to a double-necked round flask under argon atmosphere and stirred under exclusion of light at 180 °C overnight. The hot reaction mixture was filtered over celite and washed with hot toluene. After solvent evaporation, the crude product was purified by silica gel column chromatography (eluent: hexane) to give a white solid, yield: 5.793 g (60 %). ^1H NMR (400 MHz, $\text{C}_2\text{D}_2\text{Cl}_4$): δ 7.80 - 7.75 (m, 2H), 7.51 - 7.40 (m, 6H), 7.34 (ddd, $J = 8.0$, 5.5, 1.4, 2H); ^{13}C NMR (101 MHz, $\text{C}_2\text{D}_2\text{Cl}_4$): δ (ppm) 140.3, 136.5, 133.1, 128.4, 126.1, 123.2, 120.7, 120.3, 120.2, 109.5; MS (APLI) 320.996 [321.015] (M^+).

5.4.1.7. Synthesis of 1,1,2,2-tetra[4'-(carbazol-9-yl)-(1,1'-biphenyl)-4-yl]ethene (TPETPTCz)

1,1,2,2-tetra[4-(4,4,5,5-tetramethyl-1,3,2-dioxaborolan-2-yl)phenyl]ethene (0.50 g, 0.60 mmol), 9-(4-bromophenyl)-carbazole (0.828 g, 2.57 mmol), sodium carbonate (0.570 g, 5.38 mmol), anhydrous toluene (20 mL), degasified butanol (12 mL) and degasified water (15 mL) were added to a two-necked round flask under argon atmosphere. After heating up to

80 °C, tetrakis(triphenylphosphine)palladium(0) (0.07 g, 0.06 mmol) in toluene (10 mL) was added and the mixture refluxed under exclusion of light at 120 °C for 10 h. After cooling down to room temperature, the crude product was diluted with chloroform and washed with aqueous 2 N HCl. The organic phase was dried over anhydrous magnesium sulfate and the solvent removed by evaporation. The residue was purified by silica gel column chromatography (eluent: hexane/dichloromethane 7:3) to give a yellow solid, yield: 0.25 g (32 %). ¹H NMR (400 MHz, C₂D₂Cl₄): δ 8.17 (d, *J* = 7.8 Hz, 8H), 7.95 – 7.85 (m, 8H), 7.71 – 7.58 (m, 16H), 7.54 – 7.41 (m, 16H), 7.40 – 7.25 (m, 16H); ¹³C NMR (101 MHz, C₂D₂Cl₄): δ 143.0, 140.6, 139.3, 137.7, 137.6, 136.5, 132.1, 128.1, 127.0, 126.2, 126.0, 123.1, 120.2, 120.0, 109.8; MS (MALDI TOF) 1297.612 [1297.516] (M⁺).



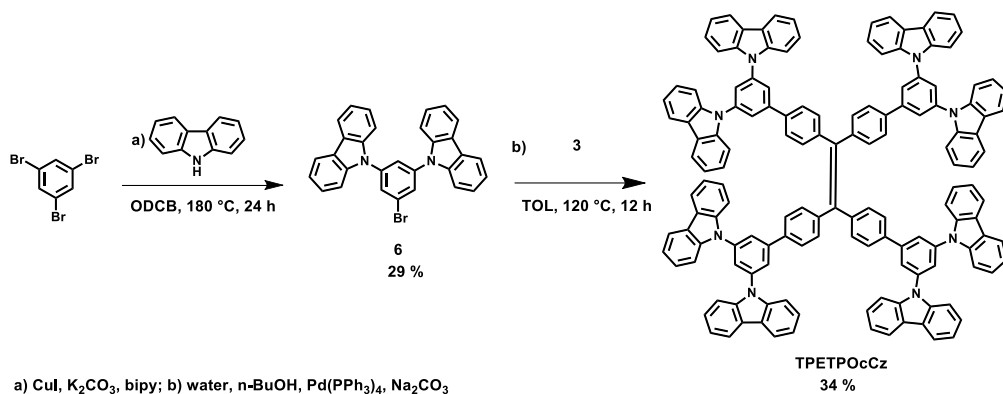
5.4.1.8. Synthesis of 2-(4-bromophenyl)thiophene (5)

1,4-Dibromobenzene (4.00 g, 16.96 mmol), tributyl(thiophen-2-yl)stannane (3.16 g, 8.48 mmol) and dry toluene (10 mL) were added to a 20 ml microwave vial under argon atmosphere. After adding tetrakis(triphenylphosphine)palladium(0) (0.49 g, 0.424 mmol) in 5 ml dry toluene, the mixture was stirred under exclusion of light at 140 °C for 10 h. The crude was purified by silica gel column chromatography (eluent: hexane) to give a white solid, yield: 1.13 g (55 %). ¹H NMR (400 MHz, C₂D₂Cl₄): δ H 7.55-7.47 (m, 4H), 7.35-7.32 (m, 2H), 7.11 (dd, *J* = 5.0, 3.7, 1H); ¹³C NMR (101 MHz, C₂D₂Cl₄): δ 142.8, 133.2, 131.9, 128.2, 127.3, 125.4, 123.6, 121.1; MS (FD) 240.2 [239.132] (M⁺).

5.4.1.9. Synthesis of 1,1,2,2-tetra[4'-(thiophen-2-yl)-(1,1'-biphenyl)-4-yl]ethene (TPETPTTh)

1,1,2,2-Tetra[4-(4,4,5,5-tetramethyl-1,3,2-dioxaborolan-2-yl)phenyl]ethene (0.70 g, 0.84 mmol), 2-(4-bromophenyl)thiophene (0.86 g, 3.60 mmol), sodium carbonate (0.80 g, 7.53 mmol), anhydrous toluene (20 mL), degasified butanol (12 mL) and degasified water (15 mL) were added to a two-necked round flask under argon atmosphere. After heating up to 80 °C, tetrakis(triphenylphosphine)palladium(0) (0.10 g, 0.08 mmol) in toluene (10 mL) was

added to the mixture and the mixture refluxed under exclusion of light at 120 °C for 10 h. After cooling down to room temperature, chloroform was added to the crude product. The mixture was washed with aqueous 2 N HCl, the organic phase was filtrated and finally washed with chloroform to give a greenish solid, yield: 0.41 g (50 %). ^1H NMR (400 MHz, $\text{C}_2\text{D}_2\text{Cl}_4$): δ 7.69-7.63 (m, 16H), 7.50-7.38 (m, 8H), 7.39-7.35 (m, 4H), 7.34-7.31 (m, 4H), 7.26-7.15 (m, 8H), 7.14-7.10 (m, 4H); MS (APLI) 964.228 [964.233] (M^+).



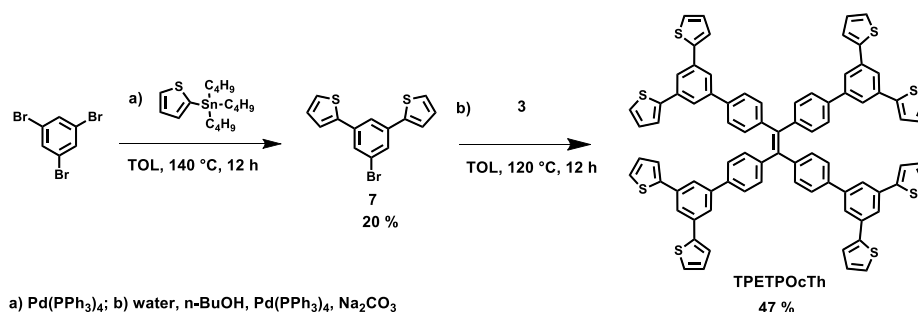
5.4.1.10. Synthesis of 9,9'-(5-bromo-1,3-phenylene)bis(carbazole) (6)

1,3,5-Tribromobenzene (7.00 g, 22.2 mmol), carbazole (7.44 g, 44.5 mmol), copper(I)iodide (0.85 g, 4.5 mmol), potassium carbonate (27.7 g, 200 mmol), 2,2'-bipyridine (1.74 g, 11.1 mmol) and o-dichlorobenzene (70 mL) were added to a double-necked round flask under argon atmosphere and stirred under exclusion of light at 180 °C for 10 h. The hot reaction mixture was filtered over celite and washed with hot toluene. After solvent evaporation, the crude product was purified by silica gel column chromatography (eluent: hexane) to give a white solid, yield: 3.11 g (29 %). ^1H NMR (400 MHz, $\text{C}_2\text{D}_2\text{Cl}_4$): δ 8.18 (d, $J = 7.6$ Hz, 1H), 7.90 (d, $J = 1.9$ Hz, 2H), 7.83 (t, $J = 1.8$ Hz, 1H), 7.60 (d, $J = 8.2$ Hz, 4H), 7.53 – 7.48 (m, 4H), 7.40 – 7.35 (m, 4H); ^{13}C NMR (101 MHz, $\text{C}_2\text{D}_2\text{Cl}_4$): δ 140.2, 140.0, 128.4, 126.4, 124.1, 123.5, 123.5, 120.8, 120.5, 109.6; MS (APLI) 488.054 [488.072] (M^+).

5.4.1.11. Synthesis of 1,1,2,2-tetra[3',5'-di(carbazol-9-yl)-(1,1'-biphenyl)-4-yl]ethene (TPETPOcCz)

1,1,2,2-Tetra[4-(4,4,5,5-tetramethyl-1,3,2-dioxaborolan-2-yl)phenyl]ethene (0.50 g, 0.60 mmol), 9,9'-(5-bromo-1,3-phenylene)bis(carbazole) (1.25 g, 2.57 mmol), sodium carbonate (0.57 g, 5.38 mmol), anhydrous toluene (20 mL), degasified butanol (12 mL) and degasified water (15 mL) were added to a two-necked round flask under argon atmosphere. After heating up to 80 °C, tetrakis(triphenylphosphine)palladium(0) (0.07 g, 0.06 mmol) in

toluene (10 mL) was added. The mixture was refluxed under exclusion of light at 120 °C for 10 h. After cooling down to room temperature, the crude product was diluted with chloroform and washed with aqueous 2 N HCl. The organic phase was dried over anhydrous magnesium sulfate and the solvent was evaporated. The resulting residue was purified by silica gel column chromatography (eluent: hexane/dichloromethane 6:4) to give a yellow solid, yield: 0.40 g (34 %). ¹H NMR (600 MHz, C₂D₂Cl₄): δ 8.18 (d, *J* = 7.8 Hz, 16H), 7.93 (d, *J* = 1.8 Hz, 8H), 7.77 (t, *J* = 1.8 Hz, 4H), 7.59 (t, *J* = 7.4 Hz, 24H), 7.47-7.40 (m, 16H), 7.35-7.28 (m, 24H); ¹³C NMR (141 MHz, C₂D₂Cl₄): δ 143.9, 143.6, 140.4, 140.3, 140.3, 139.4, 136.9, 132.1, 126.5, 126.2, 123.8, 123.3, 120.4, 120.4, 109.6; MS (APLI) 1957.127 [1957.747] (M⁺).



5.4.1.12. Synthesis of 2,2'-(5-bromo-1,3-phenylene)dithiophene (7)

1,3,5-Tribromobenzene (3.00 g, 9.53 mmol), tributyl(thiophen-2-yl)stannane (7.11 g, 19.06 mmol) and dry toluene (10 mL) were added to a 20 ml microwave vial under argon atmosphere. After adding tetrakis(triphenylphosphine)palladium(0) (0.15 g, 0.13 mmol) in toluene (5 mL), the mixture was stirred under exclusion of light at 140 °C for 10 h. The crude product was purified by silica gel column chromatography (eluent: hexane) and sublimation (100 °C, 10⁻² torr) to give yellow crystalline needles, yield: 0.60 g (20 %). ¹H NMR (600 MHz, C₂D₂Cl₄): δ 7.74 (t, *J* = 1.6 Hz, 1H), 7.66 (d, *J* = 1.6 Hz, 2H), 7.40 – 7.37 (m, 4H), 7.13 (dd, *J* = 5.1, 3.6 Hz, 2H); ¹³C NMR (141 MHz, C₂D₂Cl₄): δ 142.3, 137.0, 128.7, 127.8, 126.5, 124.8, 123.7, 122.4; MS (APLI) 321.913 [321.931] (M⁺).

5.4.1.13. Synthesis of 1,1,2,2-tetra[3',5'-di(thiophen-2-yl)-(1,1'-biphenyl)-4-yl]ethene (TPETPOcTh)

1,1,2,2-Tetra[4-(4,4,5,5-tetramethyl-1,3,2-dioxaborolan-2-yl)phenyl]ethene (0.32 g, 0.41 mmol), 2,2'-(5-bromo-1,3-phenylene)dithiophene (0.57 g, 1.77 mmol), sodium carbonate (0.39 g, 3.71 mmol), anhydrous toluene (20 mL), degasified butanol (12 mL) and degasified water (15 mL) were added to a two-necked round flask under argon atmosphere. After heating

up to 80 °C, tetrakis(triphenylphosphine)palladium(0) (0.05 g, 0.04 mmol) in toluene (10 mL) was added and the mixture refluxed under exclusion of light at 120 °C for 10 h. After cooling down to room temperature, the crude product was diluted with chloroform and washed with aqueous 2 N HCl. The organic phase was dried over anhydrous magnesium sulfate and the solvent was evaporated. The resulting residue was purified by silica gel column chromatography (eluent: hexane/dichloromethane 6:1 to 3:1) to give a white solid, yield: 0.25 g (47 %). ¹H NMR (400 MHz, C₂D₂Cl₄): δ 7.79 (d, *J* = 1.4 Hz, 4H), 7.75 (d, *J* = 1.5 Hz, 8H), 7.55 (d, *J* = 8.3 Hz, 8H), 7.44 (dd, *J* = 3.5, 0.9 Hz, 8H), 7.35 (dd, *J* = 5.1, 0.8 Hz, 8H), 7.31 (d, *J* = 8.3 Hz, 8H), 7.13 (dd, *J* = 5.0, 3.6 Hz, 8H); ¹³C NMR (101 MHz, C₂D₂Cl₄): δ 143.5, 143.1, 141.8, 140.4, 138.0, 135.3, 132.0, 128.1, 126.4, 125.3, 123.8, 123.6, 122.3; MS (APLI) 1292.988 [1292.183] (M⁺).

5.4.1.14. Synthesis of bulk polymers by oxidative coupling with FeCl₃

All monomers were chemically polymerized in a similar procedure as described here for the TPEPOcCz monomer: 1,1,2,2-tetra[3',5'-di(carbazol-9-yl)-(1,1'-biphenyl)-4-yl]ethene (0.10 g, 0.051 mmol) was dissolved in anhydrous chloroform (20 mL) and added dropwise to a suspension of iron(III) chloride (0.21 g, 1.29 mmol) in anhydrous chloroform (30 mL) under argon atmosphere. The resulting mixture was stirred at room temperature for one day. After addition of methanol (100 mL), the mixture was stirred for one more hour. The resulting precipitate was collected by filtration and washed with methanol. The powder was treated with aqueous hydrochloric acid (37 %) for 2 h, filtered off and washed with water and methanol. After Soxhlet extraction with methanol and THF for 24 h, the product was treated with ethanol (p.a.) for three days and finally washed with supercritical carbon dioxide. PTPETPOcCz was isolated as yellow powder, yield: 0.084 g (84 %). PTPETCz as yellow powder (99 %), PTPETTh as orange powder (73 %), PTPEPTCz was obtained as yellow powder (80 %), PTPEPTTh as dark yellow powder (85 %), and finally PTPEPOcTh as yellow powder (99 %).

5.4.2. Electrochemical Studies

Dichloromethane (HPLC grade) was refluxed over phosphorus pentoxide for 3 h and distilled. Tetrabutylammonium tetrafluoroborate (TBABF₄, ≥ 99 %) was purchased from Alfa Aesar. Borontrifluoride diethyletherate (BFEE, ≥ 46.5 % BF₃), nitrobenzene (NB, analytical standard), 1,3-dinitrobenzene (DNB, analytical standard) and 2,4,6-trinitrophenol (TNP, ≥ 98%, moistened with water) were purchased from Sigma-Aldrich; 1,3,5-trinitrobenzene

(TNB, neat) from Supelco; 4-nitrotoluene (NT, 99 %) from Across; and 4-nitrophenol (NP, 99 %) from ABCR. Potassium chloride (KCl, ≥ 99.5 %, ACS) was purchased from Roth. Indium tin oxide-coated transparent electrodes on glass (ITO, ≤ 20 Ohm m^{-2}) were purchased from pgo. For electrochemical polymerization and characterization, an electrochemical workstation PAR VersaSTAT 4 was used in combination to a three-electrode cell. The AFM images were recorded on an atomic force microscope Bruker diInnova operated in tapping mode. Average surface roughness and thickness of the films were extracted from the topography images.

5.4.2.1. Electrochemical polymerization and characterization on Pt disc electrodes

10 mL of 0.1 mM solutions of the carbazole- or thiophene-based monomers were prepared in dichloromethane or BFEE/dichloromethane (1:4), respectively, using 0.1 M TBABF₄ as supporting electrolyte. The solutions were placed in a three-electrode cell under argon atmosphere at 25 °C. A platinum disc electrode (Pt, 1 mm diameter) was used as working electrode (WE), a platinum wire as counter electrode (CE), and Ag⁰/AgNO₃ (0.01 M AgNO₃/0.1 M TBAP, 0.56 V vs NHE) as reference electrode (RE). Multiple cyclic voltammograms were repeatedly recorded in a potential range from -1.0 V to 1.2 V (TPETCz, TPETPTCz, TPETPOcCz, TPETPTTh, and TPETPOcTh) or -1.0 V to 1.4 V (TPETTh) with a scan rate of 0.1 Vs⁻¹. The resulting deposits on Pt were placed as WE in 0.1 M monomer-free solutions of TBABF₄ in dichloromethane. Multiple cyclic voltammograms at different scan rates from 0.005 to 0.20 Vs⁻¹ were recorded in the potential range from 0 V to 1.1 V (TPETCz, TPETPTCz, and TPETPOcCz) or 1.0 V (TPETTh, TPETPTTh, and TPETPOcTh).

5.4.2.2. Electrochemical polymerization on ITO electrodes for porosity measurements and optical characterization

10 mL of the monomers solutions were placed in a three-electrode cell. ITO (~ 1.5 cm x 1.2 cm deposited area) on glass and a platinum gauze (2.5 cm x 1.2 cm area), separated by 1 cm, were used as WE and CE, respectively (Ag⁰/AgNO₃ as RE). For krypton gas sorption measurements, thick films were produced by applying an oxidative potential of 1.2 V (TPETCz, TPETPTCz, TPETPOcCz, TPETPTTh, and TPETPOcTh) or 1.4 V (TPETTh) for 20 min. Afterwards, a potential of -1.0 V was applied for 120 s in order to dedope the deposits. After rinsing the deposits with acetonitrile and dichloromethane, they were dried for 20 min at 100 °C. The collection of ca. 2 mg of material was necessary for reliable BET measurements. For morphological characterization, carbazole-based MPN films on ITO were prepared by applying ten voltammetric cycles in the potential range of -1.0 V to 1.1 V at scan

rate of 0.01 Vs^{-1} . After rinsing the films with acetonitrile and dichloromethane, they were dried for 20 min at $100 \text{ }^\circ\text{C}$.

5.5. References

- (1) Palma-Cando, A.; Woitassek, D.; Brunklaus, G.; Scherf, U. *Mater. Chem. Front.* **2017**, DOI: 10.1039/C6QM00281A.
- (2) Chen, Q.; Luo, M.; Hammershøj, P.; Zhou, D.; Han, Y.; Laursen, B. W.; Yan, C.-G.; Han, B.-H. *J. Am. Chem. Soc.* **2012**, *134*, 6084.
- (3) Xu, Y.; Jin, S.; Xu, H.; Nagai, A.; Jiang, D. *Chem. Soc. Rev.* **2013**, *42*, 8012.
- (4) Chen, Q.; Liu, D.-P.; Luo, M.; Feng, L.-J.; Zhao, Y.-C.; Han, B.-H. *Small* **2014**, *10*, 308.
- (5) Palma-Cando, A.; Scherf, U. *Macromol. Chem. Phys.* **2016**, *217*, 827.
- (6) Ringk, A.; Lignie, A.; Hou, Y.; Alshareef, H. N.; Beaujuge, P. M. *ACS Appl. Mater. Interfaces.* **2016**, *8*, 12091.
- (7) Hu, X.-M.; Salmi, Z.; Lillethorup, M.; Pedersen, E. B.; Robert, M.; Pedersen, S. U.; Skrydstrup, T.; Daasbjerg, K. *Chem. Commun.* **2016**, *52*, 5864.
- (8) Palma-Cando, A.; Scherf, U. *ACS Appl. Mater. Interfaces.* **2015**, *7*, 11127.
- (9) Palma-Cando, A.; Preis, E.; Scherf, U. *Macromolecules* **2016**.
- (10) Luo, J.; Xie, Z.; Lam, J. W. Y.; Cheng, L.; Chen, H.; Qiu, C.; Kwok, H. S.; Zhan, X.; Liu, Y.; Zhu, D.; Tang, B. Z. *Chem. Commun.* **2001**, 1740.
- (11) Mei, J.; Hong, Y.; Lam, J. W. Y.; Qin, A.; Tang, Y.; Tang, B. Z. *Adv. Mater.* **2014**, *26*, 5429.
- (12) Hong, Y.; Lam, J. W. Y.; Tang, B. Z. *Chem. Commun.* **2009**, 4332.
- (13) Qin, A.; Lam, J. W. Y.; Tang, B. Z. *Prog. Polym. Sci.* **2012**, *37*, 182.
- (14) Hu, R.; Kang, Y.; Tang, B. Z. *Polym. J.* **2016**, *48*, 359.
- (15) Gu, C.; Huang, N.; Wu, Y.; Xu, H.; Jiang, D. *Angew. Chem. Int. Ed.* **2015**, *54*, 11540.
- (16) Qiao, S.; Du, Z.; Yang, R. *J. Mater. Chem. A* **2014**, *2*, 1877.
- (17) Preis, E.; Dong, W.; Brunklaus, G.; Scherf, U. *J. Mater. Chem. C* **2015**, *3*, 1582.
- (18) Zhang, X.; Lu, J.; Zhang, J. *Chem. Mater.* **2014**, *26*, 4023.
- (19) Zhang, X.; Lv, Y.-Z.; Liu, X.-L.; Du, G.-J.; Yan, S.-H.; Liu, J.; Zhao, Z. *RSC Advances* **2016**, *6*, 76957.
- (20) Jiang, F.; Sun, J.; Yang, R.; Qiao, S.; An, Z.; Huang, J.; Mao, H.; Chen, G.; Ren, Y. *New J. Chem.* **2016**, *40*, 4969.

- (21) Inzelt, G.; Pineri, M.; Schultze, J. W.; Vorotyntsev, M. A. *Electrochim. Acta* **2000**, *45*, 2403.
- (22) Palma-Cando, A.; Brunklaus, G.; Scherf, U. *Macromolecules* **2015**, *48*, 6816.
- (23) Kaafarani, B. R.; El-Ballouli, A. a. O.; Trattnig, R.; Fonari, A.; Sax, S.; Wex, B.; Risko, C.; Khnayzer, R. S.; Barlow, S.; Patra, D.; Timofeeva, T. V.; List, E. J. W.; Bredas, J.-L.; Marder, S. R. *J. Mater. Chem. C* **2013**, *1*, 1638.
- (24) Heinze, J.; Frontana-Uribe, B. A.; Ludwigs, S. *Chem. Rev.* **2010**, *110*, 4724.
- (25) Zhao, Z.; Lam, J. W. Y.; Tang, B. Z. *Curr. Org. Chem.* **2010** *14* 2109.
- (26) Baysec, S.; Preis, E.; Allard, S.; Scherf, U. *Macromol. Rapid Commun.* **2016**, DOI: 10.1002/marc.201600485.
- (27) Content, S.; Trogler, W. C.; Sailor, M. J. *Chem. Eur. J.* **2000**, *6*, 2205.
- (28) Dong, W.; Fei, T.; Palma-Cando, A.; Scherf, U. *Polym. Chem.* **2014**, *5*, 4048.
- (29) Raupke, A.; Palma-Cando, A.; Shkura, E.; Teckhausen, P.; Polywka, A.; Gorrn, P.; Scherf, U.; Riedl, T. *Sci. Rep.* **2016**, *6*, 29118.
- (30) Fei, T.; Jiang, K.; Zhang, T. *Sens. Actuator B-Chem.* **2014**, *199*, 148.

Chapter 6

Summary and Outlook

6.1. Summary of Chapters 2 – 5

Thin films of microporous polymer networks (MPN) were generated by electrochemical polymerization of a series of di-, tri- and tetrafunctional carbazole-based monomers. The microporous films show high BET surface areas (S_{BET}) up to $1300 \text{ m}^2\text{g}^{-1}$ as directly measured by krypton sorption experiments. A correlation between the number of polymerizable carbazole units of the monomer and the resulting surface area is observed. Electrochemical sensing experiments with 1,3,5-trinitrobenzene demonstrate an up to 180 times increased current response of MPN-modified glassy carbon electrodes in relation to non-modified electrodes based on intermolecular interactions between the electron-poor nitroaromatic analytes and the electron-rich, high surface area microporous deposits. Further on, fluorescent thin MPN films were used in the gas-phase detection of 2,4,6-trinitrotoluene up to trace (ppb) concentrations.

Chemical polymerization of tetraphenylmethane or -silane, tetra- and octacarbazolyl-substituted monomers resulted in powdery MPNs with BET surface areas of up to $1331 \text{ m}^2\text{g}^{-1}$. Slightly increased S_{BET} values result for the materials made from the octacarbazolyl monomers if compared to the tetracarbazolyl analogues, while the exchange of the central carbon by a silicon atom leads to decreased surface areas. Moreover, electrochemical oxidative coupling enables the formation of thin polymer films. Electrochemical quartz microbalance measurements allow for an in-situ characterization of the electrochemical MPN generation. The electrochemical reduction of various nitroaromatic compounds (NACs) on MPN-modified glassy carbon electrodes was studied and applied for high sensitivity NAC detection up to the ppb level.

Thiophene-based monomers were synthesized by Stille- or Suzuki-type couplings followed by chemical or electrochemical polymerization into microporous polymer networks with high BET surface areas. Similar S_{BET} values of up to $2135 \text{ m}^2\text{g}^{-1}$ were determined for tetraphenylmethane-cored bulk MPN powders and thin films. Electrochemical polymerization in boron trifluoride diethyletherate/dichloromethane mixtures allows for the generation of MPN films with optimized porosity. A distinct effect of boron trifluoride on the connectivity

of the monomeric units during electropolymerization was observed for 3-thienyl-substituted monomers. The influence of the specific surface area of MPNs on the electrochemical response towards 1,3,5-trinitrobenzene was studied for these materials.

Finally, microporous polymer networks were prepared from AIE-active tetraphenylethene (TPE)-cored, multifunctional carbazole- or thiophene-based monomers by using chemical and electrochemical oxidative coupling methods. Octacarbazolyl monomers lead to MPNs with high degree of cross-linking and optimized S_{BET} values of up to $2200 \text{ m}^2\text{g}^{-1}$. These MPN films were tested for application in the chemical sensing of nitroaromatic analytes by fluorescence quenching.

6.2. Outlook

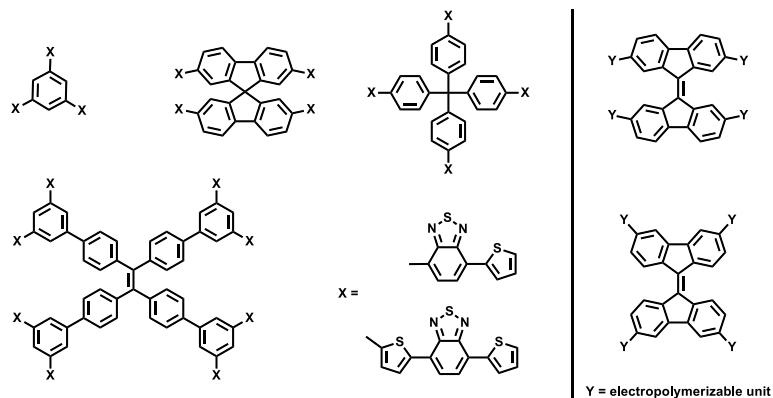
Regarding the electrochemical detection of nitroaromatic compounds (NACs) at MPN-modified electrodes, different approaches could help in improving the sensitivity of the method: i) Inclusion of additional electron-rich moieties into the monomers for facilitating the formation of charge-transfer complexes between MPN deposit and NACs; ii) Use of thicker MPN deposits with higher specific surface areas in order to increase the interfacial interactions; iii) Linear scan voltammograms at higher scan rates in diffusion-controlled regime for boosting the amperometric response; iv) Utilization of other electrochemical techniques with higher sensitivities e.g. differential pulse voltammetry (DPV);¹ and v) Use of the electrochemical quartz crystal microbalance (EQCM) for an electrogravimetric detection of NACs at MPN-modified electrodes.²

On the other hand, the application potential of electrogenerated MPN films that contain benzotrithiophene as electron donor phase in the active layer of organic solar cells (OSCs) has been described by Jiang and co-workers.³ They reported maximum power conversion efficiency (PCE) of 5.02 %. The incorporation of donor/acceptor couples as frequently used for the design of linear polymers⁴ may be applied for generation of related donor/acceptor tectons for MPNs (see Scheme 1) that can be used for the fabrication of efficient OSC.

Finally, OSCs based on non-fullerene electron acceptors have been described with 9,9'-bifluorenylidene derivatives.⁵ The electrochemical generation of MPNs based on tectons with 9,9'-bifluorenylidene cores could be possible by attaching multiple electropolymerizable

Summary and Outlook

substituents (see Scheme 1). Combining both approaches, fully electrogenerated, interdigitated donor and acceptor phases of MPNs may be tested as active layer of OSCs, possibly assembled by a layer-by-layer electrodeposition.



Scheme 1. Proposed chemical structures of multifunctional monomers for electrogeneration of electron donor (left) or electron acceptor (right) MPNs.

6.3. References

- (1) Ma, H.; Yao, L.; Li, P.; Ablikim, O.; Cheng, Y.; Zhang, M. *Chem. Eur. J.* **2014**, *20*, 11655.
- (2) Schlupp, M.; Weil, T.; Berresheim, A. J.; Wiesler, U. M.; Bargon, J.; Müllen, K. *Angew. Chem. Int. Ed.* **2001**, *40*, 4011.
- (3) Gu, C.; Huang, N.; Chen, Y.; Qin, L.; Xu, H.; Zhang, S.; Li, F.; Ma, Y.; Jiang, D. *Angew. Chem.* **2015**, *127*, 13798.
- (4) Kesters, J.; Verstappen, P.; Raymakers, J.; Vanormelingen, W.; Drijkoningen, J.; D'Haen, J.; Manca, J.; Lutsen, L.; Vanderzande, D.; Maes, W. *Chem. Mater.* **2015**, *27*, 1332.
- (5) Kim, H. U.; Kim, J.-H.; Suh, H.; Kwak, J.; Kim, D.; Grimsdale, A. C.; Yoon, S. C.; Hwang, D.-H. *Chem. Commun.* **2013**, *49*, 10950.

List of Abbreviations

A	Absorbance
AFM	Atomic force microscopy
AIE	Aggregation-induced emission
APLI	Atmospheric pressure laser ionization
BET	Brunauer-Emmett-Teller
BFEE	Boron trifluoride diethyletherate
ca.	<i>circa</i> (approximately)
CBP	4,4'-Di(carbazol-9-yl)-1,1'-biphenyl
CBPBT	4,7-Di[4-(carbazol-9-yl)phenyl]benzo[c]-[1,2,5]thiadiazole
CE	Counter electrode
CP	Conducting polymer
CPMAS	Cross-polarization magic-angle spinning
CV	Cyclic voltammogram
Cz	Carbazole
DCM	Dichloromethane
DNB	1,3-Dinitrobenzene
DNT	2,4-Dinitrotoluene
E	Potential
e.g.	<i>exempli gratia</i> (for example)
E_p	Potential peak
EQCM	Electrochemical quartz crystal microbalance
FD	Field desorption
FT-IR	Fourier transform infrared spectroscopy
GC	Glassy carbon
HOMO	Highest occupied molecular orbital
i	Current
I	PL intensity
I_0	Initial PL intensity
i_p	Current peak
ITO	Indium tin oxide
K_{SV}	Stern-Volmer quenching constant

LSV	Linear scan voltammogram
LUMO	Lowest unoccupied molecular orbital
MALDI-TOF	Matrix-assisted laser desorption/ionization time-of-flight
MeCN	Acetonitrile
MPN	Microporous polymer network
NAC	Nitroaromatic compound
NB	Nitrobenzene
NHE	Normal hydrogen electrode
NLDFT	Nonlocal density functional theory
NMR	Nuclear magnetic resonance
NP	4-Nitrophenol
NT	4-Nitrotoluene
OFET	Organic field effect transistor
OLED	Organic light emitting diode
OPV	Organic photovoltaic
OSC	Organic solar cell
P	Pressure
P ₀	Atmospheric pressure
PBS	Phosphate buffer solution
PL	Photoluminescence
ppb	Parts per billion
ppm	Parts per million
ppt	Parts per trillion
Q	Electric charge
QY	Quantum yield
RE	Reference electrode
RMS	Root-mean-square roughness
R _q	Root-mean-square roughness
S _{BET}	Specific surface area calculated by applying BET equation
S _{EQCM}	Electrochemically accessible surface area
Sp ³ Th	2,2',7,7'-Tetra(thien-3-yl)-9,9'-spirobifluorene
SpCz	2,2',7,7'-Tetra(carbazol-9-yl)-9,9'-spirobifluorene
SpTh	2,2',7,7'-Tetra(thien-2-yl)-9,9'-spirobifluorene
TBABF ₄	Tetrabutylammonium tetrafluoroborate

TBAP	Tetrabutylammonium perchlorate
TCB	1,3,5-Tri(carbazol-9-yl)benzene
TCTA	Tri[4-(carbazol-9-yl)phenyl]amine
TGA	Thermogravimetric analysis
Th	Thiophene
THF	Tetrahydrofuran
TNB	1,3,5-Trinitrobenzene
TNP	2,4,6-Trinitrophenol
TNT	2,4,6-Trinitrotolunene
torr	Torricelli
TPE	Tetraphenylethene
TPETCz	1,1,2,2-Tetra[4-(carbazol-9-yl)phenyl]ethene
TPETPOcCz	1,1,2,2-Tetra[3',5'-di(carbazol-9-yl)-(1,1'-biphenyl)-4-yl]ethene
TPETPOcTh	1,1,2,2-Tetra[3',5'-di(thiophen-2-yl)-(1,1'-biphenyl)-4-yl]ethene
TPETPTCz	1,1,2,2-Tetra[4'-(carbazol-9-yl)-(1,1'-biphenyl)-4-yl]ethene
TPETPTTh	1,1,2,2-Tetra[4'-(thiophen-2-yl)-(1,1'-biphenyl)-4-yl]ethene
TPETTh	1,1,2,2-Tetra[4-(thiophen-2-yl)phenyl]ethene
TPOcCz	Tetra[3,5-di(carbazol-9-yl)phenyl]methane
TPOcCzSi	Tetra[3,5-di(carbazol-9-yl)phenyl]silane
TPT3Th	Tetra[4-(thien-3-yl)phenyl]methane
TPTCz	Tetra[4-(carbazol-9-yl)phenyl]methane
TPTCzSi	Tetra[4-(carbazol-9-yl)phenyl]silane
TPTTh	Tetra[4-(thien-2-yl)phenyl]methane
v	Scan rate
V _a	Volume of adsorbate
vs.	<i>versus</i> (against)
WE	Working electrode

List of Publications

Papers Published as Base of This Thesis

1. **Palma-Cando, A.**; Woitassek, D.; Brunklaus, G.; Scherf, U.: Luminescent Tetraphenylethene-Cored, Carbazole- and Thiophene-Based Microporous Polymer Films for the Chemosensing of Nitroaromatic Analytes. *Mater. Chem. Front.* **2017**, DOI: 10.1039/C6QM00281A. (Chapter 5)
2. **Palma-Cando, A.**; Preis, E.; Scherf, U.: Silicon- or Carbon-Cored Multifunctional Carbazolyl Monomers for the Electrochemical Generation of Microporous Polymer Films. *Macromolecules* **2016**, 49, 8041. (Chapter 3)
3. Rüpke, A.; **Palma-Cando, A.**; Shkura, E.; Teckhausen, P.; Polywka, A.; Görrn, P.; Scherf, U.; Riedl, T.: Highly Sensitive Gas-Phase Explosive Detection by Luminescent Microporous Polymer Networks. *Sci. Rep.* **2016**, 6, 29118. (Chapter 2)
4. **Palma-Cando, A.**; Scherf, U.: Electrochemically Generated Thin Films of Microporous Polymer Networks: Synthesis, Properties, and Applications. *Macromol. Chem. Phys.* **2016**, 217, 827. (Chapter 1)
5. **Palma-Cando, A.**; Brunklaus, G.; Scherf, U.: Thiophene-Based Microporous Polymer Networks via Chemical or Electrochemical Oxidative Coupling. *Macromolecules* **2015**, 48, 6816. (Chapter 4)
6. **Palma-Cando, A.**; Scherf, U.: Electrogenerated Thin Films of Microporous Polymer Networks with Remarkably Increased Electrochemical Response to Nitroaromatic Analytes. *ACS Appl. Mater. Interfaces.* **2015**, 7, 11127. (Chapter 2)

Papers Published Outside the Scope of This Thesis

7. Chochos, C. L.; Drakopoulou, S.; Katsouras, A.; Squeo, B. M.; Sprau, C.; Colsmann, A.; Gregoriou, V.G.; **Palma-Cando, A.**; Allard, S.; Scherf, U.; Gasparini, N.; Ameri, T.; Brabec, C.J.; Avgeropoulos, A. Beyond Donor-Acceptor (D-A) Approach: Structure-Optoelectronic Properties-Organic Photovoltaic Performance Correlation in New D-A1-D-A2 Low Band Gap Conjugated Polymers. *Macromol. Rapid Commun.* **2017** (Accepted)
8. Gasparini, N.; García-Rodríguez, A.; Prosa, M.; Bayseç, Ş.; **Palma-Cando, A.**; Katsouras, A.; Avgeropoulos, A.; Pagona, G.; Gregoriou, V. G.; Chochos, C. L.; Allard,

- S.; Scherf, U.; Brabec, C. J.; Ameri, T.: Indacenodithienothiophene (IDTT)-Based Ternary Organic Solar Cells. *Front. Energy Res.* **2017**, DOI: 10.3389/fenrg.2016.00040.
9. Squeo, B. M.; Gasparini, N.; Ameri, T.; **Palma-Cando, A.**; Allard, S.; Gregoriou, V. G.; Brabec, C. J.; Scherf, U.; Chochos, C. L.: Ultra Low Band Gap α,β -Unsubstituted BODIPY-Based Copolymer Synthesized by Palladium Catalyzed Cross-Coupling Polymerization for Near Infrared Organic Photovoltaics. *J. Mater. Chem. A* **2015**, 3, 16279.
 10. **Palma-Cando, A.**; Frontana-Urbe, B.; Maldonado, J.; Rivera-Hernández, M.: Control of Thickness of PEDOT Electrodeposits on Glass/ITO Electrodes from Organic Solutions and its Use as Anode in Organic Solar Cells. *Procedia Chem.* **2014**, 12, 92
 11. Dong, W.; Fei, T.; **Palma-Cando, A.**; Scherf, U.: Aggregation Induced Emission and Amplified Explosive Detection of Tetraphenylethylene-Substituted Polycarbazoles. *Polym. Chem.* **2014**, 5, 4048.
 12. **Palma-Cando, A.**; Rivera-Hernández, M.; Frontana-Urbe, B.: Electrodepósitos de Poli-3,4-etilendioxitiofeno sobre Electrodo Transparentes de Oxido de Indio y Estaño. Control del Espesor y Morfología. *Química Central* **2013**, 3, 9.

Conference Publications

- **Alex Palma-Cando**, Gunther Brunklaus, Ullrich Scherf; Thiophene-Based Microporous Polymer Networks via Chemical or Electrochemical Oxidative Polymerization; **Poster**; *67th Annual Meeting of the International Society of Electrochemistry, ISE – 2016*; The Hague – Netherlands, **2016**
- **Alex Palma-Cando**, Gunther Brunklaus, Ullrich Scherf; Thiophene-Based Microporous Polymer Networks via Chemical or Electrochemical Oxidative Polymerization; **Poster**; *6th Baltic Electrochemistry Conference*; Helsinki – Finland, **2016**
- **Alex Palma-Cando**, Ullrich Scherf; Films of Electrogenenerated Microporous Polymer Networks for Electrochemical Determination of Nitroaromatic Compounds; **Oral**; *GDCh-Wissenschaftsforum Chemie – 2015*; Dresden - Germany, **2015**
- **Alex Palma-Cando**, Ullrich Scherf; Thin Films of Microporous Polymer Networks for the Electrochemical Detection of Nitroaromatic Compounds; **Poster**; *International Workshop on the Electrochemistry of Electroactive Materials WEEM – 2015*; Bad Herrenalb - Germany, **2015**
- **Alex Palma-Cando**, Ullrich Scherf; Electrochemical Polymerization of Carbazole Derivatives; **Poster**; *65th Annual Meeting of the International Society of Electrochemistry, ISE – 2014*; Lausanne - Switzerland, **2014**

Acknowledgements

First of all, I would like to thank Prof. Dr. Ullrich Scherf for giving me this amazing opportunity and welcoming me to his excellent working group at the Bergische Universität Wuppertal in Germany. Not only his scientific advice and vast knowledge are greatly appreciated but also his kindness and friendly temperament.

I thank Prof. Dr. Bernardo Frontana-Uribe and Prof. Dr. Arne Thomas for the revision of this thesis.

I gratefully thank the German Academic Exchange Service (DAAD) for providing me a Research Grant for Doctoral Candidates and Young Academics and Scientists (91540663).

I would also like to thank the help and technical support from Kerstin Müller, Sylwia Adamczyk and Anke Helfer.

I greatly acknowledge the support from Dr. Gunther Brunklaus for the solid state ^{13}C NMR spectra measurements, as well as Andre Raüpke and Prof. Dr. Thomas Riedl for the gas-phase detection of nitroaromatic analytes experiments.

My sincere thanks to Dr. Suman Samanta, Şebnem Bayseç, Dr. Sebastian Kowalski, Dr. Edward Preis, Dr. Kai Yuan as well as the rest of my colleagues at the Macromolecular Chemistry Group for making these three and a half years of doctoral work a really enjoyable and unforgettable experience.

Finally, my special thanks to my cheerful wife for all your selfless help and love during our stay in Germany; Ibeth, you are the light of my life! My final thanks go to my parents and family in Ecuador, like I said back in Mexico – despite the even greater distance between us I can feel you close to me.